“Sapienza” Università di Roma

Facoltà di Ingegneria
Dipartimento di Ingegneria Strutturale e Geotecnica
Dottorato di ricerca – XXIII Ciclo

IMPROVING THE SAFETY OF STEEL BRIDGES THROUGH MORE ACCURATE AND AFFORDABLE MODELING OF CONNECTIONS

Candidate: Chiara Crosti
Advisor: Prof. Franco Bontempi
Co-Advisor: Dott. Dat Duthinh

Dissertazione presentata per il conseguimento del titolo di
Dottore di Ricerca in Ingegneria delle Strutture

A.A. 2009/2010

Acknowledgements

I would like to express my gratitude to my mentor Prof. Franco Bontempi, for his scientific contribution and for giving me the passion for the world of research.

Professor Marcello Ciampoli and Professor Paolo Pinto, who revised this work and gave me precious suggestions, are also gratefully acknowledged.

Thanks are also due to the coordinator of Ph.D. activities Prof. Rega and to the committee members for the effort and time devoted to read this thesis.

A special thank is addressed to Dr. Dat Duthinh, for the contribution given to this research and for all the support he gave me.

My gratitude goes also to the Building and Fire Research Laboratory (BFRL) in particular to Prof. Emil Simiu and the Metallurgy division (MSEL) of the National Institute of Standard and Technology (NIST), for allowing me to spend almost two years there and making me feel like one of them.

An important thank is for Eng. Piergiorgio Perin for providing the use of the finite element code STRAUS7, and to NTSB and FHWA for allowing the access to the detailed FE model used in the investigation of the collapse of the I-35 W Bridge.

I wish to thank Aurelien, Coralie, Diane, Julien, Mauro, Silvia, Xenia for being my friends and my family in most of my “Ph.D American trip”, having them always by my side made/make my life much easier.

I thank my colleagues and friends Filippo, Francesco, Francesca, Konstantinos, Luisa, Pierluigi, Sauro, Stefania for the help and the continuous support.

I would like to thank my parents, my brother and Fabiola for being always there no matter what and giving me the strength to fight for what I really want.

And I thank all the people who tried to be an obstacle in the achievement of this goal, because it is thanks to them that after each “downfall” I found the motivation to stand up even stronger than before.

THESIS OUTLINE

THESIS OUTLINE 1

SYNTHESIS 5

KEYWORDS 6

SUMMARY 6

SCHEME OF THE THESIS 8

LIST OF FIGURES 9

LIST OF TABLES 15

LIST OF ACRONYMCS 17

INTRODUCTION

1 AIM OF THE THESIS 21

PART I: GENERAL ASPECTS OF STRUCTURAL SAFETY

2 STUCTURAL SAFETY IN CODES AND REGULATIONS 25

2.1 DEFINITION OF STUCTURAL SAFETY 25

2.2 SAFETY IN CODES AND REGULATIONS 26

2.2.1 AMERICAN CODES 26

2.2.2 EUROPEAN CODES 28

3 STRUCTURAL INTEGRITY 31

3.1 INTRODUCTION 31

3.2 STRUCTURAL INTEGRITY 31

3.3 SUBSTRUCTURING ANALYSIS 34

3.3.1 STRUCTURAL PROBLEM BREAKDOWN 34

4 STRUCTURAL STABILITY 37

4.1 INTRODUCTION 37

4.2 STRUCTURAL STABILITY 37

4.2 STABILITY FOR STEEL STRUCTURAL ELEMENTS 38

4.3 INSTABILITY COLLAPSES 40
4.4 STEEL TRUSS BRIDGES 41
4.5 FRACTURE CRITICAL BRIDGES 43
4.6 REDUNDANCY IN TRUSS BRIDGES 45
    4.6.1 INTERNAL REDUNDANCY 45
    4.6.2 STRUCTURAL REDUNDANCY 46
    4.6.3 LOAD PATH REDUNDANCY 47

PART II: STEEL CONNECTIONS

5 STEEL GUSSET PLATE CONNECTIONS 51
5.1 INTRODUCTION 51
5.2 STEEL GUSSET PLATES CONNECTIONS 51
5.3 REGULATIONS AND CODES FOR STEEL GUSSET PLATE CONNECTIONS 52
    5.3.1 EUROPEAN CODES 53
    5.3.2 AMERICAN CODES 55
5.4 REVIEW OF THE LITERATURE ON APPROXIMATE METHODS FOR GUSSET PLATES 56
    5.4.1 APPLICATION OF THESE METHODS TO THE CASE UNDER STUDY 65

6 CRITICAL REVIEW OF THE FHWA GUIDELINES ON GUSSET PLATES 69
6.1 INTRODUCTION 69
6.2 BUCKLING BEAHVIOR 69
    6.2.1 CURRENT GUIDELINES 69
    6.2.2 EXPERIMENTAL RESULTS 73
    6.2.3 EDGE BUCKLING VS GUSSET PLATE BUCKLING 88
6.3 BLOCK SHEAR FAILURE 91
    6.3.1 CURRENT GUIDELINES 91
    6.3.2 FINITE ELEMENT MODEL 93
6.4 CONCLUSION 108

PART III: GLOBAL RESPONCE OF I-35W BRIDGE BY MEANS OF AFFORDABLE AND ACCURATE MODELING OF CONNECTIONS

7 STORY OF I-35W 111
7.1 GENERAL DESCRIPTION 111
7.2 I35-W HISTORY 112
    7.2.1 I35-W COLLAPSE 112
7.1 DISCUSSION OF ANALYSES DEVELOPED 114

8 STRATEGIES OF ANALYSIS BY SUB-STRUCTURING METHOD 117
8.1 INTRODUCTION 117
8.2 FINITE ELEMENT MODEL OF I-35W 118
8.3 JOINT IN DETAIL 119
8.3.1 LINEAR ELASTIC ANALYSES 123
8.3.2 THEORITICAL CALCULATION OF THE STIFFNESS MATRIX 123
8.3.3 STIFFNESS MATHOD 123
8.3.4 JOINT MODELING 129
8.4 MODEL WITH BEAM ELEMENT 136
8.5 CONCLUSION 139

9 GLOBAL ANALYSIS 140
9.1 INTRODUCTION 140
9.2 TWO-DIMENSIONAL MODEL OF THE BRIDGE 140
9.2.1 LINEAR ANALYSES 143
9.2.2 NONLINEAR ANALYSES 144
9.3 THREE-DIMENSIONAL MODEL OF THE BRIDGE 145
9.3.1 NONLINEAR CONNECTION MODEL 147
9.3.2 NONLINEAR ANALYSES 150
9.4 CONCLUSION 155

CONCLUSIONS

CONCLUSION 159
FUTURE WORK 160
APPENDIX 165
REFERENCES 173

SYNTHESIS OF THE WORK

1. KEYWORDS
2. SUMMARY
3. SCHEME OF THE THESIS

SYNTHESIS

1. KEYWORDS

Fracture of Steel Bridges, Gusset Plates, Semi-rigid Nodes, Complex Structures, Structural Safety, Structural Integrity, Robustness, Bridge Collapses, Nonlinear Finite Element Analysis, Sub-Structuring Techniques

2. SUMMARY

This thesis develops an improved and affordable method to model the connections of steel truss bridges with a view of improving their design, analysis and safety.

The issue came to the fore when the I35-W Bridge in Minnesota collapsed on August1, 2007 [NTSB, 2008]. After many Finite Element Analyses, the National Transportation Safety Board (NTSB) found the buckling of an under-designed gusset plate to be the main cause of the disaster. After this tragedy, the Federal Highway Administration (FHWA) focused its attention on all the 465 steel deck truss bridges present in the National Bridge Inventory [NTSB, 2008], and provided guidelines to bridge owners to verify the safety of these kind of bridges.

The present work focuses on the means to assess the structural safety for these particular types of steel truss bridges, and proposes a method for the correct and efficient modeling of the connections.

It starts with the basic question: “how safe is it to consider all the connections in these types of bridges as rigid joints?”

The work is organized in three parts:

- the first gives an overview of the problem of the structural safety of complex structure such as bridges, and proposes the use of the sub-structuring method, [Przemieniecki, 1968], [Bontempi and Arangio, 2008];
- the second part reviews the relevant literature, standards and codes. Both the Eurocodes and the American codes are missing a way to assess the stiffness and strength of gusset plate connections. This work aims at filling the gap between advanced computing

methods that can be brought to bear on a failure investigation, and the rigid connections, linear beam analysis typical of routine design, [AASHTO, 1994], [Astaneh, 2010], [Ballio and Mazzolani, 2005], [Crosti and Duthinh, 2010], [Chambers and Ernst, 2005], [EN 1993-1-8, 2003];

- in the third part, the proposed method is applied to the I-35W Bridge. The I-35W is classified as a Fracture Critical Truss Bridge, meaning that the failure of one major element would cause the collapse of the whole structure. The method makes use of the detailed finite element models of the NTSB and FHWA to find the strength and stiffness of the joint in question and replace it with five spring elements. The method provides accuracy and substantial computational savings for repeated load cases, particularly if many joints in the structure are similar, [NTSB, 2008], [FHWA, 2009].

The goal of the thesis then is to develop accurate but computationally affordable connection models to improve global analysis and thus allow bridge owners to predict the effects of joint deterioration, design deficiencies and to guide the requirements for structural monitoring..

3. SCHEME OF THE THESIS

IMPROVING THE SAFETY OF STEEL BRIDGES TROUGH MORE ACCURATE AND AFFORDABLE MODELING OF CONNECTION

Fact:
I-35W Collapse

"How safe is it to consider all the connections in these types of bridges as rigid joints?"
"How to model these types of connections in steel truss bridges?"

General aspects of Structural Safety

Structural Safety | Structural Integrity | Structural Stability

Steel Connections

Steel gusset plate connections | Critical review of FHWA guidelines on gusset plates

Global response of I-35W Bridge by means of affordable modeling of connections

History of I-35W

Buckling of an under-designed gusset plate

Sub-structuring method

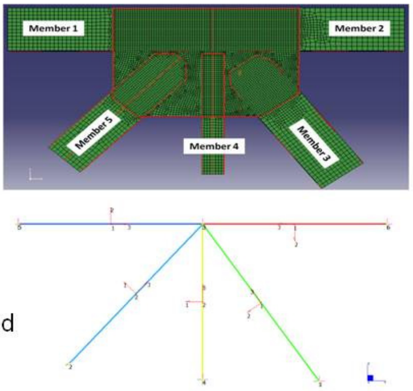

Global analyses

Rigid Joints;
Semi-rigid Joints;

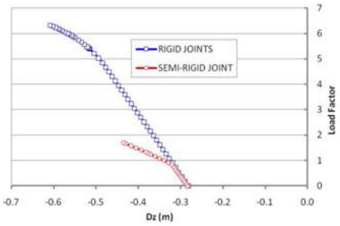

Conclusion and future work

Figure 1. Flowchart of the thesis.

LIST OF FIGURES

Figure 1. Flowchart of the thesis……………………………………………………………………………… 8

Figure 1.1. Picture of U10 W connection taken on June 2003, [NTSB, 2008]…………………………………. 20

Figure 2.2. Individuation of Serviceability, Safety and Structural Robustness on Load-Displacement curve….. 29

Figure 3.1. Structural Integrity vs. Discrete event and Continuous occurrence………………………………… 32

Figure 3.2. Trend of Structural Integrity with continuous occurrence and discrete event, for the I-35W Bridge. 33

Figure 3.3. Hierarchical breakdown of a system, [Bontempi and Arangio, 2010]……………………………… 35

Figure 3.4. Breakdown model of the I 35W bridge……………………………………………………………... 36

Figure 4.1. N-d curve for steel elements with and without imperfections………………………………………. 38

Figure 4.2. Non symmetric N-d curve for steel elements……………………………………………………….. 40

Figure 4.3. Different members in a typical steel truss bridge…………………………………………………… 42

Figure 4.4. Different types of truss bridges. ……………………………………………………………………. 43

Figure 4.5. Configuration of the 20 bridges from plans submitted by various states. The bridges are drawn to the same scale to illustrate the relative size. [FHWA,2009]…………………………………………………….. 44

Figure 4.6. ”Multi-element” riveted members, example of internal redundancy……………………………….. 46

Figure 4.7. Newport Southbank Bridge in Ohio. (Wikipedia)…………………………………………………... 46

Figure 4.8. Bridge with X diagonal, First Whhan Bridge in China. (Wikipedia)……………………………….. 47

Figure 5.1. Example of truss bridge with gusset plates. (Photo by NTSB Report)……………………………... 52

Figure 5.2. Classification of hollow section connections, (prEN1993 Part 1.8)………………………………... 52

Figure 5.3. Failure modes for joints between RHS brace members and RHS chord members, (EN1993 Part 1.8)……. 52

Figure 5.4: Stress trajectories, [Whitmore, 1952]……………………………………………………………… 55

Figure 5.5: Tension cracks in the Stresscoat [Whitmore, 1952]………………………………………………… 55

Figure 5.6: Wedge model, [Astaneh, 1989]……………………………………………………………………... 56

Figure 5.7: Fin truss model, [Astaneh, 1989]…………………………………………………………………..... 56

Figure 5.8: Thornton's Uniform Force Method [Thornton, 1991]…………………………………………… 57

Figure 5.9. [McGuire]……………………………………………………………………………………… 60

Figure 5.10: Pseudo gusset plate frame, from Dowswell and Barber (2004)…………………………………… 61

Figure 5.11: Critical section for edge buckling of gusset plate, from Brown (1988)…………………………… 62

Figure 5.12: Regions of yielding or local buckling………………………………………………………... 66

Figure 6.1. Equivalent column………………………………………………………………………………... 70

Figure 6.2. Column curves……………..……………………………………………………………….. 72

Figure 6.3. Factored column curves……………………………………………………………………... 72

Figure 6.4. University of Alberta tests [Walbridge, Grondin and Cheng, 1998]………………………………. 73

Figure 6.5. Summary of the analyses developed………………………………………………………... 74

Figure 6.6. Finite-element model meshed with 2000 elements…………………………………………………. 75

Figure 6.7. Mesh convergence study…………………………………………………………………………. 76

Figure 6.8. Framing member stiffness……………………………………………………………………….. 77

Figure 6.9. Effects of framing member stiffness (edge loading)………………………………………………... 78

Figure 6.10. Effects of initial deformations, edge loading, Case (B)…………………………………………… 79

Figure 6.11. Effects of initial deformations, edge loading, Case (C)…………………………………………… 79

Figure 6.12. Effects of initial deformations, compression on first row of bolts, Case (C)……………………… 81

Figure 6.13. Effects of initial deformations, compression on first row of bolts, Case (C)……………………… 82

Figure 6.14. Pre- and post-buckling gusset plates………………………………………………………………. 82

Figure 6.15. Triangular load, Case C……………………………………………………………………………. 83

Figure 6.16. Uniform load, Case C………………………………………………………………………………… 83

Figure 6.17. Bilinear load distribution……………………………………………………………………... 84

Figure 6.18. Gusset plate framing I-section loaded in 2 ways……………………………………………… 85

Figure 6.19. Gusset plate loaded eccentrically by I-member…………………………………………………… 86

Figure 6.20 Gusset plate framing I-member loaded by F and M…………………………………………….. 87

Figure 6.21. Effects of initial imperfections of opposite direction to load eccentricity on gusset plate loaded by I-member………………………………………………………………………………………………... 87

Figure 6.22. Effects of initial imperfections of opposite direction to moment on gusset plate framing I-section loaded by F & M……………………………………………………………………………………………… 88

Figure 6.23. Buckling of non compact gusset plates……………………………………………………………. 89

Figure 6.24. Compressive strength of non compact gusset plates………………………………………………. 90

Figure 6.25. Example of potential block shear rupture planes for gusset plates in tension [FHWA, 2009]……. 92

Figure 6.26. Summary of the analyses developed for the block shear failure…………………………………... 92

Figure 6.27. University of Alberta gusset plate test (Nast, Grondin and Cheng, 1999)………………………… 93

Figure 6.28. Finite-element model meshed with 9520 elements………………………………………………... 93

Figure 6.29. Application of bolt loads…………………………………………………………………………... 94

Figure 6.30. Mesh refinement around holes…………………………………………………………………….. 95

Figure 6.31. Results of mesh study……………………………………………………………………………… 96

Figure 6.32. Coarse and fine bolt load application……………………………………………………………… 96

Figure 6.33. Results for coarse and fine bolt load applications…………………………………………………. 97

Figure 6.34. Strain contours of Plate 2 ($A_{tn}< 0.58A_{vn}$)………………………………………………………….. 99

Figure 6.35. Load displacement for Plate 2……………………………………………………………………... 100

Figure 6.36. Strain contours of Plate 3 ($A_{tn}< 0.58A_{vn}$)…………………………………………………………. 101

Figure 6.37. Load-displacement curve for Plate 3………………………………………………………………. 102

Figure 6.38. Strain contours of Plate 4 ($A_{tn} > 0.58A_{vn}$)…………………………………………………………. 103

Figure 6.39. Load-displacement curve for Plate 4………………………………………………………………. 104

Figure 6.40. Strain contours of Plate 5 ($A_{tn} > 0.58A_{vn}$)…………………………………………………………. 105

Figure 6.41. Load-displacement curve for Plate 5………………………………………………………………. 106

Figure 6.42. Plate 6……………………………………………………………………………………………... 107

Figure 6.43. Load-displacement curve for Plate 6……………………………………………………………… 107

Figure 7.1. I 35W bridge. [NTSB, 2008]………………………………………………………………………... 111

Figure 7.2. Drawing of the bridge, [Ocel, 2008].1064 ft = 324.3 m…………………………………………… 112

Figure 7.3. http://content.asce.org/I-35W/NTSBI35W.html... 113

Figure 7.4. Stress with the load at time of accident, [Ocel, 2008]……………………………………………. 114

Figure 7.5. Crossing the threshold of failure, [Ocel, 2008]…………………………………………………... 115

Figure 8.1. NTSB model…………………………………………………………………………………... 119

Figure8.2. Joint dimensions (m)…………………………………………………………………………... 120

Figure 8.3. Position of the rigid links modeling the rivets…………………………………………………… 121

Figure8.4. Members in joint U10………………………………………………………………………….. 121

Figure8.5. Dimensions of the members composing the joint………………………………………………... 122

Figure 8.6. Beam element………………………………………………………………………………….. 123

Figure 8.7. Beam element in STRAUS…………………………………………………………………….. 125

Figure 8.8. Properties of the beam element………………………………………………………………... 125

Figure 8.9. Partition of the stiffness matrix………………………………………………………………... 127

Figure 8.10. Definition of the terms of the stiffness matrix for the user-defined element in STRAUS……… 127

Figure 8.11. Transformation from global to local coordinates……………………………………………….. 127

Figure 8.12. User defined elements with local axes………………………………………………………….. 130

Figure 8.13. a) Joint built with beam elements, b) detailed model…...………………………………………. 136

Figure 9.1. Drawing of the truss of I-35W Bridge…………………………………………………………. 140

Figure 9.2. Restraints in the model………………………………………………………………………… 141

Figure 9.3. West truss……………………………………………………………………………………… 141

Figure 9.4. Load components for the west main truss……………………………………………………... 142

Figure 9.5. Four different 2D models of the bridge………………………………………………………... 143

Figure 9.6. Typical vertical displacements………………………………………………………………… 143

Figure 9.7. Node where the vertical displacement is measured……………………………………………. 144

Figure 9.8. Load factor vs. out of plane displacement for the midspan node in the out-of- plane direction……. 145

Figure 9.9. 3D model………………………………………………………………………………………. 145

Figure 9.10. Traffic load…………………………………………………………………………………… 146

Figure9.11. Concentrated load for the construction load………………………………………………………….. 147

Figure 9.12. Stress-strain curve………………………………………………………………………………. 148

Figure 9.13. Member 1………………………………………………………………………………………... 149

Figure 9.14. Member 2, (the F_x should have been plotted with negative values to be coherent with the XYZ coordinates system, but for simplicity in the graph has been plotted with positive values)…………………….. 149

Figure 9.15. Member 3………………………………………………………………………………………... 149

Figure 9.16. Member 4………………………………………………………………………………………... 150

Figure 9.17. Member 5………………………………………………………………………………………... 150

Figure 9.18. Rigid joints model. Deformed shape of 10 scaling at load factor of 6.36…………………………. 151

Figure 9.19. Localization of the yield hinge. Trend of stress in the 5 elements around the joint U10-W………. 151

Figure 9.20. Load Factor-Vertical Displacement at the node in the midspan…………………………………... 152

Figure 9.21. Tension and compression axial capacity in the five connection elements, (local coordinates)…… 153

Figure9.22. Semi-rigid joint. Trend of the axial forces in the 5 connection elements of the joint chosen……... 154

Figure9.23. Deformation of the detailed model at F (compression) of 1.21E+7……………………………….. 155

Figure 9.24. Picture of U10 W connection taken on June 2003, [NTSB, 2008]………………………………... 159

Figure C.1. On the left the detailed and simplified model used to model the joint, on the right the trend of the axial force of each connection elements modeling the join under study……………………………..…. 160

Figure C.2. Comparison between the two models used………………………………………………………. 161

Figure C.3. Test performed at FHWA in Virginia, USA……………………………………………………... 161

Figure C.4. Results of these tests, buckling of the gusset plates……………………………………………... 162

Figure C.5. Displacement monitoring for a gusset plate of the FHWA tests…………………………………… 165

Figure A.1. Geometry of the truss bridge…………………………………………………………………….. 166

Figure A.2. Typical example in literature of bridges with the same geometry………………………………. 166

Figure A.3. Bridge with X diagonal, First Whhan Bridge in China. (Wikipedia)……………………………… 167

Figure A.4. Two load cases considered……………………………………………………………………… 168

Figure A.5. The four different models considered…………………………………………………………. 168

Figure A.6. Load factor-vertical displacement……………………………………………………………….. 168

Figure A.7. Rigid joints, (Deformed scale of 10)………………………………………………………….. 169

Figure A.8. Model 2, Semi-rigid joints, 5 connection elements in one joint…………………………………… 170

Figure A.9. Model 2, Semi-rigid joints, 5 connection elements in one joint. Trend of the axial forces in the 5 connection elements of the joint chosen……………………………………………………………………… 170

Figure A.10. Semi-rigid connections (5 connection elements in the 5-members joints)………………………... 171

Figure A.11. Model 3, Semi-rigid joints, 5 connection elements in all the 5-member joints. Trend of the axial forces in the 5 connection elements of the joint chosen………………………………………………………… 171

Figure A.12. Model 4, Pinned joints, (Deformed scale of 10)…………………………………………………... 171

LIST OF TABLES

Table 5.1: Concentric gusset plate design models. H = horizontal force, V = vertical force, R = resultant force, M =moment Subscript B for beam, C for column………………………………………………………… 60

Table 5.2: Safety factors for various characteristic loads. P_d = design load; P_y^u = load at which plastic zone penetrates web of chord; P_y = initial yield load; P_{cr} = initial buckling load; P_u = ultimate strength………….. 66

Table 5.3: Buckling constant from FEA of idealized triangular plate………………………………………... 67

Table 6.1. Calculation of block shear capacity………………………………………………………………. 94

Table 8.1. Flexibility matrix for the beam element 1 (units: N, m, rad)………………………………………… 127

Table 8.2. Stiffness matrix for the beam element 1 (units: N, m, rad)………………………………………….. 127

Table 8.3. Transformation matrix, T………………………………………………………………………….. 129

Table 8.4. Stiffness matrix in local coordinates………………………………………………………………. 129

Table 8.5. Stiffness matrix calculated by means of the theoretical approach………………………………….. 130

Table 8.6. Displacements obtained by using the user-defined element with the matrix of Table 9.4………….. 130

Table 8.7. Displacements obtained by using the user-defined element with the matrix of Table 9.5………….. 130

Table 8.8. Stiffness matrix element 1 in global coordinates…………………………………………………….. 132

Table 8.9. Transformation matrix T_1, (rotation around 2 of 90 degrees)……………………………………… 132

Table 8.10. Stiffness matrix for element 1 in local coordinates………………………………………………… 133

Table 8.11. Stiffness matrix element 2 in local coordinates…………………………………………………….. 133

Table 8.12. Stiffness matrix element 3 in local coordinates…………………………………………………….. 133

Table 8.12. Stiffness matrix element 4 in local coordinates…………………………………………………….. 133

Table 8.14. Stiffness matrix element 5 in local coordinates………………………………………………….... 134

Table 8.15. Forces and moments applied one at a time………………………………………………………. 134

Table 8.16. Element 1, displacements obtained in STRAUS with user defined elements node 5……………… 134

Table 8.17. Element 1, displacements obtained in ABAQUS node 5…………………………………………... 135

Table 8.18. Element 2, displacements obtained in STRAUS with user defined elements node 6……………… 135

Table 8.19. Element 2, displacements obtained in ABAQUS node 6………………………………………….. 135

Table 8.20. Element 3, displacements obtained in STRAUS with user defined elements node 1……………… 135

Table 8.21. Element 3, displacements obtained in ABAQUS node 1………………………………………….. 136

Table 8.22. Element 4, displacements obtained in STRAUS with user defined elements node 4……………… 136

Table 8.23. Element 4, displacements obtained in ABAQUS node 4………………………………………….. 136

Table 8.24. Element 5, displacements obtained in STRAUS with user defined elements node 2……………… 136

Table 8.25. Element 5, displacements obtained in ABAQUS node 2………………………………………….. 137

Table 8.26. Element 1, displacements obtained in STRAUS with beam elements, node 5, those have to be compared with the results shown in Table 8.17………………………………………………………………. 138

Table 8.27. Element 2, displacements obtained in STRAUS with beam elements, node 6, those have to be compared with the results shown in Table 8.19………………………………………………………………... 138

Table 8.28. Element 3, displacements obtained in STRAUS with beam elements, node 1, those have to be compared with the results shown in Table 8.21………………………………………………………………. 138

Table 8.29. Element 4, displacements obtained in STRAUS with beam elements, node 4, those have to be compared with the results shown in Table 8.23………………………………………………………………. 139

Table 8.30. Element 5, displacements obtained in STRAUS with beam elements, node 2, those have to be compared with the results shown in Table 8.25……………………………………………………………… 139

Table 8.30: Comparison of displacements and rotations of STRAUS model with rigidly connected beams and ABAQUS FE model with various gusset plate thicknesses, Element 1………………………………………… 140

Table 9.1: Midspan vertical deflection for different models…………………………………………………. 145

ACRONYMS

ASD	Allowable Stress Design
AISC	American Society of Civil Engineers
AASHTO	American Association of State Highway and Transportation Officials
CBT	Center for Building Technology
DoFs	Degrees of Freedom
FEM	Finite Element Method
FEA	Finite Element Analysis
FHWA	Federal Highway Administration
ILS	Integrity Limit States
LRFD	Load Factor and Resistance Design
LRF	Load Reduction Factor
Mn/ DOT	Minnesota Department of Trasportation
NCHRP	National Cooperative Highway Research Program
NTSB	National Transportation Safety Board
SLS	Serviceability Limit States
ULS	Ultimate Limit States

INTRODUCTION

1. AIM OF THE THESIS

1 AIM OF THE THESIS

The August 1st, 2007 catastrophic collapse of the I-35 W Bridge in Minnesota, United States, under ordinary traffic and construction loads, was triggered by a design flaw that had remained undetected for 40 years. It took very intensive Finite Element Analysis (FEA) to prove that the cause was the buckling of an undersized gusset plate [NTSB, 2008]. Constructed in 1967, Bridge 9340 was designed in the early days of computer structural analysis, and did not include load-path redundancy. Connections (gusset plates) were designed with hand formulas that verified strength across critical sections, and were subsequently assumed to be stronger than the structural members they connected. The truss bridge was designed, most likely by matrix linear structural analysis, as an assemblage of rigidly connected beams. The bridge was inspected every two years, as recommended by the FHWA, [FHWA, 2009], and was load tested in 2000. It is worth nothing that an inspector had actually photographed gusset plate U10 because of its bowed- out appearance, but did not judge that to be alarming, [O'Connell et al., 2001].

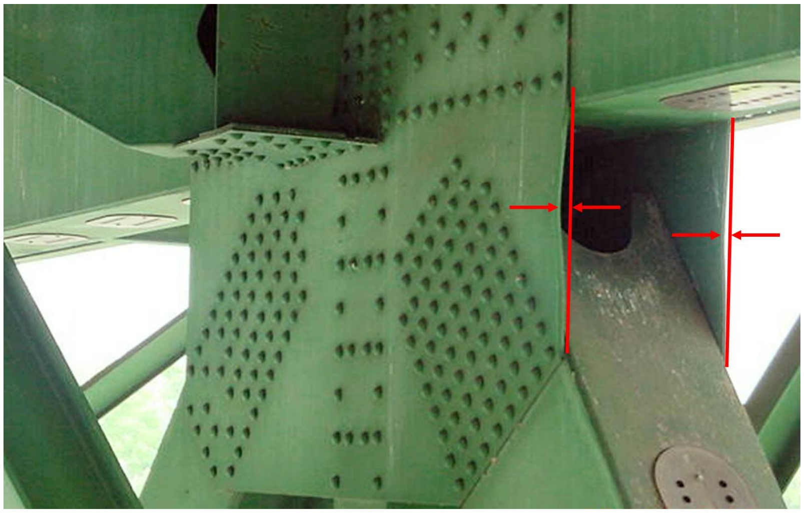

Figure 1.1. Picture of U10 W connection taken on June 2003, [NTSB, 2008].

Although the state of computer structural analysis has vastly improved in the last 45 years, the state of practice has not changed so dramatically. The NTSB used massive computing to model the bridge and several connections with finite elements, but the Guidance issued by FHWA for the load rating of gusset plates relied very much on hand calculation methods.

The literature review provides information on the strength and the design of gusset plates but no guidance on the actual load displacement behavior of the connections [Astaneh-Asl, 2010]. Both the Eurocodes and the American Codes are missing a way to assess the stiffness of those particular connections [PrEN 1993-1-8, 2003], [AISC, 2008].

Current design and maintenance software use FE models in the form of beam elements connected by fixed joints. Yet, the investigation, made by FHWA and NTSB, only revealed the cause of the collapse after highly detailed and computationally intensive modeling of the joints using solid elements.

This thesis aims at filling the gap between advanced computing noted that are too expensive for routine design, and design methods that rely on highly approximate hand calculations to dimension gusset plates and then assume they behave rigidly in a global analysis.

The idea is to properly account for the behavior of connections in the global analysis with the use of equivalent springs. The spring properties, in the linear and nonlinear ranges up to failure, are derived from FEA, but this need to be done only once or a few times. If a bridge contains similar joints, the same set of equivalent springs, suitably modified to account, for example, for changes in thickness of the gusset plates, can be used repeatedly. Moreover, computational savings can be gained in repeated load cases, as each analysis run makes use of the simplified connection. This techinque can also be used for verifying the load rating of existing bridges and identify potential locations in need of strengthening.

The goal of the thesis then is to develop accurate but computationally affordable connection models to improve global analysis and thus allow bridge owners to predict the effects of joint deterioration, design deficiencies and to guide the requirements for structural monitoring. The method is therefore to perform nonlinear analyses on detailed joint model in order to assess the characteristics of non linear springs that will replace the gusset plate in a global model of the bridge and produce significant savings in computational effort at the cost of little loss of accuracy.

PART I:

GENERAL ASPECTS OF STRUCTURAL SAFETY

2. STRUCTURAL SAFETY IN REGULATIONS AND CODES
3. STRUCTURAL INTEGRITY
4. STRUCTURAL STABILITY

2 STRUCTURAL SAFETY IN REGULATIONS AND CODES

2.1 DEFINITION OF STRUCTURAL SAFETY

Safety is a central theme in Structural Engineering. From a general dictionary the definition of this word is:

> *"the state of being "safe", the condition of being protected against physical, social, spiritual, financial, political, emotional, occupational, psychological, educational or other types or consequences of failure, damage, error, accidents, harm or any other event which could be considered non-desirable. This can take the form of being protected from the event or from exposure to something that causes health or economical losses. It can include protection of people or of possessions".*

Nevertheless, if a general consensus can be found among structural engineers on the importance of achieving safety, not the same can be said on the ways of pursuing it. The divergences start from the definition of the term "safety" itself, that is either referred primarily to the safety of people as in [SIA260] or to the structural integrity of the building as in [ISO 2394]. The first code states that:

> *"A structure can be declared safe if during a critical event, such as impact, fire, downfall, safety of people assured",*

While the International Standard above mentioned [ISO 2394] states that:

> *"Structures and structural elements should be designed, built and maintained in such a way as to serve properly and economically their intended use during their design life. Particularly they should satisfy, with proper levels of reliability:*
>
> *a. serviceability state requirements,*
>
> *b. ultimate load state requirements,*
>
> *c. structural integrity requirements".*

In Structural Engineering, the word ``safety'' is used more narrowly. A safe structure is one that will not be expected to fail. This could sometimes be quantified by saying that the probability of failure is less than a specific value, but such a value is not normally stated or known explicitly. For the most part, safety is determined by other means: first of all by reliance on codes, for example. Historically, the emphasis on personal safety, of preventing death and injury, has tended to underlie the structural view of safety. This view is now changing. Particularly since the Northridge earthquake, the emphasis has been shifting towards minimization of economic losses. In a sense, the focus has changed from ensuring safety to managing risk. Nevertheless, safety is still an important concept. Below are reported some definitions and ways to assess structural safety [Giuliani L., 2008].

2.2 SAFETY IN REGULATIONS AND CODES

Structural Codes and Standards provide the foundation of sound engineering practice and a framework for addressing safety and serviceability issues in structural design. They identify natural and man-made actions that must be considered, define magnitudes of the resulting forces for design, and prescribe methods for determining structural resistance to these forces. The frame of these documents on which the structural engineer places so much reliance must address the question: “How safe is safe enough?” on behalf of the Society as a whole.

Structural Codes are linked to computational methods of safety assessment, and their primary purpose is to manage risk and maintain the safety of buildings, bridges and other facilities at socially acceptable levels.

2.2.1 AMERICAN CODES

Until the 1960s, the safety criteria in Structural Codes were based on allowable stress principle, ASD (Allowable Stress Design). The structural system being designed was analyzed under the assumption that it behaved elastically (the fact that structures did not necessarily behave elastically up to failure was disregarded). Uncertainties were addressed by requiring that the computed stresses did not exceed a limiting stress (at yielding, rupture, instability) divided by a factor of safety. These factors of safety were selected subjectively; one might, for example, identify the load acting on a structure and then design the structure so that the elastic stresses due to that load remain below 60 % of the stress at yield. It is not entirely subjective, but rather depends on the consequence of reaching the limit state. Yielding in tension does not cause failure necessarily, due to material ductility, therefore the allowable stress can be as high as 0.9 F_y. On the other hand, yielding in compression can lead to buckling and collapse, therefore the allowable stress is lower. Likewise, shear failure is more brittle and sudden than tensile failure and the allowable stress is also lower.

During the past century, with the advance of rational structural and materials calculations and testing, the trend in the factor of safety generally has been downward.

During the late 1960s and 1970s, a number of natural disasters occurred worldwide that caused extensive loss of life and property damage and focused the attention of the structural engineering community and the public on the need to advance building practices for disaster mitigation. In Professional staff from the Structures Division in the Center for Building Technology (CBT) of the National Bureau of Standards, now the National Institute of Standards and Technology were involved in a number of the damage surveys and failure investigations that followed these disasters. Among the more notable of these were the structural failure investigations that followed the San Fernando, California, Earthquake of 1971, the Managua, Nicaragua, Earthquake of 1972, and the Miyagi-ken-oki Earthquake of 1978; the investigation of snow and rain load conditions prior to the collapse of the Hartford Civic Arena roof in 1978; and the evaluations of wind loads, wind load effects, and building performance following Hurricane Camille on the Gulf Coast (1969) and Cyclone Tracy in Darwin, Australia (1974). These and other investigations of building performance revealed a number of deficiencies in the provisions for structural safety appearing in the codes of practice of the time, and emphasized the need for improvements in design for natural hazards.

Concurrently, the new field of structural reliability was developing around the notion that many of the uncertainties in loads and strengths could be modeled probabilistically. Advances were being made in first-order reliability analysis, stochastic load modeling and supporting statistical databases. Several probabilistic code formats were suggested including an early version of Load and Resistance Factor Design (LRFD) for steel buildings.

The change from ASD to LRFD was proposed in the late 1970's, early 1980's because of LRFD's ability to better handle certain sources of uncertainty.

In a deterministic context, structural safety requires that:

$$\text{Required Strength} < \text{Design Strength} \tag{1}$$

where the required strength is determined from structural analysis utilizing the specified design loads, and the design strength is calculated from principles of structural mechanics with specified material strengths and structural element dimensions.

Equation (1) can be therefore written in the following way to reflect uncertainties:

$$\Sigma \gamma_i \ Q_i < \phi R_n \tag{2}$$

In this equation, R_n is the nominal strength corresponding to the limit state of interest and Q_i is the nominal load. These strengths and loads traditionally have been provided in codes and standards, and most engineers are familiar with them. The factors ϕ and γ_i are resistance and load factors that reflect (1) uncertainty in strength and load, and (2) consequence of failure, measured by the target reliability. The right hand side of Eq. (2) is the purview of material specification (steel, concrete, engineered wood, etc.).

The left-hand side is defined for all construction materials by American Society of Civil Engineers ASCE 7, Minimum Design Loads for Buildings and Other Structures [ASCE 7-10], the national load standard referenced by the Model Codes and other regulatory documents in the United States.

2.2.2 EUROPEAN CODES

The "EN 1990: Basis of structural design" is the main document of the European set of Structural Design Standards known as the Structural Eurocodes [EN 1990]. It provides comprehensive information and guidance on the principles and requirements for safety, serviceability and durability that are normally necessary to consider in the design of buildings and civil engineering structures.

The EN1990 states that structures shall be designed and executed in such a way that they meet fundamental requirements for serviceability, safety and robustness. Focusing on the structural safety, this regulation affirms that:

> *"The structure will sustain all actions likely to occur during execution and use during its intended life with appropriate degrees of reliability, and in an economic way".*

All the Eurocodes use the concept of limit state design. Limit states are states beyond which the structure no longer satisfies the design performance requirements. EN1990 makes a distinction between ultimate limit states and serviceability limit states.

The ultimate limit states are those associated with collapse or with other forms of structural failure. They concern the safety of the structure and its contents and the safety of people. Serviceability limit states correspond to conditions beyond which specified service requirements for a structure or structural element are no longer met. They concern the functioning of the construction, the comfort of the people and the appearance, Figure 2.1.

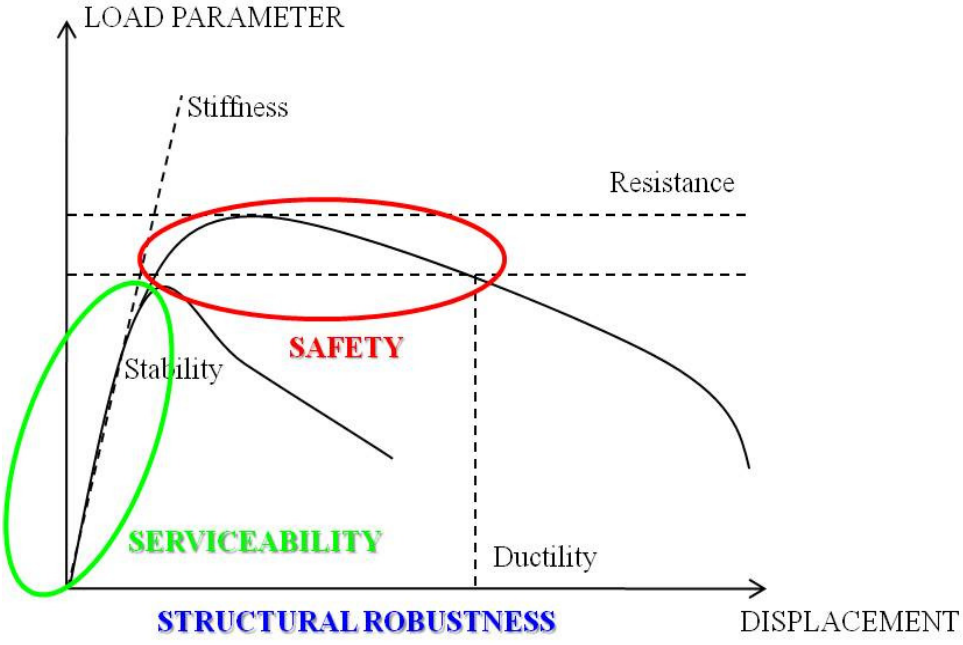

Figure 2.1. Individuation of Serviceability, Safety and Structural Robustness on Load-Displacement curve.

The requirement linked to serviceability is:

- Stiffness, to limit vibrations and deformations.

The ones linked to safety are instead:

- Resistance, the capacity of bearing load,

- Stability, the capacity to not deviate far from nominal equilibrium; and
- Ductility, that is the capacity of the structure to absorb energy and therefore to tolerate a defined level of deformation without collapse.

Therefore, for the ultimate limit state verification, EN1990 stipulates that the effects of design actions do not exceed the design resistance of the structure at the ultimate limit state. Satisfaction of limit state requirements is verified in combinations that take in account appropriate load and resistance coefficients.

3 STRUCTURAL INTEGRITY

3.1 INTRODUCTION

In recent times, events such as the 1994 Northridge Earthquake, 1995 Kobe Earthquake, 1995 Murrah Federal Building bombing and 2001 attack to the World Trade Center have brought the engineering community, including Codes and Standards development organizations and public regulatory agencies, to pay greater attention to the performance of buildings when subjected to local damage sustained from abnormal events.

In this chapter a review regarding the structural integrity and the way to approach the study of a complex system is reported.

3.2 STRUCTURAL INTEGRITY

In Structural Engineering, relevant attributes are reliability, safety, maintainability and integrity. [Arangio et al., 2010]. These properties are essential to guarantee:

- the “safety” of the structure under the relevant hazard scenarios, that in current practice is evaluated by checking a set of ultimate limit states (ULS);
- the “survivability” of the system under accidental or exceptional scenarios, considering also the security issues; in recent guidelines, this property is quantified by the robustness of the system and evaluated by checking a set of “integrity” limit states (ILS);
- the “functionality” of the system under operative conditions, that in current practice is evaluated by checking a set of serviceability limit states (SLS);
- the “durability” of the system.

Bontempi et al, 2010, defines structural integrity as the capacity of a structure to function as designed/required. Integrity is a term which refers to the quality of being whole and complete, or the state of being unimpaired.

It was introduced in the 1970 as safety requirement for buildings, as a direct effect that the collapse of Ronan Point in 1968 had on building codes in UK. Ronan Point was a 22 storyapartment building where a gas explosion on the 18th story blew out a living room wall. The loss of the wall led to the collapse of the whole corner of the building. Better continuity and ductility might have reduced the amount of damage in this building [Griffiths et al., 1968].

Another example of lack of integrity is the Alfred P. Murrah Federal Building where a blast caused the disintegration of one of the perimeter column and the brittle failures of two others, [FEMA, 1996].The transfer girder at the third level above these columns failed and the upper-story floors collapsed in a progressive fashion. Even in this case all of that could have been avoided if there had been better detailing for ductility and greater redundancy and if there had been better resistance for uplift loads on floor slabs [Giuliani, 2008].

Figure 3.1 shows the trend of the structural integrity in function with the continuous occurrence (due to environmental actions, like corrosion, or antropic actions, such as fatigue, etc) and the discrete event, like for example a human design error. In case of discrete event the capacity of the structure decreases suddenly and the curve of the capacity becomes the green one, much lower than the red one.

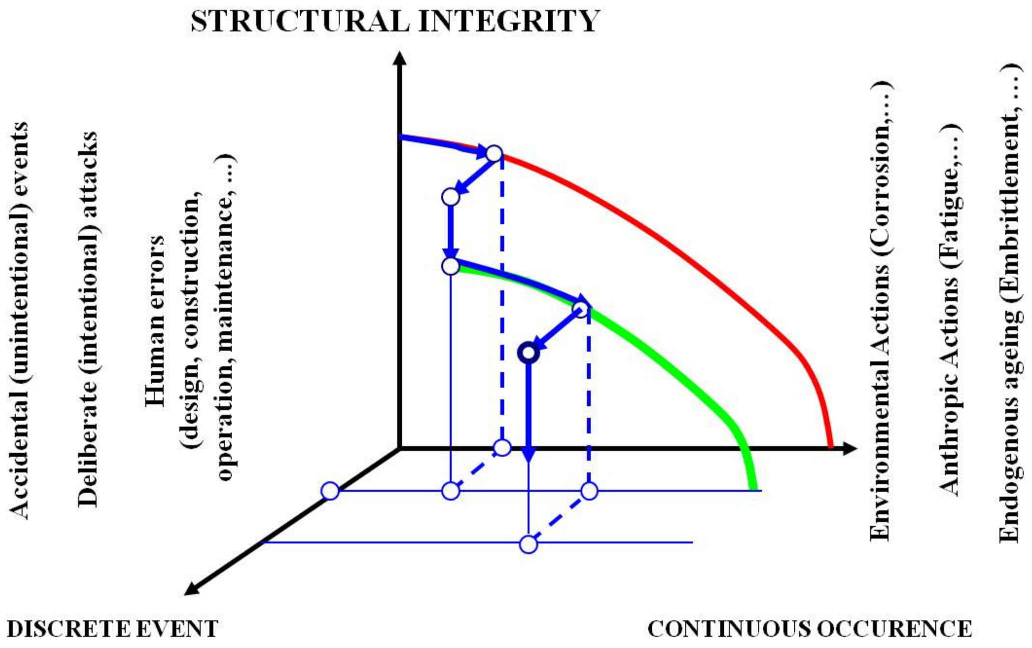
STRUCTURAL INTEGRITY
Accidental (unintentional) events
Deliberate (intentional) attacks
Human errors
(design, construction,
operation, maintenance, ...)
Environmental Actions (Corrosion,...)
Anthropic Actions (Fatigue,...)
Endogenous ageing (Embrittlement, ...)
DISCRETE EVENT
CONTINUOUS OCCURENCE

Figure 3.1. Structural Integrity vs. Discrete event and Continuous occurrence.

Adapting this graph to the specific case of I35-W Bridge disaster for example, it could be possible to point out four phases, see Figure 3.2:

0- it is the nominal configuration of the bridge;
1- after the time passing, some continuous occurrences, such as for instance the corrosion in the connections, lead to the decreasing of the structural performance, (pink curve);
2- a discrete event happens, for the specific case of I35-W Bridge, that event was the buckling of the gusset plate in the joint U10-W due to the under-designed thickness of the gusset plate (human error); after this, the structural capacity of the bridge is much lower, green curve and it keeps decreasing due to the time passing, until it reaches the point 3;
3- at this point the structure crosses its maximum capacity and it collapses.

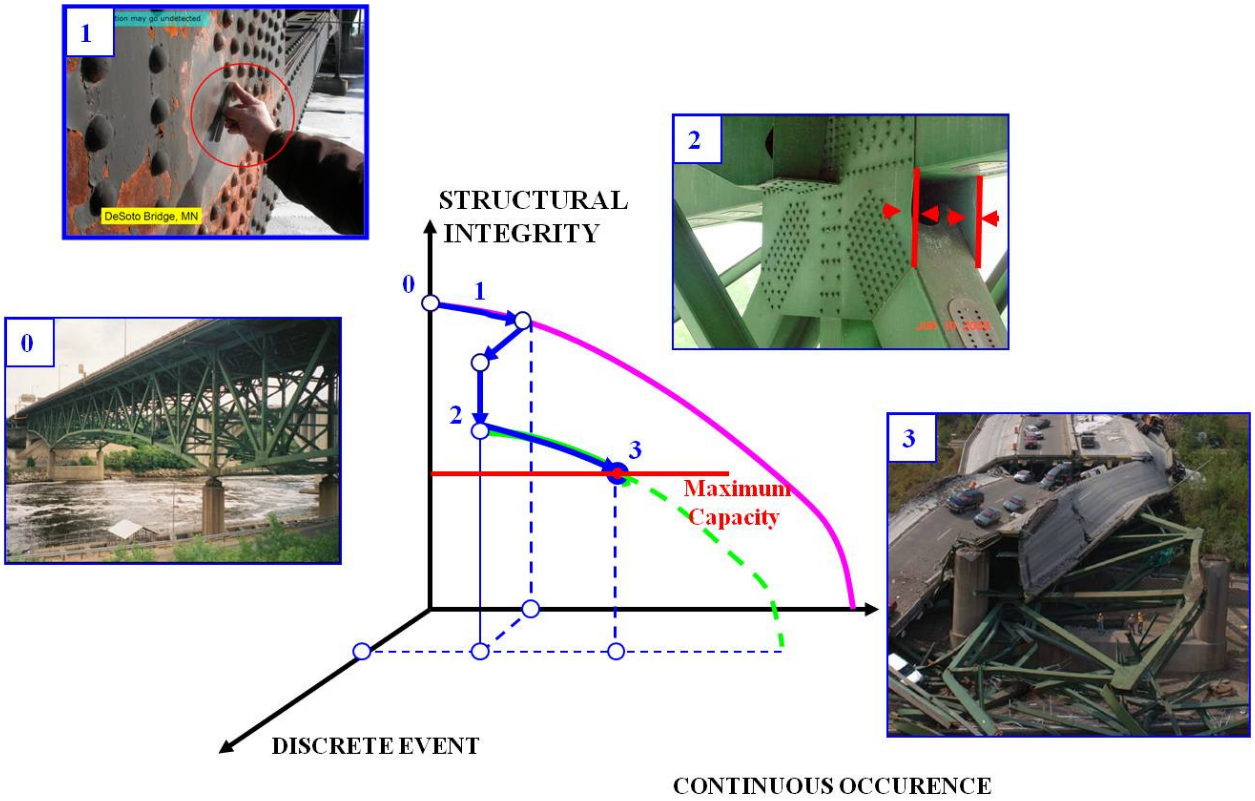
1
tion may go undetected
DeSoto Bridge, MN
2
0
3
STRUCTURAL INTEGRITY
0
1
2
3
Maximum Capacity
DISCRETE EVENT
CONTINUOUS OCCURENCE

Figure 3.2. Trend of Structural Integrity with continuous occurrence and discrete event, for the I-35W Bridge.

3.3 SUB-STRUCTURING ANALYSIS

In recent years more and more demanding structures are designed, built and operated to satisfy the needs of the society. This kind of structures can be denoted as complex systems.

The concept of mechanical system is derived as being a combination of individual elements organized and working as a sum of elements in order to perform a predetermined function [Park et al, 2004]. Talking about structural systems, a "system" can be defined as an organized assembly of elements connected and regulated by interactions in order to satisfy specific functions; the elements can be imagined therefore as beams or columns and the interactions can be the restraints or control devices, [Bontempi, 2006].

On this point, Ciampoli, 2005, says that:

> *"The complexity of a structure can be related to several aspects, which originate from the following observations:*
>
> - *when subjected to accidental action, like earthquakes and windstorms, building constructions may exhibit a strongly nonlinear dynamic behavior and a realistic evaluation of the structural response can be extremely cumbersome, as analytical models usually cannot be exploited;*
> - *while safety checks are carried out considering each structural element per se, structures are usually "systems" composed by strongly interacting components;*
> - *the structural response shall be evaluated taking into account the influence of the several sources of uncertainty that characterize both the actions and the structural properties, as well as the efficiency and consistency of the adopted structural model."*

Only if these aspects are properly considered, the structural response can be reliably evaluated, and the performance of the building/bridge construction ensured [Arangio et al., 2010].

3.3.1 STRUCTURAL PROBLEM BREAKDOWN

Generally speaking about the process of searching the solution of the structural problem, it is important to recognize that the way in which one describes the object of investigation influences how one organizes the knowledge and the decision about the object itself [Sinon, 1998]. As anticipated by the top-down approach shows how to deploy a system: one starts from the definition of the global structure and then, subsequently and orderly, develops further magnification of the description.

The differentiation of the modeling level is adopted to reduce the uncertainties. The level of a generic model of the structure is here identified by means of two parameters: the maximum degree of detail and the scale of the model; if the finite element method is adopted, at each model level it is possible to associate a certain typology of finite element which is mainly used to build the model. This global behavior is obtained by assembling different parts, each of them with a specific function itself. For this reason, among different graphical representations of the concept of system, a useful one is presented in Figure 3.3.

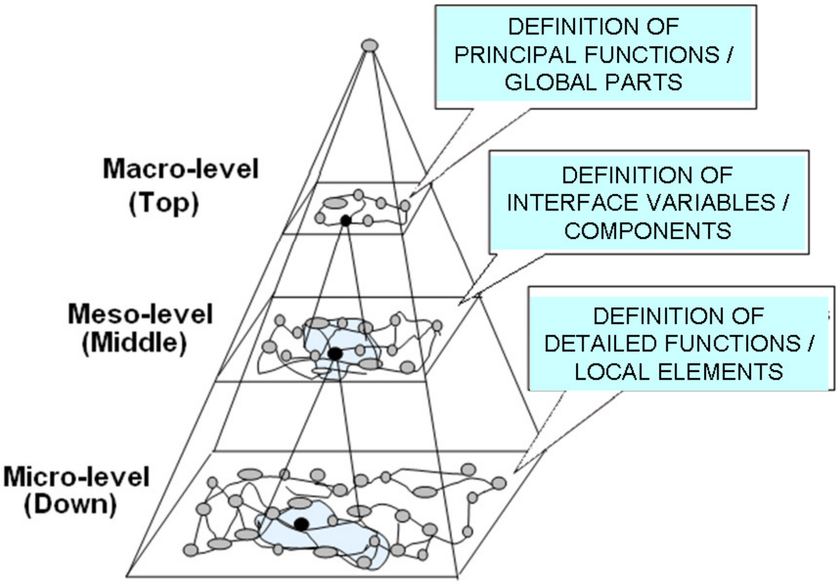
DEFINITION OF PRINCIPAL FUNCTIONS / GLOBAL PARTS
DEFINITION OF INTERFACE VARIABLES / COMPONENTS
DEFINITION OF DETAILED FUNCTIONS / LOCAL ELEMENTS
Macro-level (Top)
Meso-level (Middle)
Micro-level (Down)

Figure 3.3. Hierarchical breakdown of a system [Bontempi and Arangio, 2010].

Here one considers different hierarchical levels:

- Macro-level (Top), where are explicated the principal functions, related integral variables and global response;
- Meso-level (Middle), where interface functions are considered, connecting global and local variables and responses;

- Micro-level (Down), where detailed functions are considered relating local variables and responses.

This point of view is useful because it puts the light on the presence of the interface layer connected with the Meso-level, which connects global and local aspects. This layer can be eventually critical for reaching the expected performance.

In the case of the bridge that will be taken under study (I35-W Bridge) the hierarchical breakdown of the structural system can be summarized by Figure 3.4. Starting from the global model of the bridge (Macro-level), the aim of this sub-structuring system will be to extrapolate some of the main elements and joints going from the Meso-level, analyzing the main trusses and some detailed joints, to the Micro-level, focusing on part of the detailed joint model and in particular on the gusset plates composing it.

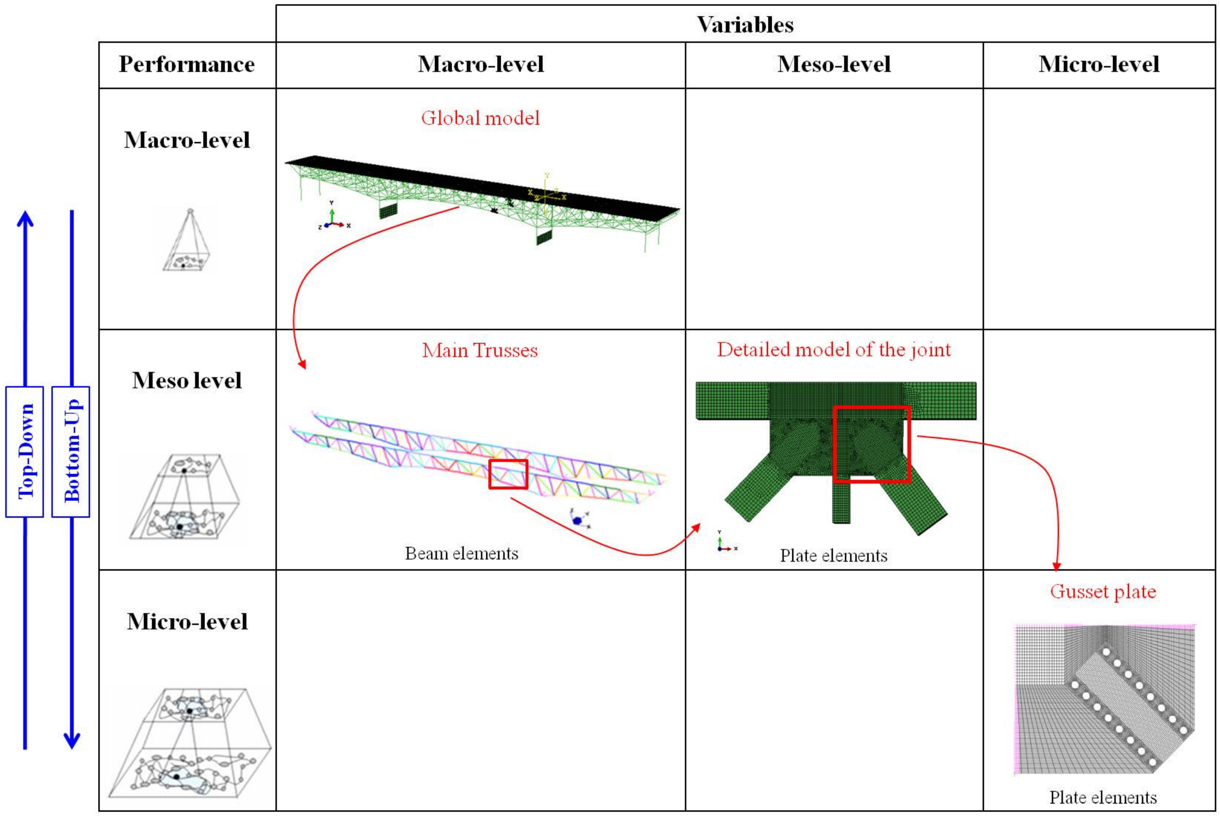
Variables
Performance
Macro-level
Meso-level
Micro-level
Macro-level
Global model
Meso level
Main Trusses
Beam elements
Detailed model of the joint
Plate elements
Micro-level
Gusset plate
Plate elements
Top-Down
Bottom-Up

Figure 3.4. Structural decomposition of the I-35W Bridge, [Bontempi, 2006].

4 STRUCTURAL STABILITY

4.1 INTRODUCTION

Absolute safety is not a goal that can be considered achievable, as it is well known to structural engineers. The tragedy of the World Trade Center collapse provides understanding of how a design may be safe under any expected circumstances, but may become unsafe under extreme and unforeseen circumstances.

Failure could be defined as the behavior of the structure when it crosses a limit state. There are many limit states that the structural design engineer has to consider, such as excessive deflection, large rotation at joints, cracking of metal or concrete, corrosion or excessive vibration under dynamic loads.

One of the limit states, which would be considered in this contest, is the limit state where the structure passes from a safe to an unsafe condition.

4.2 STRUCTURAL STABILITY

A stable elastic structure will have displacements that are proportional to the loads placed on it. A small increase in the load will result in a small increase of displacement. It is intuitive therefore that an instable structure is the one where a small increase in load corresponds a large change in the displacements. It is important to specify that in case of axially loaded members, the large displacement is not in the same direction as the load causing the instability [Galambos and Surovek, 2008].

Instability is a condition wherein a compression member looses the ability to resist increasing loads and exhibits instead a decrease in load-carrying capacity. Problems in instability of compression members can be subdivided in two categories: those associated with the bifurcation of equilibrium, and those in which instability occurs when the system reaches a maximum load without previous bifurcation.

In the first case a perfect member, when subjected to increasing load, initially deforms in one mode and then, once the load reaches the so called critical load, the deformation suddenly changes into a different pattern. This type of instability is typical of axially compressed columns, plates and cylindrical shells.

The members belonging to the latter category deform in a single mode from the beginning of loading until the maximum load is reached. Shallow arches and spherical caps subjected to uniform external pressure are examples of the second type of instability [Galambos, 1998].

4.3 STABILITY FOR STEEL STRUCTURAL ELEMENTS

In this chapter a quick review on the main aspects of structural stability for steel elements is done. Considering a compressed element loaded by a force N acting along its longitudinal axis, its behavior could be explained by the N-d curve, Figure 4.1, where N is the axial force and d the displacement.

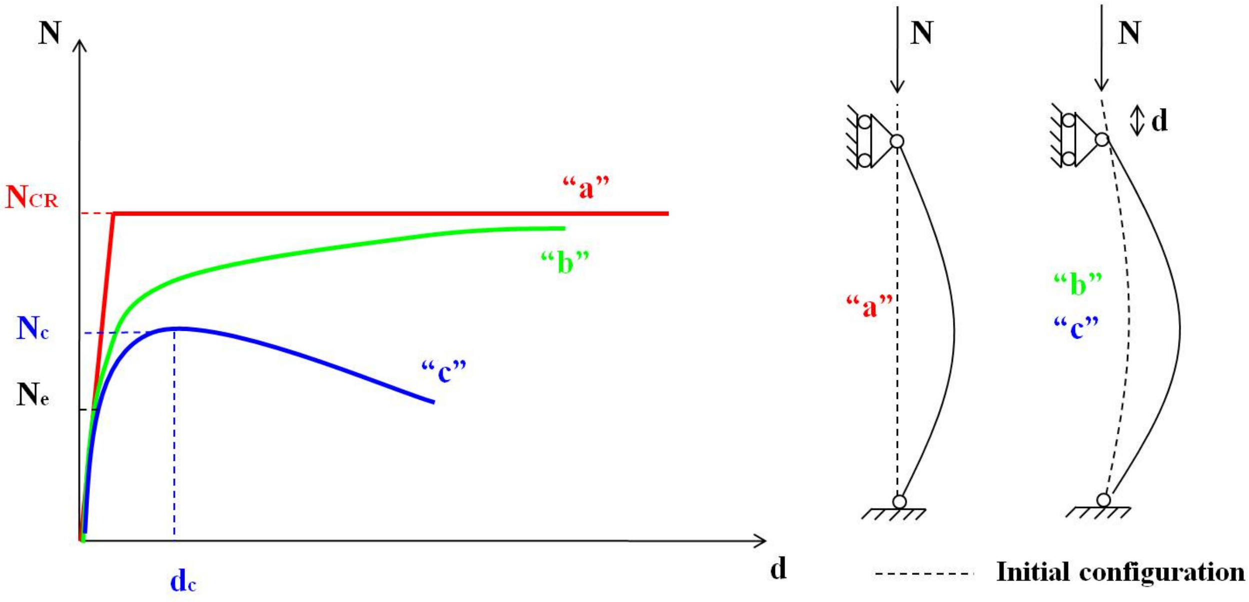

Figure 4.1. N-d curve for steel elements with and without imperfections.

If the member is in the elastic field, perfectly straight and compressed by a perfect centroidal load, its behavior is defined by the curve "a" in Figure 4.1. In case of small displacement theory, the element remains straight until the N load is lower than the N_{CR} of Euler:

$$N_{CR} = \frac{\pi^2 EA}{\lambda^2} \tag{1}$$

The N_{CR} is called in literature the critical load, the buckling load or the load at the bifurcation of the equilibrium.

In reality the steel elements have geometric imperfections that change the behavior of the element. These imperfections are practically unavoidable and represent acceptable construction tolerance which are, as a general rule, not visible to the naked eye, and cannot be quantified precisely beforehand, [Galambos, 1998]. In case of material still elastic the trend of F-d becomes the curve “b”, Figure 4.1. With the increasing of the load the displacements increase more than linearly and a bending effect is added to the axial one due to the gap of the beam from the longitudinal axis where the load is applied. The N_{cr} is still the asymptotic value that the beam can bear, as long as the material remains elastic. The reason for this dual representation, perfect and imperfect, is that for practical purposes some types of columns such as cold-formed steel and aluminum columns, can be idealized as perfect, while for other columns, for example hot-rolled or welded built-up structural steel columns. It is therefore necessary to consider the effects of the imperfections.

Nevertheless the element does not have a material indefinitely elastic, for a value of $N< N_{CR}$, many practical columns where in the section more loaded the elastic limit value of the material could be achieved. Essentially, the stiffness of the column /element is reduced by yielding. The degradation of the stiffness may be the result of a nonlinearity in the material itself or it may be due to partial yielding of the cross section at points of compressive residual stress, [Galambos, 1998]. For $N>N_e$ the element is in the elasto-plastic field and its displacements are bigger than the one evaluated in the hypothesis of elastic material. In fact, with the entrance in a plastic field, the Euler’s equation, used to determinate the critical buckling load in elastic field, can be still used on the condition that, the Young’s modulus, is replaced by the value of tangent modulus. This formula is called in literature as Shanley’s equation [Crosti and Bontempi, 2008]. The post buckling behavior is radically different from the elastic column, as bifurcation buckling occurs at the tangent-modulus load:

$$N_t = \frac{\pi^2 E_t I}{L^2} \tag{2}$$

Where E_t is the tangent modulus that is the slope of the stress-strain curve when the material is nonlinear. The F-d curve is therefore represented by the curve “c”.

Concluding, the element subjected to axial load has a non symmetric N-d curve. In tension the behavior could be rounded up to have an elasto-perfectly-plastic behavior and the maximum achievable limit is $N_{pl} = f_y A$, where A is the area of the section and f_y the yielding stress of the material. In compression the trend of the F-d is curved and its maximum limit depends also from the geometric and structural imperfection and from the slenderness λ of the element [Ballio and Mazzolani, 2005].

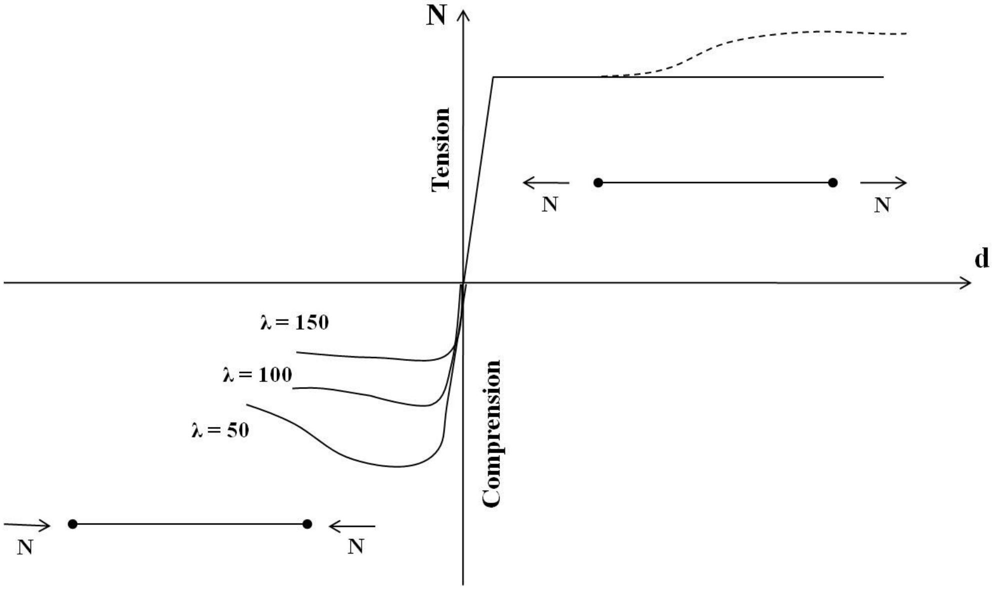

Figure 4.2. Non symmetric N-d curve for steel elements.

4.4 INSTABILITY COLLAPSES

Instability of structures, as already said, is characterized by small perturbations (imperfections, transverse loading) leading to large deformations or collapse. Structures are designed such that instability will not normally occur.

The failure of a bracing element due to some small triggering event, however, can make a system unstable and result in collapse. This could apply to truss or beam structures in which bracing elements are used to stabilize bars or cross-sectional elements in compression.

An instability-type collapse exhibits the following features:

- initial failure of the elements that brace or stiffen load-carrying elements in compression;
- instability of the elements in compression that have lost their bracing or stiffeners;
- sudden failure of these destabilized elements due to small perturbations;
- failure progression.

The progression of failure can vary. If the element firstly affected by destabilization is one of a few primary components, for example the leg of a truss tower, complete collapse can happen immediately without cascading failure of similar, consecutively affected elements. Although strong disproportion between cause and effect is apparent in such an event, it might be felt that this is not a progressive collapse. But then the definition of progressive collapse would have to be expanded by adding the feature of cascading failure of similar, consecutively affected elements [Starossek, 2007].

On the other hand, the element firstly affected by destabilization can also be a relatively small component, and failure can progress as a consecutively occurring stability failure of similar elements. This would be the case in a continuous girder where spans fail consecutively due to buckling of compression chords. In this example, however, the subsequently affected elements fail due to overloading resulting from redistribution of forces and not because of the failure of bracing or stiffeners [Starossek 2007].

Instability failures are often catastrophic and occur most often during erection. An example could be given by the collapse of the Yarra River Crossing in Melbourne, Australia. The Royal Commission attributed the failure of the bridge to two causes: the structural design and an unusual method of erection [Royal Commission, 1971].

4.5 STEEL TRUSS BRIDGES

A truss bridge is a structure composed of elements connected at joints, called nodes. Trusses, due to their triangular geometry, resist bending and shear primarily by axial strength and stiffness of their members. The behavior of a truss as a whole is determined by the behavior of the single members composing it, such as the members and the connections.

In a typical truss bridge few different elements can be pointed out, Figure 4.3:

- Upper chord;
- Lower chord;
- Web diagonals;
- Web verticals;
- Connections.

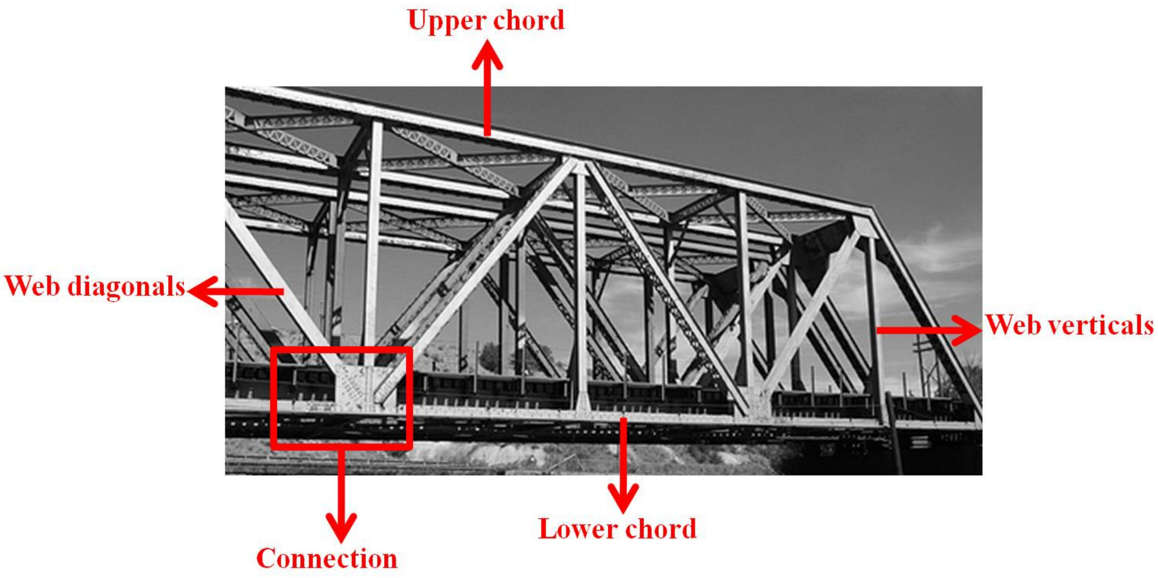

Figure 4.3. Different members in a typical steel truss bridge.

In a classical pin-jointed truss, the ends of the members are connected by pins that allow free rotation so the members only carry direct tension or compression with no bending. In large structures, pin joints are impractical and members are joined with gusset plates. Geometry ensures that the members are still primarily loaded in direct tension or compression, but the gusset plate joints allow the transfer of some secondary bending stress.

In Figure 4.4 the most common types of steel bridge trusses are reported. The trusses can be classified in trough-deck trusses, in case the deck of the bridge is supported at the level of the bottom chord, or deck trusses, where the deck is supported on the upper chord level. To connect each members of the truss gusset plates are used in both cases.

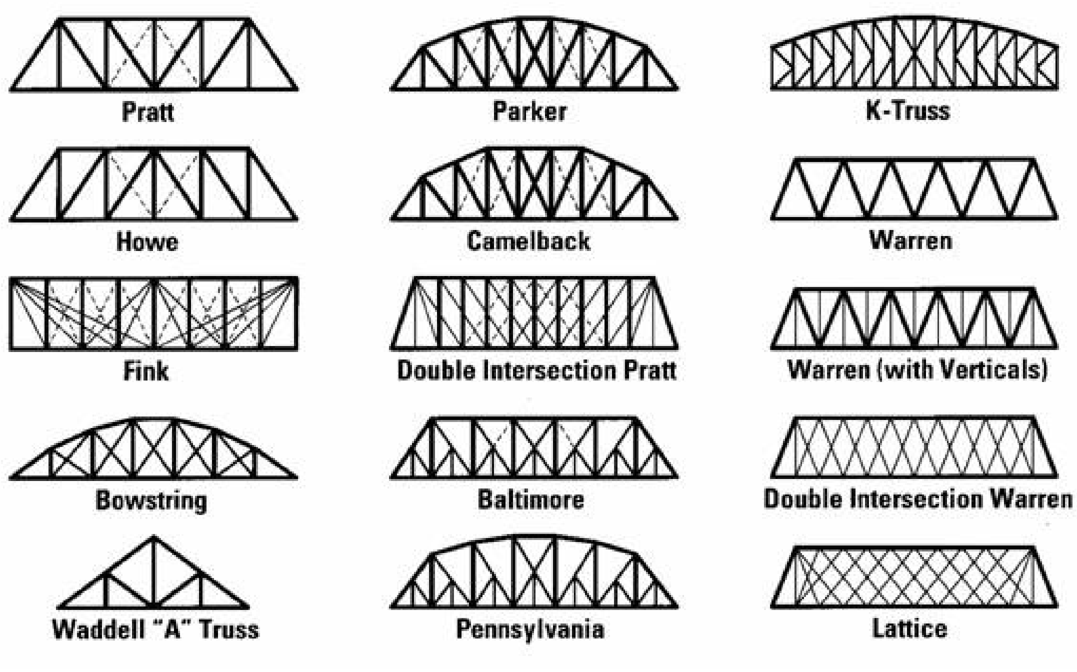
Pratt
Parker
K-Truss
Howe
Camelback
Warren
Fink
Double Intersection Pratt
Warren (with Verticals)
Bowstring
Baltimore
Double Intersection Warren
Waddell "A" Truss
Pennsylvania
Lattice

Figure 4.4. Different types of truss bridges (http://www.prhs.k12.ny.us/fac/HerskowitzM/bridges.htm)

Failure modes of the substructures, as for instance a connection, can therefore lead at the collapse of the whole structure. The main failure modes for a steel truss are:

- Global instability failure of the truss: the compression chord can buckle and even the tension chord can move out of plane when the lateral braces are not stiff enough to provide the instability of the nodes;
- Failure of the truss members: compression members of a truss bridge can fail in overall buckling or in local buckling modes and members in tension can fail in yielding of the gross area or fracture of the net area;
- Failure of truss connections such as the gusset plates and splices and supports.

4.6 FRACTURE CRITICAL BRIDGES

After the disaster of I35-W Bridge, the FHWA focused its attention on all the 465 steel deck truss bridges present in the National Bridge Inventory [NTSB, 2008]. These bridges, shown in Figure 4.5, provide a "snapshot" of highway truss bridges that were designed in the period from 1929 to 1990 in the US.

The load paths in many of these bridges are non-redundant and thus failure of a major truss member or connection may cause collapse of the structure. As a result, these structures are classified as Fracture Critical and are required by law to have hands-on inspections at intervals not to exceed 24 months (so do all other bridges). In addition to these periodic inspections, structural evaluations are crucial for these types of bridges.

In fracture critical bridges, it is not necessary to have fracture of a tension member or a connection to initiate total collapse. Buckling failure of a single compression member or compression areas of a critical connection, such as a gusset plate of a main truss, can also cause total or partial collapse of a steel truss span.

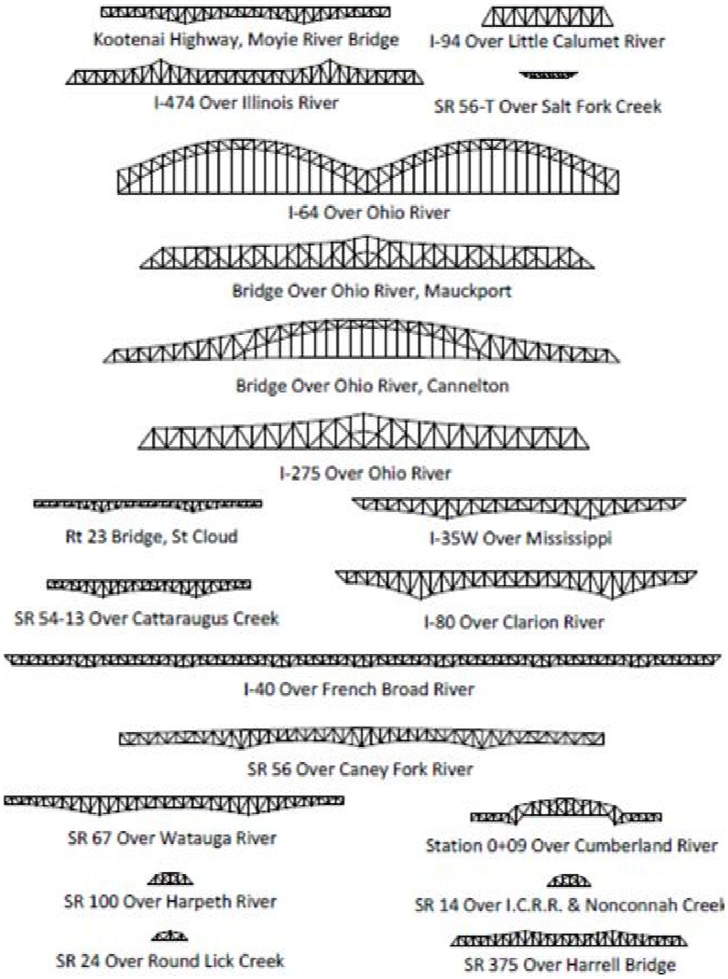
Kootenai Highway, Moyie River Bridge
I-94 Over Little Calumet River
I-474 Over Illinois River
SR 56-T Over Salt Fork Creek
I-64 Over Ohio River
Bridge Over Ohio River, Mauckport
Bridge Over Ohio River, Cannelton
I-275 Over Ohio River
Rt 23 Bridge, St Cloud
I-35W Over Mississippi
SR 54-13 Over Cattaraugus Creek
I-80 Over Clarion River
I-40 Over French Broad River
SR 56 Over Caney Fork River
SR 67 Over Watauga River
Station 0+09 Over Cumberland River
SR 100 Over Harpeth River
SR 14 Over I.C.R.R. & Nonconnah Cree
SR 24 Over Round Lick Creek
SR 375 Over Harrell Bridge

Figure 4.5. Configuration of the 20 bridges from plans submitted by various states. The bridges are drawn to the same scale to illustrate the relative size. [FHWA,2009].

4.7 REDUNDANCY IN TRUSS BRIDGES

As said before for fracture critical bridges, being determinate systems, the fracture of a single major member or connection could cause the collapse of the whole structure. It is therefore important to recognize a non-redundant bridge. There are three types of redundancy in bridge structures [NCHRP, 2005]:

- Internal redundancy of bridge trusses;
- Structural redundancy;
- Load path redundancy.

4.7.1 INTERNAL REDUNDANCY OF BRIDGE TRUSSES

The NCHRP (2005) defines the internal redundancy in this way:

> *“Internal redundancy, also called member redundancy, exists when a member is comprised of multiple elements and a fracture that formed in one element cannot propagate directly into adjacent elements”.*

An example on internal redundancy in a truss bridge is a riveted built up truss members made of multiple angles and plates. An example of non multiple load path is instead a single rolled wide flange shape, where if a fatigue cracks happens it will propagate in the cross section causing the fracture of the whole member. Most of the bridge in the US have pinned or riveted/bolted connections. The pinned ones do not have internal redundancy because the failure of one pin will precipitate the progressive collapse of the structure. Bridges with riveted/bolted connections, however, have multiple lines of rivets or bolts and a high degree of redundancy even though the failure of one rivet would overload the next one and so on.

Gusset plates connections in truss bridges have always double plates; these types of connections have at least two separated load path, in a way that when one of them fails, its load can be carried by the other one.

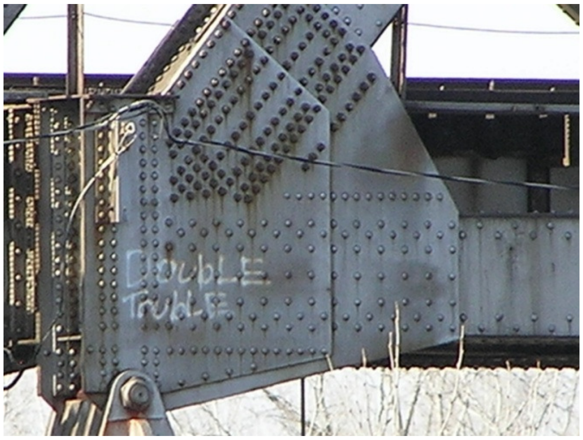

Figure 4.6. "Multi-element" riveted members, example of internal redundancy. Photo by http://okbridges.wkinsler.com/verdigrisbridge4.html

4.7.2 STRUCTURAL REDUNDANCY

According to the NCHRP (2005):

> *"Structural redundancy is external static indeterminacy and can occur in a two or more span continuous girder or truss"*

If a plane truss has more external supports than are necessary to ensure a stable equilibrium configuration, the truss as a whole is statically indeterminate, and the extra supports constitute external redundancy.

A typical example of external redundancy can be provided by multiple trusses or girders, see for example the case of the Newport Southbank Bridge in Ohio, which thanks to the four main trusses has a high level of redundancy, Figure 4.7. This is not typical for steel truss bridges, which are built usually with just two main trusses.

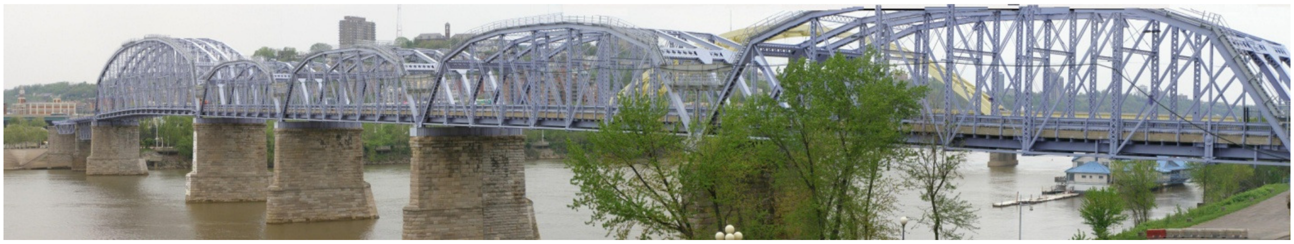

Figure 4.7. Newport Southbank Bridge in Ohio. (Wikipedia)

When a fracture happens in a cross section of the middle span the cantilevered segments of the fractured girder will be able to carry some of its load and shed to rest to the adjacent girders through internal redundancy of the deck or the cross bracings [Astaneh A., 2010].

Structural redundancy can be defined therefore as the ability of a system to redistribute among its members the load which can no longer be sustained by some other members due to their damage [Biondini et al, 2008].

4.7.3 LOAD PATH REDUNDANCY

According to the NCHRP (2005):

> *"Load-path redundancy is internal static indeterminacy arising from having three or more girders or redundant truss members"*

In case of trusses the load path redundancy can be expressed in terms of number of main trusses in the bridge and number of redundant members in each truss.

Usually truss bridges have only two main trusses. It is therefore desirable that primary members be redundant.

A good example of a bridge with this type of redundancy is the one with trusses with "X" web diagonals instead of "/" diagonals, see Figure 4.8.

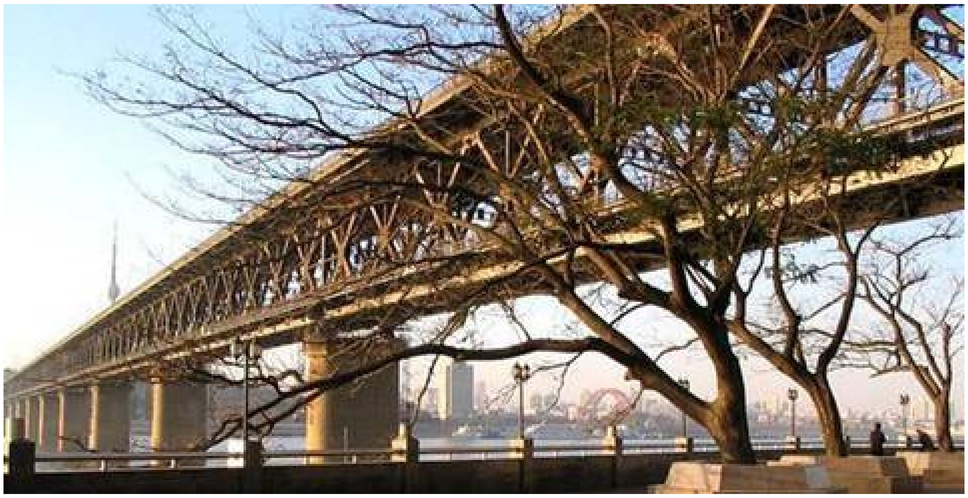

Figure 4.8. Bridge with X diagonal, First Whhan Bridge in China. (Wikipedia)

PART II:

STEEL CONNECTIONS

5. STEEL GUSSET PLATE CONNECTIONS
6. CRITICAL REVIEW OF FHWA GUDELINES ON GUSSET PLATES

5 STEEL GUSSET PLATE CONNECTIONS

5.1 INTRODUCTION

The 2007 catastrophic collapse of the I-35 W Bridge in Minnesota, United States, under ordinary traffic and construction loads, was triggered by the buckling of an undersized gusset plate [NTSB, 2008].

Four lanes (out of eight) of the bridge had been closed to traffic due to a repaving operation that also caused construction material and equipment to be on the bridge at that time. The National Transportation Safety Board investigation determined that several gusset plates had been under-designed from the beginning and that construction material piled near gusset plate U10 contributed to the failure [NTSB, 2008]. Inspection photographs also showed significant out-of-plane bowing of this particular plate, about 13 mm or one plate thickness, but this had not caused any alarm. The day after the tragic event in Minneapolis, the FHWA issued the first of its advisories regarding steel truss bridges and called for the state departments of transportation to immediately inspect all non load path-redundant steel truss bridges to verify the stress level in all the members including gusset plates.

5.2 STEEL GUSSET PLATE CONNECTIONS

In civil engineering, gusset plates are frequently used to connect beams columns, braces or truss members to load-bearing columns. They are used in steel bridge trusses and braced steel towers to connect the steel members to each other. The members can be bolted, riveted or welded to the gusset plates, whose function in fundamental for the integrity of the structure.

In the United States, welded gusset plates are used occasionally in building connections involving lateral braces and they are often found singly in buildings and in pairs in bridges, see Figure 5.1.

Their use in buildings and bridges go back many decades, if not centuries, and certainly predate the use of computers in structural analysis and design.

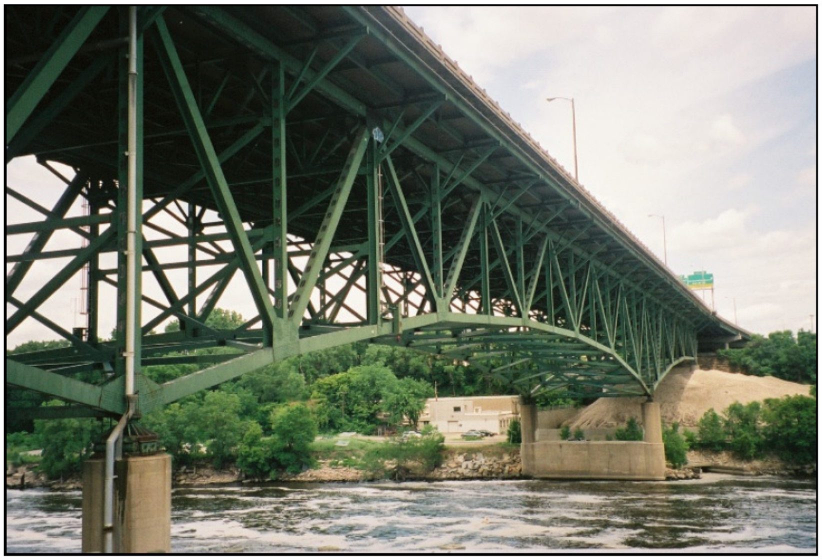

Figure 5.1. Example of truss bridge with gusset plates. (Photo by NTSB Report).

5.3 REGULATIONS AND CODES ABOUT STEEL CONNECTIONS

5.3.1 EUROPEAN CODES

Traditional design methods for connections are based on a series of capacity checks and do not include methods for calculating the connection stiffness and rotational capacity. Over the last ten years the understanding of connection behavior has improved and methods are now available for calculating the stiffness and the rotational capacity of bolted and welded connections.

EN1993-1-8, 2005, takes advantage of these developments and includes a consistent approach for calculating the stiffness, strength and rotational capacity of a limited range of bolted and welded connections. The method proposed in EN1993-1-8 is called the component approach and uses the behavior of the individual components within a connection (bolts, welds, end-plate, column flange, etc) to build a realistic picture of a connection load-deformation characteristic.

The component approach is based on Zoetemijer's work [Zoetemijer, 1983]. Later, other researchers worked on this method to determine the mechanical properties of more components and to refine the calculation methods, in order to obtain more accuracy in the description of the mechanical behavior.

Well explained in the EN1993 is the case of beam-column connections, for which is possible to assess the resistance, the stiffness and the rotational capacity by just evaluating the single components in the joint, but nothing is specified regarding the modeling of these connections.

European standard, precisely in chapter 7, gives detailed application rules to determine the static resistances of uni-planar and multi-planar joints in lattice structures composed of circular, square or rectangular hollow sections, and of uni-planar joints in lattice structures composed of combinations of hollow sections with open section. The static resistances of the joints are expressed in terms of maximum design axial and/or moment resistances for the brace members.

In Figure 5.2 all the types of joints in hollow section lattice girders considered in EN1993-1-8 which have similar geometry of the ones in the bridges are shown.

From EN1993-1-8:

> *"The design joint resistances of connections between hollow sections and of connections of hollow sections to open sections, should be based on the following failure modes as applicable:*
>
> *a) Chord face failure (plastic failure of the chord face) or chord plastification (plastic failure of the chord cross-section);*
>
> *b) Chord side wall failure (or chord web failure) by yielding, crushing or instability (crippling or buckling of the chord side wall or chord web) under the compression brace member;*
>
> *c) Chord shear failure;*
>
> *d) Punching shear failure of a hollow section chord wall (crack initiation leading to rupture of the brace members from the chord member);*
>
> *e)Brace failure with reduced effective width (cracking in the welds or in the brace members);*
>
> *f) Local buckling failure of a brace member or of a hollow section chord member at the joint location."*

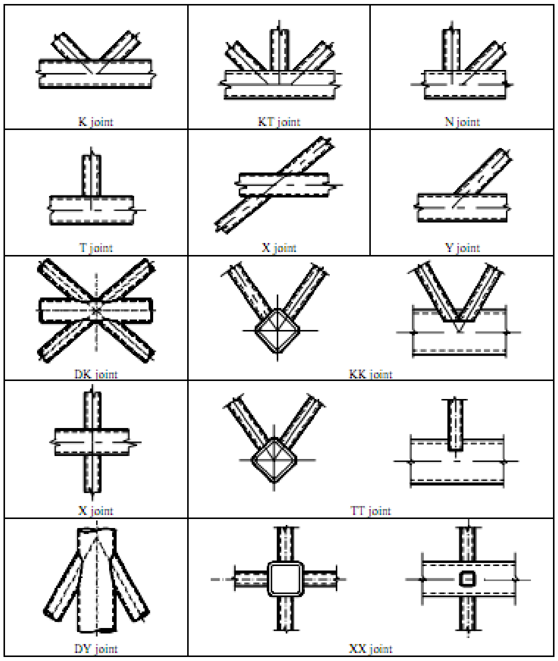
K joint
KT joint
N joint
T joint
X joint
Y joint
DK joint
KK joint
X joint
TT joint
DY joint
XX joint

Figure 5.2. Classification of hollow section connections (EN1993 Part 1.8).

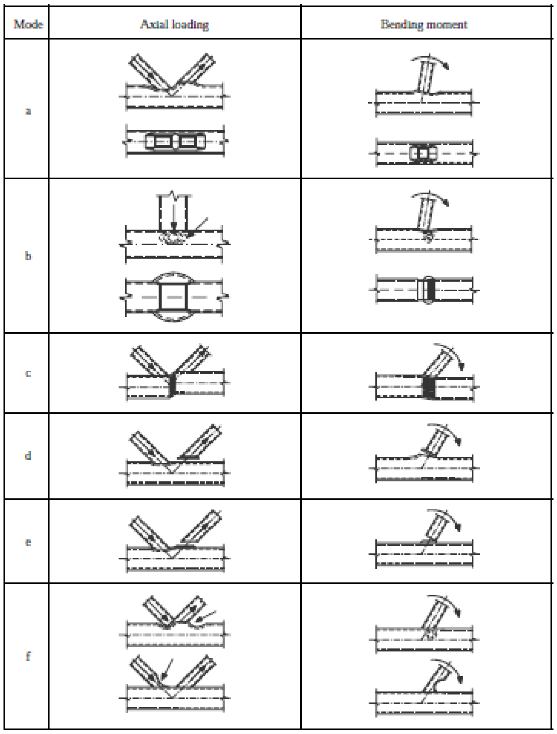
Mode
Axial loading
Bending moment
a
b
c
d
e
f

Figure 5.3. Failure modes for joints between RHS brace members and RHS chord members, (EN1993 Part 1.8)

No advices are given by the European code about the gusset plates and the eventual possibility to assess stiffness, resistance and rotation capacity of a joint composed by different shape of sections, as well as hollow and I section, all linked together by gusset plates.

5.3.2 AMERICAN CODES

5.3.2.1 ASSHTO

(AASHTO-LRFD) Specifications (2004) in section 6.14.2.8 prescribes design of gusset plates. Section 6.14.2.8 recommends the gusset plates to be symmetrical with the axis of the member (concentric loading), as far as practicable, and to allow the full development of the members (connection designed to be stronger than members). The maximum stress form combined factored flexural and axial loads should not exceed $\varphi_f F_y$ based on the gross area. Shear stress on a section due to the factored loads should be less than $\varphi_v F_u/\sqrt{3}$ for uniform shear and less than $\varphi_v 0.74\ F_u/\sqrt{3}$ for flexural shear. Unsupported edges should be stiffened if their length exceeds $2.06\sqrt{E/F_y}$.

If gusset plates in compression are designed as equivalent columns, their nominal compressive resistance P_n should be taken as (Section 6.9.4.1).

If $\lambda \leq 2.25$, $P_n = 0.66^{\lambda} F_y A_s$

If $\lambda > 2.25$, $P_n = \frac{0.88 F_y A_s}{\lambda}$

where $\lambda = \left(\frac{Kl}{r_s \pi}\right)^2 \frac{F_y}{E}$

Notation:

φ_f = 1.00 = resistance factor for flexure

φ_v= 1.00 = resistance factor for shear

F_y= specified minimum yield strength

F_u= specified minimum tensile strength

E = Young’s modulus

K = effective length factor

l = unbraced length

r_s = radius of gyration about plane of buckling

A_s = grossl area of the cross section

These provisions are also listed in the FHWA *Guidance*.

5.3.2.2 FHWA

As a result of the structural failure of the I35-W, the FHWA issued guidelines for the load rating of gusset plates [FHWA, 2009] and recommended to verify the capacity of the plates in non-load-path-redundant steel truss bridges. The guidelines provide the state departments of transportation with simple hand formulas based on laboratory tests, but the absence of a commentary makes it difficult to assess the level of safety of the formulas. In the guidelines the resistance of a gusset plate is determined as the least between the resistances of the plates in compression, shear, and tension including block shear.

More details on these guidelines are given in the next chapter.

5.4 REVIEW OF THE LITERATURE ON APPROXIMATE METHODS FOR GUSSET PLATES

Practical design methods ensure safety by providing a load path that satisfies equilibrium and boundary conditions and does not exceed material yield limits. The resulting stress field is by definition a statically possible yield state of stress. Safety against plastic failure is assured because, according to the Lower Bound Theorem of the Limiting Load [Kachanov, L.M., 1974] a statically possible yield state of stress is due to the load that is less than or equal to the limiting load, which is characterized by unrestricted plastic flow. However, there is no guarantee that the design load path is the actual one, and thus the design methods provide no information on the load-displacement behavior or stiffness in the elastic range. Current procedures [FHWA, 2009] for the design and load rating of multi-member gusset plates consist in checking axial, bending and shear stresses along various sections deemed critical, using elastic beam theory. These procedures are intended to ensure a safe and conservative design, but produce results that can be quite different from more realistic finite-element (FE) results, and cannot predict stiffness nor actual behavior. To do so would require highly sophisticated and detailed FE models, such as the ones used in the investigation of the I-35 W collapse [NTSB, 2008].

Extensive reviews of the literature were performed by Chambers and Ernst, 2005 and Astaneh-Asl, 2010. Here the attention is focused on approximate methods of analysis and design, with the hope of finding formulas for the stiffness of springs equivalent to a gusset plate.

Whitmore, 1952, tested 1:4 scale specimens of gusset plates for Warren trusses made of aluminum, masonite and bakelite using wire-bonded strain gages (a novelty at the time). Based on these experiments (Figures 5.4 and 5.5), he devised the effective width which now bears his name, “by constructing lines making 30 degrees with the axis of the member which originate at the outside rivets in the first row and continue until they intersect a line perpendicular to the member through the bottom row of rivets.” The maximum tensile and compressive stresses may be approximated by assuming the force in each diagonal to be uniformly distributed over this width.

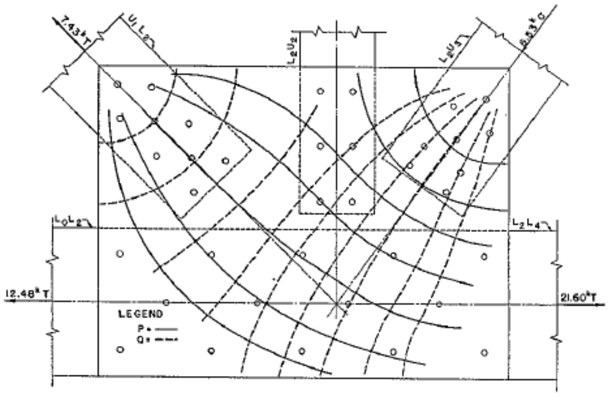

Figure 5.4: Stress trajectories [Whitmore, 1952].

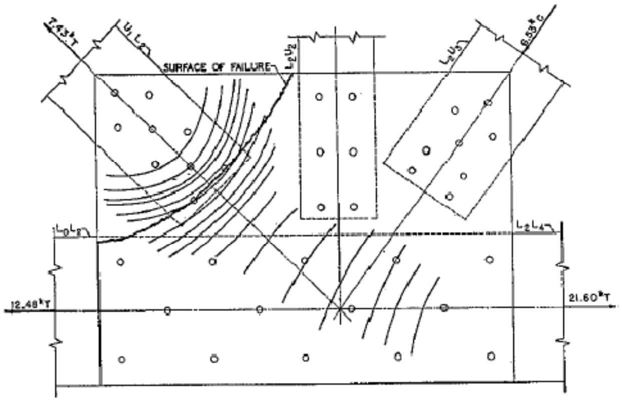

Figure 5.5: Tension cracks in the Stresscoat [Whitmore, 1952].

Astaneh, 1989, proposed modeling gusset plates as wedges under a point load (Figure 5.6). In the elastic range, closed-form solutions exist for infinite wedges, but cannot account for the actual boundary conditions. Furthermore, actual loads are transferred to gusset plates by rows of rivets or bolts, rather than at a single point. The author also indicates that wedge models cannot predict buckling, for which he proposes a fin truss model (Figure 5.7), where the cross section of each bar is the average of the cross section of the triangle it bisects. The author suggests an effective length factor of 0.7 for the struts to account for the restraint provided by the transverse direction to account for two-dimensional plate buckling, as opposed to one-dimensional column buckling. The use of multiple fin trusses to model gusset plates that connect multiple members rapidly becomes cumbersome, and makes the finite-element method very attractive in comparison for its accuracy and automation.

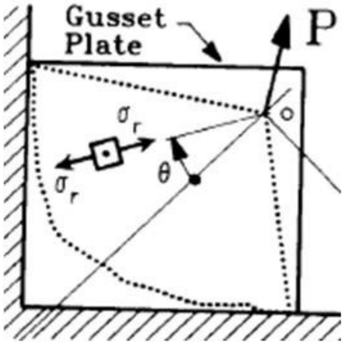

Figure 5.6: Wedge model, [Astaneh, 1989].

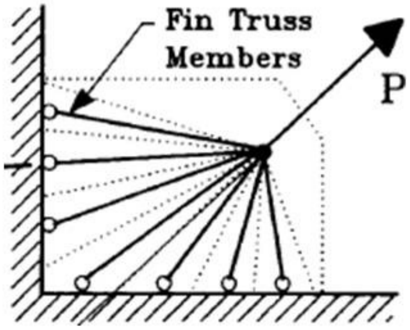

Figure 5.7: Fin truss model, [Astaneh, 1989].

An elegant, statically possible load path with no moment in the gusset-to-beam and gusset-to-column connections was developed and called the Uniform Force Method by Thornton, 1991. Because it achieved a certain importance in practice, and the original paper is rather cryptic, it is explained in some detail here. The problem can be stated as follows: given a (diagonal) bracing force P at angle θ to the vertical, design a gusset plate of height 2β and width 2α such that force P is transferred to the column face, beam face and beam-column intersection with zero moment. Thornton's solution is to dimension the gusset plate so that the bracing force P passes through the intersection of the centerlines of the beam and column, the so-called working point A in Figure 5.8. The connection is therefore concentric. Furthermore, the gusset plate, the weld between it and the top of the beam, and the rows of bolts between it and the column flange are dimensioned so that lines CD and BF meet the line of force P at the same point I. B, C and F are the middle of the joints between gusset and beam, gusset and column, and beam and column respectively, whereas D is the intersection of the top of the beam with the centerline of the column. Note that in Figure

5 there is no moment at B and C. In order to calculate the connection forces at B and C, we first need to derive a geometrical relationship. Consider the lines that intersect at point I (Figure 6.8):

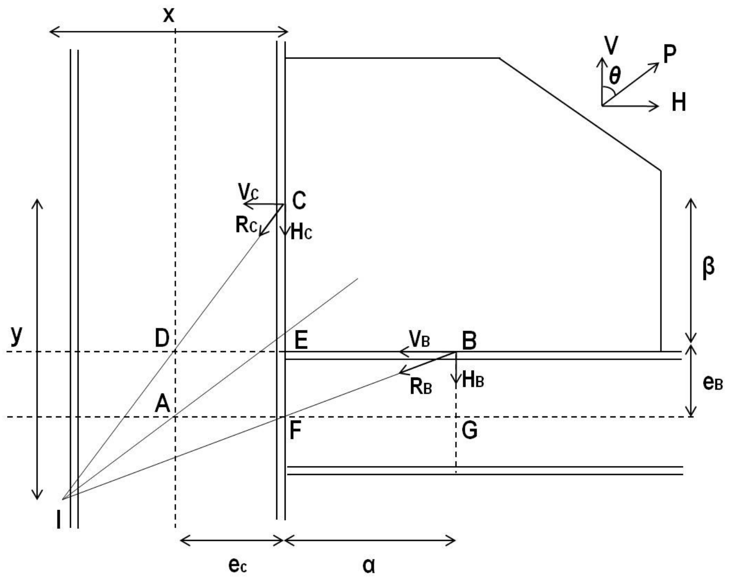

Figure 5.8: Thornton's Uniform Force Method [Thornton, 1991].

$$\frac{x}{y} = \frac{e_C}{\beta} \;\Rightarrow\; y = x\frac{\beta}{e_C} \tag{1}$$

$$\frac{H}{V} = \frac{x-e_C}{y-\beta-e_B} = \tan\theta \;\Rightarrow\; y-\beta-e_B = \frac{x-e_C}{\tan\theta} \tag{2}$$

$$\frac{\alpha}{e_B} = \frac{x}{y-\beta-e_B} \;\Rightarrow\; y-\beta-e_B = \frac{xe_B}{\alpha} \tag{3}$$

Equating (2) and (3):

$$\frac{x-e_C}{\tan\theta} = \frac{xe_B}{\alpha} \;\Rightarrow\; x = \frac{e_C}{1-\frac{e_B}{\alpha}\tan\theta} \tag{4}$$

From (1) and (4):

$$y = \frac{\beta}{1-\frac{e_B}{\alpha}\tan\theta} \tag{5}$$

Substituting (4) and (5) into (3):

$$\alpha = \frac{e_C\, e_B}{\beta-(\beta+e_B)\left(1-\frac{e_B}{\alpha}\tan\theta\right)} = \frac{e_C\,\alpha}{\tan\theta\,(\beta+e_B)-\alpha} \tag{6}$$

which simplifies to:

$$\alpha - e_B \tan\theta = \beta \tan\theta - e_C \tag{7}$$

Eq. (6) was presented by Thornton (1991), but the above derivation is from Chambers and Ernst, 2005.

We can now calculate the forces at B and C. Equilibrium requires:

$$V \tan\theta = H \;\Rightarrow\; (V_B + V_C)\tan\theta = H_B + H_C \;\Rightarrow\; V_C \tan\theta - H_C = H_B - V_B \tan\theta \tag{8}$$

Consider triangle CDE and the forces at C

$$\frac{V_C}{\beta} = \frac{H_C}{e_C} = \frac{V_C \tan\theta - H_C}{\beta \tan\theta - e_C} \tag{9}$$

triangle BFG and the forces at B:

$$\frac{V_B}{e_B} = \frac{H_B}{\alpha} = \frac{H_B - V_B \tan\theta}{\alpha - e_B \tan\theta} \tag{10}$$

triangle JAG and force P:

$$\frac{V}{\beta + e_B} = \frac{H}{\alpha + e_C} = \frac{P}{r} \tag{11}$$

$$r = \sqrt{(\alpha + e_C)^2 + (\beta + e_B)^2} \tag{12}$$

From (6) to (10):

$$\frac{V_C}{\beta} = \frac{H_C}{e_C} = \frac{V_B}{e_B} = \frac{H_B}{\alpha} = \frac{V_C + V_B}{\beta + e_B} = \frac{H_B + H_C}{\alpha + e_C} = \frac{P}{r} \tag{13}$$

The connection forces are given by:

$$H_B = \frac{\alpha}{r}P \qquad V_B = \frac{e_B}{r}P \qquad V_C = \frac{\beta}{r}P \qquad H_C = \frac{e_C}{r}P \tag{14}$$

The equations of equilibrium (6), (11) and (12) are in Thornton's 1989 paper, with no derivation, even though they are not obvious. Thornton neither offered any guidance on the thickness of the gusset plate, nor showed that stresses were below yield in his solution, as a complete application of the Lower Bound Theorem of the Limiting Load would require. He did, however, a comparison between the predictions of the Uniform Force Method and a number of experimental results and confirmed the accuracy on the method. Variations of concentric design, where the bracing force P goes through the working point A, include [Thornton, 1991]:

- Ricker's model where the resultants of the connection forces at B and C are parallel to the bracing force P. Moments must be present at B and C to satisfy equilibrium.
- Modified Richard's model, where the resultants of the connection forces at B and C are not parallel and do not intersect the line of the bracing force P at the same point. Moments must be present at B and C to satisfy equilibrium. The model includes empirical factors from Richard's experiments.
- The AISC method (American Institute of Steel Construction), where the gusset-beam connection at B has a moment and a horizontal but no vertical force component, and the gusset-column connection at C has both vertical and horizontal components but no moment.
- The KISS model (Keep It Simple, Stupid), where the gusset-beam connection at B has a moment and a horizontal but no vertical force component, and the gusset-column connection at C has a moment and a vertical, but no horizontal force component. This method satisfies equilibrium and the design and analysis assumptions and it is applicable to all the geometries and boundary condition. However the presence of the large moments at the connection interfaces makes it an uneconomical choice in practice.

Table 5.1: Concentric gusset plate design models. H = horizontal force, V = vertical force, R = resultant force, M =moment Subscript B for beam, C for column.

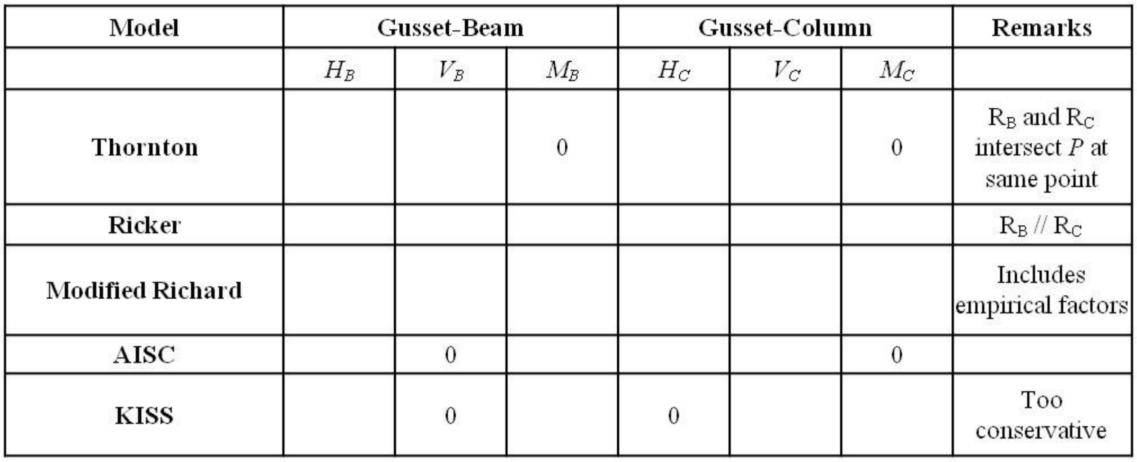

Model	Gusset-Beam			Gusset-Column			Remarks
	H_B	V_B	M_B	H_C	V_C	M_C	
Thornton			0			0	R_B and R_C intersect P at same point
Ricker							R_B // R_C
Modified Richard							Includes empirical factors
AISC		0				0	
KISS		0		0			Too conservative

Dowswell and Barber (2004) provided guidance on the required thickness to prevent buckling of gusset plates and a quantitative definition of compact gussets. They started out with the minimum stiffness β_{br} required by AISC (LRFD Manual of Steel Construction, 3rd Edition, American Institute of Steel Construction, 2001) to control the relative movement of two adjacent brace points separated by a distance L_b in a column subjected to a compressive load P_u:

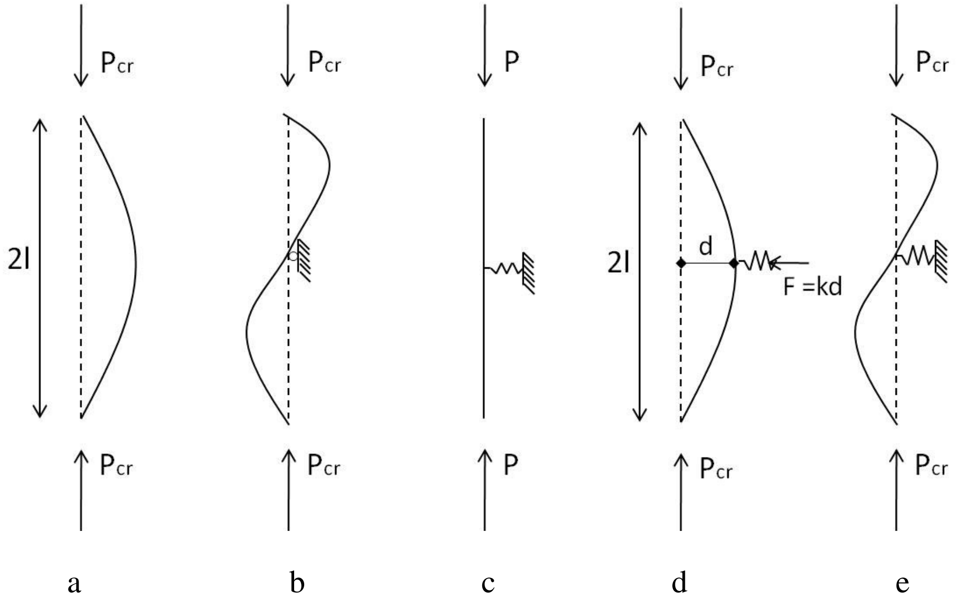

Figure 5.9. [McGuire, 1968].

$$\beta_{br} = \frac{2P_u}{\varphi L_b} = \frac{2P_u}{0.75L_b} \qquad (15)$$

This equation expresses the stiffness needed for a mid-span brace to force two half-waves in the column of length $2l$ shown in Figure 5.9d. For an infinitesimal displacement d at mid-span, equilibrium of moments requires:

$$Fl/2 = P_{cr}d \qquad (15)$$

The spring constant necessary for full bracing of a straight, axially loaded column is:

$$k = F/d = 2P_{cr}/l \qquad (16)$$

For a gusset plate, the equivalent column of unit width has thickness t and length l_1 (the equivalent column length from the middle of the Whitmore width) and the compressive stress is limited to 0.85 F_y, where F_y is the yield stress.

Thus,

$$\beta_{br} = \frac{2 \times 0.85 F_y t}{0.75 l_1} = \frac{2.27 F_y t}{l_1} \tag{17}$$

The gusset plate is considered as an equivalent column with a pseudo brace of unit width, thickness t and length c equal to the shorter of the distances from the corner bolt or rivet to the adjacent beam or column (see Figure 5.10). As a guided cantilever, the pseudo brace stiffness is:

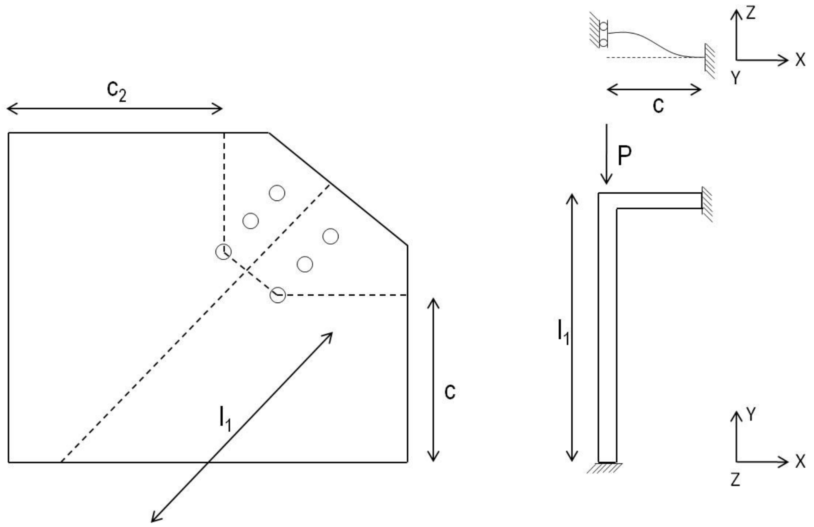

Figure 5.10: Pseudo gusset plate frame, from Dowswell and Barber (2004).

$$\frac{P_u}{\delta} = \frac{12EI}{c^3} = \frac{Et^3}{c^3} \tag{18}$$

Setting Eq. (13) = Eq. (14) gives the required plate thickness:

$$t_\beta = 1.5\sqrt{\frac{F_y c^3}{E l_1}} \tag{19}$$

The gusset plate is compact if $t \geq t_\beta$ and no-compact if $t < t_\beta$. Dowswell and Barber (2004) compared their theoretical buckling capacities, P_{th}, with experimental or finite-element calculations available in the literature P_{lit}. They used the average of the lengths from the middle and the ends of the Whitmore width for the equivalent column length. For compact gusset plates, using an effective length factor of 0.5, they found the ratio P_{lit} /P_{th} = 1.47 and for no-compact gusset plates, using an effective length factor of 1.0, P_{lit} / P_{th} = 3.08. Thus, the separation of compact from non compact gusset plates and the subsequent different effective length factors result in inconsistent and problematic factors of safety for design against buckling.

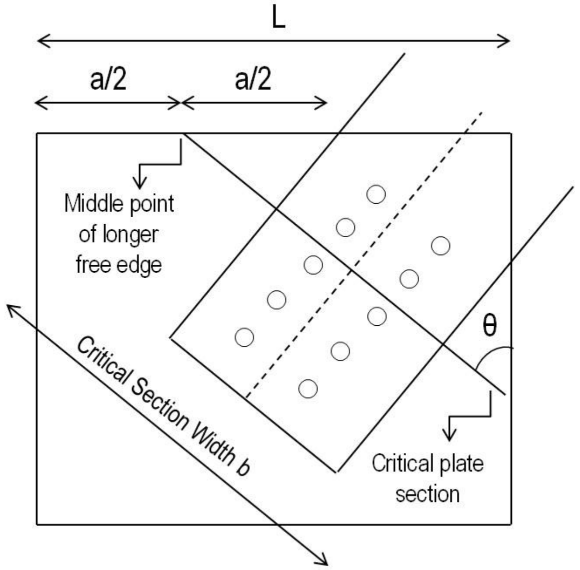

Figure 5.11: Critical section for edge buckling of gusset plate, from Brown (1988).

Brown (1988, 1990) developed analytical expressions for the edge buckling of gusset plates, based on the elastic buckling stress σ_{CR} of a plate of thickness *t*, modulus of elasticity *E* and Poisson ratio υ supported on its loaded edges, but otherwise unrestrained:

$$\sigma_{cr} = \frac{\pi^2 E}{12(1-\nu^2)(Ka/t)^2} \tag{20}$$

where K = 1.2 reflects the end conditions of the strip along edge *a* (one end fixed, the other end restrained against rotation but free to translate at the brace). This stress can also be expressed in terms of the elastic column buckling:

$$\sigma_{cr} = \frac{\pi^2 E}{\left(\frac{Kl}{r}\right)^2} \tag{21}$$

Setting Eq. (15) = Eq. (16) with $\nu = 0.3$ produces

$$\frac{Kl}{r} = \frac{\sqrt{12(1-\nu^2)}Ka}{t} = \frac{4a}{t} \tag{22}$$

For edge buckling, the critical section bisects the long free edge and is perpendicular to the brace. Its width is different from the Whitmore width (Figure 5.11):

$$b = \frac{L-a/2}{\sin\theta} \tag{23}$$

Only a fraction f of the total brace load contributes to edge buckling of the gusset, the rest being transferred directly to the steel frame. Assuming the bolts or rivets carry uniform loads (Figure 5.11):

$$f = \frac{(a/2)\cos\theta + p - e}{np} \tag{24}$$

where n = number of bolt rows in load direction; p = bolt pitch, and e = edge distance.

From Eqs. (16) to (19), the edge buckling load is therefore:

$$P_b = \frac{\sigma_{cr} bt}{f} = \left(\frac{\pi t}{4a}\right)^2 \frac{Etnp(2L-a)}{\sin\theta(a\cos\theta + 2p - 2e)} \tag{25}$$

Comparison of the predictions of this formula with 18 experiments produces 16 ratios of experimental values to predicted values ranging from 1.01 to 1.38, and 2 values below 1 (0.99 and 0.81).

5.4.1 APPLICATION OF THESE METHODS TO THE CASE UNDER STUDY

An independent (from the official investigation) finite-element study by researchers from the University of Minnesota [Liao et al., 2011] started with a 2-D model of the I-35 W Bridge, with all member ends assumed pinned, and the deck not acting in a composite manner with the trusses. Influence lines showed the dramatic effect of the location of the construction loads on the truss forces at the panel that triggered the collapse. These truss forces were then applied to a detailed finite-element model of gusset plate U10. The study attributes the cause of the collapse to be the fracture and not the buckling of gusset plate U10 under the combination of compression and shear stresses.

> *"The U10 connection was affected substantially by yielding in the region in front of the connection." As a consequence, stresses "redistributed from the front of the*

> *connection to the shear lines along the perimeter of rivet holes, resulting in the wide yielded region surrounding member L9/U10."*

Although the yielded region replicated the fracture lines observed on U10, the authors point out that "in this study, the initiation of fracture is not quantified." If the linkage between yielding and fracture is not established, could yielding of part of the gusset plate have precipitated local buckling followed by global failure? The authors' buckling study "indicated only minor sensitivity to the initial imperfections / deformed shapes", and implied that buckling did not play a role in the collapse. These conclusions differ significantly from those of the NTSB investigation.

Higgins et al. (2010) propose a screening and ranking method to identify possible vulnerable connections for detailed evaluation and field inspection. The procedure considers member demands relative to the connection geometric and material properties for four different parameters: fasteners, plate tension, plate compression, and overall horizontal shear. Examples include the (collapsed) I-35 W Bridge in Minnesota and a bridge in Oregon.

Gross and Cheok (1988) and Gross (1990) tested three diagonally braced steel beam-column gusseted connections at ¾ scale. The first two connections were in the plane of the column strong axis, the first one concentric (where the axes of beam, column and brace intersect at one point), and the second eccentric, whereas the third specimen, also eccentric, used the weak axis column. The strong axis specimens failed by buckling of the gusset plate connecting the compression brace, whereas the third specimen failed by tearing of the gusset plate connecting the tension brace. The more compact gusset plate (eccentric) was stronger than the longer (concentric) one, and specimens 2 and 3 had the same strength, although they failed differently. The moment introduced by the eccentricity was distributed to the beam and column in the strong axis column specimen 2, but was carried almost entirely by the beam in the weak axis column specimen 3. Compared with test results, design equations [AISC, Richard's, Thornton's] were conservative.

Yamamoto et al. (1988) tested eight gusset plates (each connecting two horizontal chord members and two diagonal braces, Figure 5.12) to establish stability design criteria for the joints of the stiffening Warren truss of the Honshu-Shikoku suspension bridge. They focused on the development of plastic zones, local buckling (Figure 5.13) and ultimate strength, and obtained the following safety factors.

Local yielding and local buckling preceded global buckling of the gusset plates. The load at which local buckling started depended on the extent of yielding, which covered the inner portions of the gusset plate, whose in-plane stiffness was constrained by the surrounding elastic region. The authors performed a FEA of a simplified triangular plate which represented region A (Figure 5.12) under various boundary conditions with the load assumed uniformly applied along the chord. The elastic buckling stress σ_{CR} for a plate has the following form:

$$\sigma_{cr} = \frac{K\pi^2 E}{12(1-\upsilon^2)\left(\frac{b}{t}\right)^2} \qquad \text{or} \tag{26}$$

$$\frac{\sigma_{cr}}{\sigma_y} = \frac{K\pi^2}{12(1-\upsilon^2)\left(\frac{b}{t}\sqrt{\frac{\sigma_y}{E}}\right)^2} = \frac{k}{\left(\frac{b}{t}\sqrt{\frac{\sigma_y}{E}}\right)^2} \tag{27}$$

Where:

E = modulus of elasticity,

υ = Poisson’s ratio,

b = plate width,

t = plate thickness,

σ_y = yield stress,

and K, k = constants dependent on edge conditions.

Table 5.2: Safety factors for various characteristic loads. P_d = design load; P_y^u = load at which plastic zone penetrates web of chord; P_y = initial yield load; P_{cr} = initial buckling load; P_u = ultimate strength.

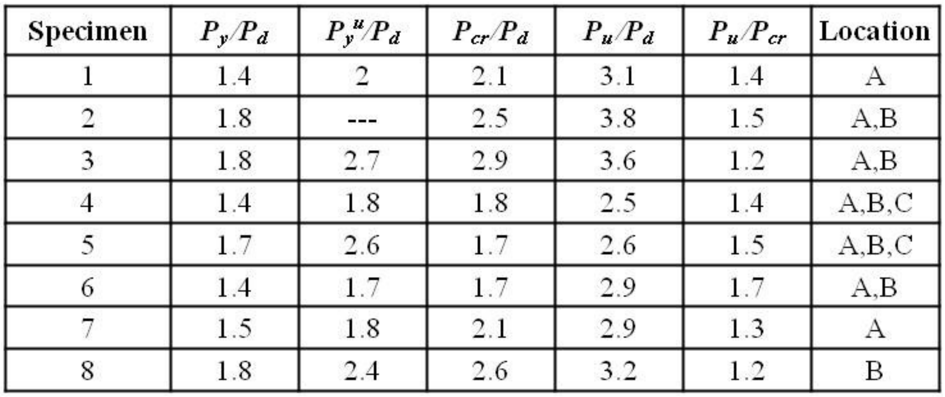

Specimen	P_y/P_d	P_y^u/P_d	P_{cr}/P_d	P_u/P_d	P_u/P_{cr}	Location
1	1.4	2	2.1	3.1	1.4	A
2	1.8	---	2.5	3.8	1.5	A,B
3	1.8	2.7	2.9	3.6	1.2	A,B
4	1.4	1.8	1.8	2.5	1.4	A,B,C
5	1.7	2.6	1.7	2.6	1.5	A,B,C
6	1.4	1.7	1.7	2.9	1.7	A,B
7	1.5	1.8	2.1	2.9	1.3	A
8	1.8	2.4	2.6	3.2	1.2	B

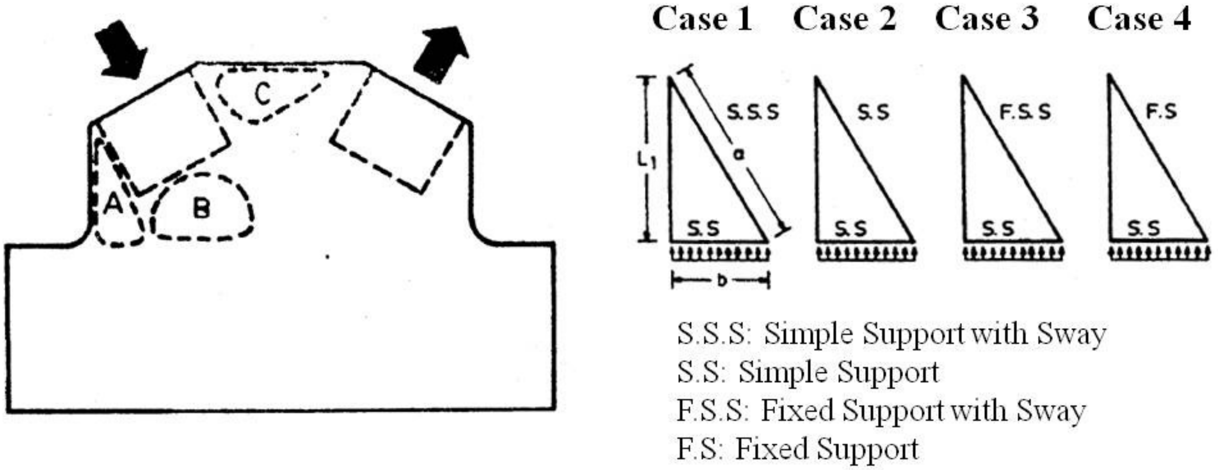
C
A
B
Case 1
Case 2
Case 3
Case 4
L1
a
b
S.S.S
S.S
F.S.S
F.S
S.S: Simple Support
S.S.S: Simple Support with Sway
S.S: Simple Support
F.S.S: Fixed Support with Sway
F.S: Fixed Support

Figure 5.12: Regions of yielding or local buckling and FEA of simplified plate model A.

Under the assumption that buckling occurred when the stress in region A reached the allowable stress in the material, $\sigma_a = 0.58\ \sigma_y$, and with L_1 = length of the vertical free edge, the authors proposed the following design thickness for local buckling:

$$t_{cr} = 1.10 L_1 \sqrt{\frac{\sigma_a}{E}} \tag{28}$$

If $\sigma_{cr} = \sigma_a$ and k = 0.276, the previous two equations are equivalent for $L_1 = b\sqrt{3}$. Test specimens 4 and 5 (Table 5.2) used a plate thickness less than that given by the above equation, and resulted in the lowest factor of safety $P_u\ /P_d$. For all the other test specimens, this factor equaled or exceeded 2.9. Specimen 5 did not benefit from the stiffening effect of a chord flange, thus causing $P_{cr}\ /P_d$ to be much less than P_{yu}/P_d. The authors further noted that P_u/P_{cr} was independent of structural details and gusset type.

Table 5.3: Buckling constant from FEA of idealized triangular plate.

Case	Diagonal edge	Horizontal edge	*k*
1	Simple support with sway	Simple support	0.276
2	Simple support	Simple support	0.918
3	Fixed support with sway	Simple support	1.85
4	Fixed support	Simple support	2.156

6 CRITICAL REVIEW OF FHWA GUIDELINES ON GUSSET PLATES

6.1 INTRODUCTION

As a result of the structural failure, the Federal Highway Administration issued guidelines for the load rating of gusset plates [FHWA, 2009] and recommended to verify the capacity of these plates in non-load-path-redundant steel truss bridges be verified.

The guidelines provide state departments of transportation with simple hand formulas based on laboratory tests, but the absence of a commentary makes it difficult to assess the level of safety of these formulas.

The purpose of this chapter is to examine with a critical point of view:

- the buckling behavior of steel gusset plates in greater detail, accounting for parameters that were not explicitly included in the guidelines, such as initial deformations, stiffness of the framing members, load distribution from the framing members to the gusset plate and load eccentricity; and
- the behavior of gusset plates in tension, resulting in possible failure by block shear, focusing on the level of detail required in the finite-element mesh and the transfer of load from the bolts to the plate, with reference to experimental results. Next, the influence of the number and arrangement of bolt holes on the mode of failure and the ultimate strength of the gusset plate for block shear is addressed through a series of examples.

6.2 BUCKLING BEHAVIOR OF STEEL GUSSET PLATES

6.2.1 CURRENT GUIDELINES

The compressive strength of a gusset plate is that of an equivalent column determined as follows:

- The thickness of the column is that of the gusset plate;

- The width is the Whitmore (1952) effective width determined by the intersections of the last row of rivets or bolts with two lines originating from the ends of the first row of bolts and extending at 30° to the framing member (Figure 6.1).

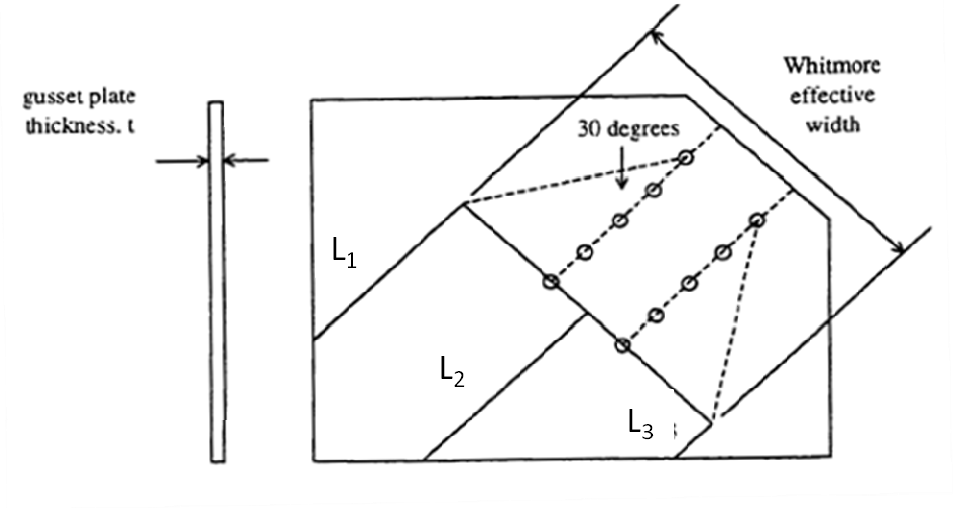

Figure 6.1. Equivalent column.

The length of the column is the average of three lengths extending in the direction of the framing member from the middle and the ends of the last row of bolts to the edges of the gusset plate or adjacent groups of bolts (L_1, L_2 and L_3 Figure 6.1). This approximation is attributable to Thornton (1984).

In general, this equivalent column is not slender, and its buckling behavior would be in the inelastic range. The following quantities are used in defining the column strength:

$$\sigma_E = E\left(\frac{\pi r}{KL}\right)^2 \qquad (1)$$

$$\lambda = \frac{\sigma_y}{\sigma_E} \qquad (2)$$

Where: σ_E = Euler buckling strength; σ_y = yield strength; E = modulus of elasticity; ρ= radius of gyration; L = column length; K = end fixity coefficient.

The guidelines allow two different methods.

For Load and Resistance Factor Rating (LRFR), the nominal (unfactored) compressive resistance is:

for $\lambda \leq 2.25$, (inelastic buckling):

$$\frac{\sigma_{LRFR}}{\sigma_Y} = 0.66^{\lambda} \tag{3}$$

for $\lambda > 2.25$, (elastic buckling):

$$\sigma_{LRFR} = 0.88\ \sigma_E \tag{4}$$

The Commentary of the American Association of State Highway and Transportation Officials (AASHTO) Specifications C6.9.4.1 (1994) states that Equations (3) and (4) are the same as in the American Institute of Steel Construction (AISC) Load Resistance Factor Design (LRFD) 1986 Specifications and come from column strength curve 2P of the Structural Stability Research Council (SSRC 1988). They are based on the maximum strength theory and incorporate an out-of-straightness value of L/1500 (the maximum permissible out-of-straightness is L/1000).

For Load Factor Rating (LFR), the nominal (unfactored) compressive resistance is:

for $\lambda \leq 2.0$, (inelastic buckling):

$$\frac{\sigma_{LFR}}{\sigma_Y} = 1 - \frac{\lambda}{4} \tag{5}$$

for $\lambda > 2.0$, (elastic buckling):

$$\sigma_{LFR} = \sigma_E \tag{6}$$

Equation (5) is based on the tangent modulus theory and is generally known as the CRC Column Strength Curve named after the Column Research Council, now the Structural Stability Research Council (SSRC). It was recommended in the first edition of the CRC Guide (1960) and widely used (e.g., in AISC 1979).

> *"It is based on the average critical stress for small and medium-sized hot-rolled wide-flanged sections of mild structural steel, with a symmetrical residual stress distribution typical of such members" (SSRC Guide 1998).*

These curves are plotted in Figure 6.3. The FHWA guidelines do not contain Eqs. (4) and (6), which are included here for completeness.

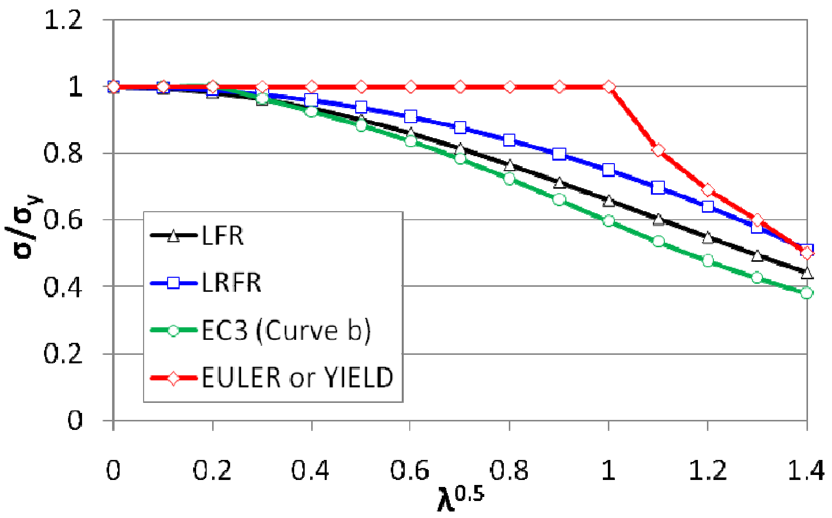

Figure 6.2. Column curves.

In the inelastic buckling range, the design values factored with different safety coefficients are close to each other (Figure 6.3):

for stub columns, $0.90\ \sigma_{LRFR} / (0.85\ \sigma_{LFR}) \leq 1.06$; (7)

at $\lambda = 2$, $0.85\ \sigma_{LFR} / (0.90\ \sigma_{LRFR}) = 1.08$; and (8)

at $\lambda = 0.611^2 = 0.373$, the two quantities are equal,

i.e., $0.90\ \sigma_{LRFR} / \sigma_y = 0.85\ \sigma_{LFR} / \sigma_y = 0.7707$. (9)

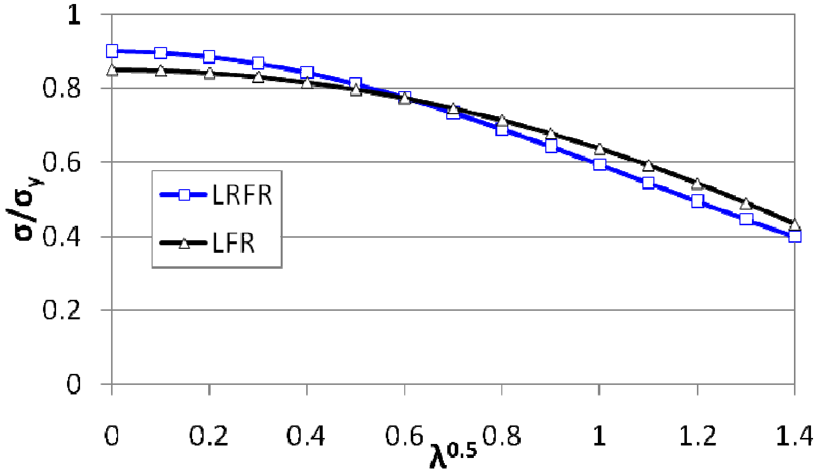

Figure 6.3. Factored column curves.

6.2.2 EXPERIMENTAL RESULTS

Experimental results were obtained from tests of gusset plates performed at the University of Alberta, Figure 6.4 [Walbridge, Grondin and Cheng, 1998]. The test parameters included thickness and size of the gusset plate, and angle, moments and restraint conditions of the framing members. The researchers measured out-of-plane displacements of the gusset plate and applied loads. They found that the compressive capacity was almost proportional to the thickness of the gusset plate, and framing member moments only had a small effect on the compressive capacity and the strain distribution in the gusset plate.

The test selected for modeling resulted in a gusset plate ultimate capacity of *1956 kN*. The plate, of dimensions *500 mm* × *400 mm* × *13.3 mm*, was made of steel with a modulus of elasticity of *207.6 GPa*, a yield strength of *295 MPa* and an ultimate strength of *501 MPa*. Initial imperfections were not recorded.

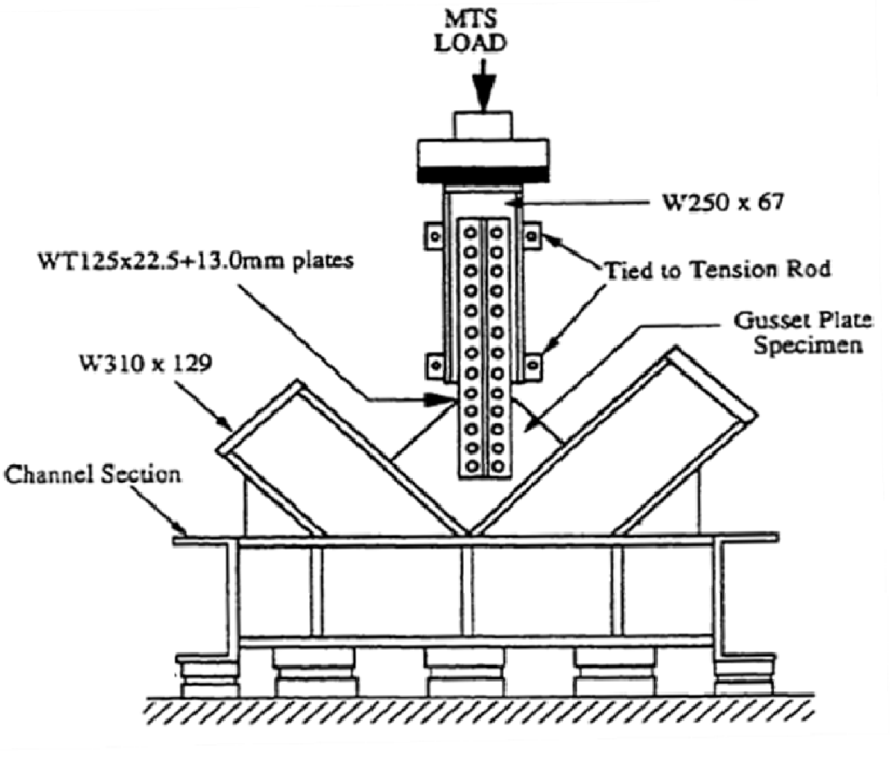

Figure 6.4. University of Alberta tests [Walbridge, Grondin and Cheng, 1998].

6.2.2.1 FINITE ELEMENT ANALYSES

Linear or nonlinear finite-element analyses of the tested gusset plate were performed using shell elements with four-nodes available in software STRAND7/STRAUS7. Figure shows a summary of the analyses developed.

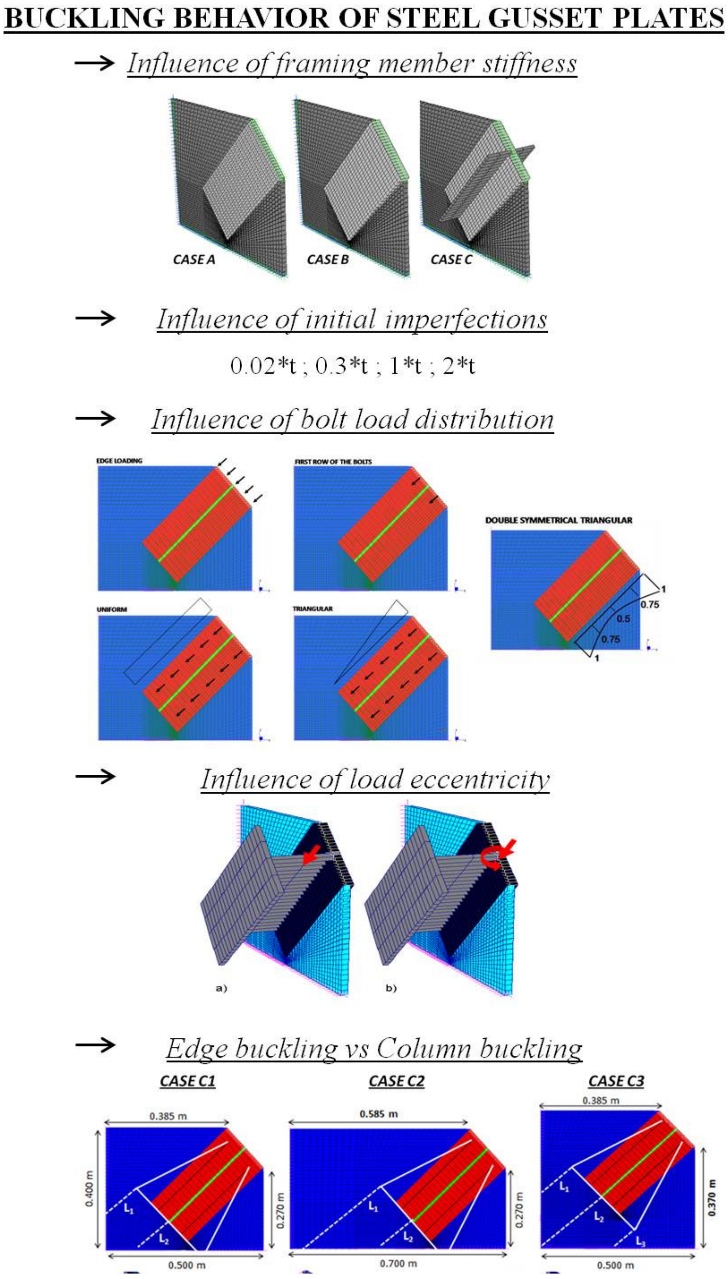
BUCKLING BEHAVIOR OF STEEL GUSSET PLATES
→ Influence of framing member stiffness
CASE A
CASE B
CASE C
→ Influence of initial imperfections
0.02*t ; 0.3*t ; 1*t ; 2*t
→ Influence of bolt load distribution
EDGE LOADING
FIRST ROW OF THE BOLTS
DOUBLE SYMMETRICAL TRIANGULAR
1
0.75
0.5
0.75
1
UNIFORM
TRIANGULAR
→ Influence of load eccentricity
a)
b)
→ Edge buckling vs Column buckling
CASE C1
CASE C2
CASE C3
0.385 m
0.400 m
L1
L2
0.500 m
0.585 m
0.270 m
0.270 m
0.700 m
0.385 m
L1
L2
L3
0.370 m
0.500 m

Figure 6.5. Summary of the analyses developed.

6.2.2.2 MESH CONVERGENCE STUDY

In the first model (A), the gusset plate considered has a uniform thickness *t = 13.3 mm*, is fixed along the two perpendicular edges at bottom and left and is restrained against rotation at the oblique edge (end fixity coefficient *K = 1.2*). The compression load was applied by 21 equal point loads at *32.5°* to the x axis, perpendicular to the oblique edge.

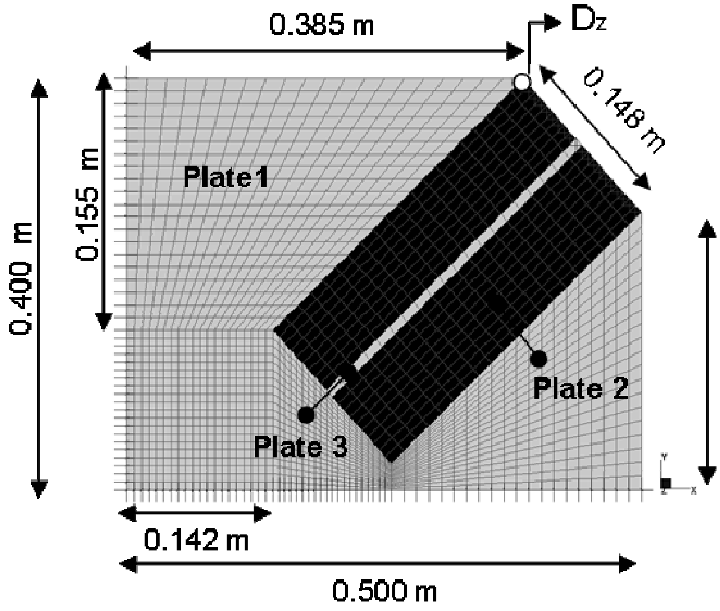

Figure 6.6. Finite-element model meshed with 2000 elements.

Note that the gusset plate does not require stiffeners along its unsupported edges, as

$\frac{l}{t} = \frac{385}{13.3} = 29$ is less than $2.06\sqrt{\frac{E}{F_y}} = 2.06\sqrt{\frac{207600}{295}} = 55\ (\text{LRFR})$ or $\frac{11000}{\sqrt{F_y}(psi)} = \frac{11000}{\sqrt{42780}} = 53\ (\text{LFR})$

where l is the length of the free edge of interest, t is the thickness of the gusset plate and Guidance criteria are used.

Analyses were performed to assess the level of mesh refinement required to ensure convergence. Figure 6.6 shows that there is little difference in results between a model meshed with 1280, 1620 or 5120 shell elements (D_z is the load-induced out-of-plane deformation at the intersection of the upper and the oblique edges, see Figure 6.5). In the rest of the study, a mesh of 2000 elements is used.

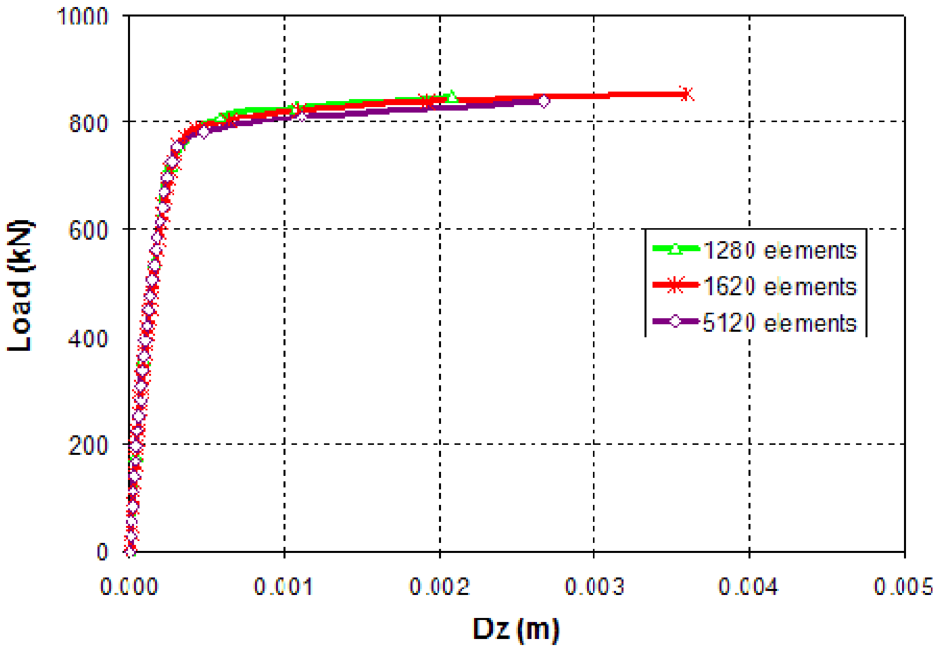

Figure 6.7. Mesh convergence study.

6.2.2.3 INFLUENCE OF FRAMING MEMBER SYSTEM

Three cases were investigated (Figure 6.8):

A. uniform thickness *t* = *13.3 mm*,

B. the flange thickness of the framing member is added to that of the gusset plate, so plate 2 and plate 3 have a thickness of *26.3 mm*, and

C. both the flange and the web of the framing member add to the stiffness of the gusset plate.

All three cases are symmetrical with respect to the mid-plane of the gusset plate to reflect experimental conditions. The effect of load eccentricity will be discussed in a later section. For bridges, members usually frame into pairs of parallel and symmetrical gusset plates, so they introduce no bending moment into the gusset plates.

All three cases are symmetrical with respect to the mid-plane of the gusset plate to reflect experimental conditions. The effect of load eccentricity will be discussed in a later section. For

bridges, members usually frame into pairs of parallel and symmetrical gusset plates, so their axial loads introduce no bending moment into the gusset plates.

Figure 6.9 shows, as expected, that the stiffness of the framing member plays an important role in the buckling strength of the gusset plate. The experimental value falls between (B) and (C). Unfortunately, the experimenters reported neither a load–deflection curve nor measurements of initial imperfections, but only the buckling strength [Yam and Cheng, 1993].

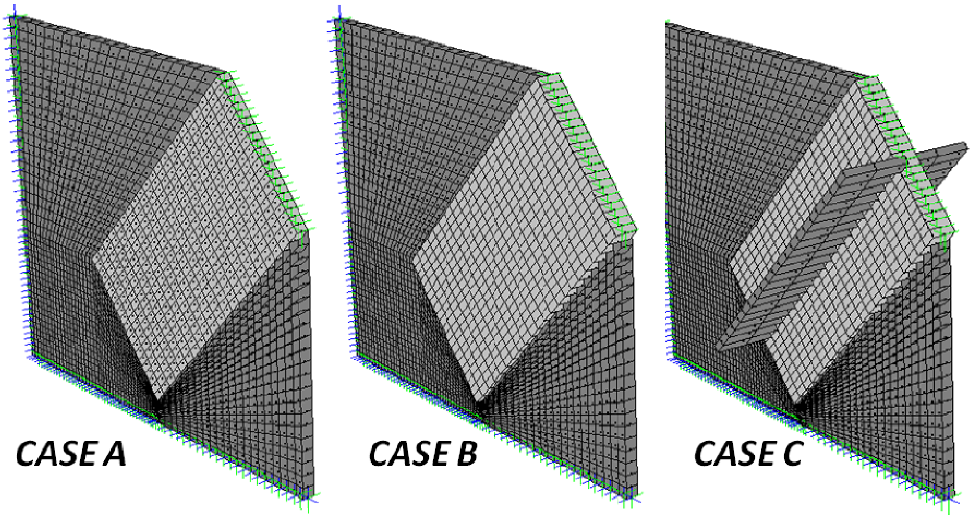

Figure 6.8. Framing member stiffness.

The calculations here (Figure 6.8) used a small initial imperfection in the same shape as the first elastic buckling mode for a plate of similar geometry and loading and of maximum amplitude 0.02 t = 0.02×13.3 mm = 0.266 mm = 310 mm/1165 = L/1165, where L = 310 mm is the Thornton length for the gusset plate.

An initial imperfection greater than that value and/or a small eccentricity of the applied load might have made the test value less than case (C), which is closest to the experimental set-up. All three cases calculated here were edge-loaded as described in the previous section.

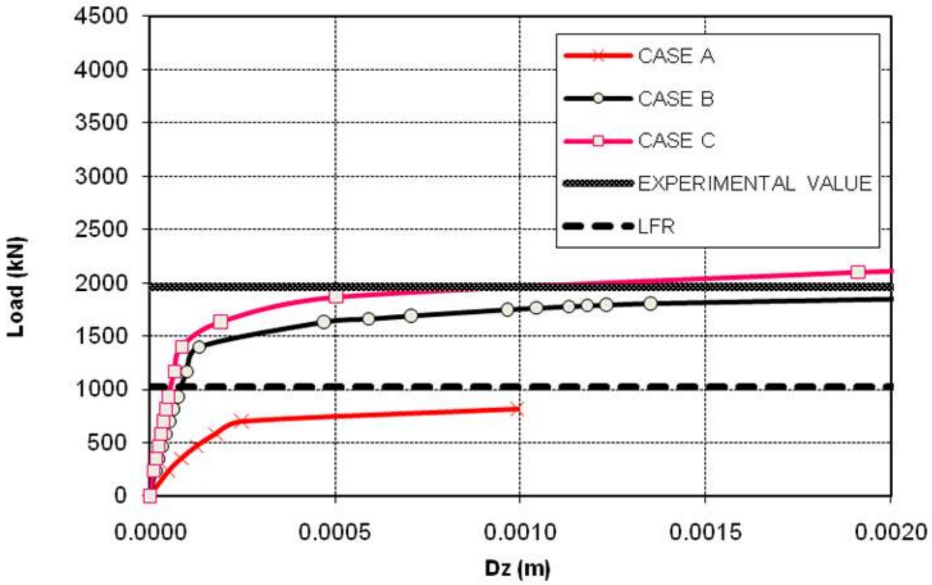

Figure 6.9. Effects of framing member stiffness (edge loading).

6.2.2.4 INFLUENCE OF INITIAL IMPERFECTION

As initial imperfections increase in magnitude, the column strength decreases. Figure 6.10 shows results for case (B), where only the contribution of the framing member flange to the plate stiffness is accounted for, and with loading applied to the plate edge. Even with these conservative assumptions, the unfactored LFR strength is acceptable up to an initial deformation of $1t = 13.3\ mm = 310\ mm/23.3$, although the plate would have to undergo an additional out-of-plane deformation of the same order before its strength is reached. Initial imperfections in excess of *1t* would be unsafe. Note that on the scale of the graph, LRFR and LFR values are indistinguishable.

Figure 6.10 shows, as expected, that the stiffness of the framing member plays an important role in the buckling strength of the gusset plate. The experimental value falls between (B) and (C). Unfortunately, the experimenters reported neither a load–deflection curve nor measurements of initial imperfections, but only the buckling strength (Yam and Cheng, 1993). The calculations here (Figure 6.10) used a small initial imperfection in the same shape as the first elastic buckling mode for a plate of similar geometry and loading and of maximum amplitude $0.02\ t = 0.02 \times 13.3\ mm = 0.266\ mm = 310\ mm/1165 = L/1165$, where $L = 310\ mm$ is the average of L_1 , L_2 and

L_3 for the gusset plate. An initial imperfection greater than that value and/or a small eccentricity of the applied load might have made the test value less than case (C), which is closest to the experimental set-up. All three cases calculated here were edge-loaded as described in the previous section.

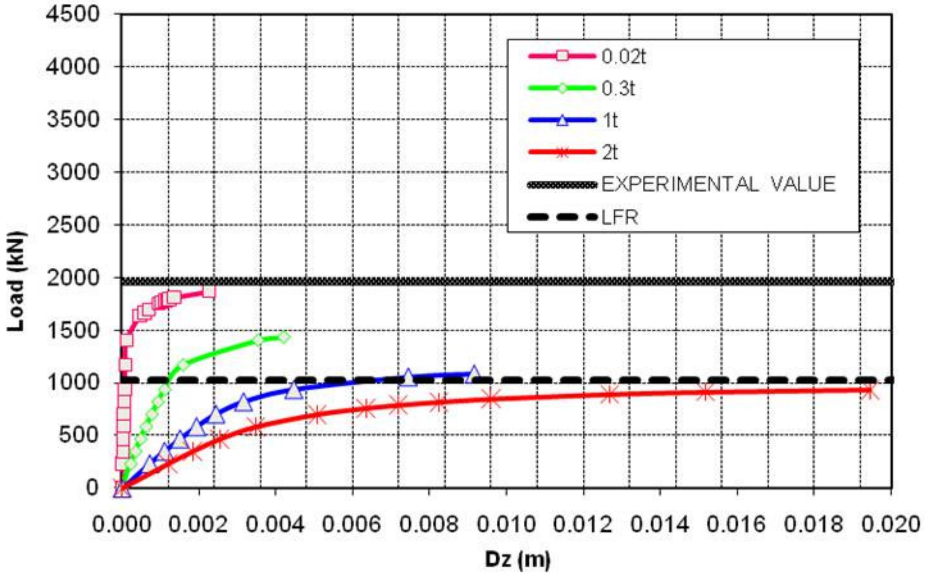

Figure 6.10. Effects of initial deformations, edge loading, Case (B).

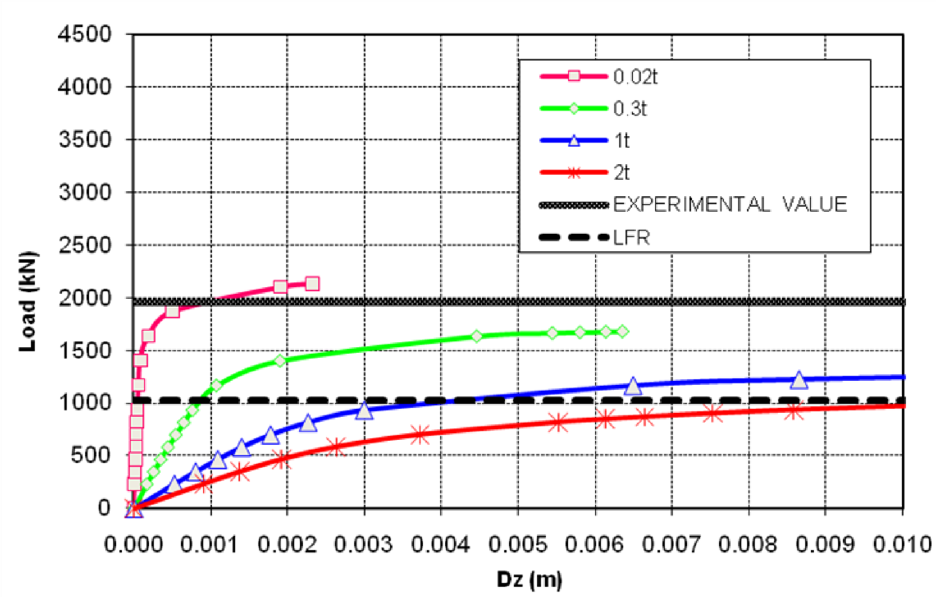

Figure 6.11. Effects of initial deformations, edge loading, Case (C).

Schmidt et al. (2008) documented the failure of a small steel truss caused by the buckling of a pair of non compact gusset plates. They attributed the buckling to be caused by the excessive overall length of the plates, rather than to the length of the free edges. Their calculations used a similar approach to Whitmore (30° spread) except that the thickness of their equivalent column included the flange of the framing member as well as the gusset plate. They took the effective length as ⅔ of the strip of maximum length (⅔ L_1 in Figure 6.1), from which they calculated the strength of the equivalent column and compared it to a column curve (EC3, Figure 6.2) used in DIN 18800-3 (and in EN 1993-1-1:2005 E). This column curve is similar to Eqs. (3) and (5) and described by the following equation. (Notation has been modified to conform to this paper, σ_b is the column strength corresponding to curve b of the standard):

$$\frac{\sigma_b}{\sigma_y} = \frac{1}{\Phi+\sqrt{\Phi^2+\lambda}} \leq 1.0, \tag{10}$$

$$\text{where } \Phi = \frac{1+\alpha\left(\sqrt{\lambda}-0.2\right)+\lambda}{2} \tag{11}$$

and α is an imperfection factor (= 0.34 in this case).

Interestingly, their FEA shows that an initial imperfection of only 1 mm for this 20 mm thick plate produces strength (*3752 kN*) very close to the actual failure load (*3700 kN*). This means that a ratio of initial imperfection to plate thickness of 5% is not tolerable, a very stringent requirement indeed. Their conclusion differs from this chapter because their FEA does not account for the web of the framing member, which stiffens the gusset plate considerably and makes it more tolerant to initial imperfections.

6.2.2.5 INFLUENCE OF BOLT LOAD DISTRIBUTION

The finite-element model was not refined enough to determine the load carried by individual bolts, so various load distributions were assumed, see Figure 6.12.

Figure 6.12 shows the gusset plate buckling strength for various values of the initial imperfections assuming the compression is carried by the first row of bolts (closest to the plate edge).

Figure 6.13 shows the buckled shape. Results are very similar to the previous case of edge loading, except for the almost perfect plates, which show a small strength increase. As initial deformations increase, the effect of a small change in column length decreases.

Figure 6.14 uses a triangular or linear load distribution, with the first row of bolts (near the edge of the plate) carrying the highest load and the last row of bolts (near the center of the plate) carrying no load. Here the plate buckling strength is considerably greater than for edge loading, and the LFR value is adequate even for an initial deformation of *2t*. The uniform load distribution and the bilinear distribution shown in Figures 6.15 and 6.16 produce similar results and greater resistance to compression than the triangular or edge loading. In the absence of more detailed analysis, the uniform distribution is recommended.

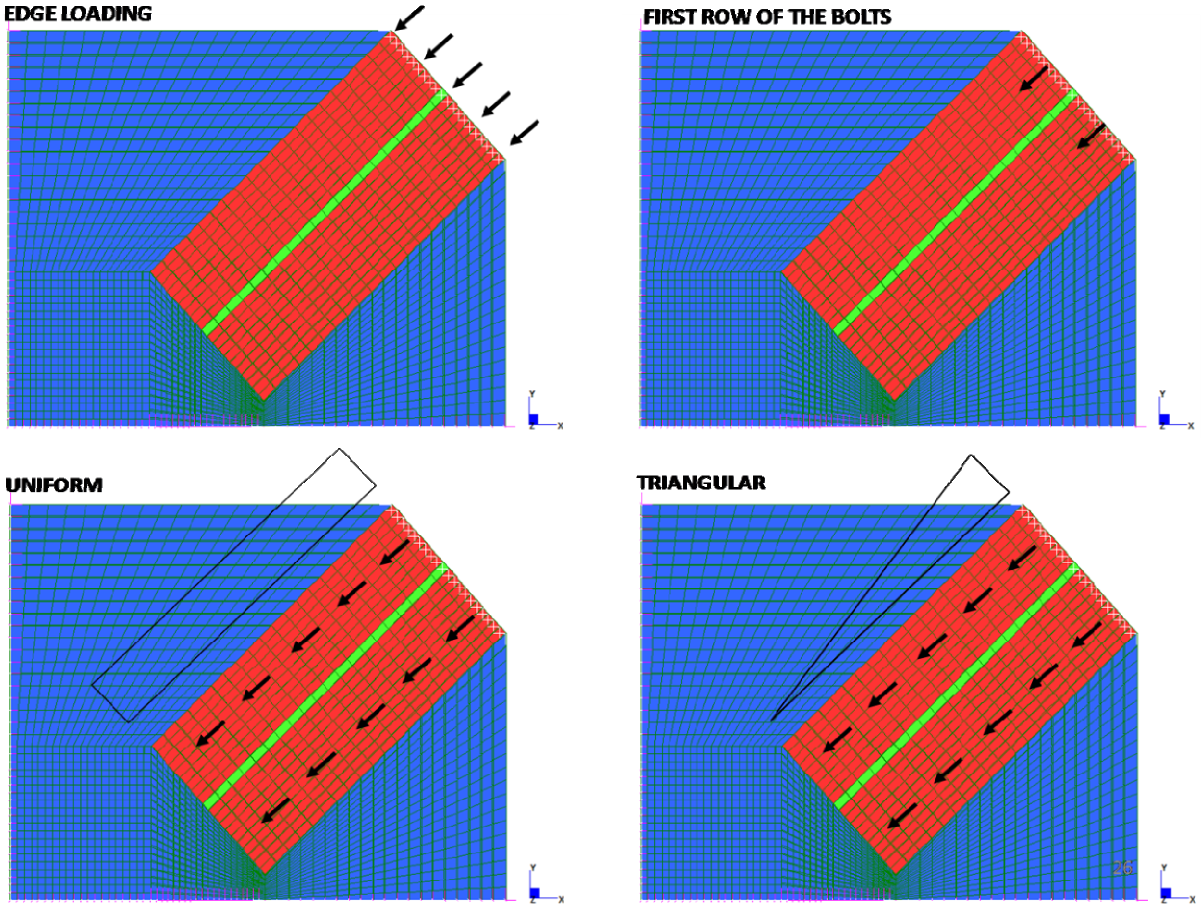

Figure 6 12. Effects of initial deformations, compression on first row of bolts, Case (C).

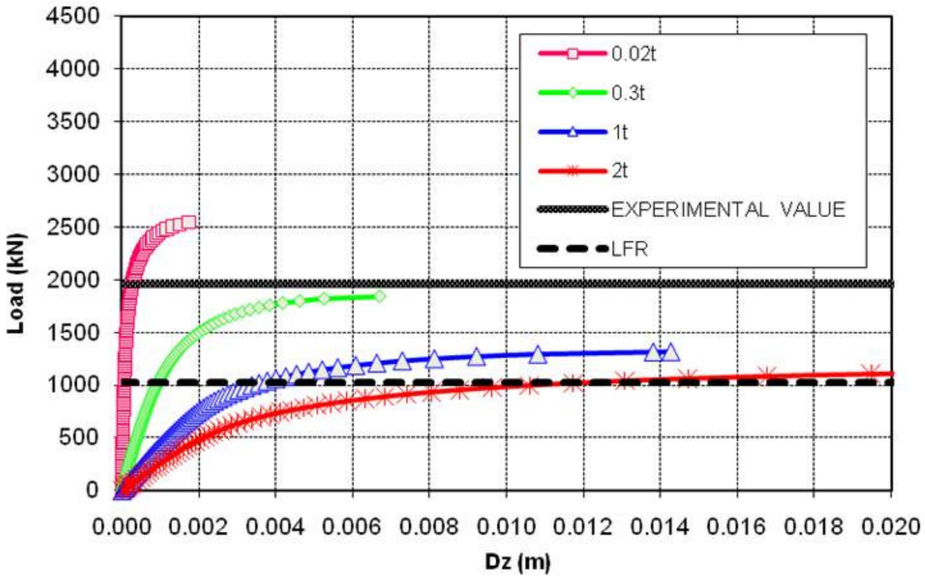

Figure 6.13. Effects of initial deformations, compression on first row of bolts, Case (C).

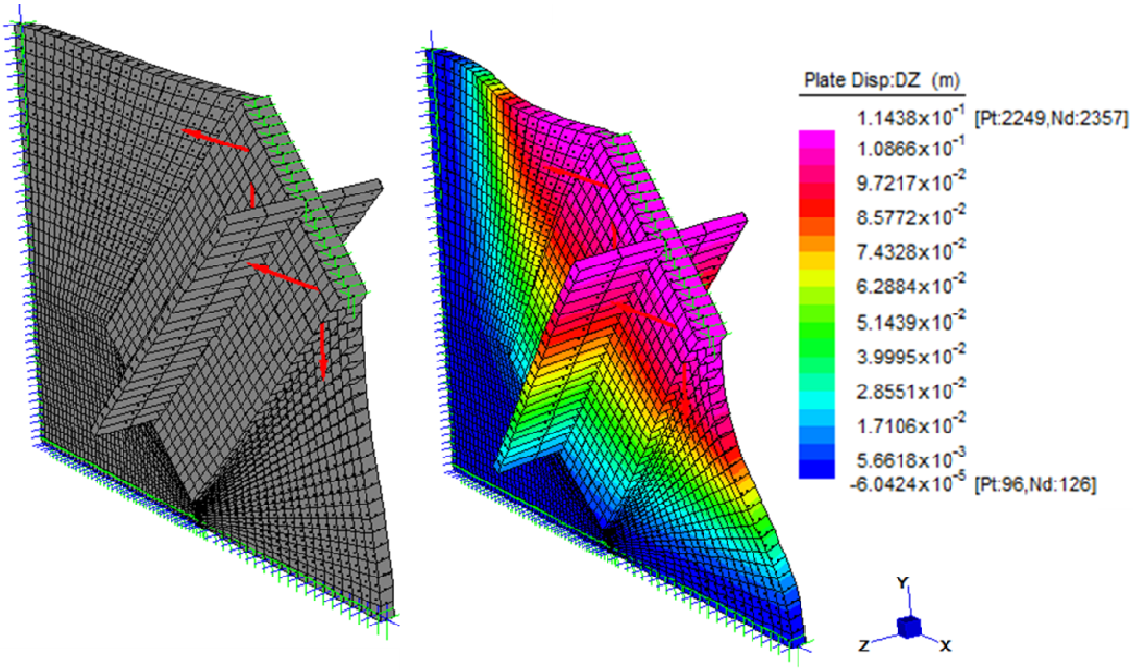
Plate Disp:DZ (m)
1.1438x10^-1 [Pt:2249,Nd:2357]
1.0866x10^-1
9.7217x10^-2
8.5772x10^-2
7.4328x10^-2
6.2884x10^-2
5.1439x10^-2
3.9995x10^-2
2.8551x10^-2
1.7106x10^-2
5.6618x10^-3
-6.0424x10^-3 [Pt:96,Nd:126]
Y
Z
X

Figure 6.14. Pre- and post-buckling gusset plates.

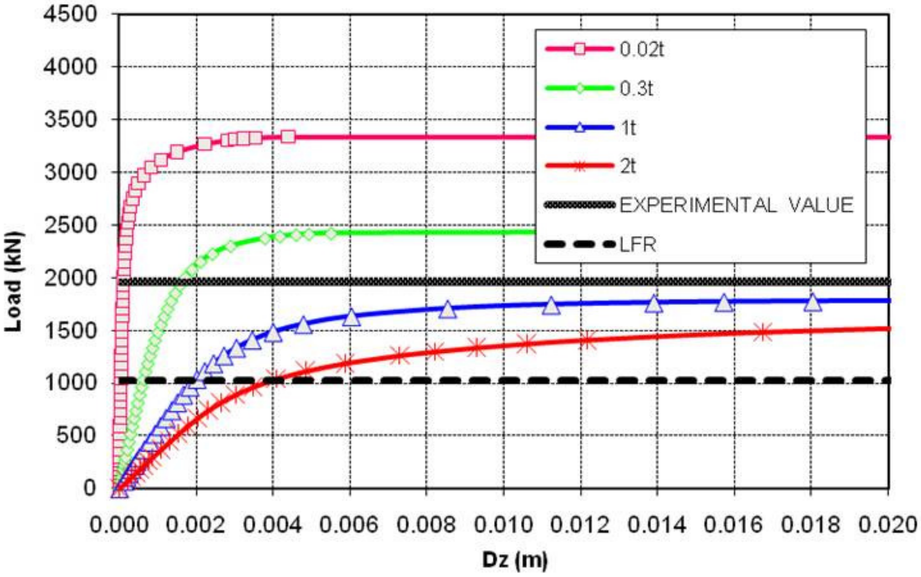

Figure 6.15. Triangular load, Case C.

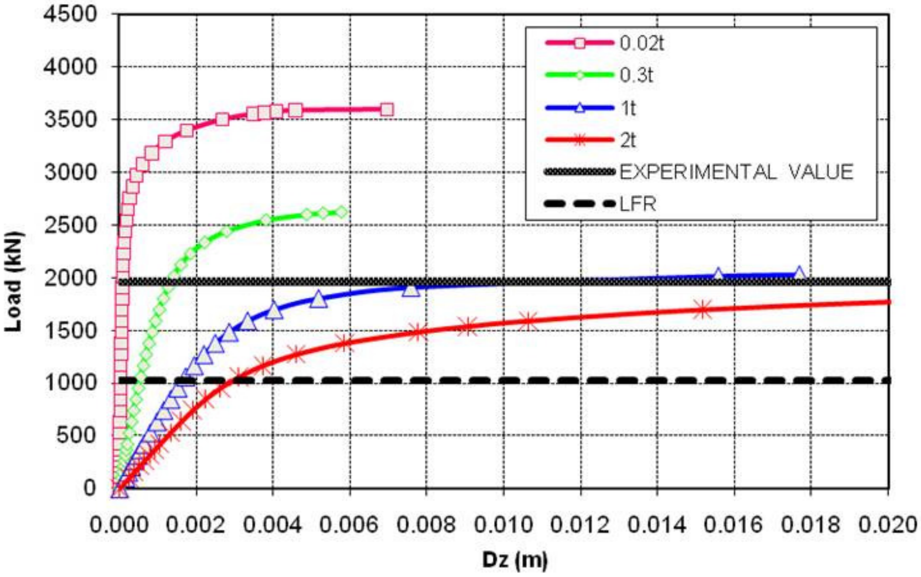

Figure 6.16. Uniform load, Case C

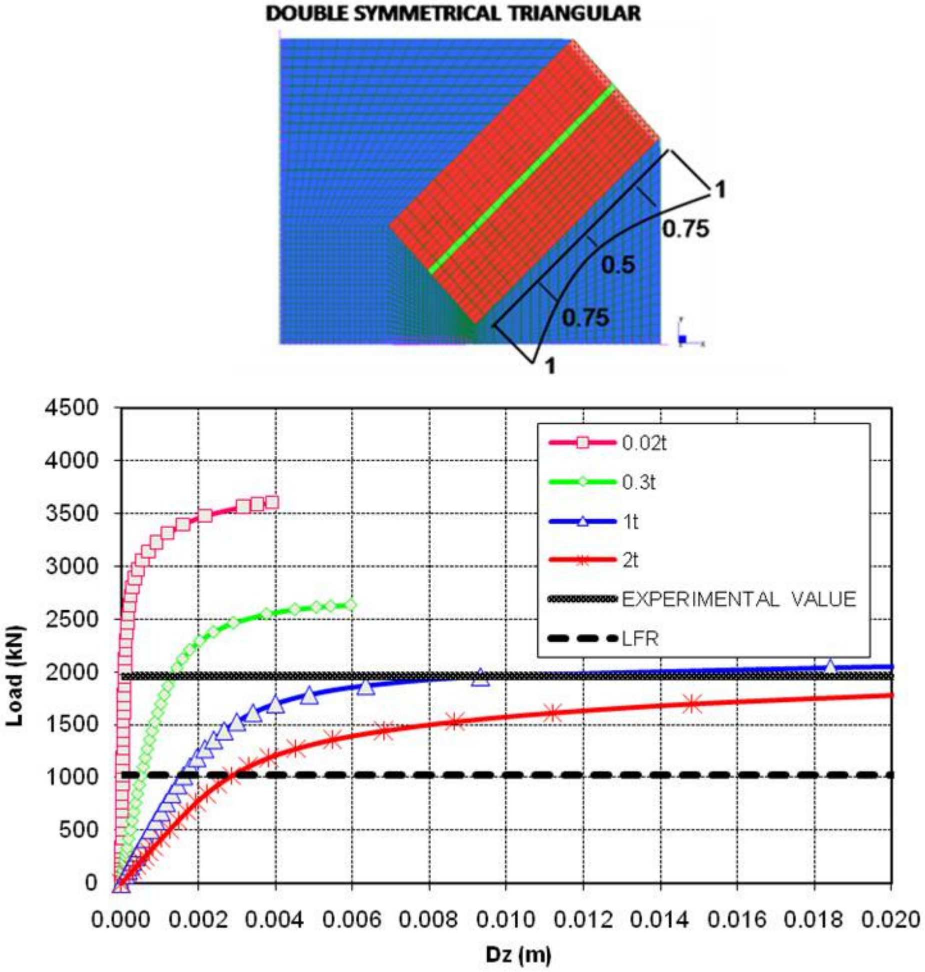

Figure 6.17. Bilinear load distribution.

The actual load distribution in a long row of rivets is complex and depends on many factors, such as the relative stiffness of the rivets and the plates they connect. Very flexible rivets carry equal loads, whereas, for very stiff rivets, all the force is transmitted by the end rivets. For intermediate situations, Hrennikoff's approximate elastic theory (1934) predicts, for example, a distribution from either end toward the middle of *0.360*F*, *0.104*F* and *0.036*F* for a row of six rivets transmitting a force *F* between two plates of equal stiffness. More recently, Huang et al. (2010) finite-element analysis and physical measurements confirmed that the highest loads are carried by the ends of the connection: for four rows of bolts transmitting a force F in double shear between a single plate and two cover plates, they measured a force distribution of *0.489*F*, *0.098*F*, *0.080*F* and *0.334*F* (the highest load is closest to the end of the cover plate, the second highest is closest to the end of the single plate). The load distribution also depends on the amount of slip in the connection: in the last stage before failure, plastic deformation permits load redistribution leading to a uniform distribution with all rivets in bearing. In the absence of more detailed analysis, the uniform distribution is currently used in design practice.

6.2.2.6 INFLUENCE OF LOAD ECCENTRICITY

In all the cases studied above, loads were applied in the mid-plane of the gusset plate, which is also a plane of symmetry, to reflect the experimental set-up as well as the actual conditions in bridges. In buildings, however, gusset plates are often used singly and not in pairs, with the framing members on one side of the plate, and thus load eccentricity must be accounted for.

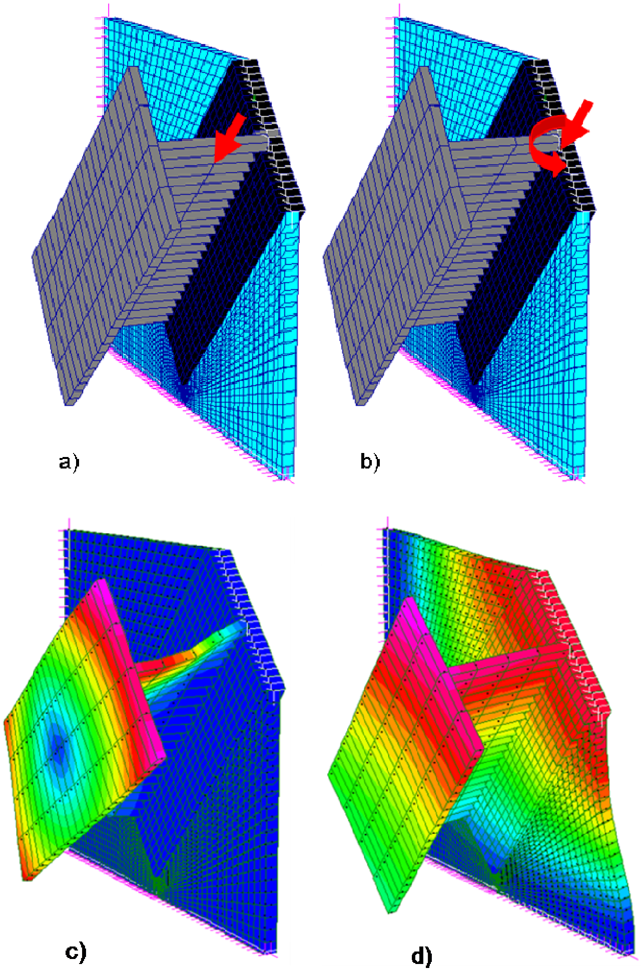

Figure 6.18. Gusset plate framing I-section loaded in 2 ways.

Figure 6.18 shows a gusset plate framing an I-section. In Figure 6.18a, the gusset plate is loaded, at the level of the first row of bolts, by a force *F* applied at mid-depth of the I-section. In Figure 6.18b, the gusset plate is loaded, at the level of the first row of bolts, by a statically equivalent combination of in-plane compressive force *F* and moment $M = Fe$, where *e* equals half of the depth of the I-section and *F* is the applied force.

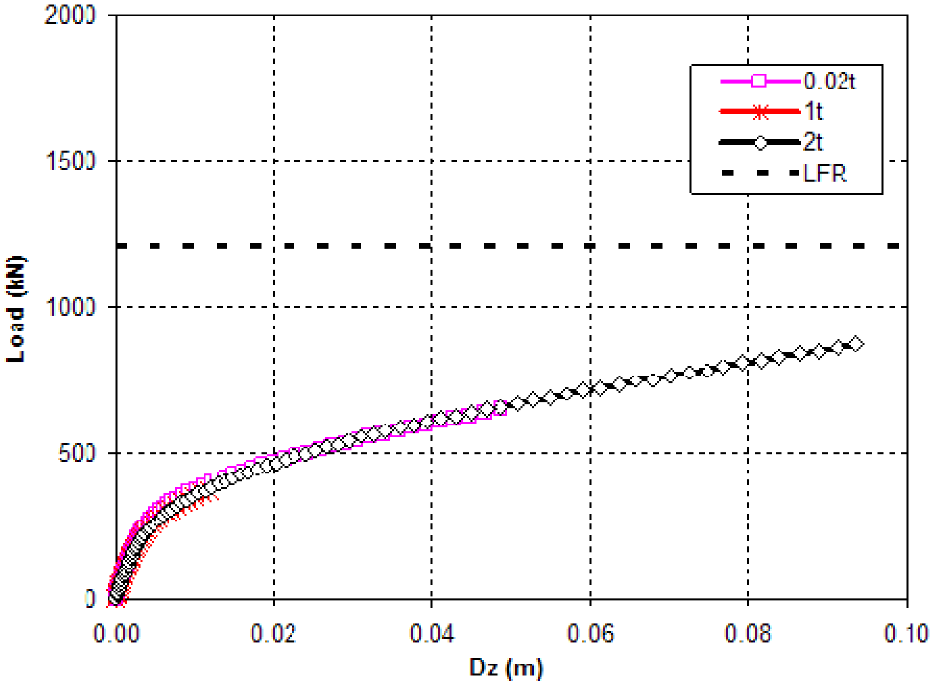

Figure 6.19. Gusset plate loaded eccentrically by I-member.

In the first case, Figure 6.19 indicates that the LFR value cannot be achieved even for an almost perfect plate, and initial deformations of *1t* and *2t* produce negligible effects compared to the load eccentricity. In the second case, Figure 6.20, the effects of various values of initial deformation are still felt, and the LFR value is achievable by an initially almost perfect plate. The difference in behavior is due to the different initial imperfections shown in Figures 6.21 and 6.22.

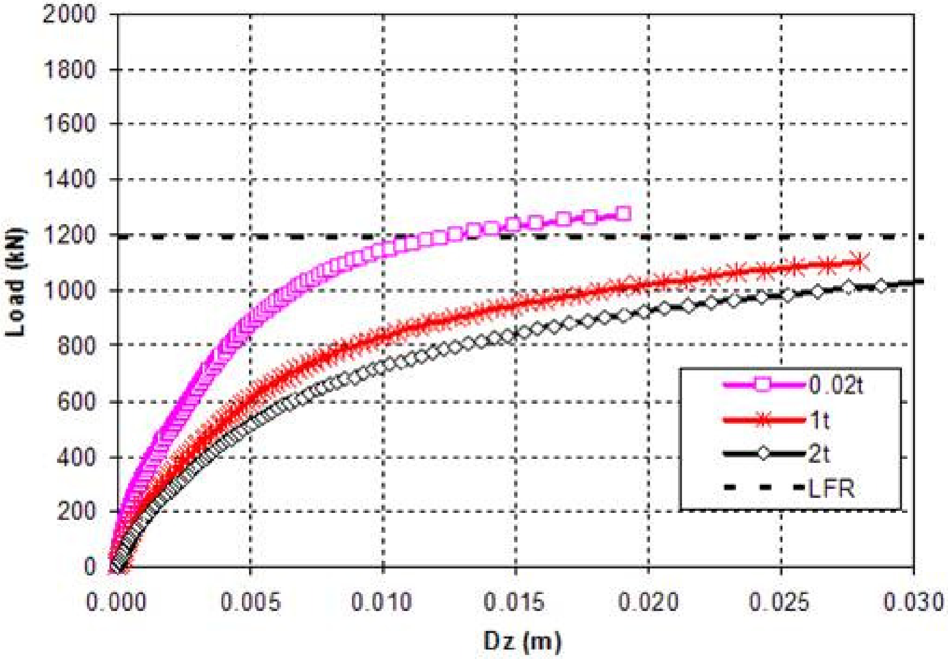

Figure 6.20. Gusset plate framing I-member loaded by F and M.

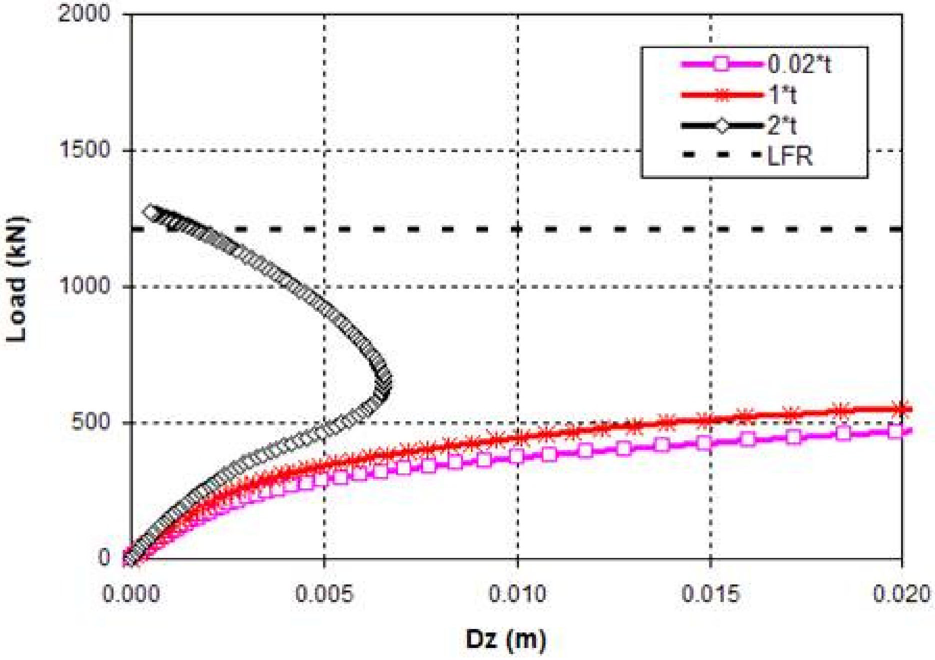

Figure 6.21. Effects of initial imperfections of opposite direction to load eccentricity on gusset plate loaded by I-member.

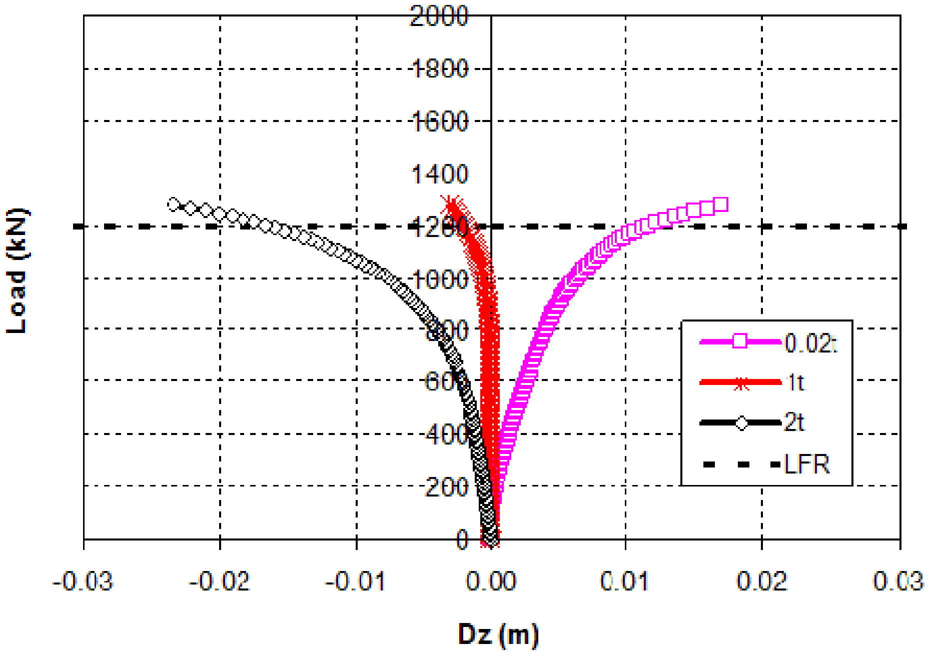

Figure 6.22. Effects of initial imperfections of opposite direction to moment on gusset plate framing I-section loaded by F & M.

Figures 6.21 and 6.22 correspond to Figures 6.19 and 6.20, except now the applied moment or load eccentricity tends to make D_z positive, whereas the initial imperfections act in the opposite direction. Figure 6.21 shows that for all three values of initial imperfection studied (*0.02t*, *1t*, *2t*), the plate starts out deflecting in the direction of the applied moment, but for 2t, snap-through occurs and the load-induced deflection reverses direction, thus allowing the plate to reach the LFR value, a much greater load than an almost perfectly flat plate can bear. Figure 6.22 shows that, for a small initial imperfection of *0.02t*, $M = Fe$ governs, for a large initial imperfection of *2t*, the imperfection governs, and for an initial imperfection of *1t*, the two effects compensate each other resulting in no additional deflection until a fairly large load is attained. In this last case, the LFR value is achievable for a small additional deflection.

6.2.3 EDGE BUCKLING VS GUSSET PLATE BUCKLING

To prevent the free edges of gusset plates from buckling, the Guidance limits the slenderness ratio of free edges:

$$\frac{l}{t} < 2.06\sqrt{\frac{E}{F_y}} \quad \text{for LRFR} \quad or \quad \frac{l}{t} < \frac{11000}{\sqrt{F_y}\ \text{psi}} \quad \text{for LFR} \qquad (12)$$

The buckling of the gusset plate documented by Schmidt et al. (2008) appears not to be caused by a long free edge, but rather by too long a middle length L_1 (Figure 6.1).

Figure 6.23 shows that, even though the LFR values are still conservative compared to the strengths calculated by FEA, gusset plate C3 is weaker than C2 according to FEA, but stronger according to the Guidance approach. C3 has the longer middle length L_1 , whereas C2 has the longer free edge.

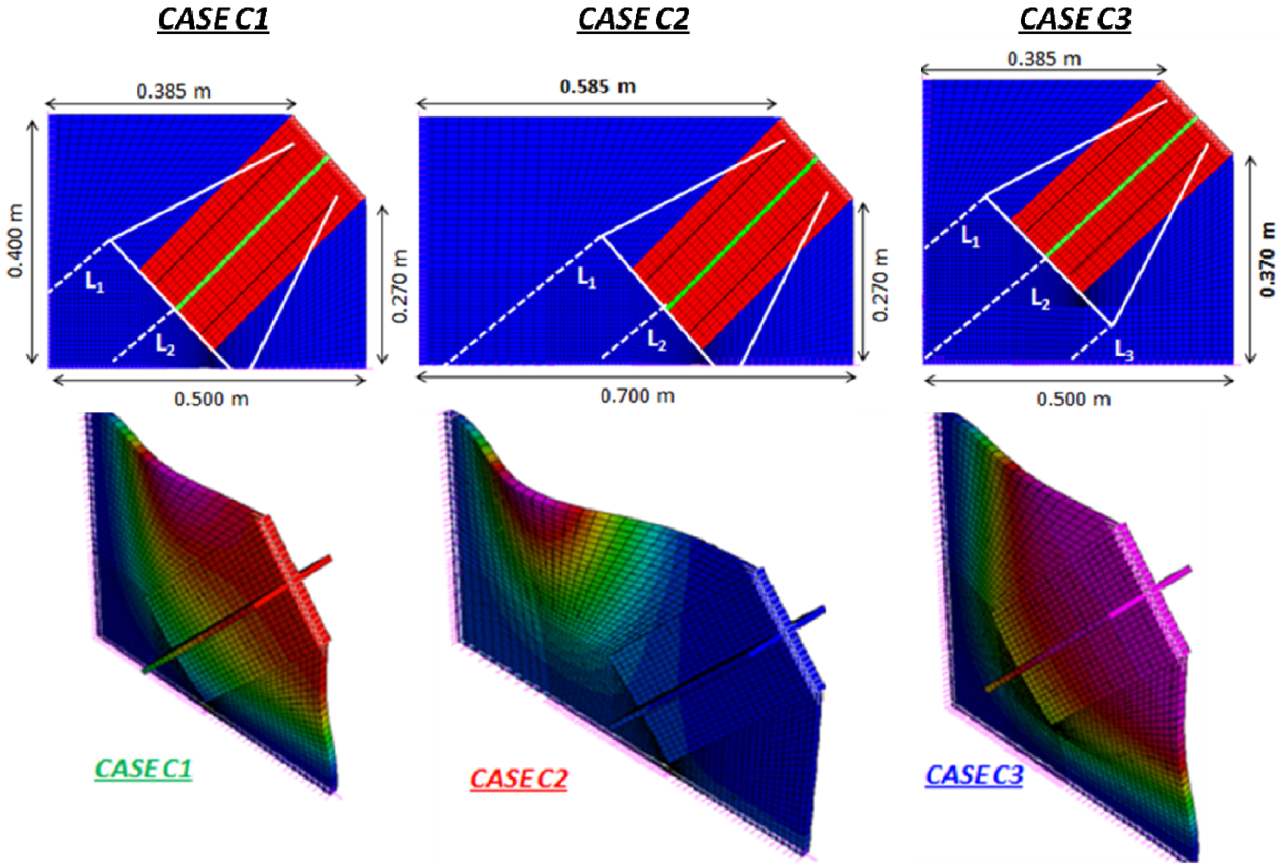
CASE C1
CASE C2
CASE C3
0.385 m
0.400 m
L1
L2
0.270 m
0.500 m
0.585 m
L1
L2
0.270 m
0.700 m
0.385 m
L1
L2
L3
0.370 m
0.500 m
CASE C1
CASE C2
CASE C3

Figure 6.23. Buckling of non compact gusset plates.

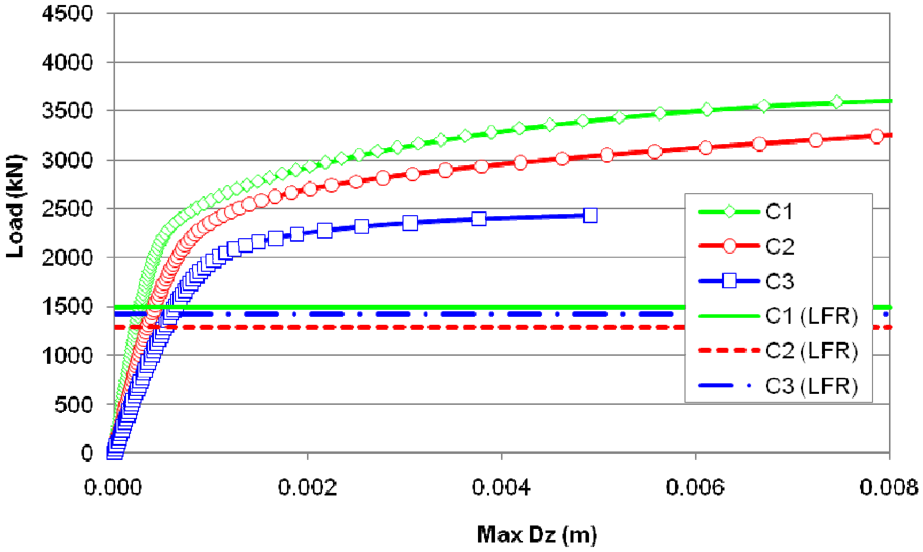

Figure 6.24. Compressive strength of non compact gusset plates.

6.3 BLOCK SHEAR FAILURE

6.3.1 CURRENT GUIDELINES

Block shear failure is a limit state that combines tension failure on one plane and shear failure on a perpendicular plane (Figure 6.24). The guidelines [FHWA, 2009] assume that rupture occurs when one plane reaches the ultimate strength, while the other plane reaches the yield strenght. Therefore, two possible failure modes can develop:

- in the first mode, rupture occurs along the net tension plane and full yield develops along the gross shear plane;
- in the second mode, rupture occurs along the net shear plane while full yield develops along the gross tension plane.

If $A_{tn} \geq 0.58\ A_{vn}$, then (14)

$$P_r = \varphi\ (0.58\ F_y\ A_{vg} + F_u\ A_{tn}) \quad (15)$$

Otherwise: $P_r = \varphi\ (0.58\ F_u\ A_{vn} + F_y\ A_{tg})$ (16)

where:

φ = resistance factor = 0.80 for Load and Resistance Factor Rating (LRFR), or

φ = 0.85 for Load Factor Rating (LFR);

A_{tg} = gross area along plane resisting tension;

A_{tn} = net area along plane resisting tension;

A_{vg} = gross area along plane resisting shear;

A_{vn} = net area along plane resisting shear;

F_u = minimum tensile strength of gusset plate;

F_y = minimum yield strength of gusset plate, and

P_r = rupture load.

Next, we compare these formulas with numerical and experimental results.

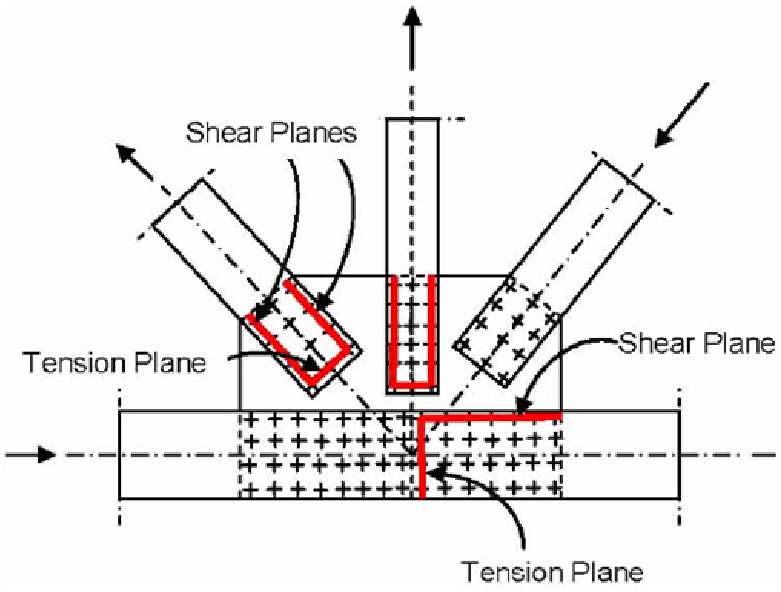
Shear Planes
Tension Plane
Shear Plane
Tension Plane

Figure 6.21. Example of potential block shear rupture planes for gusset plates in tension [FHWA, 2009].

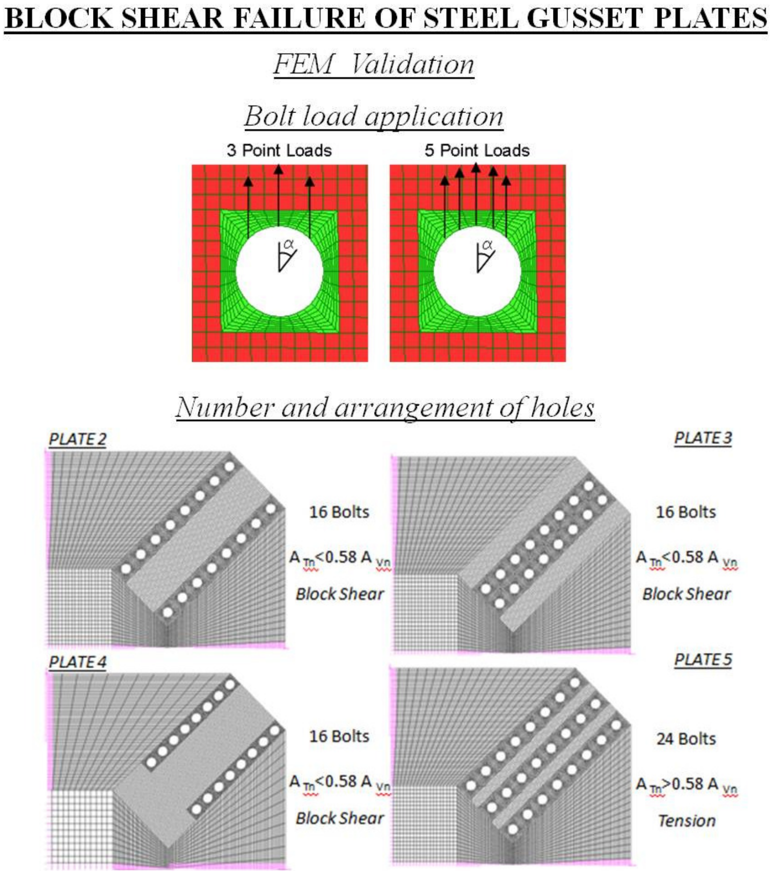
BLOCK SHEAR FAILURE OF STEEL GUSSET PLATES
FEM Validation
Bolt load application
3 Point Loads
5 Point Loads
α
α
Number and arrangement of holes
PLATE 2
16 Bolts
A Tn<0.58 A Vn
Block Shear
PLATE 3
16 Bolts
A Tn<0.58 A Vn
Block Shear
PLATE 4
16 Bolts
A Tn<0.58 A Vn
Block Shear
PLATE 5
24 Bolts
A Tn>0.58 A Vn
Tension

Figure 6.22. Summary of the analyses developed for the block shear failure.

6.3.2 FINITE ELEMENT MODEL

The study uses shell elements with four-nodes, available in commercial software STRAND7 / STRAUS7, to perform nonlinear finite-element analyses of gusset plates under tension. For validation, a test (Figure 6.25) performed at the University of Alberta [Nast, Grondin and Cheng, 1999] is simulated.

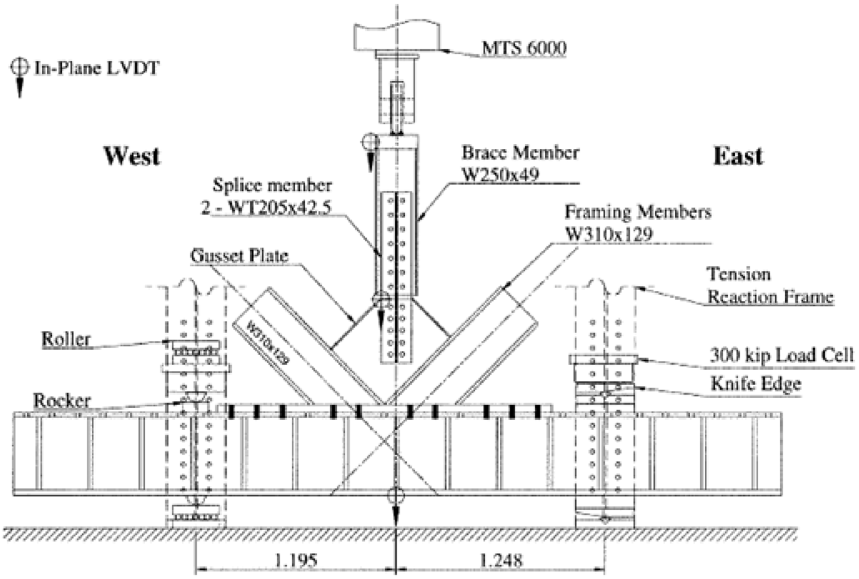
MTS 6000
In-Plane LVDT
West
East
Brace Member
W250x49
Splice member
2 - WT205x42.5
Framing Members
W310x129
Gusset Plate
Tension
Reaction Frame
W310x129
Roller
300 kip Load Cell
Knife Edge
Rocker
1.195
1.248

Figure 6.23. University of Alberta gusset plate test (Nast, Grondin and Cheng, 1999).

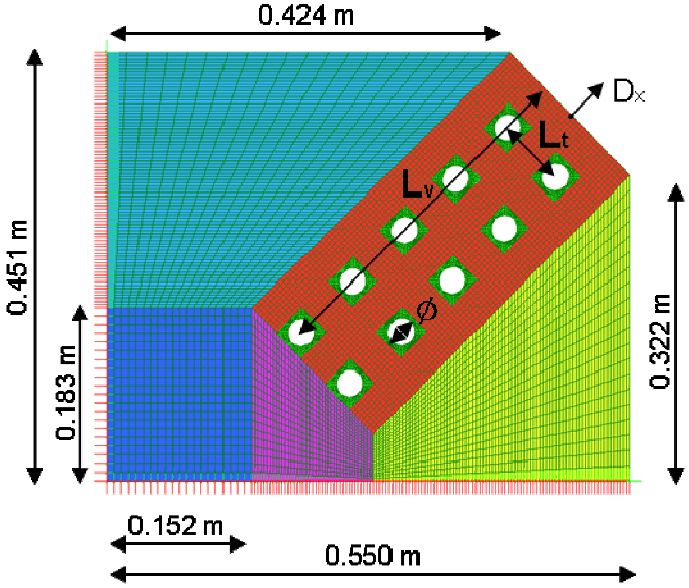
0.424 m
Dx
Lt
Lv
Ø
0.451 m
0.183 m
0.322 m
0.152 m
0.550 m

Figure 6.24. Finite-element model meshed with 9520 elements.

Plate 1 has the dimensions shown in Figure 6.26 (colors are arbitrary), a thickness of *9.61 mm* and ten bolt holes of diameter *24.3 mm* (bolt failure is not part of this study). The model is fixed along the two perpendicular edges at the bottom and left. The analysis accounts for the nonlinearity of the material and large displacements. The material is bilinear elasto-plastic, with Young's modulus of *215 GPa*, yield strength of *410 MPa* and tangent modulus of *2.15 GPa*. The analysis uses true stress and true strain. The tension load is applied by three point loads on the upper half of each bolt hole (Figure 6.27).

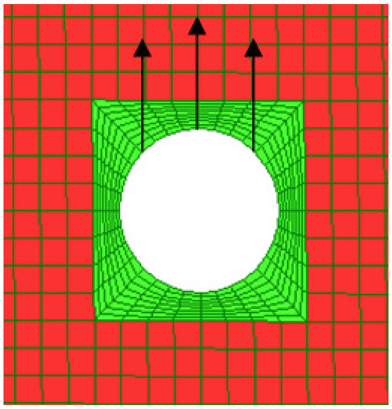

Figure 6.25. Application of bolt loads.

From Equations 15 and 16 and as detailed in Table 6.1 (net area calculations conform with AASHTO, 1994), the gusset plate fails in block shear at an unfactored load ($\varphi = 1.0$) of *1512 kN.*

Table 6.1. Calculation of block shear capacity.

Tension	Eq. (15)	Shear	Eq. (16)
L_t	73.8 mm	L_v	306 mm
t	9.61 mm	t	9.61 mm
Ø	24.3 mm	Ø	24.3 mm
$Ø_{nom}$	27.5 mm	$Ø_{nom}$	27.5 mm
A_{tg}	710 mm^2	A_{vg}	5880 mm^2

f_y	410 MPa	f_y	410 MPa
f_u	600 MPa	f_u	600 MPa
A_{tn}	446 mm^2	A_{vn}	3510 mm^2
		0.58 A_{vn}	2030 mm^2
P_u	1819 kN	P_u	1512 kN

Note: P_u is P_r with $\varphi = 1.0$

6.3.2.1 FINITE ELEMENT MESH

Two levels of mesh refinement were used to model the regions of stress concentration around the bolt holes (Figure 6.28) where failure would likely initiate. In Figure 6.29 the load-displacement response of the node in the middle of the oblique edge is used to compare the test and numerical results from the University of Alberta with the unfactored FHWA value P_u, the LRFR value 0.80*P_u, and the finite-element results for the coarse and the fine mesh.

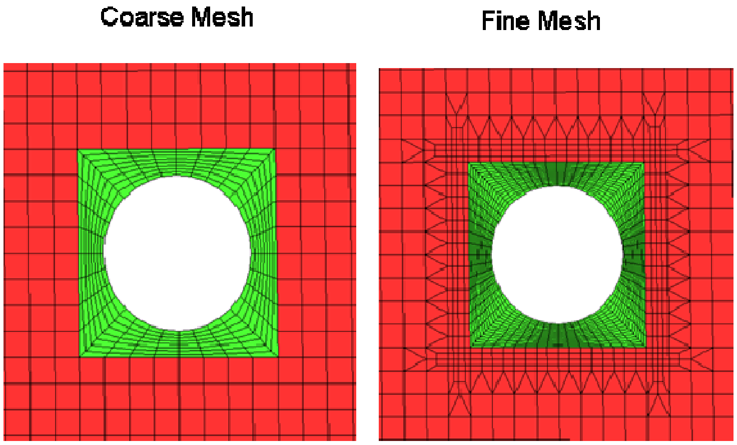

Figure 6.26. Mesh refinement around holes.

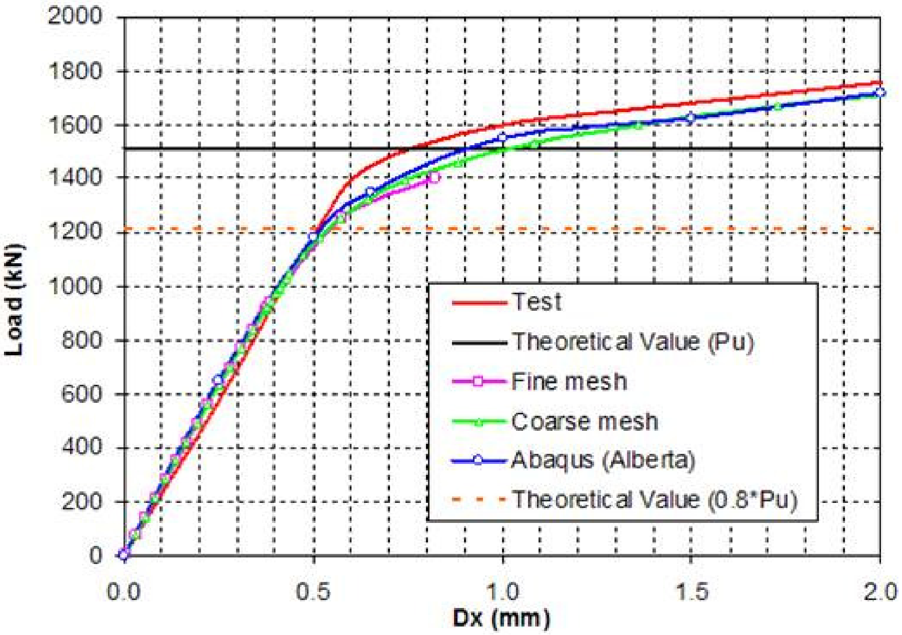

Figure 6.27. Results of mesh study.

Results from the present two STRAND7/STRAUS7 meshes agree well with the ABAQUS model used by the University of Alberta. All three finite-element results slightly underestimate the test results, especially at the onset of yielding. The LRFR value falls on the limit of the elastic range, whereas the unfactored FHWA value produces a small amount of yielding. The time-consuming fine mesh analysis was deliberately terminated prematurely once it had exceeded the elastic range and appeared to track the coarse mesh results. The coarse mesh was used in the rest of this study.

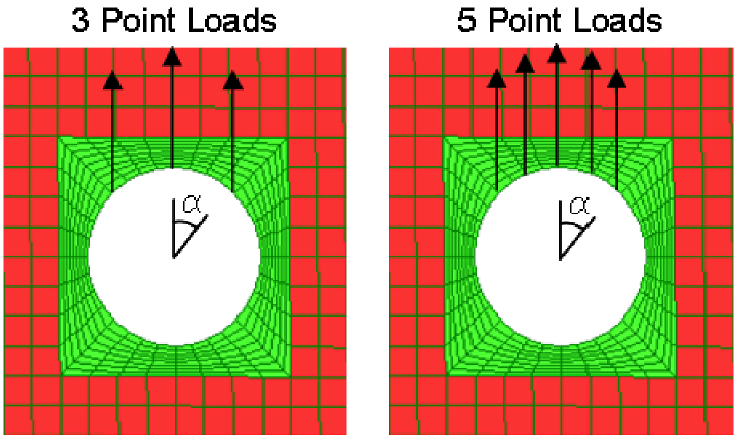

Figure 6.28. Coarse and fine bolt load application.

6.3.2.2 BOLT LOAD APPLICATION

The previous finite-element results predict premature yielding compared to test results. One possible reason is the bolt load, which is applied in a concentrated fashion at three nodal points for each bolt hole. In the next step, the bolt load are distributed to five points over a 90° arc (Figure 6.28), following a sinusoidal distribution, $P = P_0 \cos \alpha$, where $-45° \leq \alpha \leq 45°$.

Figure 6.29 compares the FHWA values, the test results and the results for the coarse and fine bolt load applications. There is not much difference between the results for the two bolt load applications. Figure 6.29 also shows results for one point load per hole, which has numerical convergence issues. In the rest of the study, three point loads per hole are used.

It is not clear from Huns, Grondin and Driver, 2002, whether they measured the yield strength of the plate they tested or reported the nominal yield strength. Since the nominal value could be 5 to 10% less than the actual value, its use could explain the difference between the numerical and the experimental results.

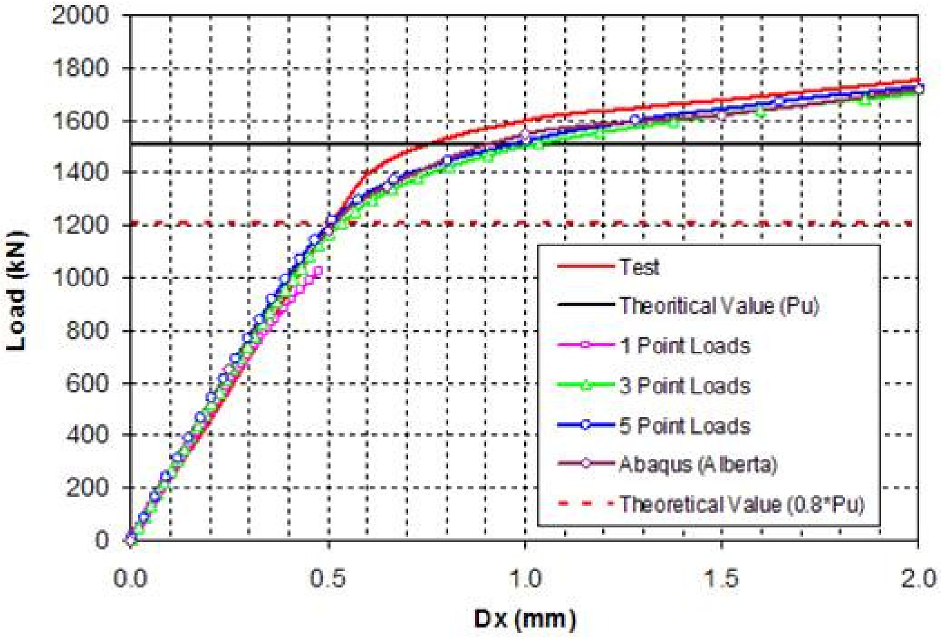

Figure 6.29. Results for coarse and fine bolt load applications.

6.3.2.3 NUMBER OF ARRANGEMENT OF HOLES

Next the influence of the number and arrangement of the perimeter bolt holes on the maximum load and displacement at failure was investigated (previous finite-element parametric studies, such as Topkaya, 2004, are acknowledged). It is therefore possible to show that, although the FHWA loads are safe, the degree of safety and the ductility of the connection vary with geometry. In the following analyses, the chosen criterion for structural failure is the attainment, anywhere, of a maximum strain of ± 100 %, as justified in Huns, Grondin and Driver, 2002. In the next three cases, the number of holes is increased to 16, but their diameter and all the other plate dimensions are the same as before. As well, the displacements of interest continue to be at the middle of the oblique side (Figure 6.24).

Plate 2

Plate 2 has a tension length L_t of *0.139 m*, a shear length L_v of *0.358 m* and bolt holes arranged as shown in Figure 6.30. Since $A_{tn} < 0.58\ A_{vn}$, failure is by block shear. Figure 6.30 show the maximum and minimum principal strain (ε_1, ε_3) contours and the load-displacement curve of this gusset plate at various load steps. In Figure 6.30, elastic regions are in color whereas plastic regions (ε_y is the yield strain) and the holes are in white. As expected, straining is most intense between the holes, yielding initiates near the holes, then spreads to the connecting regions. The strain contours are compatible with eventual rupture along the shear plane while full yield develops across the tension plane between the two end holes. Figure 6.33 shows an ultimate load of *2720 kN* at a displacement of *14 mm*, and thus the LRFR value provides a factor of safety of ultimate load/LRFR value = *2720 kN/1267 kN = 2.15.*

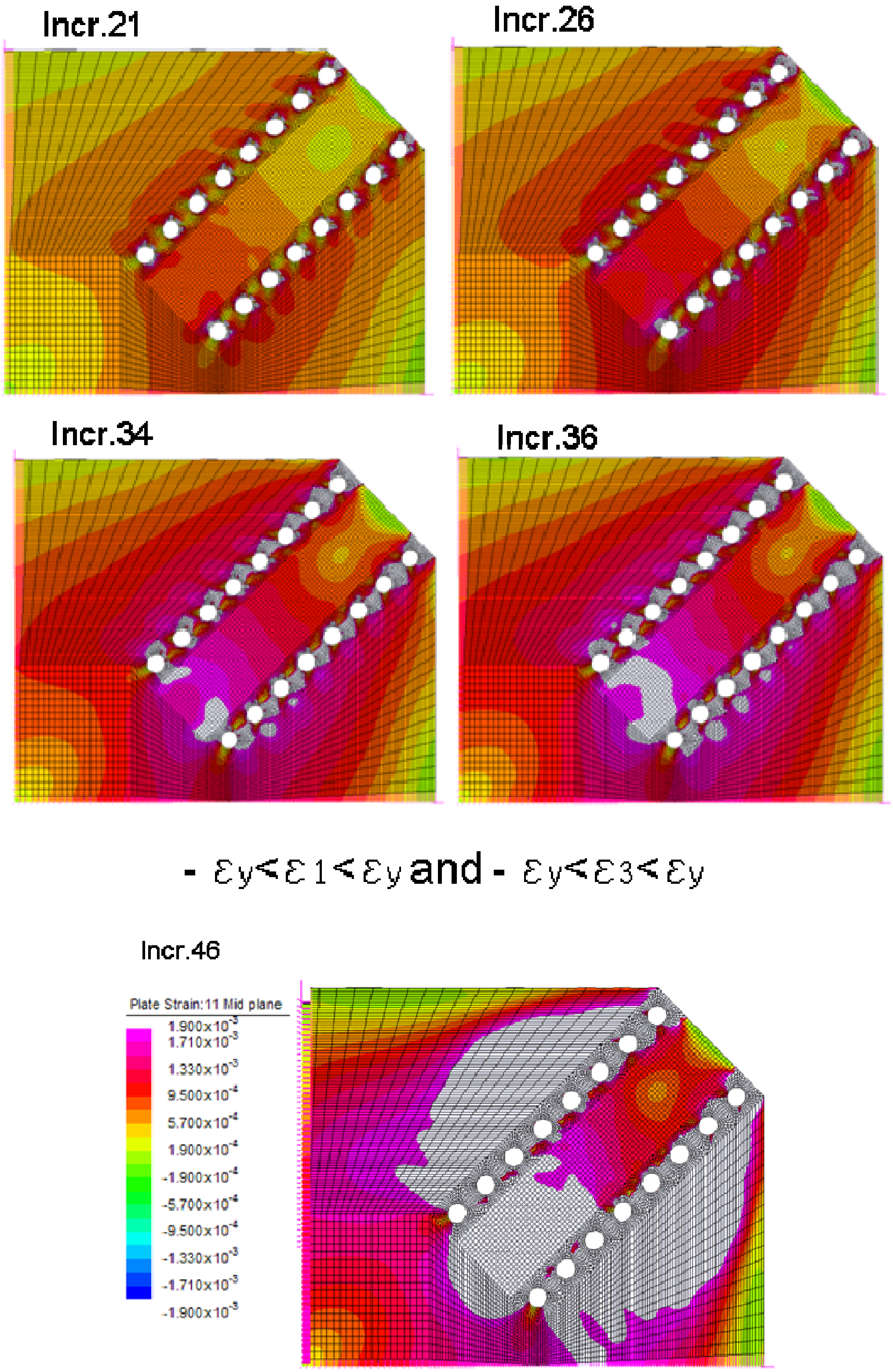

Figure 6.30. Strain contours of Plate 2 (A_{tn}< $0.58A_{vn}$).

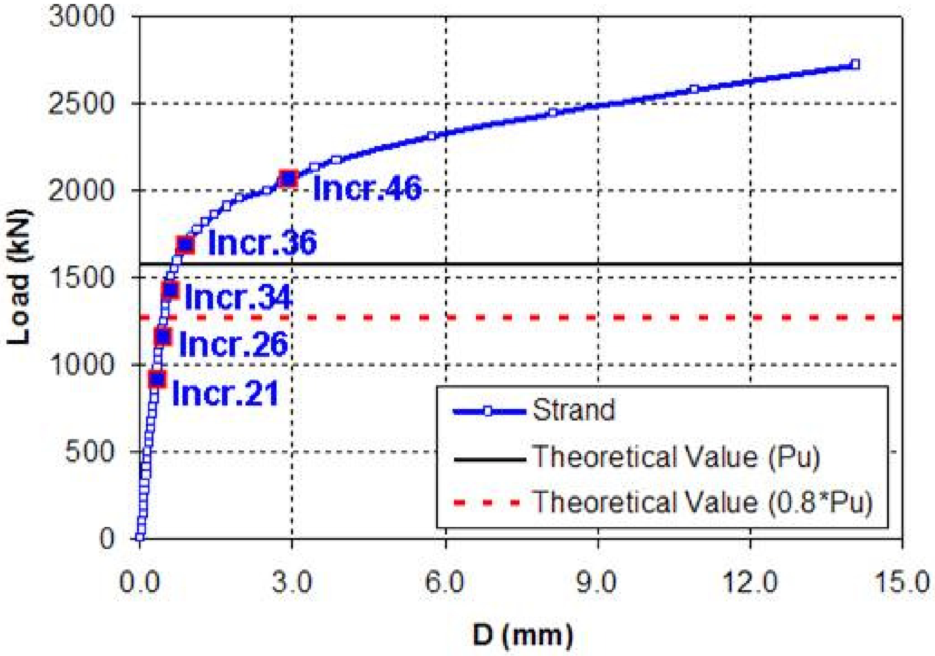

Figure 6.31. Load displacement for Plate 2.

Plate 3

The bolts in Plate 3, shown in Figure 6.32, are distributed over a narrower width. The gusset plate has a tension length $L_t = 0.0462\ m$ and a shear length $L_v = 0.358\ m$. Again, since $A_{tn} < 0.58\ A_{vn}$, failure is by block shear.

Similar observations about the maximum and minimum principal strain contours and the load-displacement curve can be made for plate 3 as for plate 2.

Figure 6.33 shows an ultimate load of *2088 kN* at a displacement of *14 mm*, and thus the LRFR value provides a factor of safety of ultimate load/LRFR value = *2088 kN/974.4 kN= 2.14.*

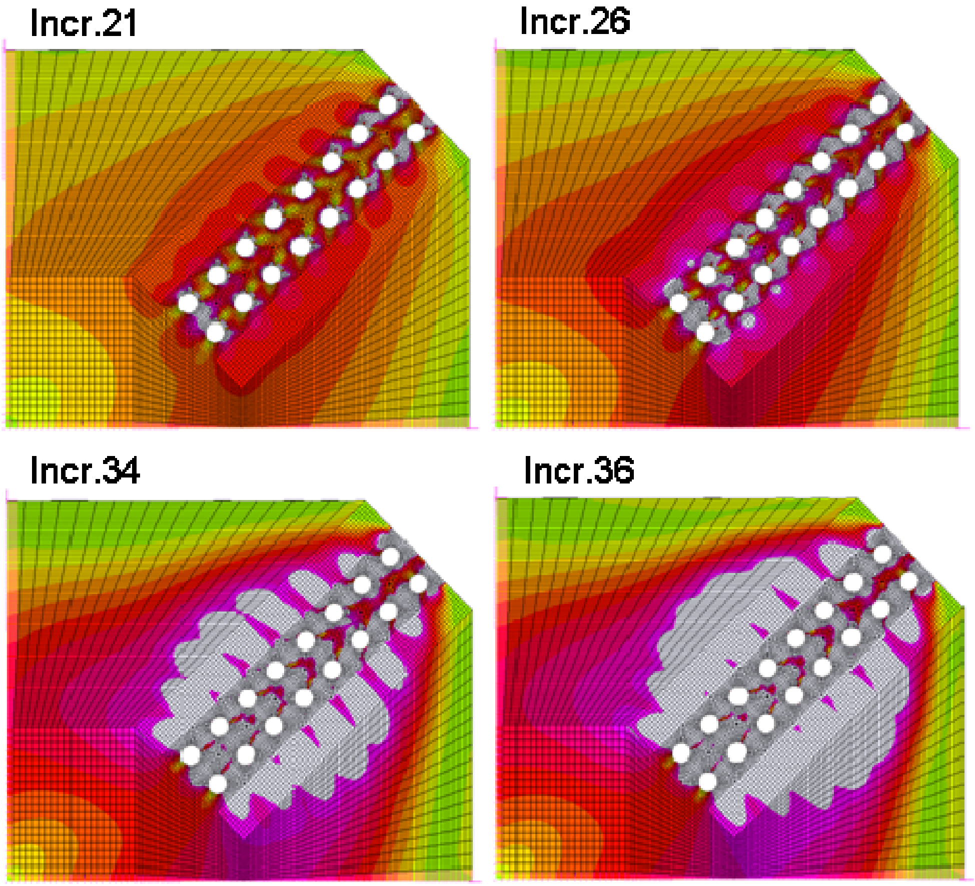

$- \varepsilon_y < \varepsilon_1 < \varepsilon_y$ and $- \varepsilon_y < \varepsilon_3 < \varepsilon_y$

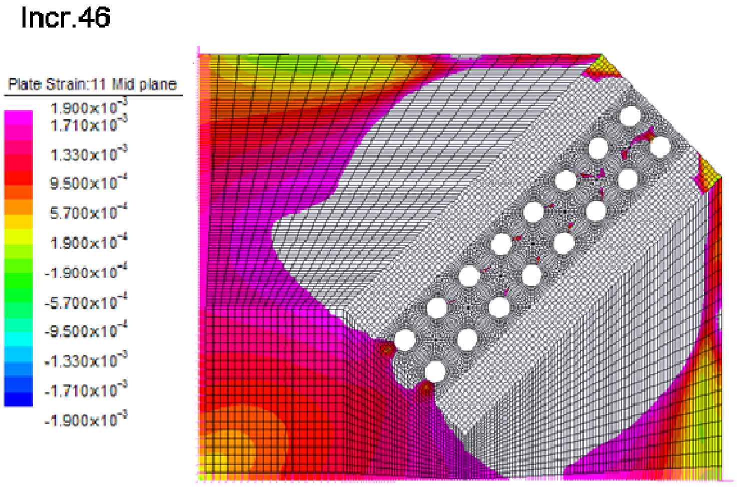

Figure 6.32. Strain contours of Plate 3 ($A_{tn} < 0.58A_{vn}$).

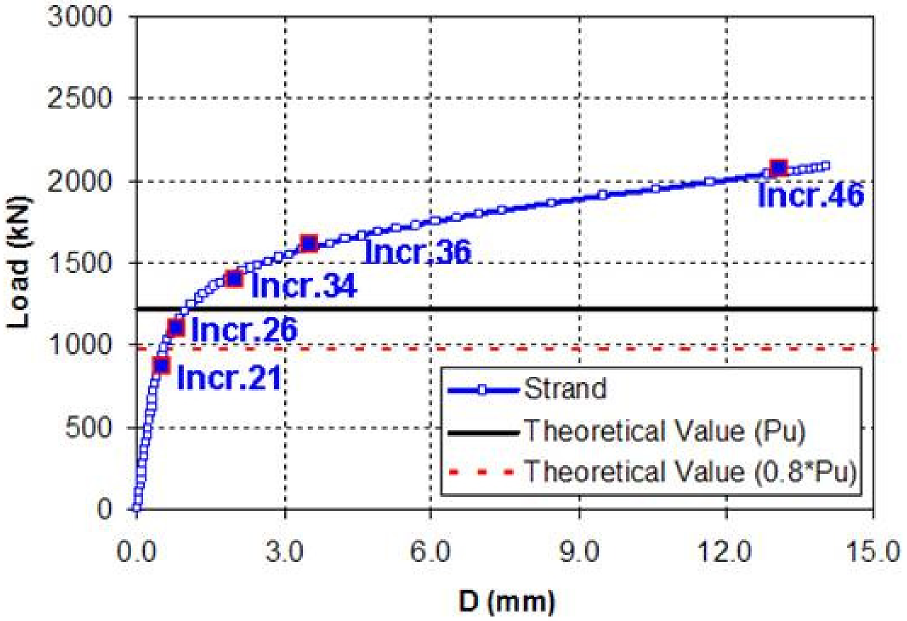

Figure 6.33. Load-displacement curve for Plate 3.

Plate 4

Figure 6.34 shows the results for Plate 4 with tension length $L_t = 0.150\ m$ and shear length $L_v = 0.273\ m$. In this case, $A_{tn} > 0.58\ A_{vn}$ and failure is by tension. Figure 6.35 shows an ultimate load of *2190 kN* at a displacement of *7.8 mm*, and thus the LRFR value provides a factor of safety of ultimate load/LRFR value = *2190 kN/918.2 kN = 2.38.*

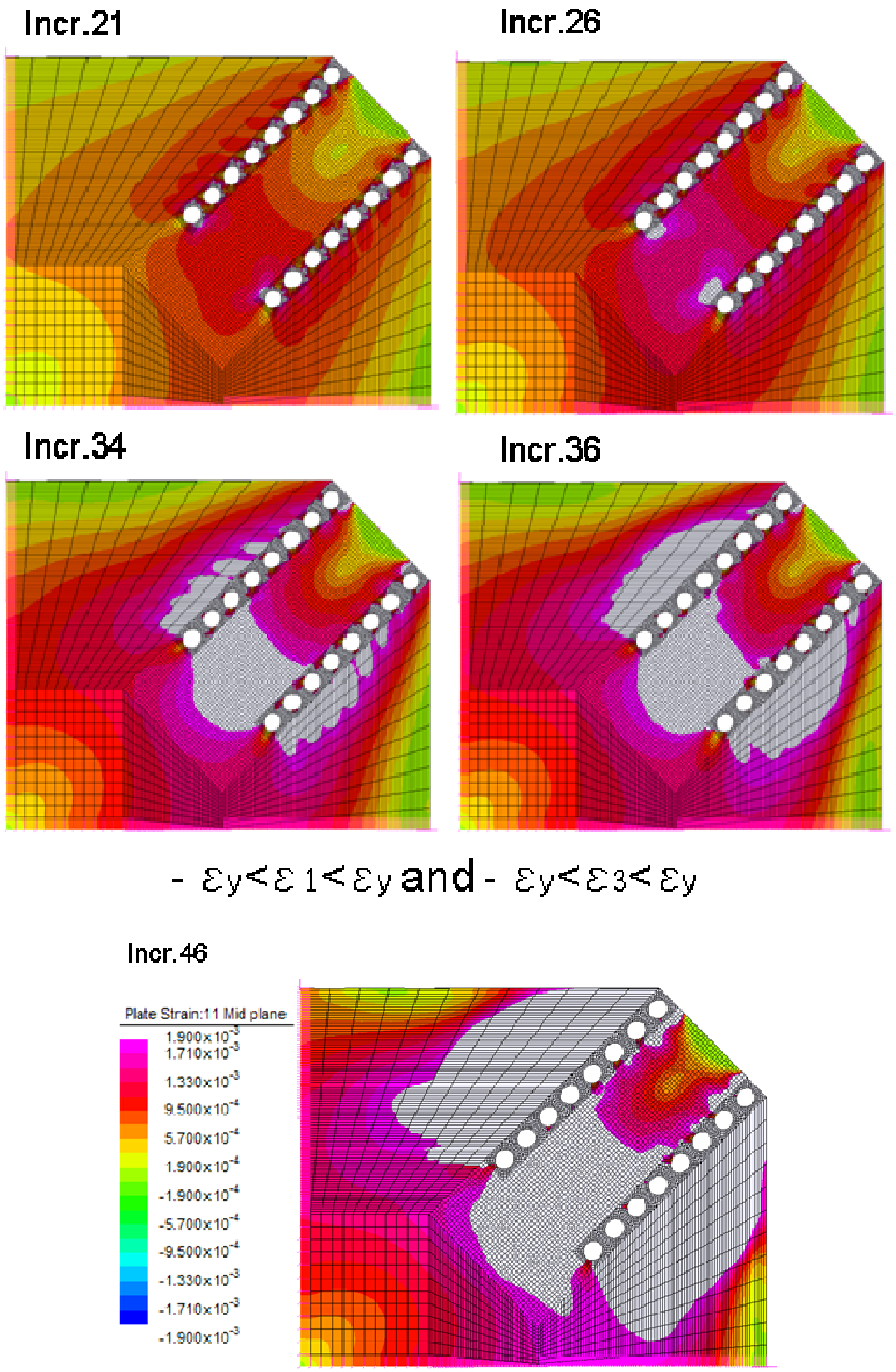

Figure 6.34. Strain contours of Plate 4 ($A_{tn} > 0.58A_{vn}$).

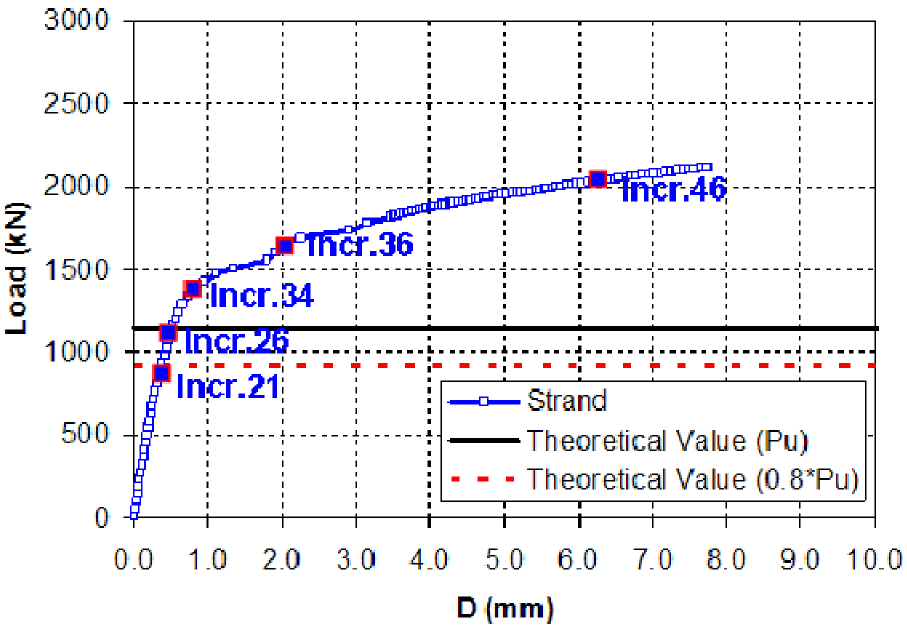

Figure 6.35. Load-displacement curve for Plate 4.

Thus, Plates 2 and 3, which failed by block shear, even though they had rather different hole arrangement, behaved very similarly. Plate 4, which failed by tension, had a slightly higher factor of safety but less overall ductility than Plates 2 and 3. In all cases, the FHWA values are safe and adequate.

Plate 5

Compared to Plate 2, Plate 5 has a third row of bolts. The strain contours shown in Figure 6.36 resolve the strains that exceed yield at the last load step, when the highest strains reach 100 % (at a few localized points). The plot has better resolution and is more instructive when it is limited to strains of 50%. In the last plot of Figure 6.36, the elastic regions and the holes are in white. Figure 6.37 shows an ultimate load of *3468 kN* at a displacement of *47.3 mm*, and thus the LRFR value provides a factor of safety of ultimate load/LRFR value = *3468 kN/1267 kN = 2.73*. Figure 6.37 also shows the beneficial effect of adding internal bolts, which increase the strength and overall ductility of the gusset plate. A simplified analysis that only accounts for the perimeter bolts would underestimate the strength and ductility of the gusset plate.

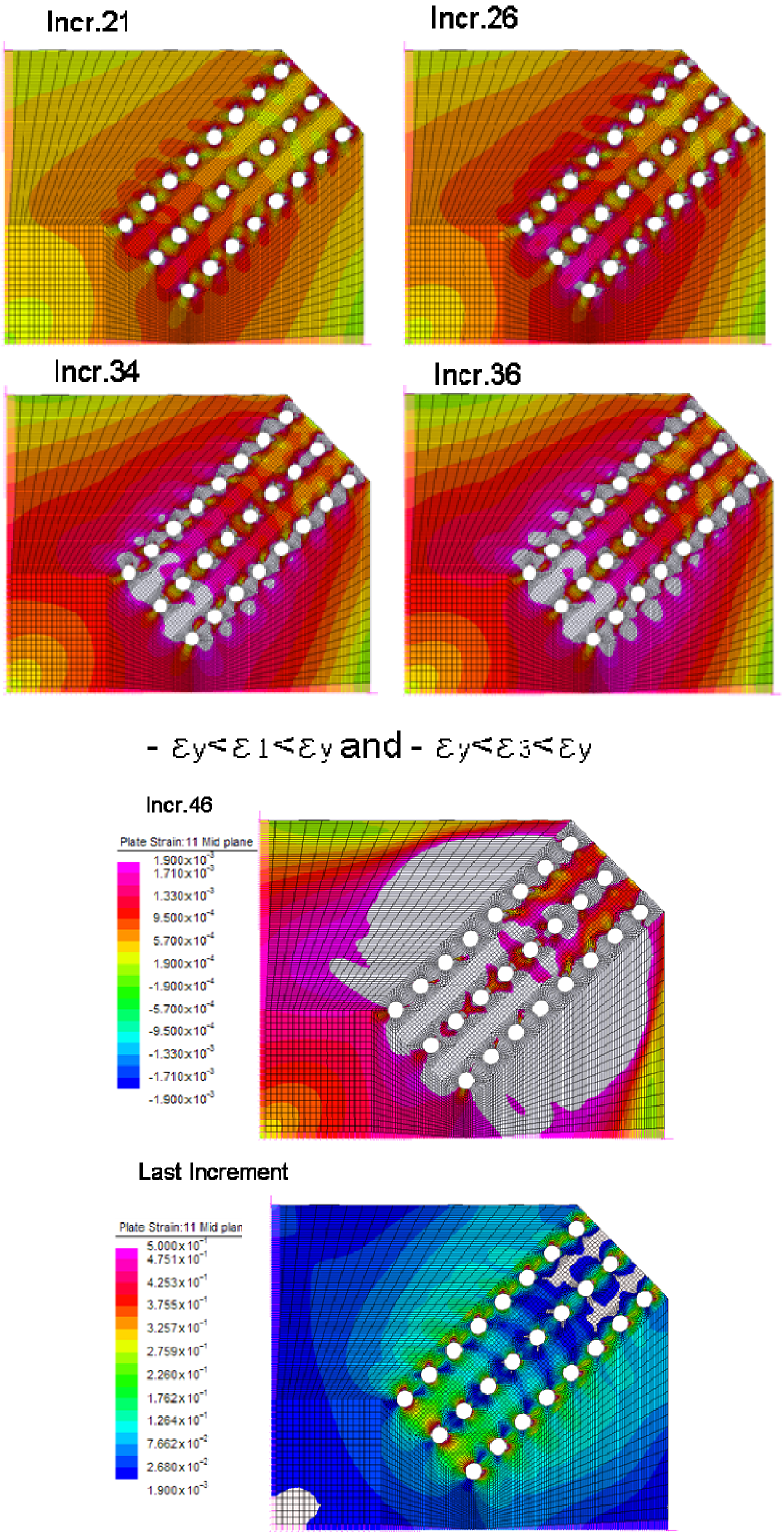

Figure 6.36. Strain contours of Plate 5 ($A_{tn} > 0.58A_{vn}$).

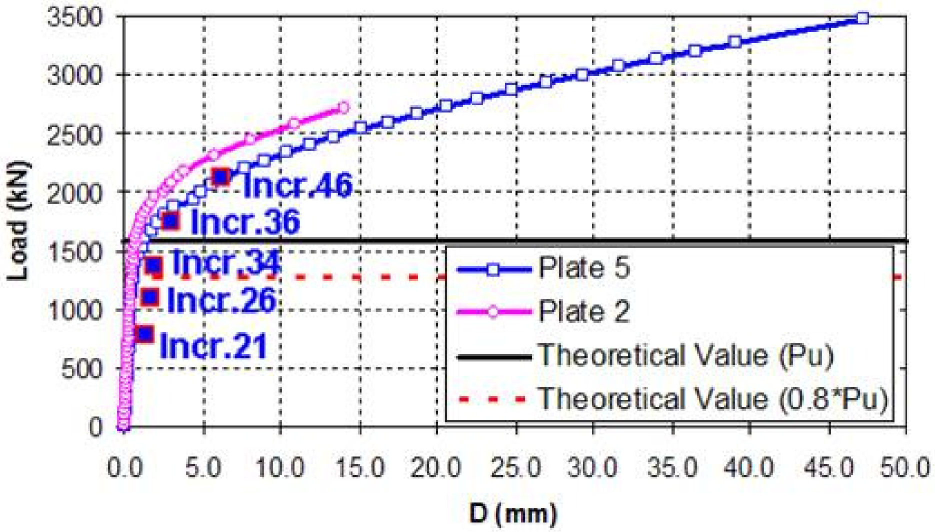

Figure 6.37. Load-displacement curve for Plate 5.

Plate 6

In this last example one of the example plates from the guidance document is analyzed (FHWA, 2009). The gusset plate considered is shown in Figure 6.38 and its steel is elasto-plastic, with Young's modulus of *200 GPa*, a yield strength of *248 MPa*, and a tangent modulus equal to *1%* of the elastic modulus. Failure is by block shear. Figure 6.39 shows an ultimate load of *10750 kN* at a displacement of *43.2 mm*, and thus the LRFR value provides a factor of safety of ultimate load/LRFR value = *10750 kN/4704 kN = 2.28.*

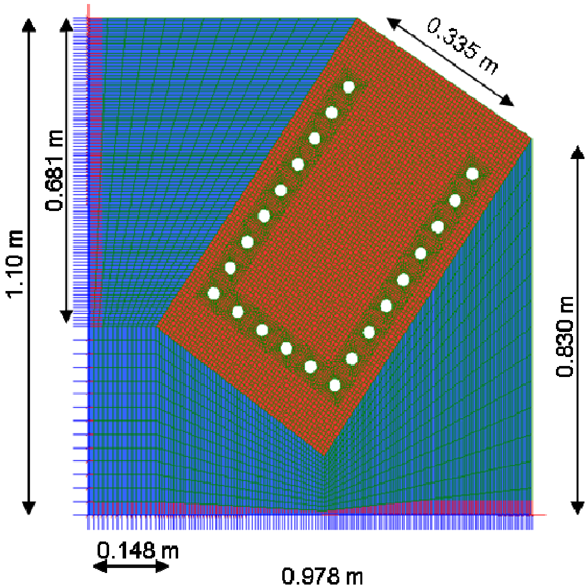
0.335 m
0.681 m
1.10 m
0.830 m
0.148 m
0.978 m

Figure 6.38. Plate 6.

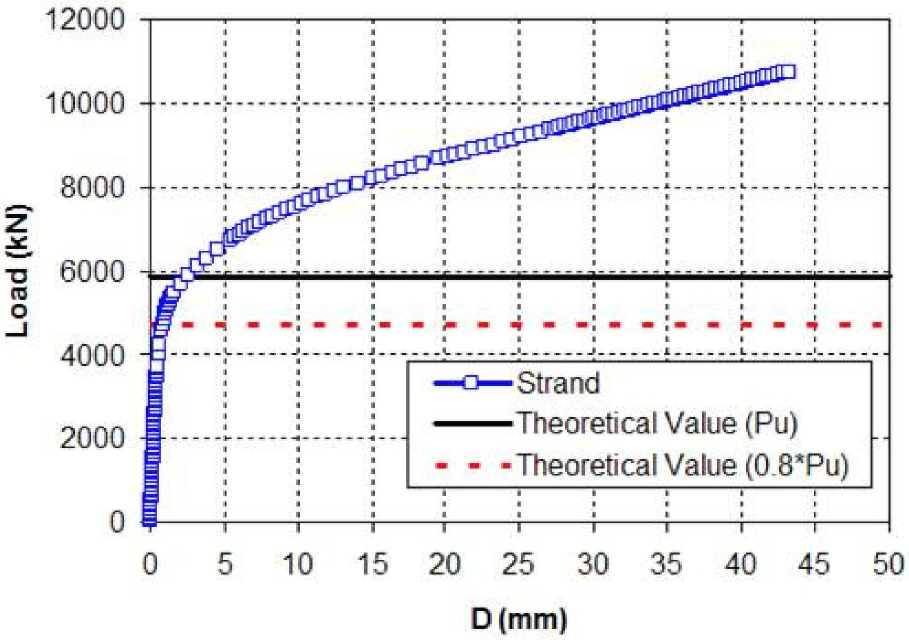

Figure 6.39. Load-displacement curve for Plate 6.

6.4 CONCLUSION

Regarding the bucking failure, a finite-element model of a gusset plate has been developed and verified against experimental measurements. It shows that the FHWA guidelines for load rating, based on the Whitmore equivalent column width, the Thornton column length and SSRC column curves, which assume an initial out-of-straightness of L/1500, are conservative and safe for larger initial out-of-plane deformations up to one plate thickness. This is true for in-plane compressive loads with no moment and no eccentricity. By monitoring the out-of-plane deformations of gusset plates and their rate of change with respect to compressive load, one could obtain a warning of impending instability when these measurements increase suddenly, whether one knows the magnitude of the initial deformations or not.

Moreover, nonlinear finite-element analysis validated by experimental data confirms the safety and validity of the FHWA load rating formulas for the block shear strength of riveted and bolted gusset plates. For a variety of geometries, the LRFR value produces factors of safety between 2.1 and 2.7. This study also provides guidance on the mesh density required around the holes, the application of bolt loads, the effects of geometry, and the approximation involved in modeling the perimeter holes only.

PART III:

GLOBAL RESPONSE OF I35-W BRIDGE BY MEANS OF AFFORDABLE AND ACCURATE MODELING OF CONNECTIONS

7. STORY OF I35-W BRIDGE
8. STRATEGY OF ANALYSIS BY SUBSTRUCTURING METHOD
9. GLOBAL MODEL

7 STORY OF I-35W BRIDGE

7.1 GENERAL DESCRIPTION

The I-35W Highway Bridge spanned across the Mississippi River in Minneapolis, Minnesota. The bridge was designed by the engineering consulting firm Sverdrup & Parcel and Associates and the design plans were approved by the Minnesota Department of Transportation (Mn DOT) in 1965.

The bridge consisted of a three span continuous Warren deck truss with a cantilever overhang at each end, and 11 multi-girder approach span. A view of the main truss from the north side of the I-35W Bridge is shown in Figure 7.1.

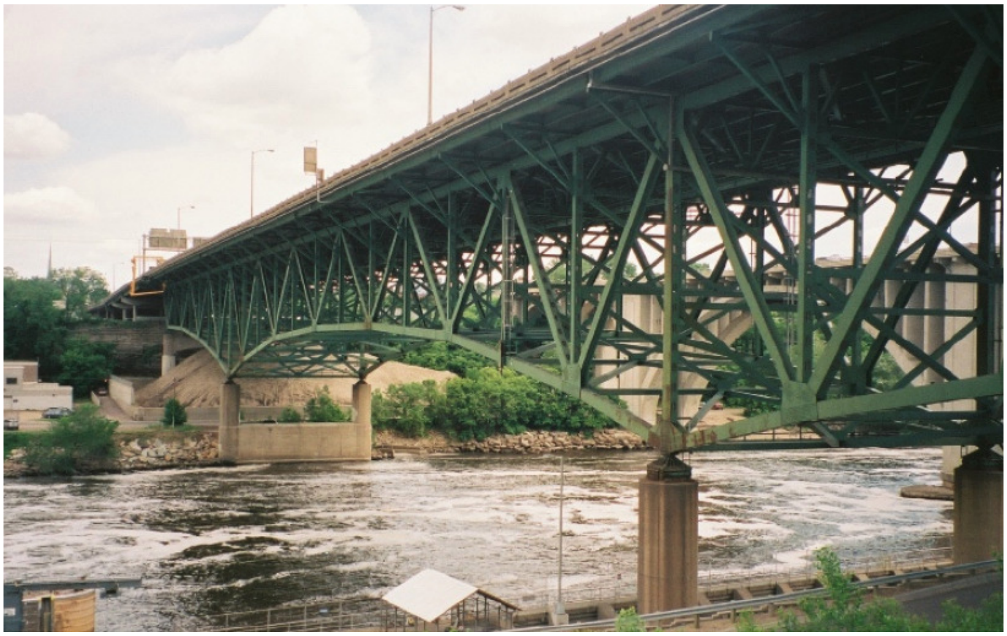

Figure 7.1. I-35W Bridge [NTSB, 2008].

The truss portion of the bridge consisted of two parallel main trusses (east and west) connected through transverse floor trusses supporting the reinforced concrete desk. The end of the beams in the main trusses was connected by riveted gusset plates at 112 nodes (joints) along the truss portion of the bridge. Since it was built, the truss portion of the bridge has undergone at least two major renovations, which led to an increase of the deck thickness from 6.5 inches (165 mm) to 8.5 inches (216 mm) and an increase in size of the center median barrier and outside barrier walls.

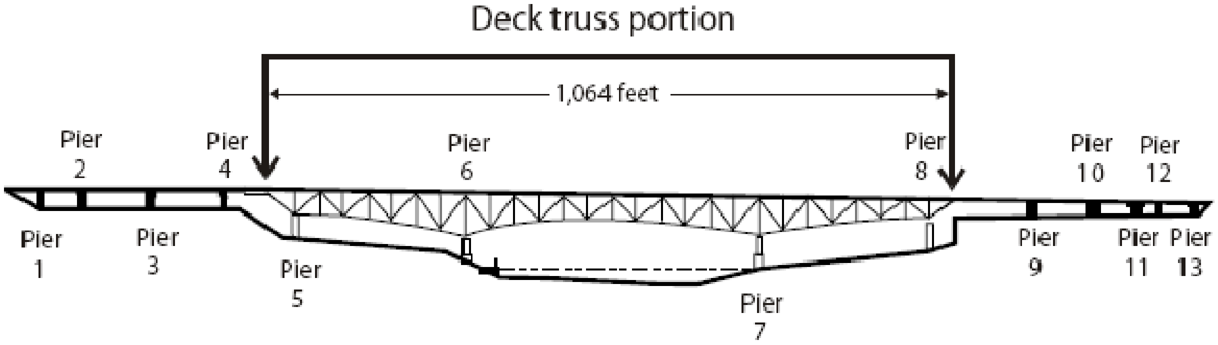

Figure 7.2. Drawing of the bridge, [Ocel, 2008].1064 ft = 324.3 m.

7.2 I35-W HISTORY

The design plans for the I-35W Bridge (Bridge # 9340) were based on the AASHTO 1961 specifications and approved in their final form in 1965. The 1907 ft (581 m) long bridge was opened to traffic in 1967. It is comprised of 14 spans, with the main spans (6 to 8) consisting of a “fracture critical” (i.e., statically determinate) steel deck truss. Over the years, two major renovations increased the dead weight of the bridge. In 1977, the bridge deck surface was milled down to a depth of ¼ in (6 mm) and a 2 in (51 mm) concrete wearing surface was added. The original deck had 1.5 in (38 mm) concrete cover over the top reinforcing bars. The dead load was thus increased by 13.4 % or more than 3 million pounds (13 MN). In 1998, the median barrier was replaced and traffic railings upgraded, resulting in a further increase in dead load of 1.13 million pounds (5 MN) or 6.1 %. At the time of collapse, the bridge deck was being repaved.

7.2.1 I 35W COLLAPSE

At the time of collapse, Wednesday 1 August 2007, loads on the bridge consisted of vehicular traffic as well as construction loads. The NTSB (2008) estimated the construction loads to be 184 380 lbf (820 kN) of gravel, 198 820 lbf (884 kN) of sand, and 195 535 lbf (870 kN) of parked construction vehicles and personnel, for a total estimated weight of 578 735 lbf (2.574 MN). Traffic loads were estimated to be 1 260 326 lbf (5.606 MN).

A video surveillance camera captured the collapse sequence. It showed the south end of span 7 dropping down first. In the north end of the span, a bend appeared in the lower chord members. Over the next 3 seconds, the entire center span separated from the rest of the bridge and fell 108 ft (33 m) into the 15 ft (4.6 m) deep river, with the north end remaining higher than the south end, but the deck remaining level east to west. 13 lives were lost, 145 people were injured, and 17 vehicles were recovered from the water.

The NTSB (2008) investigation showed the collapse was triggered by the buckling of an undersized gusset plate, which was only half as thick (½ in or 13 mm) as it should have been (1 in or 25 mm).

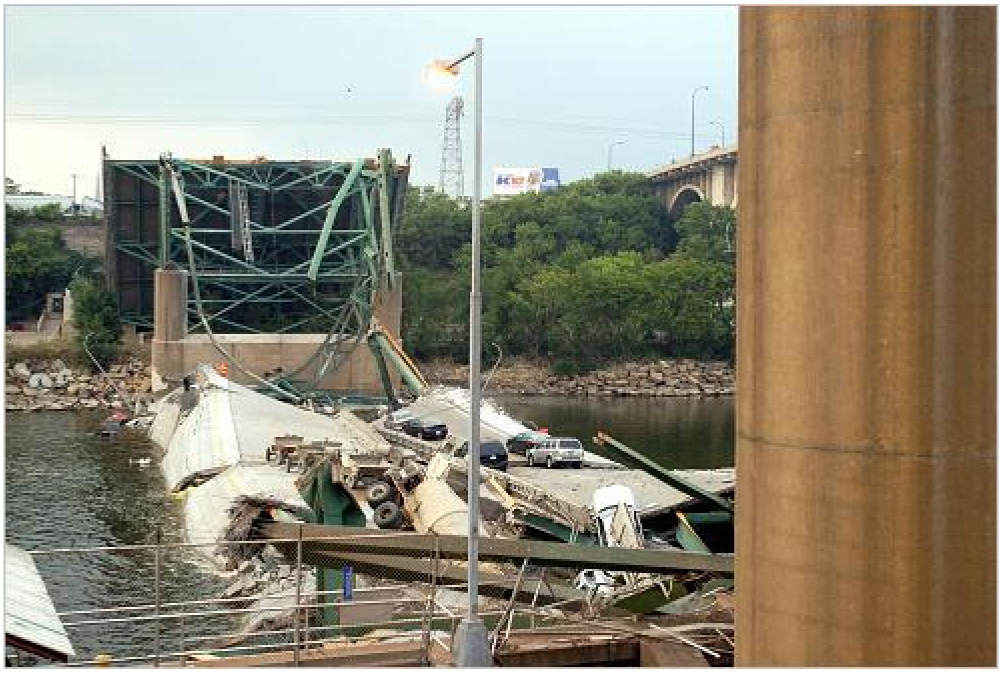

Figure 7.3. http://content.asce.org/I-35W/NTSBI35W.html

7.3 DISCUSSION OF THE ANALYSES DEVELOPED

The bridge was considered to be fracture-critical because the load paths in the structure were non-redundant, meaning that the failure of any major structural element in the bridge would cause a collapse of the entire bridge. The type of bridge is also referred to as non-load-path-redundant bridge.

The main causes of failure that NTSB found was that the gusset plates at joints U10, L11 and a few other locations were undersized for both the design forces and the forces present in the I-35W Bridge at the time of collapse.

Nonlinear stress analysis of the U10 gusset plates without initial imperfection predicts that the region immediately at the end of the compression diagonal (U10-L9) would have been at its yield strength when the bridge was initially constructed in 1967, Figure 8.4. Then the additional dead load and the presence of construction/traffic loads at the time of collapse increased the area of yielding even more, as shown in Figure 7.4.

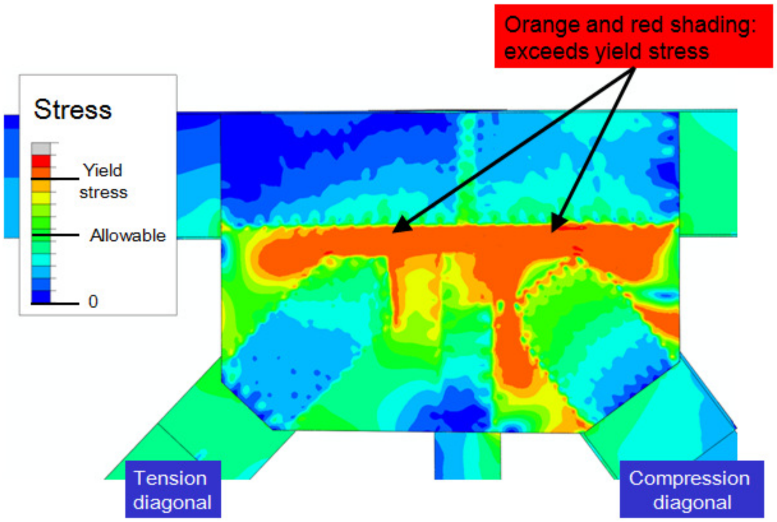

Figure 7.4. Stress with the load at time of accident [Ocel, 2008].

Two different alternative design scenarios were investigated by the NTSB for the gusset plates at U10. In one case the gusset plate thickness was doubled from 0.5 inch (12.7 mm) to 1.0 inch (25.4 mm). In the second case the yield strength of the 0.5 inch (12.7 mm) gusset plate was doubled from 50 ksi (345 MPa) to 100 ksi (689 MPa). Both scenarios eliminated the areas of yielding observed in the as-built gusset plates.

From the analyses conducted, NTSB ruled out any thermal effects on the collapse.

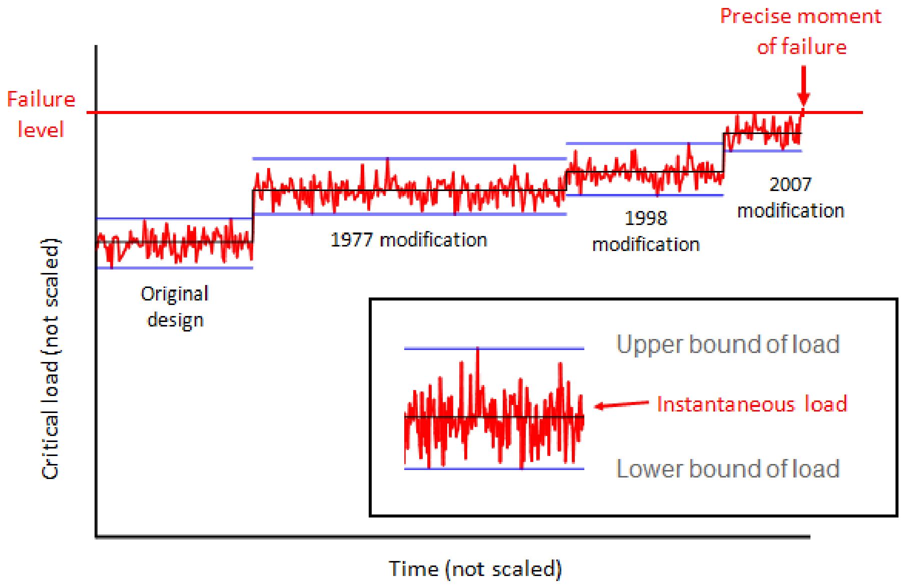

Figure 7.5. Crossing the threshold of failure [Ocel, 2008].

The effect of the corrosion was studied as well, but even that aspect did not change the failure mode predicted by the detailed model that was the inelastic buckling of the gusset plates at the end of the compression diagonal in both the east and west U10 joints.

The presence of initial bowing of the free edge of the gusset plates had a significant effect on the critical buckling load and the mode shape. In fact when an imperfection was added in accordance to photographic evidence, the failure mode of U10 gusset plates changed to side-sway buckling to the west with significant lateral movement of the compression diagonal, as was observed in the field. Perfectly flat gusset plates would have withstood a 26 % increase in the applied construction load over the collapse load, which could have allowed the bridge to serve normally until its planned replacement.

In conclusion, the initiating event in the collapse of the I-35W Bridge was a lateral instability of the upper end of the L9/U10W diagonal member and the subsequent failure of the U10 node plates on the center portion of the deck truss. Because the deck truss portion of the I-35W Bridge was non-load-path-redundant, the total collapse of the deck truss was unavoidable once the gusset plates at the U10 nodes failed [Ocel, 2008].

The Highway Accident Report of the NTSB further points out that, if the gusset plates had been designed in accordance with the American Association of State Highway Officials specifications (with their thickness doubled), they would have been able to safely sustain these loads, and the accident would not have occurred.

Moreover contributing to the accident was the inability among State transportation officials of gaging the effects of distortion or bowing of members and connections during inspection, and of excluding connections in load rating analyses.

The present work aims at developing a methodology that accounts for the stiffness and strength of gusset plate connections in global analysis without having to go to the kind of detailed analysis required for a collapse investigation. It follows other detailed investigation of the effects of initial imperfection, stiffness of framing members, and distribution of loading from members to gusset plates.

8 STRATEGY OF ANALYSIS BY SUBSTRUCTURING METHOD

8.1 INTRODUCTION

From the literature review, chapter 6, it is seen that there are simple design methods based on equilibrium and elastic behavior and prove to be safe by experiments. There is, however, no simple way of calculating the actual behavior of a gusset plate, even in the elastic range. Designers ensure that the connections are stronger than the members and then proceed with a structural analysis that assumes rigid connections. Such a structural analysis is incapable of predicting connection failure, or account for the flexibility of the connection in the global behavior of the structure.

At the other extreme of structural analysis they are detailed models such as the one analyzed by the National Transportation Safety Board (NTSB) as a result of the collapse of the I-35 W Bridge (NTSB report). Forensic investigation had already pinpointed and preliminary analysis confirmed that the trigger of the collapse was the buckling of the undersized joint U10. So there was a justification in performing a detailed FE analysis of joint U10 to replicate the collapse.

The approach proposed here is to replace the FEM of gusset plates with springs to incorporate into global analysis. These springs are capable of capturing the linear and non linear behavior of gussets up to failure. The spring stiffnesses are determined from FEA and once they are installed in the global model, they can simulate the actual behavior of the structure.

The results will not be as accurate as NTSB, but the cost will also be much less, especially if many load cases need to be run, and if the connection can be generalized to other locations. On the other hand, results will be more accurate than those obtained with rigid connection, linear analysis, as is currently done.

8.2 FINITE-ELEMENT MODEL OF I-35W

All the modeling was done using the ABAQUS software [ABAQUS, 2007] with nonlinear material and geometry effects included. Each gusset plate of the detailed model was composed of *289 000* elements, whose in-plane size was *5 mm* (*0.2 in*) in highly stressed regions and less than *15 mm* (*0.6 in*) elsewhere [NTSB, 2008].

The gusset plates were modeled using four-node shell elements (S4R) as were truss members for a distance equal to *2d* from the edge of the gusset plate (*d* is the member depth). The rest of the members and all the other steel members not connected to the joint were modeled using two-node beam elements, with the concrete deck and piers modeled with shell elements. Except for a couple of connections modeled in detail, all connections are fixed.

The approach of concentrating computational resources on the suspected joint improves the efficiency of the finite element analysis. All the plates were modeled at mid-thickness. The members were assumed to be elastic, while the gusset plates and the splice plates were modeled with non linear material properties.

The global beam and shell models of the bridge provided by FHWA will be called “FHWA structural element bridge models” [FHWA, 2008].

Eight FEM of the whole I-35W bridge were used by FHWA throughout the investigation. Each model iteration was slightly modified by FHWA as more information became available, better techniques were incorporated and different local models and their combination were embedded.

Such a detailed analysis is clearly beyond routine design and requires advanced skills and powerful computers.

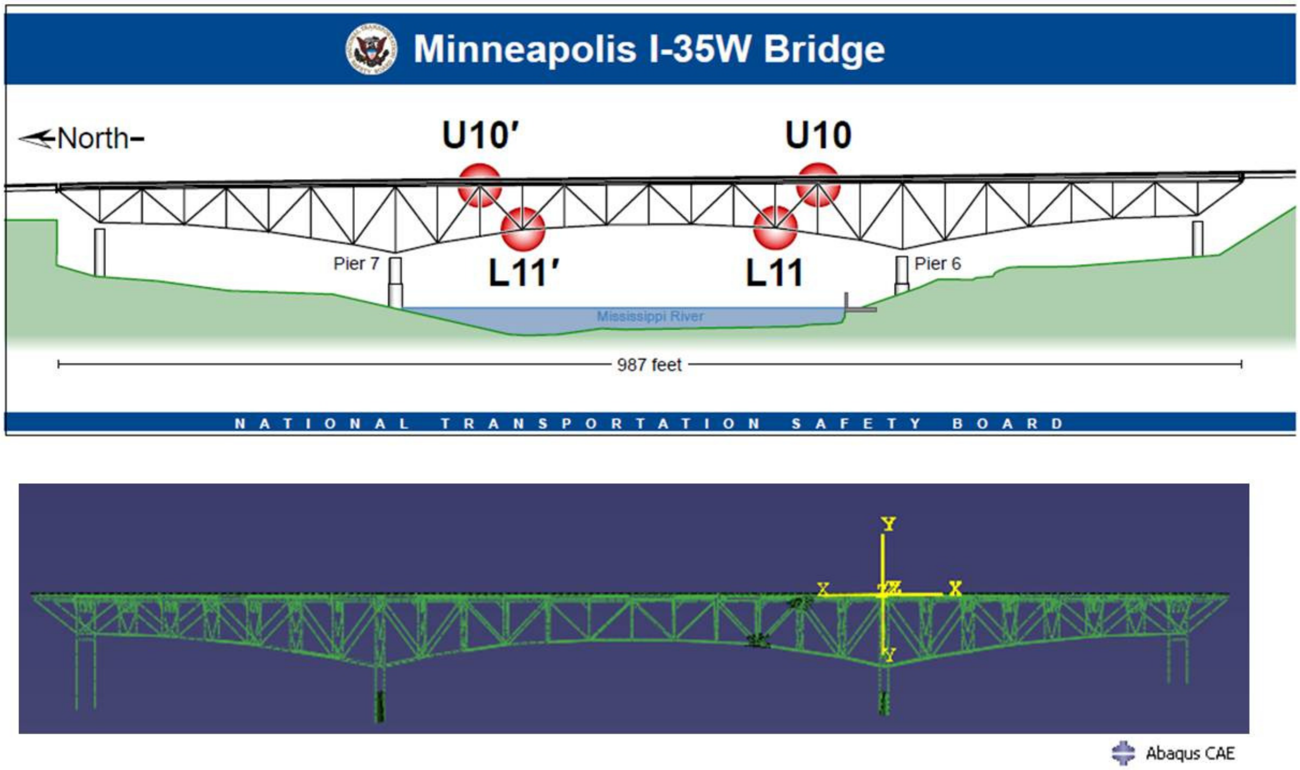
Minneapolis I-35W Bridge
North
U10′
U10
L11′
L11
Pier 7
Pier 6
Mississippi River
987 feet
NATIONAL TRANSPORTATION SAFETY BOARD
Y
X
X
Y
Abaqus CAE

Figure 8.1. NTSB model.

8.3 JOINTS IN DETAIL

Detailed finite element analyses are conducted using ABAQUS (ABAQUS, 2007).

The main truss members are extended for *0.97-1.48* m (depending on the member, see Fig.8.2) beyond the gusset plate to ensure there are no localized stress effects near the connection due to the beam to shell element transition in the global model of the bridge.

The ends of each element are capped with 50.8 mm thick steel shell elements In Figure 8.2 the dimensions of the joint U10-W taken under study are shown. This joint is created by 5 members with different sections and by two gusset plates with thickness of *13 mm*.

Figure 8.3 shows the l dimensions of these sections.

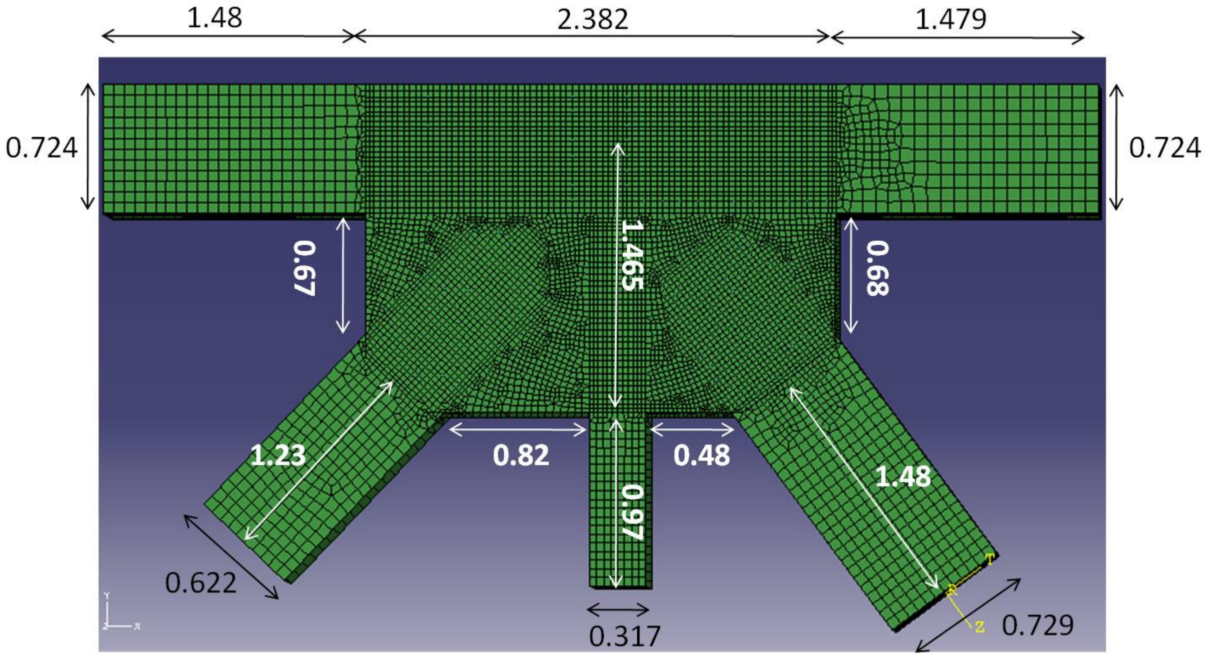

Figure 8.2. Joint dimensions (m).

Rivets and rivet holes are not modeled in either the gusset plates or the truss members. Instead, a node is purposely placed at the center of each rivet in both the gusset and the main member plates. A rigid link between these adjoining nodes is used to represent the rivet. The rigid link element is the ABAQUS *MPC BEAM which is a multi-point constraint that locks all the degrees of freedom together between the linked nodes.

Nonlinear springs were meshed between the truss members and the gusset plate around the perimeter of the truss members at the points of contact. These springs were assigned a low opening stiffness of 0.0001 kips/inch (17.5 N/m) and a high closing stiffness of 10000 kips/inch (1.75 MN/mm) [Ocel, 2008].

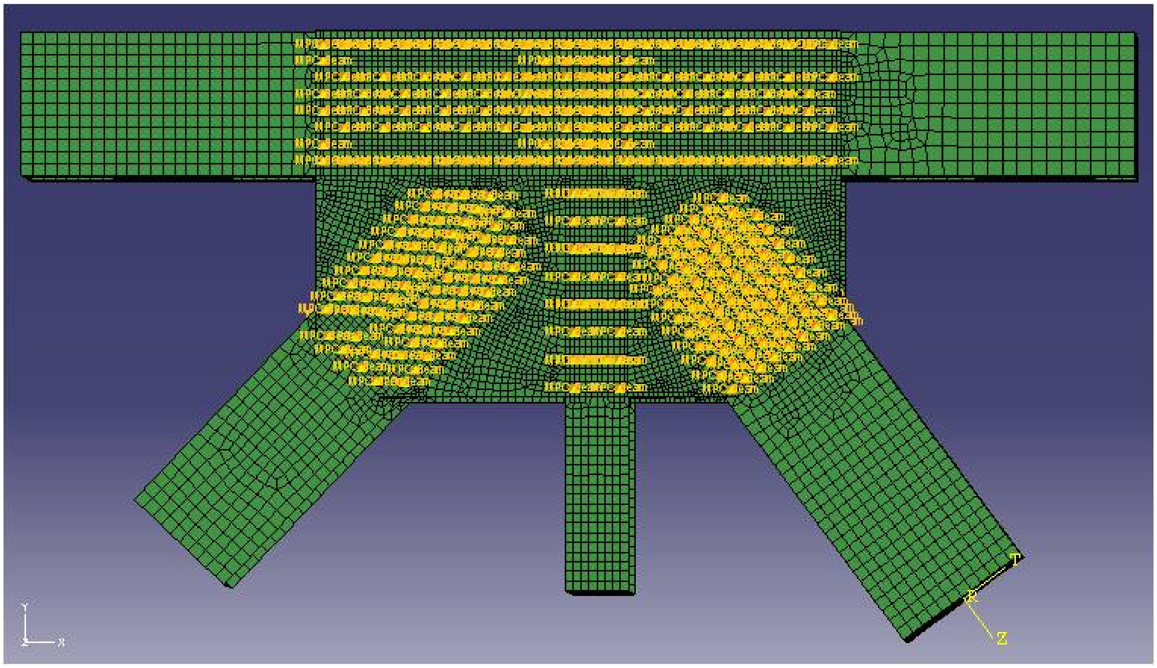

Figure 8.3. Posistion of the rigid links modeling the rivets.

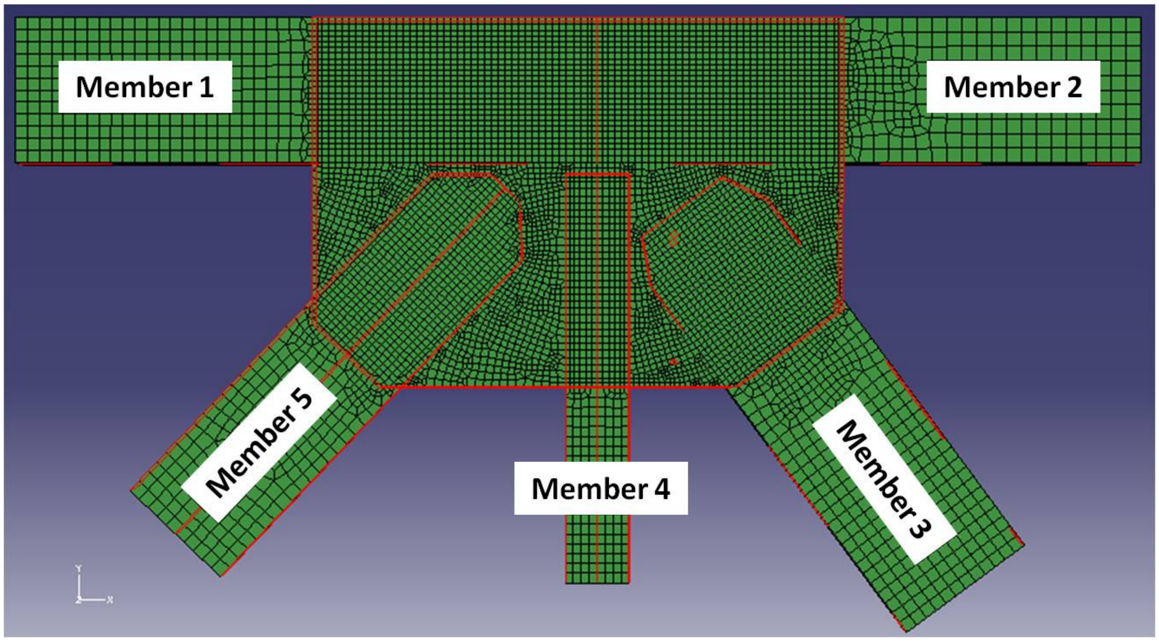
Member 1
Member 2
Member 5
Member 4
Member 3
Y
X

Figure 8.4. Members in joint U10.

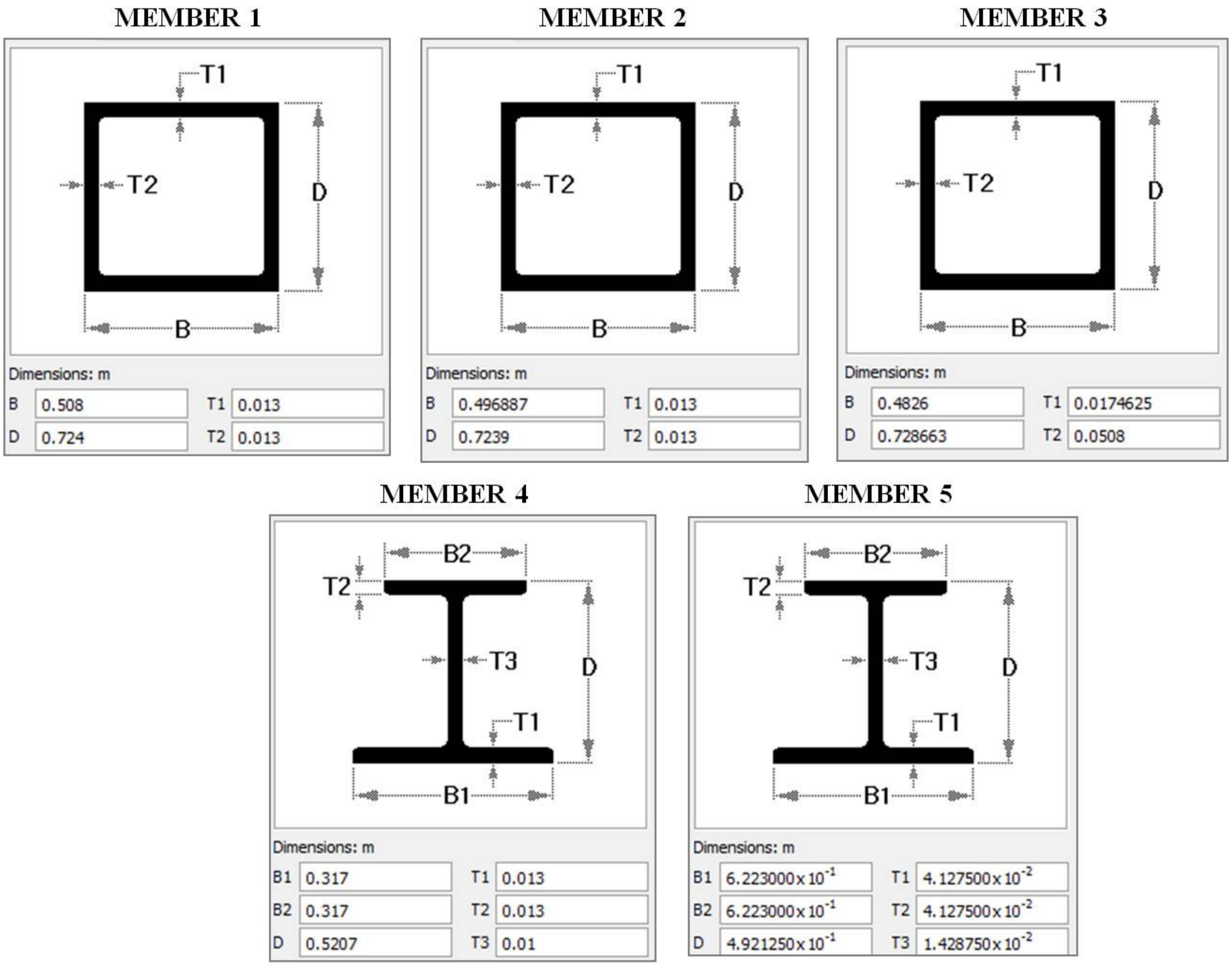

MEMBER 1

Dimensions: m

B 0.508
T1 0.013
D 0.724
T2 0.013

MEMBER 2

Dimensions: m

B 0.496887
T1 0.013
D 0.7239
T2 0.013

MEMBER 3

Dimensions: m

B 0.4826
T1 0.0174625
D 0.728663
T2 0.0508

MEMBER 4

Dimensions: m

B1 0.317
T1 0.013
B2 0.317
T2 0.013
D 0.5207
T3 0.01

MEMBER 5

Dimensions: m

B1 6.223000×10^{-1}
T1 4.127500×10^{-2}
B2 6.223000×10^{-1}
T2 4.127500×10^{-2}
D 4.921250×10^{-1}
T3 1.428750×10^{-2}

Figure 8.5. Dimensions of the members composing the joint.

The present work takes advantage of the NTSB detailed FE model (formulated in software ABAQUS) of gusset plate U10 to establish the equivalent stiffness of springs that completely model the elastic and post-elastic behavior of the connection. The FE model has 5 stub members attached to a pair of gusset plates (Figure 9.4), and the model is connected to the appropriate members in the global model. For the simplified connection model, the stub members and gusset plates are replaced by 5 user-defined structural elements, called springs for short, that can each have up to a full 6 x 6 stiffness matrix for all 6 degrees of freedoms (DoFs).

8.3.1 LINEAR ELASTIC ANALYSES

The idea is to perform linear analyses on a detailed joint model in order to develop the characteristics of 5 springs that will replace the gusset plate framing five members in the global model and produce significant savings in computational effort at the cost of some loss in accuracy, if the simplified connection can be generalized and used at other locations in the global model. The procedure is tested on a simple beam element modeled by means of the finite-element code STRAND7 STRAUS7 and the results are compared with theoretical results.

8.3.2 THEORETICAL CALCULATION OF THE STIFFNESS MATRIX

The stiffness method is an efficient way to solve complex determinate or indeterminate structures, that is used extensively in the Finite Element Method (FEM).

8.3.3 STIFFNESS METHOD

Before getting into the evaluation of the stiffness matrix of a complex structure, here below the stiffness matrix of a single beam element, Figure 1 is illustrated.

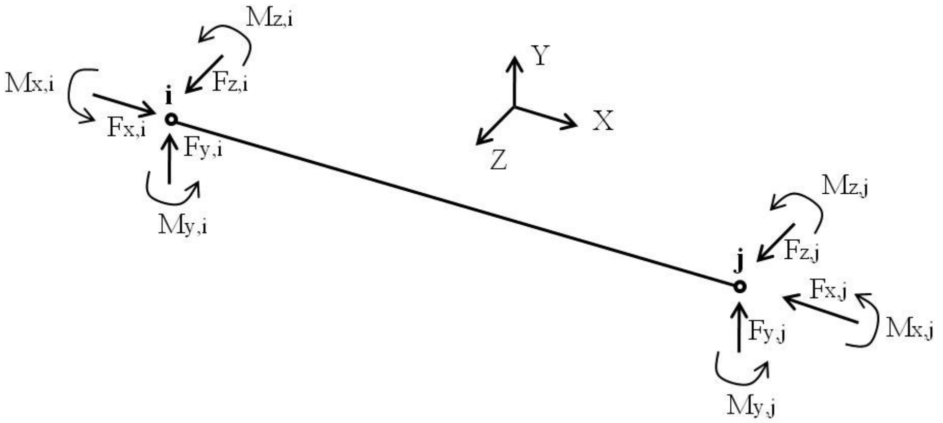

Figure 8.6. Beam element.

The forces and displacements are related through the element stiffness matrix K which depends on the geometry and properties on the element.

$$F = [K]U \tag{1}$$

Where the nodal forces F and displacements U of the beam element are referenced to the global coordinate system and are grouped in the following vectors:

$$F = \{F_x; F_y; F_z; M_x; M_y; M_z\} \tag{2}$$

$$U = \{U_x; U_y; U_z; R_x; R_y; R_z\} \tag{3}$$

Where M are moments and R are rotations and *[K]* is the stiffness matrix of the beam, which in local coordinates (in this case identical to the global coordinates) has the form shown in Equation (4) [Martin H. C., 1966].

$$[\mathrm{K}] = \begin{vmatrix} \frac{EA}{L} & 0 & 0 & 0 & 0 & 0 \\ 0 & \frac{12EI_Y}{L^3} & 0 & 0 & 0 & \frac{6EI_Y}{L^2} \\ 0 & 0 & \frac{12EI_Z}{L^2} & 0 & -\frac{6EI_Z}{L^2} & 0 \\ 0 & 0 & 0 & \frac{GJ}{L} & 0 & 0 \\ \frac{6EI_Y}{L^2} & 0 & 0 & 0 & \frac{4EI_Y}{L} & 0 \\ 0 & -\frac{6EI_Y}{L^2} & 0 & 0 & 0 & \frac{4EI_Z}{L} \end{vmatrix} \tag{4}$$

All diagonal stiffness coefficients K_i must be positive. This means that a force F_i directed toward the right will not produce a displacement toward the left. For any structure, no diagonal coefficient K_{ii} is negative or zero unless the structure is unstable.

[K] is symmetric according to Betti-Maxwell's reciprocal theorem of structural theory, which says that a force F_i acting through a displacement caused by force F_j does the same amount of work as force F_j acting through a displacement caused by force F_i. This is true for any structure that displays a linear relationship between the applied loads and the resulting displacements.

8.3.3.1 STIFFNESS MATRIX FOR A BEAM BY MEANS OF FINITE ELEMENT CODE

The global coordinate system is XYZ, the element is straight and the longitudinal axis is X. Node 1 is fully restrained, Figure 9.7. The beam element is assumed to have a uniform flexural stiffness *EI* over its length *L*; the mechanical and geometrical properties are shown in Figure 9.8.

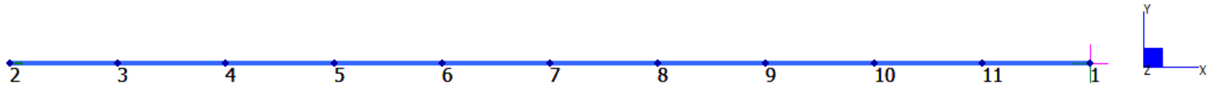

Figure 8.7. Beam element in STRAND7/STRAUS7.

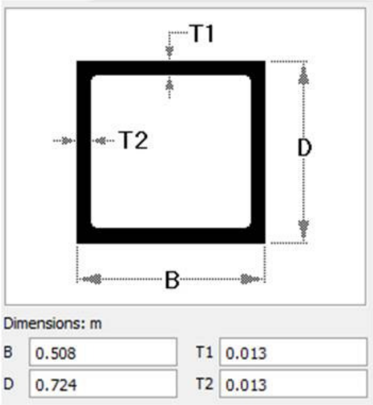

Dimensions: m

B 0.508
T1 0.013
D 0.724
T2 0.013

A = 0.031356 m^2

$\mathbf{I_1}$ = 2.406E-03 m^4

$\mathbf{I_2}$ = 1.396E-03 m^4

L = 2.896 m

J = 2.670E-03 m^4

G= 8.24E+10 Pa

E = 2.06E+11 Pa

Figure 8.8. Properties of the beam element.

Applying forces and moments on the free node 2, one obtains the flexibility matrix of the element in global coordinates XYZ.

Three forces (F_x; F_y; F_z) = (444820 N; 444820 N; 444820 N) and three moments (M_x; M_y; M_z) = (228794.1957 N·m; -112984.788 N·m; -161003.3229 N·m) of arbitrary magnitude are applied. To calculate the flexibility matrix, an individual unit force or moment is applied.

The stiffness matrix $[K]$ is the inverse of the flexibility matrix $[F]$.

$$[K] = [F]^{-1} \tag{5}$$

Table 8.1. Flexibility matrix for the beam element 1 (units: N, m, rad).

4.484E-10	0.000E+00	0.000E+00	0.000E+00	0.000E+00	0.000E+00
0.000E+00	1.634E-08	0.000E+00	0.000E+00	0.000E+00	-8.462E-09
0.000E+00	0.000E+00	2.816E-08	0.000E+00	1.459E-08	0.000E+00
0.000E+00	0.000E+00	0.000E+00	1.316E-08	0.000E+00	0.000E+00
0.000E+00	0.000E+00	1.459E-08	0.000E+00	1.007E-08	0.000E+00
0.000E+00	-8.462E-09	0.000E+00	0.000E+00	0.000E+00	5.843E-09

Table 8.2. Stiffness matrix for the beam element 1 (units: N, m, rad).

2.230E+09	0.000E+00	0.000E+00	0.000E+00	0.000E+00	0.000E+00
0.000E+00	2.448E+08	0.000E+00	0.000E+00	0.000E+00	3.545E+08
0.000E+00	0.000E+00	1.420E+08	0.000E+00	-2.057E+08	0.000E+00
0.000E+00	0.000E+00	0.000E+00	7.597E+07	0.000E+00	0.000E+00
0.000E+00	0.000E+00	-2.057E+08	0.000E+00	3.972E+08	0.000E+00
0.000E+00	3.545E+08	0.000E+00	0.000E+00	0.000E+00	6.846E+08

For the user-defined element in STRAND7/STRAUS7 it is necessary to transform the stiffness matrix $[K]$ of Table 9.2 to local coordinates, $[k]$. The user-defined beam element is used to represent a component of a structure that has known values of stiffness. In some cases the stiffness of components will be available from manufacturer's data or in other cases a detailed finite element model of the component may exist and the stiffness can be obtained from it. The user-defined matrix for the beam element provides a very general format for the input of data for the beam element. Figure 9.9 shows a general form of a beam stiffness matrix in the case of a 2-node beam element. Note that the matrix is subdivided into 3 sub-matrices *[A], [B]* and *[C]* corresponding to the degrees of freedom in Equation (4). The nodal forces and displacements of the element, referenced to the local coordinate system, are grouped in the following vectors:

$$f = \{f_x; f_y; f_z; m_x; m_y; m_z\} \quad (7)$$

$$u = \{u_x; u_y; u_z; r_x; r_y; r_z\} \quad (8)$$

$$\begin{array}{c}
\text{A} \hspace{18em} \text{B} \\
\left[\begin{array}{ccc|ccc}
\frac{12EI_2}{L^3} & 0 & 0 & 0 & \frac{6EI_2}{L^2} & 0 \\
0 & \frac{12EI_1}{L^3} & 0 & -\frac{6EI_1}{L^2} & 0 & 0 \\
0 & 0 & \frac{EA}{L} & 0 & 0 & 0 \\
\hline
0 & -\frac{6EI_1}{L^2} & 0 & \frac{4EI_1}{L} & 0 & 0 \\
\frac{6EI_2}{L^2} & 0 & 0 & 0 & \frac{4EI_2}{L} & 0 \\
0 & 0 & 0 & 0 & 0 & \frac{GJ}{L}
\end{array}\right] \\
\hspace{18em} \text{C}
\end{array}$$

Figure 8.9. Partition of the stiffness matrix.

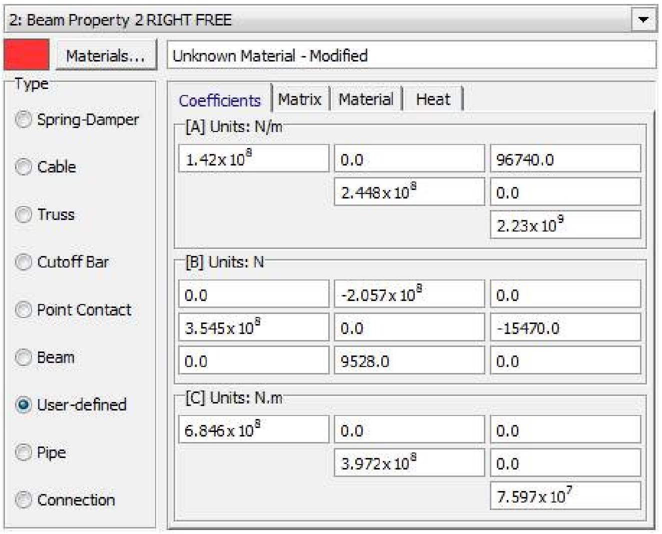

2: Beam Property 2 RIGHT FREE

Materials...

Unknown Material - Modified

Type

- ○ Spring-Damper
- ○ Cable
- ○ Truss
- ○ Cutoff Bar
- ○ Point Contact
- ○ Beam
- ● User-defined
- ○ Pipe
- ○ Connection

Coefficients | Matrix | Material | Heat

[A] Units: N/m

1.42×10^8	0.0	96740.0
	2.448×10^8	0.0
		2.23×10^9

[B] Units: N

0.0	-2.057×10^8	0.0
3.545×10^8	0.0	-15470.0
0.0	9528.0	0.0

[C] Units: N.m

6.846×10^8	0.0	0.0
	3.972×10^8	0.0
		7.597×10^7

Figure 8.10. Definition of the terms of the stiffness matrix for the user-defined element in STRAND7 / STRAND7/STRAUS77.

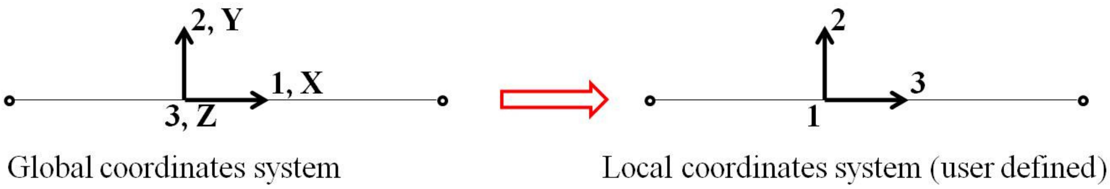
2, Y
1, X
3, Z
Global coordinates system
2
3
1
Local coordinates system (user defined)

Figure 8.11. Transformation from global to local coordinates.

In order to go from global to local system it is necessary to rotate 90 degrees around axis 2, by means of the transformation matrix, T.

$$F = [K]U \tag{9}$$

$$f = [T]F \qquad u = [T]U \tag{10}$$

$$[T]^{-1}f = [K][T]^{-1}u \rightarrow f = [T][K][T]^{-1}u \rightarrow f = [T][K][T]^{T}u \tag{11}$$

$$[k] = ([T][K])[T]^{T} \tag{12}$$

For verification, the matrix of Table 8.4 is compared with the one calculated by theoretical approach, according to Figure 8.9. Tables 8.6 and 8.7 show the displacements obtained with the two stiffness matrices. They are identical. Once the procedure is verified, it is applied to the joint modeled in ABAQUS.

All the matrices have units: N, m, rad.

Table 8.3. Transformation matrix, T.

0.000	0.000	-1.000	0.000	0.000	0.000
0.000	1.000	0.000	0.000	0.000	0.000
1.000	0.000	0.000	0.000	0.000	0.000
0.000	0.000	0.000	0.000	0.000	-1.000
0.000	0.000	0.000	0.000	1.000	0.000
0.000	0.000	0.000	1.000	0.000	0.000

Table 8.4. Stiffness matrix in local coordinates.

1.420E+08	0.000E+00	0.000E+00	0.000E+00	2.057E+08	0.000E+00
0.000E+00	2.448E+08	0.000E+00	-3.545E+08	0.000E+00	0.000E+00
0.000E+00	0.000E+00	2.230E+09	0.000E+00	-9.528E+03	0.000E+00
0.000E+00	-3.545E+08	0.000E+00	6.846E+08	0.000E+00	0.000E+00
2.057E+08	0.000E+00	-9.528E+03	0.000E+00	3.972E+08	0.000E+00
0.000E+00	0.000E+00	0.000E+00	0.000E+00	0.000E+00	7.597E+07

Table 8.5. Stiffness matrix calculated by means of the theoretical approach.

1.420E+08	0.000E+00	0.000E+00	0.000E+00	2.057E+08	0.000E+00
0.000E+00	2.448E+08	0.000E+00	-3.545E+08	0.000E+00	0.000E+00
0.000E+00	0.000E+00	2.230E+09	0.000E+00	0.000E+00	0.000E+00
0.000E+00	-3.545E+08	0.000E+00	6.846E+08	0.000E+00	0.000E+00
2.057E+08	0.000E+00	0.000E+00	0.000E+00	3.972E+08	0.000E+00
0.000E+00	0.000E+00	0.000E+00	0.000E+00	0.000E+00	7.597E+07

Table 8.6. Displacements obtained by using the user-defined element with the matrix of Table 8.4.

	u_x	u_y	u_z	r_x	r_y	r_z
F_x	1.99E-04	0.00E+00	0.00E+00	0.00E+00	0.00E+00	0.00E+00
F_y	0.00E+00	7.26E-03	0.00E+00	1.48E-06	0.00E+00	-3.76E-03
F_z	5.16E-07	0.00E+00	1.25E-02	0.00E+00	6.49E-03	0.00E+00
M_x	0.00E+00	7.61E-07	0.00E+00	3.01E-03	0.00E+00	-3.94E-07
M_y	6.67E-08	0.00E+00	1.65E-03	0.00E+00	1.14E-03	0.00E+00
M_z	0.00E+00	1.36E-03	0.00E+00	2.77E-07	0.00E+00	-9.40E-04

Table 8.7. Displacements obtained by using the user-defined element with the matrix of Table 8.5.

	u_x	u_y	u_z	r_x	r_y	r_z
F_x	1.99E-04	0.00E+00	0.00E+00	0.00E+00	0.00E+00	0.00E+00
F_y	0.00E+00	7.26E-03	0.00E+00	1.48E-06	0.00E+00	-3.76E-03
F_z	5.16E-07	0.00E+00	1.25E-02	0.00E+00	6.49E-03	0.00E+00
M_x	0.00E+00	7.61E-07	0.00E+00	3.01E-03	0.00E+00	-3.94E-07
M_y	6.67E-08	0.00E+00	1.65E-03	0.00E+00	1.14E-03	0.00E+00
M_z	0.00E+00	1.36E-03	0.00E+00	2.77E-07	0.00E+00	-9.40E-04

8.3.4 JOINT MODELING

In this paragraph, the detailed finite element model of the joint U10-W is considered. Since the aim of this work is to obtain the stiffness matrix of the complex connection and transform it into a set of springs or beams with full stiffness matrix, a model with 5 beam elements (user- defined) is built in STRAND7/STRAND7.

The procedure to obtain the stiffness matrices in global coordinates is the following:

- Node 5 is free and nodes 1, 2, 3, 4 and 6 are fixed, Figure 8.12;
- Apply F_x on node 5;
- Calculate the corresponding displacements and rotations (U_x, U_y, U_z, R_x, R_y, R_z);
- Repeat by applying F_y, F_z, M_x, M_y, M_z one at a time;
- Build the flexibility matrix for element 1 (with end nodes 5 and 3);
- Invert to obtain the stiffness matrix of member 1;
- Repeat for all joint members.

Note that the central node 3 is fully restrained, as the procedure requires for each beam. Note also that the local longitudinal local axis (3) for each beam element must point away from the loaded end in STRAND7/STRAUS7.

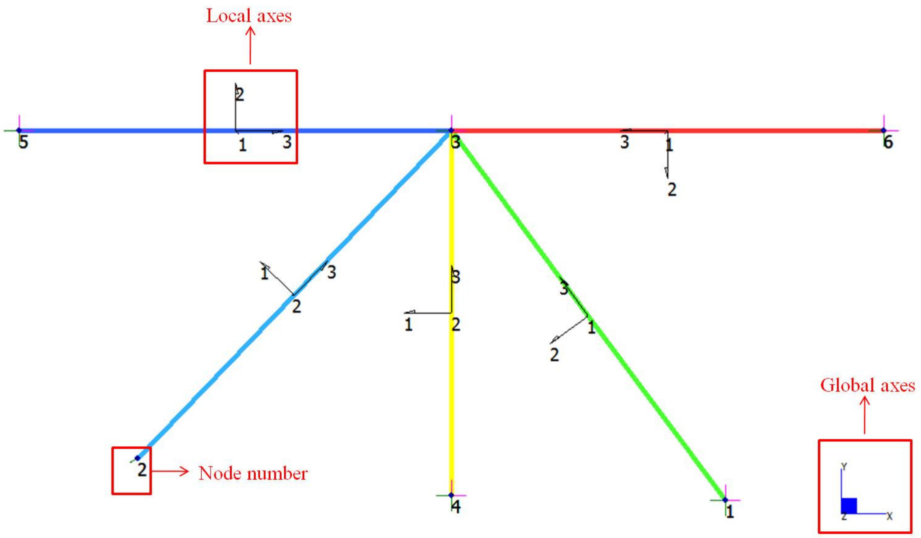

Figure 8.12. User defined elements with local axes.

Once the stiffness matrix of each member in global coordinate is found, it is necessary to transform it from the global coordinates (K) to the local ones (k).To do this, the transformation matrix (T) has to be built for each member:

- Element 1: Rotation of 90 degrees around global axis 2 (Y);

- Element 2: Rotation of 90 degrees around axis 2 (Y) and rotation of 180 degrees around axis 1 (X);
- Element 3: Rotation of 90 degrees around axis 2 (Y) and rotation of -126.5 degrees around axis 1 (X);
- Element 4: Rotation of 90 degrees around axis 1 (Y) and rotation of 180 degrees around axis 2 (X);
- Element 5: Rotation of 90 degrees around axis 1 (Y) and rotation of 133.6 degrees around axis 2 (X);

For element 1, the global stiffness matrix, the transformation matrix and the corresponding local stiffness matrix are reported, for the other elements only the local ones are written.

Table 8.8. Stiffness matrix for element 1 in global coordinates.

2.907E+09	-1.356E+08	3.902E+04	-6.129E+03	-1.546E+05	-1.209E+08
-1.355E+08	3.619E+08	1.544E+03	-1.629E+03	6.435E+03	4.147E+08
2.012E+03	3.332E+03	3.861E+07	-5.743E+06	-7.048E+07	1.998E+03
-2.574E+03	-5.802E+02	-5.746E+06	5.412E+07	7.688E+06	9.240E+01
-2.679E+03	-9.739E+02	-7.048E+07	7.676E+06	2.892E+08	-7.560E+02
-1.208E+08	4.147E+08	2.777E+02	-1.223E+03	6.219E+03	7.371E+08

Table 8.9. Transformation matrix T_1, (rotation around 2 of 90 degrees).

0.000	0.000	-1.000	0.000	0.000	0.000
0.000	1.000	0.000	0.000	0.000	0.000
1.000	0.000	0.000	0.000	0.000	0.000
0.000	0.000	0.000	0.000	0.000	-1.000
0.000	0.000	0.000	0.000	1.000	0.000
0.000	0.000	0.000	1.000	0.000	0.000

Table 8.10. Stiffness matrix for element 1 in local coordinates.

3.861E+07	-3.332E+03	-2.012E+03	1.998E+03	7.048E+07	5.743E+06
-1.544E+03	3.619E+08	-1.355E+08	-4.147E+08	6.435E+03	-1.629E+03
-3.902E+04	-1.356E+08	2.907E+09	1.209E+08	-1.546E+05	-6.129E+03
2.777E+02	-4.147E+08	1.208E+08	7.371E+08	-6.219E+03	1.223E+03
7.048E+07	-9.739E+02	-2.679E+03	7.560E+02	2.892E+08	7.676E+06
5.746E+06	-5.802E+02	-2.574E+03	-9.240E+01	7.688E+06	5.412E+07

Table 8.11. Stiffness matrix for element 2 in local coordinates.

4.104E+07	2.146E+04	-7.189E+02	-1.977E+04	8.133E+07	-6.182E+06
2.149E+04	4.528E+08	1.243E+08	-5.305E+08	-9.767E+03	-4.952E+04
-7.303E+02	1.243E+08	2.670E+09	-9.485E+07	2.878E+04	5.800E+04
-1.981E+04	-5.306E+08	-9.480E+07	9.349E+08	3.416E+03	4.441E+04
8.135E+07	-9.812E+03	2.886E+04	3.437E+03	3.467E+08	-8.508E+06
-6.205E+06	-4.953E+04	5.799E+04	4.442E+04	-8.604E+06	6.354E+07

Table 8.12. Stiffness matrix for element 3 in local coordinates.

2.916E+07	2.476E+03	-2.329E+03	3.202E+03	4.158E+07	6.708E+05
2.482E+03	4.853E+08	1.001E+08	-6.117E+08	-5.404E+04	6.732E+03
-2.322E+03	1.001E+08	2.313E+09	-9.662E+07	1.397E+05	4.023E+04
3.198E+03	-6.118E+08	-9.664E+07	1.153E+09	-1.171E+05	-4.877E+04
4.159E+07	-5.402E+04	1.396E+05	-1.172E+05	2.287E+08	-7.205E+06
6.511E+05	6.757E+03	4.021E+04	-4.872E+04	-7.303E+06	5.518E+07

Table 8.12. Stiffness matrix for element 4 in local coordinates.

8.051E+07	8.663E+01	-1.049E+06	-1.530E+03	4.731E+07	-2.470E+02
8.663E+01	4.132E+07	-3.962E+03	-3.398E+07	7.051E+01	2.954E+05
-1.049E+06	-3.962E+03	1.321E+09	8.110E+03	-2.717E+05	1.721E+03
-1.530E+03	-3.398E+07	8.110E+03	1.051E+08	-7.754E+02	-8.771E+04
4.731E+07	7.051E+01	-2.717E+05	-7.754E+02	3.938E+07	-1.237E+02
-2.470E+02	2.954E+05	1.721E+03	-8.771E+04	-1.237E+02	5.510E+06

Table 8.14. Stiffness matrix for element 5 in local coordinates.

3.424E+08	-9.033E+02	-7.573E+07	-1.052E+04	3.282E+08	-2.642E+03
-9.038E+02	2.946E+07	4.701E+03	-4.344E+07	-6.619E+02	-1.871E+05
-7.573E+07	4.700E+03	2.279E+09	3.001E+04	-6.914E+07	1.066E+04
-1.052E+04	-4.344E+07	3.000E+04	2.290E+08	-6.278E+03	5.898E+06
3.282E+08	-6.617E+02	-6.914E+07	-6.281E+03	4.964E+08	-1.655E+03
-2.642E+03	-1.907E+05	1.066E+04	5.920E+06	-1.655E+03	2.313E+07

To assess that the new model built in STRAND7/STRAUS7 with 5 user-defined beam elements is able to reproduce the behavior of the detailed model built in ABAQUS, a comparison between the displacements measured in nodes 1, 2, 4, 5, 6 is shown in Tables 8.16 to 8.25. For example, F_x= 4.48 E+5 N is applied to node 5 with nodes 2 to 6 fixed and the results in terms of displacements and rotations are shown in the first row of Table 8.16.

Table 8.15. Forces and moments applied one at a time.

	Node 5	**Node 6**	**Node 1**	**Node 4**	**Node 2**
F_x	4.448E+05	4.448E+05	4.448E+05	4.448E+05	4.448E+05
F_y	4.448E+05	4.448E+05	4.448E+05	4.448E+05	4.448E+05
F_z	4.448E+05	4.448E+05	4.448E+05	4.448E+05	4.448E+05
M_x	2.288E+05	-2.273E+05	-2.273E+05	-1.158E+05	-2.189E+05
M_y	-1.130E+05	-1.105E+05	-1.105E+05	1.401E+05	-1.095E+06
M_z	-1.610E+05	-1.610E+05	-1.610E+05	-7.062E+04	-9.549E+05

Table 8.16. Element 1, displacements obtained in STRAND7/STRAUS7 with user defined elements node 5.

El.1	**U_x**	**U_y**	**U_z**	**R_x**	**R_y**	**R_z**
F_x	1.85E-04	8.27E-05	2.51E-07	2.61E-08	1.43E-07	-2.10E-05
F_y	8.27E-05	3.50E-03	-3.29E-07	4.60E-08	-7.31E-08	-1.95E-03
F_z	2.51E-07	-3.29E-07	2.10E-02	1.51E-03	5.09E-03	1.31E-07
M_x	1.60E-08	2.83E-08	9.30E-04	5.15E-03	9.00E-05	-7.92E-09
M_y	-3.63E-08	1.86E-08	-1.29E-03	-3.71E-05	-7.06E-04	-7.14E-09
M_z	7.60E-06	7.07E-04	-4.75E-08	4.66E-09	-1.02E-08	-6.15E-04

Table 8.17. Element 1, displacements obtained in ABAQUS node 5.

El.1	U_x	U_y	U_z	R_x	R_y	R_z
F_x	1.84E-04	8.19E-05	-1.88E-08	6.72E-09	7.72E-08	-2.05E-05
F_y	8.19E-05	3.50E-03	-3.42E-07	4.51E-08	-7.66E-08	-1.96E-03
F_z	-1.88E-08	-3.39E-07	2.10E-02	1.51E-03	5.08E-03	1.37E-07
M_x	4.19E-09	1.22E-08	9.30E-04	5.15E-03	8.98E-05	-8.80E-09
M_y	7.83E-10	1.94E-08	-1.29E-03	-3.71E-05	-7.04E-04	-8.01E-09
M_z	7.43E-06	7.09E-04	-5.10E-08	4.41E-09	-1.11E-08	-6.16E-04

Table 8.18. Element 2, displacements obtained in STRAND7/STRAUS7 with user defined elements node 6.

El.2	U_x	U_y	U_z	R_x	R_y	R_z
F_x	-1.69E-04	7.96E-05	-8.06E-08	1.95E-07	3.98E-08	2.80E-05
F_y	-7.96E-05	2.99E-03	-1.46E-06	1.14E-06	4.45E-07	1.69E-03
F_z	8.06E-08	-1.46E-06	2.05E-02	1.36E-03	-4.77E-03	-4.34E-07
M_x	-1.19E-07	6.95E-07	8.30E-04	4.35E-03	-8.70E-05	1.96E-07
M_y	-9.93E-09	1.11E-07	-1.19E-03	-3.56E-05	5.98E-04	3.63E-08
M_z	1.01E-05	-6.12E-04	1.57E-07	-1.16E-07	-5.27E-08	-5.19E-04

Table 8.19. Element 2, displacements obtained in ABAQUS node 6.

El.2	U_x	U_y	U_z	R_x	R_y	R_z
F_x	-1.69E-04	7.87E-05	-8.01E-08	1.94E-07	3.96E-08	2.75E-05
F_y	-7.87E-05	2.97E-03	-1.45E-06	1.13E-06	4.42E-07	1.68E-03
F_z	8.01E-08	-1.45E-06	2.05E-02	1.36E-03	-4.78E-03	-4.29E-07
M_x	-1.19E-07	6.91E-07	8.28E-04	4.34E-03	-8.64E-05	1.91E-07
M_y	-9.84E-09	1.10E-07	-1.19E-03	-3.57E-05	5.96E-04	3.58E-08
M_z	9.95E-06	-6.07E-04	1.55E-07	-1.14E-07	-5.20E-08	-5.16E-04

Table 8.20. Element 3, displacements obtained in STRAND7/STRAUS7 with user defined elements node 1.

El.3	U_x	U_y	U_z	R_x	R_y	R_z
F_x	1.81E-03	1.26E-03	-2.59E-06	1.84E-06	1.77E-07	1.18E-03
F_y	1.26E-03	1.17E-03	-2.31E-06	1.70E-06	1.04E-07	8.90E-04
F_z	-2.59E-06	-2.31E-06	2.07E-02	-3.49E-03	-1.67E-03	-2.29E-06
M_x	8.87E-08	8.16E-08	-1.68E-04	2.40E-04	-1.31E-04	8.51E-08
M_y	-4.25E-08	-2.50E-08	4.01E-04	6.57E-04	-1.39E-03	4.90E-09
M_z	1.54E-04	1.16E-04	-2.97E-07	2.30E-07	-2.65E-09	1.52E-04

Table 8.21. Element 3, displacements obtained in ABAQUS node 1.

El.3	U_x	U_y	U_z	R_x	R_y	R_z
F_x	1.81E-03	1.26E-03	-2.59E-06	1.84E-06	1.71E-07	1.17E-03
F_y	1.26E-03	1.17E-03	-2.31E-06	1.70E-06	9.92E-08	8.88E-04
F_z	-2.59E-06	-2.31E-06	2.07E-02	-3.48E-03	-1.65E-03	-2.28E-06
M_x	8.89E-08	8.19E-08	-1.68E-04	2.39E-04	-1.32E-04	8.52E-08
M_y	-4.13E-08	-2.39E-08	3.98E-04	6.60E-04	-1.40E-03	6.65E-09
M_z	1.53E-04	1.15E-04	-2.96E-07	2.29E-07	-3.29E-09	1.51E-04

Table 8.22. Element 4, displacements obtained in STRAND7/STRAUS7 with user defined elements node 4.

El.4	U_x	U_y	U_z	R_x	R_y	R_z
F_x	1.88E-02	-1.31E-05	-1.14E-07	1.44E-07	-3.28E-07	2.26E-02
F_y	-1.31E-05	3.37E-04	1.59E-08	2.09E-08	-1.06E-07	-1.34E-05
F_z	-1.14E-07	1.59E-08	1.47E-02	-4.73E-03	-7.09E-04	-7.26E-08
M_x	-3.77E-08	-5.44E-09	1.23E-03	-1.50E-03	-4.49E-05	-1.81E-08
M_y	-1.03E-07	-3.33E-08	-2.23E-04	5.42E-05	2.54E-02	-4.53E-08
M_z	-3.59E-03	2.13E-06	1.15E-08	-1.10E-08	2.29E-08	-6.12E-03

Table 8.23. Element 4, displacements obtained in ABAQUS node 4.

El.4	U_x	U_y	U_z	R_x	R_y	R_z
F_x	1.88E-02	-1.03E-05	-1.16E-07	1.44E-07	-3.29E-07	2.26E-02
F_y	-1.03E-05	3.37E-04	1.59E-08	2.09E-08	-1.06E-07	-1.00E-05
F_z	-1.16E-07	1.59E-08	1.47E-02	-4.74E-03	-7.11E-04	-7.47E-08
M_x	-3.75E-08	-5.43E-09	1.24E-03	-1.50E-03	-4.23E-05	-1.79E-08
M_y	-1.04E-07	-3.34E-08	-2.24E-04	5.12E-05	2.54E-02	-4.53E-08
M_z	-3.58E-03	1.59E-06	1.19E-08	-1.09E-08	2.28E-08	-6.10E-03

Table 8.24. Element 5, displacements obtained in STRAND7/STRAUS7 with user defined elements node 2.

El.5	U_x	U_y	U_z	R_x	R_y	R_z
F_x	1.90E-03	-1.68E-03	-2.41E-07	-3.73E-08	-2.18E-07	1.69E-03
F_y	-1.68E-03	1.86E-03	1.12E-07	0.00E+00	9.67E-08	-1.64E-03
F_z	-2.41E-07	1.12E-07	2.09E-02	-3.47E-03	2.15E-03	-1.02E-07
M_x	1.84E-09	0.00E+00	1.71E-04	-5.61E-04	-4.12E-04	4.61E-10
M_y	5.35E-08	-2.37E-08	-5.27E-04	-2.05E-03	-2.63E-03	2.28E-08
M_z	2.17E-04	-2.11E-04	-1.31E-08	-1.20E-09	-1.20E-08	3.15E-04

Table 8.25. Element 5, displacements obtained in ABAQUS node 2.

El.5	U_x	U_y	U_z	R_x	R_y	R_z
F_x	1.90E-03	-1.68E-03	-2.41E-07	-3.89E-08	-2.20E-07	1.69E-03
F_y	-1.68E-03	1.85E-03	1.11E-07	2.18E-09	9.81E-08	-1.63E-03
F_z	-2.41E-07	1.11E-07	2.10E-02	-3.48E-03	2.16E-03	-1.02E-07
M_x	1.92E-09	-1.07E-10	1.71E-04	-5.60E-04	-4.11E-04	5.91E-10
M_y	5.42E-08	-2.41E-08	-5.31E-04	-2.06E-03	-2.64E-03	2.35E-08
M_z	2.18E-04	-2.09E-04	-1.31E-08	-1.55E-09	-1.23E-08	3.15E-04

8.4 MODEL WITH BEAM ELEMENTS

In this paragraph the results obtained by a model built in STRAND7/STRAUS7 with rigidly connected beam elements are reported. All the beams have the sections already described in Figure 8.5.

From Table 37 to 45 the stiffness matrix obtained by STRAND7/STRAUS7 and the one calculated using the theory are shown.

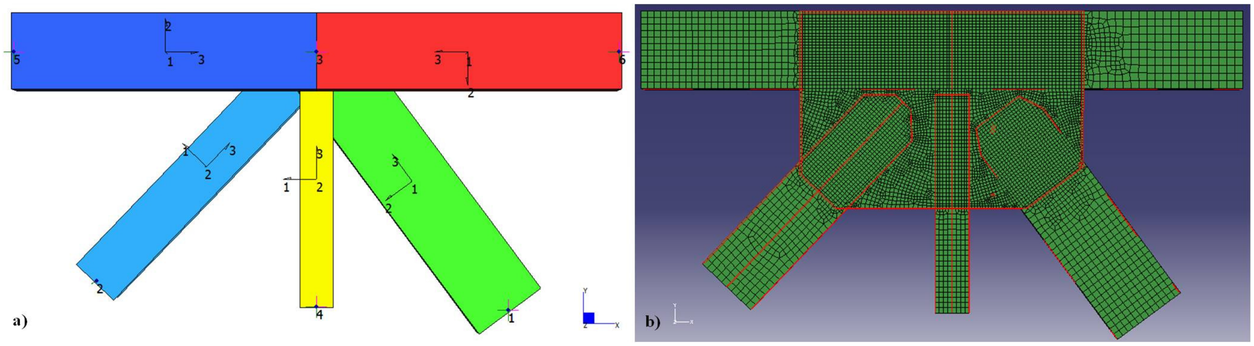

Figure 8.13. a) Joint built with beam elements, b) detailed model.

The displacements obtained in the ABAQUS model are compared with the ones obtained in STRAND7/STRAUS7 with beam elements and reported in the following Tables, from 8.26 to 8.30. The differences in the displacements and rotations reflect the influence of the gusset plates on the connection.

Table 8.26. Element 1, displacements obtained in STRAND7 / STRAUS7 with beam elements, node 5, they have to be compared with the results shown in Table 8.17.

El.1	U_x	U_y	U_z	R_x	R_y	R_z
F_x	1.84E-04	5.62E-05	0.00E+00	0.00E+00	0.00E+00	-1.60E-05
F_y	5.62E-05	7.42E-03	0.00E+00	0.00E+00	0.00E+00	-3.50E-03
F_z	0.00E+00	0.00E+00	1.28E-02	1.12E-03	5.06E-03	0.00E+00
M_x	0.00E+00	0.00E+00	6.88E-04	3.12E-03	1.05E-04	0.00E+00
M_y	0.00E+00	0.00E+00	-1.28E-03	-4.35E-05	-7.59E-04	0.00E+00
M_z	5.79E-06	1.27E-03	0.00E+00	0.00E+00	0.00E+00	-8.02E-04

Table 8.27. Element 2, displacements obtained in STRAND7 / STRAUS7 with beam elements, node 6, they have to be compared with the results shown in Table 8.19.

El.2	U_x	U_y	U_z	R_x	R_y	R_z
F_x	-1.61E-04	3.51E-05	0.00E+00	0.00E+00	0.00E+00	1.51E-05
F_y	-3.51E-05	6.40E-03	0.00E+00	0.00E+00	0.00E+00	3.01E-03
F_z	0.00E+00	0.00E+00	1.14E-02	1.01E-03	-4.30E-03	0.00E+00
M_x	0.00E+00	0.00E+00	6.17E-04	2.90E-03	-7.68E-05	0.00E+00
M_y	0.00E+00	0.00E+00	-1.07E-03	-3.14E-05	6.11E-04	0.00E+00
M_z	5.47E-06	-1.09E-03	0.00E+00	0.00E+00	0.00E+00	-6.84E-04

Table 8.28. Element 3, displacements obtained in STRAND7 / STRAUS7 with beam elements, node 1, they have to be compared with the results shown in Table 8.21.

El.3	U_x	U_y	U_z	R_x	R_y	R_z
F_x	4.03E-03	2.89E-03	0.00E+00	0.00E+00	0.00E+00	2.16E-03
F_y	2.89E-03	2.39E-03	0.00E+00	0.00E+00	0.00E+00	1.61E-03
F_z	0.00E+00	0.00E+00	1.22E-02	-4.26E-03	-2.57E-03	0.00E+00
M_x	0.00E+00	0.00E+00	-2.05E-04	1.54E-04	-2.85E-05	0.00E+00
M_y	0.00E+00	0.00E+00	6.18E-04	1.42E-04	-7.48E-04	0.00E+00
M_z	2.80E-04	2.09E-04	0.00E+00	0.00E+00	0.00E+00	2.01E-04

Table 8.29. Element 4, displacements obtained in STRAND7 / STRAUS7 with beam elements, node 4, they have to be compared with the results shown in Table 8.23.

El.4	**U_x**	**U_y**	**U_z**	**R_x**	**R_y**	**R_z**
F_x	1.55E-01	-3.92E-05	0.00E+00	0.00E+00	0.00E+00	9.53E-02
F_y	-3.92E-05	5.58E-04	0.00E+00	0.00E+00	0.00E+00	-2.34E-05
F_z	0.00E+00	0.00E+00	5.24E-02	-3.19E-02	-2.91E-05	0.00E+00
M_x	0.00E+00	0.00E+00	8.33E-03	-6.78E-03	-9.85E-04	0.00E+00
M_y	0.00E+00	0.00E+00	-9.16E-06	1.19E-03	8.01E+00	0.00E+00
M_z	-1.51E-02	3.72E-06	0.00E+00	0.00E+00	0.00E+00	-1.24E-02

Table 8.30. Element 5, displacements obtained in STRAND7 / STRAUS7 with beam elements, node 2, they have to be compared with the results shown in Table 8.25.

El.5	**U_x**	**U_y**	**U_z**	**R_x**	**R_y**	**R_z**
F_x	1.35E-02	-1.29E-02	0.00E+00	0.00E+00	0.00E+00	9.06E-03
F_y	-1.29E-02	1.27E-02	0.00E+00	0.00E+00	0.00E+00	-8.73E-03
F_z	0.00E+00	0.00E+00	1.02E-02	-3.23E-03	2.69E-03	0.00E+00
M_x	0.00E+00	0.00E+00	1.59E-04	-1.65E-02	-1.70E-02	0.00E+00
M_y	0.00E+00	0.00E+00	-6.60E-04	-8.48E-02	-8.89E-02	0.00E+00
M_z	1.17E-03	-1.12E-03	0.00E+00	0.00E+00	0.00E+00	1.05E-03

On the next step the attention is focused on the diagonal terms of the above matrices and on the comparison of the displacements and rotations predicted by the STRAND7/STRAUS7 model with rigidly connected beams and the detailed ABAQUS model with various gusset plate thicknesses (Table 8.30). In Table the results for element 1 are shown. As expected, the rigid joint produces an approximation that is not as good as the more complicated spring model, equivalent to a gusset plate of thickness t = 12.7 mm.

Table 8.30: Comparison of displacements and rotations of STRAND7/STRAUS7 model with rigidly connected beams and ABAQUS FE model with various gusset plate thicknesses, Element 1.

	STRAND7 / STRAUS7 beams with rigid joint	ABAQUS FE model with thickness:			
		12.7 mm	15.87mm	19.05 mm	25.4 mm
U_x (m)	1.84E-04	1.84E-04	1.748E-04	1.677E-04	1.575E-04
U_y (m)	7.42E-03	3.50E-03	3.276E-03	3.105E-03	2.860E-03
U_z (m)	1.28E-02	2.10E-02	1.854E-02	1.690E-02	1.483E-02
R_x (rad)	3.12E-03	5.15E-03	4.688E-03	4.393E-03	4.021E-03
R_y (rad)	-7.59E-04	-7.04E-04	-6.618E-04	-6.302E-04	-5.862E-04
R_z (rad)	-8.02E-04	-6.16E-04	-5.998E-04	-5.872E-04	-5.682E-04

Although the pair of gusset plates should have been designed with a thickness of 25.4 mm, they were in fact constructed with a thickness of 12.7 mm. Except for U_x and R_y, the assumption of a rigid joints produces fairly different results from the actual gusset plate connection. This gives a benchmark on needed improvement in connection modeling.

8.5 CONCLUSIONS

In this chapter the linear-elastic behavior of a joint modeled in detail by ABAQUS is shown. A comparison with a simplified model built with another finite element code, STRAND7/STRAUS7, with the use of different elements is reported.

Testing the linear-elastic behavior against the theoretical approach, the results show that the linear elastic behavior using “spring” elements with full stiffness matrix is reproduced with good approximation.

This is made in order to produce significant savings in computational effort at the cost of little loss of accuracy when for example analyzing a steel truss bridge, as shown in the next chapter.

In the elastic range, agreement between the simplified and the detailed models in the calculated displacements and rotations is good, especially for the diagonal terms, with acceptable errors in the off-diagonal terms, which are several orders of magnitude smaller.

9 GLOBAL ANALYSES

9.1 INTRODUCTION

Joint behavior has a significant effect on the response of the structural frame and should be included in both the global analysis and design.

In modeling joints, their stiffness and resistance have to be taken into account. In the case of elastic global frame analysis, only the stiffness properties of the joint are relevant for the joint modeling. In the case of rigid plastic analysis, the principal joint features are the resistance, and the rotational capacity both of which need to be checked. In all the other cases, both the stiffness and the resistance properties should be included in the global analysis.

In this chapter the case of the I-35W is taken under study starting from a two-dimensional model to a more complete and realistic three-dimensional one.

9.2 TWO-DIMENSIONAL MODEL OF THE BRIDGE

In order to study the overall response of the bridge, a two-dimensional bridge model was constructed and analyzed using STRAUS. The west truss of the bridge is modeled and the model geometry is based on the original construction drawings (Mn/DOT 2008).

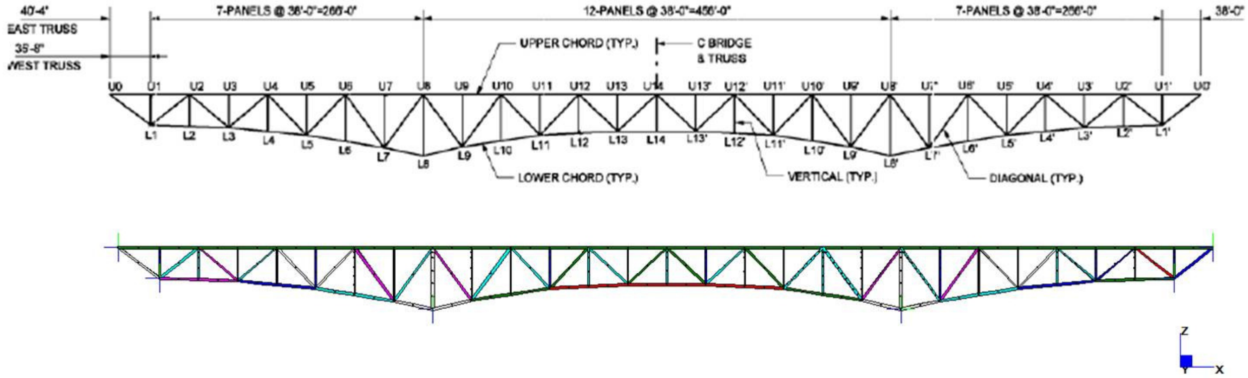
40'-4"
EAST TRUSS
35'-8"
WEST TRUSS
7-PANELS @ 38'-0"=266'-0"
12-PANELS @ 38'-0"=456'-0"
7-PANELS @ 38'-0"=266'-0"
38'-0"
UPPER CHORD (TYP.)
C BRIDGE & TRUSS
U0 U1 U2 U3 U4 U5 U6 U7 U8 U9 U10 U11 U12 U13 U14 U13' U12' U11' U10' U9' U8' U7' U6' U5' U4' U3' U2' U1' U0'
L1 L2 L3 L4 L5 L6 L7 L8 L9 L10 L11 L12 L13 L14 L13' L12' L11' L10' L9' L8' L7' L6' L5' L4' L3' L2' L1'
LOWER CHORD (TYP.)
VERTICAL (TYP.)
DIAGONAL (TYP.)
Z
Y
X

Figure 9.1. Drawing of the truss of I-35W.

In this model four types of member are identified, the upper chord members which extend for the entire length of the truss, the lower chord members, the vertical members, which vertically connect like-numbered nodes on the upper and lower chords, and diagonals, which connect adjacent nodes of the upper and lower chords.

The restraints are shown in Figure 9.2. In Figure 9.2 and 9.3 the main truss and the particular of the joint U10 West modeled, are shown.

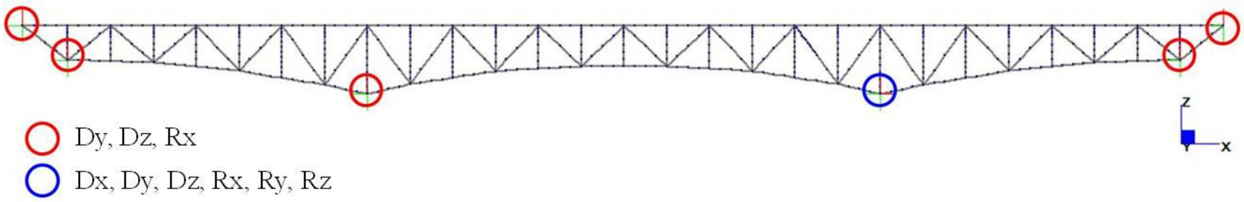

Figure 9.2. Restraints in the model.

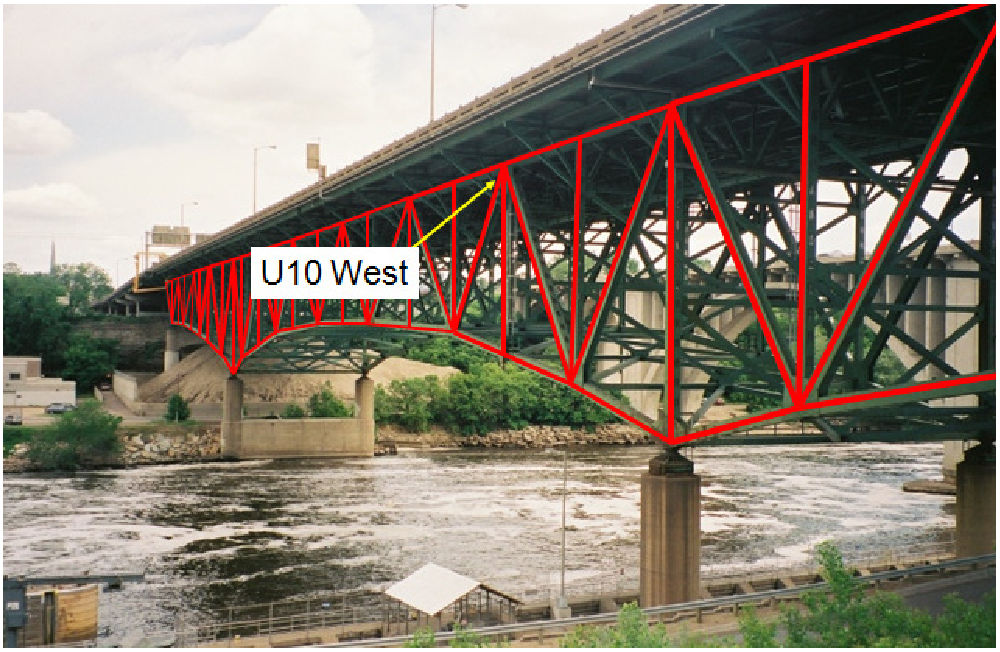

Figure 9.3. West truss.

Generic elastic properties of steel AISI 5150 were assigned to the members, E= 1.99 E+11 Pa, $\upsilon = 0.25$, $\rho = 7850\ \mathrm{kg/m^3}$.

The applied load consists of its own dead load (the concrete and steel weight), the vehicle loads (different for west and east truss) and the construction loads, all taken from the NTSB Report No. 07-115, November 8, [NTSB, 2007]. All these loads are applied to the upper chord with all the load factors equal to 1, as they are the loads present at the moment of the collapse. Liao et al., 2010 showed by influence lines that the temporary construction loads placed near U10 significantly affected the forces imposed on the bridge and contributed to the collapse.

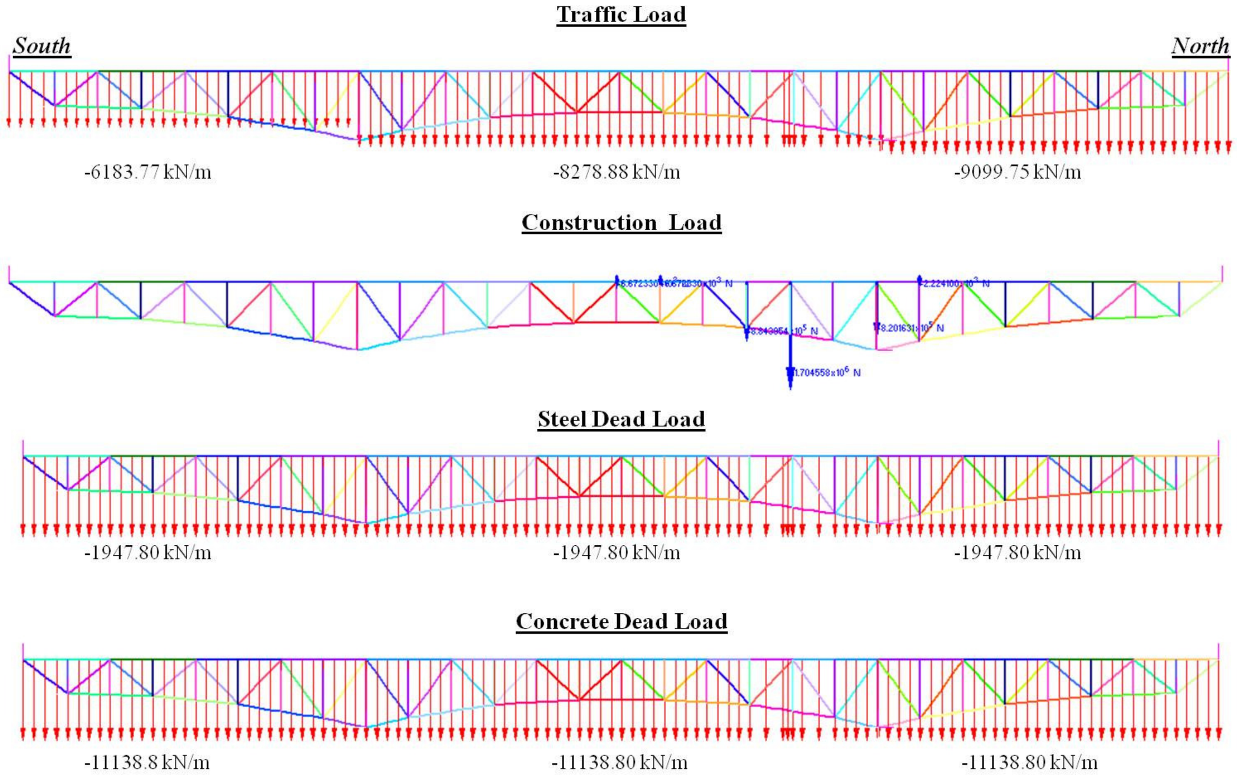
Traffic Load

Construction Load

Steel Dead Load

Concrete Dead Load

South
North
-6183.77 kN/m
-8278.88 kN/m
-9099.75 kN/m
2.224100x10^3 N
8.201631x10^5 N
1.704558x10^6 N
-1947.80 kN/m
-1947.80 kN/m
-1947.80 kN/m
-11138.8 kN/m
-11138.80 kN/m
-11138.80 kN/m

Figure 9.4. Load components for the west main truss.

The idea is to compare the 2D model built in STRAUS7/STRAND7 with user-defined elements (with full stiffness matrix) and the 2D model built in ABAQUS with beam elements and the detailed joint, in order to assess whether the “simplified” model of the joint is good enough to reproduce its real behavior.

9.2.1 LINEAR ANALYSES

Four cases, shown in Figure 9.5, were run [Crosti and Duthinh, 2010]:

1. All joints rigid;
2. U10 modeled with user-defined elements, all other joints rigid;
3. U10 modeled with detailed FE, all other joints rigid; and
4. All 5 member joints hinged and all other joints rigid.

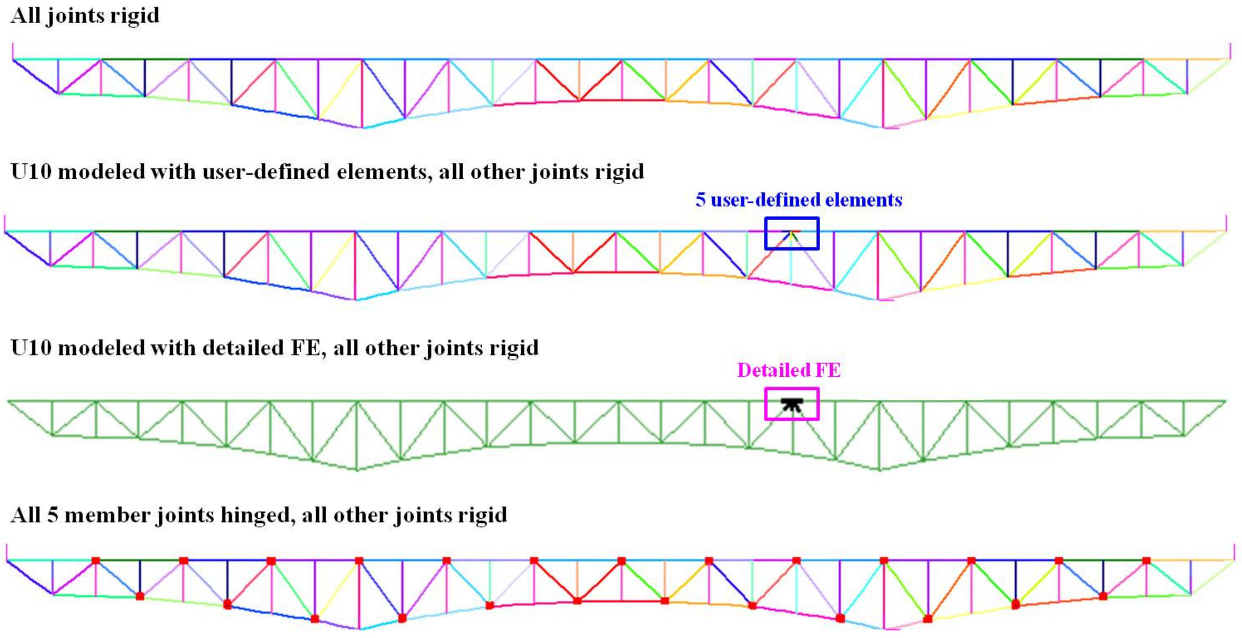
All joints rigid
U10 modeled with user-defined elements, all other joints rigid
5 user-defined elements
U10 modeled with detailed FE, all other joints rigid
Detailed FE
All 5 member joints hinged, all other joints rigid

Figure 9.5. Four different 2D models of the bridge.

Results (Table 9.1) show that modifying the stiffness of one connection within the elastic range produces no noticeable effect on the maximum vertical deflection of the bridge (at midspan).

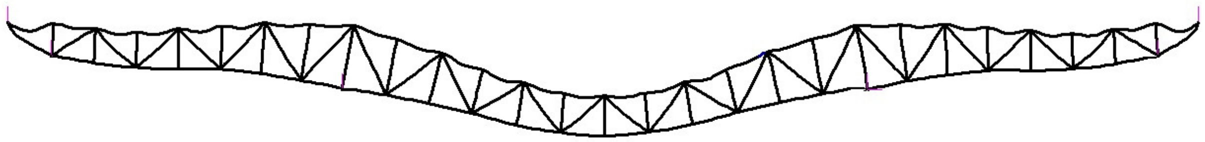

Figure 9.6. Typical vertical displacements.

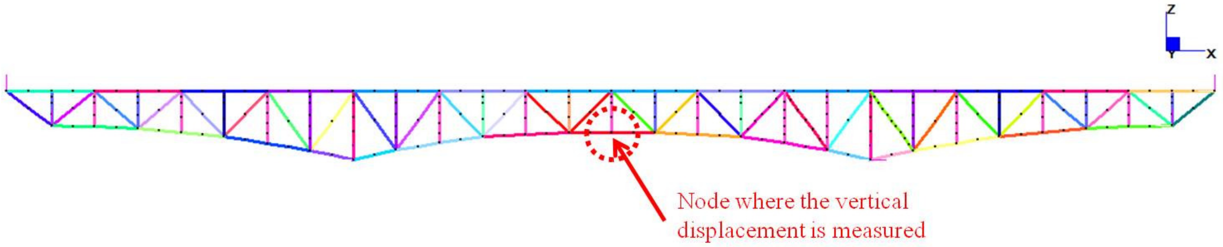

Figure 9.7. Node where the vertical displacement is measured.

Table 9.1: Midspan vertical deflection for different models.

Connection models	All rigid	Rigid + 1 set of springs	Rigid + 1 detailed FE model	All 5-member joints hinged
(m)	-0.281	-0.285	-0.2845	-0.286

The equivalent spring model produces a good approximation of the behavior of a gusset plate connection in the elastic range. A major difficulty is that it is based on a prior detailed FE model.

9.2.2 NONLINEAR ANALYSES

Nonlinear analyses of the model with large deflections, elasto-plastic and strain hardening material are run for the model with rigid connections. Figure 9.8 shows the load factor-displacement curve for the mid-span node. From this Figure a sudden failure around the load factor of 0.4, where the load factor multiplies the concentrated construction load only (with dead load and traffic load present), is shown.

The sudden increase in the out-of-plane displacement is indicative of buckling. Buckling of the compression chord in a truss bridge occurs when the lateral braces do not have the necessary strength or stiffness to keep the truss node, which is the gusset plates, from moving out of plane. For this reason a three-dimensional model with two parallel main trusses that carry the gravity load is considered in the next paragraph [Crosti, 2010].

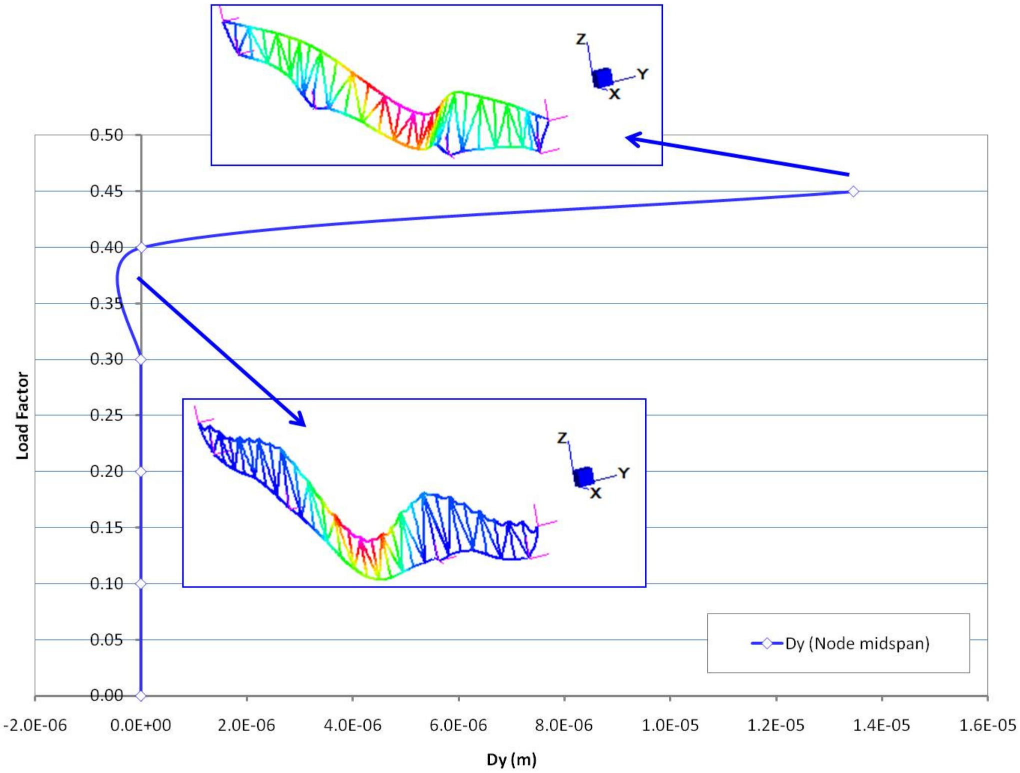

Figure 9.8. Load factor vs out of plane displacement for the midspan node in the out-of- plane direction.

9.3 THREE-DIMENSIONAL MODEL OF THE BRIDGE

In the three-dimensional model (Figure 9.9) the introduction of the lateral bracing members prevents the global buckling of the truss chord. The loads applied are the same as the two dimensional model; in Figure 9.10 and 9.11 the traffic and the construction loads are specified.

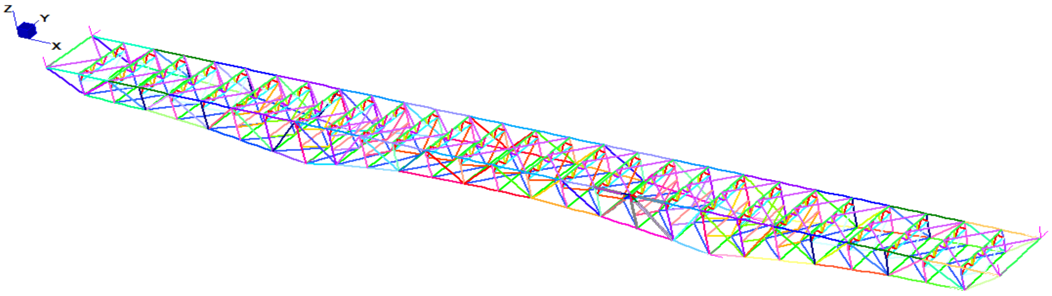

Figure 9.9. 3D model.

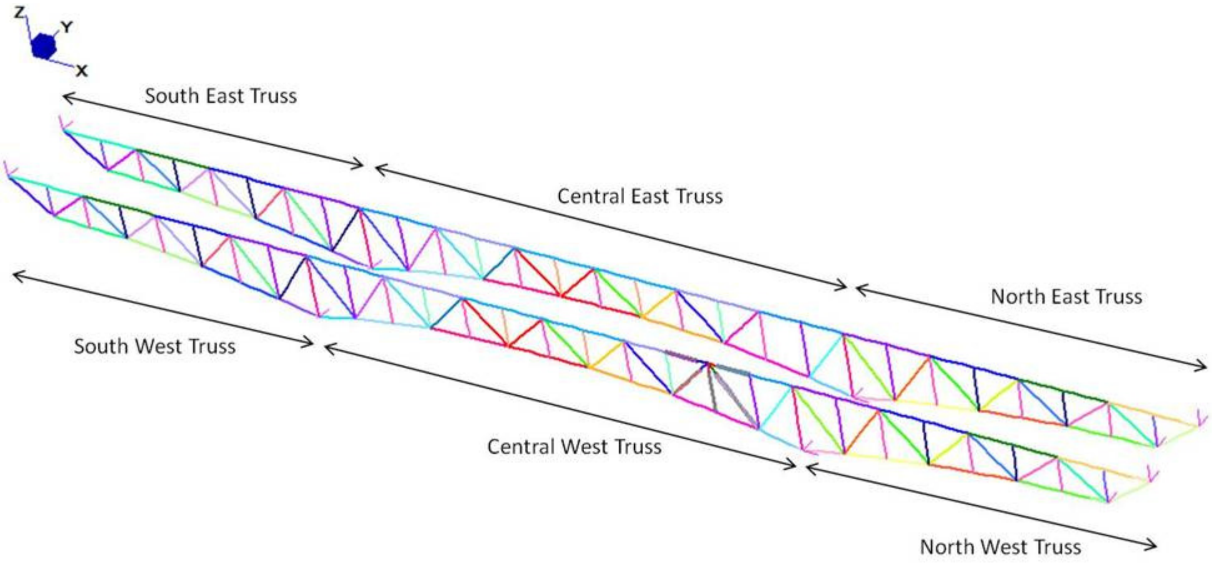
Z
Y
X
South East Truss
Central East Truss
North East Truss
South West Truss
Central West Truss
North West Truss

Load in N/m	TRAFFIC LOAD		STEEL LOAD		CONCRETE LOAD	
TRUSS	*WEST*	*EAST*	*WEST*	*EAST*	*WEST*	*EAST*
SOUTH	6183.77	3010.88	17931.14	17931.14	111390.27	111390.27
CENTRAL	8278.88	1571.38	17931.14	17931.14	111390.27	111390.27
NORTH	9099.75	2157.85	17931.14	17931.14	111390.27	111390.27

Figure 9.10. Traffic load.

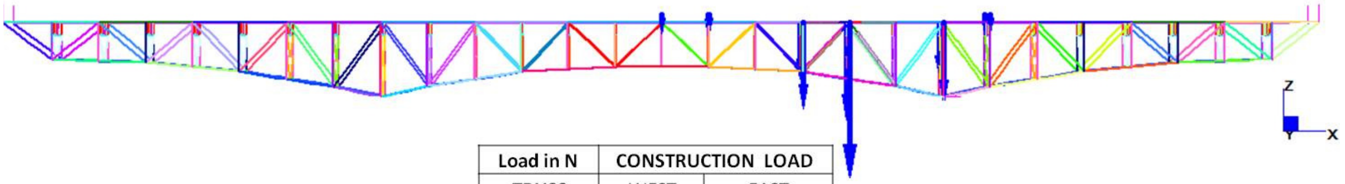

Load in N	CONSTRUCTION LOAD	
TRUSS	*WEST*	*EAST*
SOUTH	7506.34	5838.26
	7506.34	5838.26
	1105494.25	663296.55
	2130697.50	1278418.50
	1025203.88	615122.33
NORTH	2502.11	1946.09

Figure 9.11. Concentrated load for the construction load.

Two different models are taken account:

1. Rigid joints, 5 members around the U10-W elasto-plastic and the others elastic;

2. Semi-rigid joint, elasto-plastic connection elements (only the diagonal terms of the stiffness matrix) and the 5 members around the U10W joint elasto-plastic.

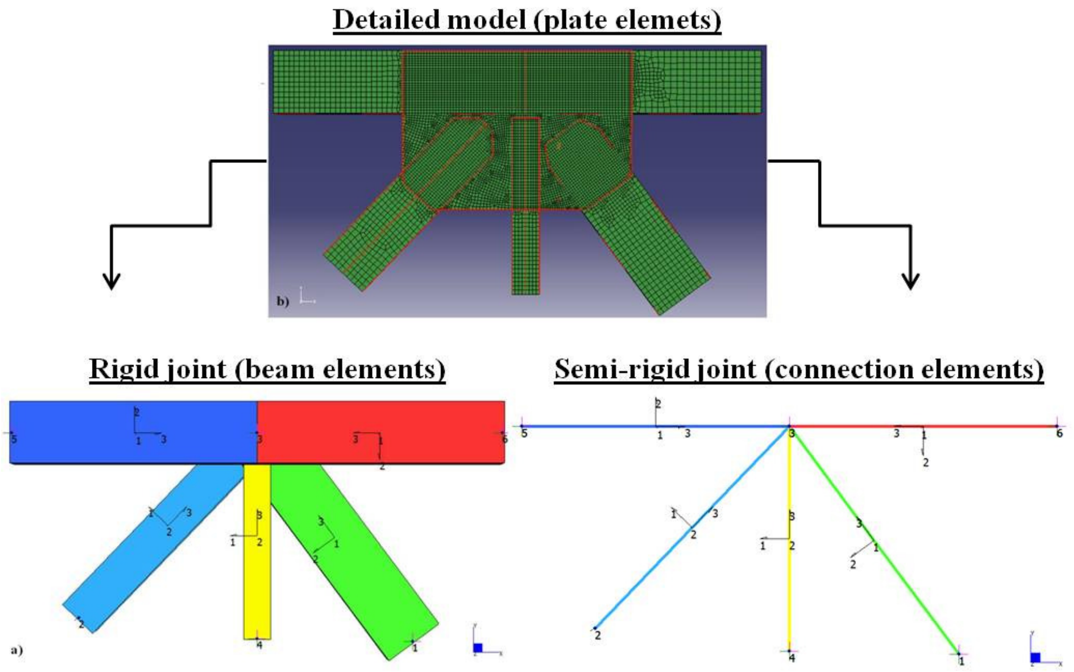

Detailed model (plate elemets)

Rigid joint (beam elements)

Semi-rigid joint (connection elements)

Figure 9.12. Different modeling of the joint.

9.3.1 NONLINEAR CONNECTION MODEL

The nonlinear behavior of the 5-member connections is now represented by means of 5 nonlinear elements using the method similar to the linear model, chapter 9. There are two essential differences:

1. The behavior must be represented by a set of load-displacement or moment-rotation points calculated from the detailed FEM (using ABAQUS);
2. The stiffness matrix of each nonlinear element is diagonal only, in order to use the connection elements available in STRAUS7/STRAND7. It is expected nevertheless that this simplification will introduce some errors compared to the detailed FEM.

Nonlinear material behavior is modeled using the Von Mises yield criterion and the isotropic hardening rule.

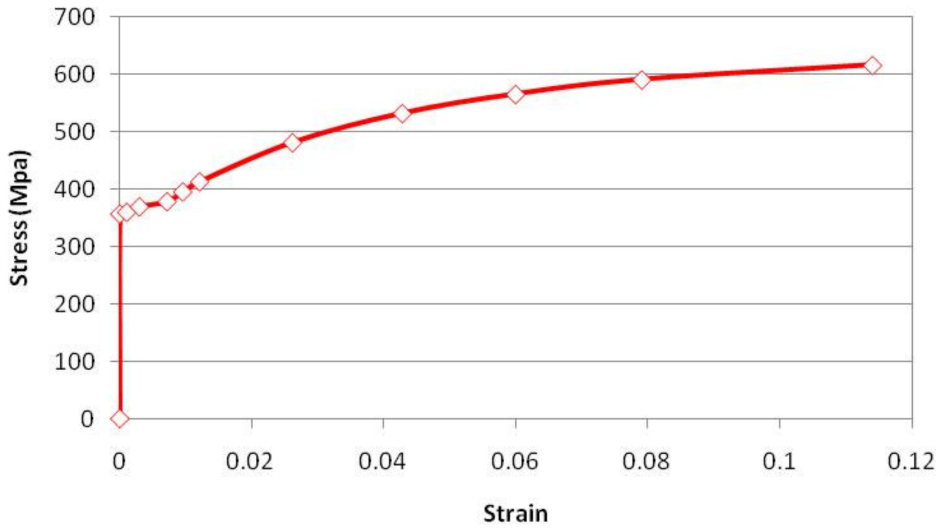

Figure 9.13. Stress-strain curve, [Bruneau, 1998].

A large strain-large displacement formulation, which is the default option for ABAQUS, is used to carry out the nonlinear analysis. Figures 9.14 to 9.18 show the load-displacement and moment-rotation curves of each element, where XYZ refers to the global coordinate system. For simplicity only the positive values are shown in the next figures.

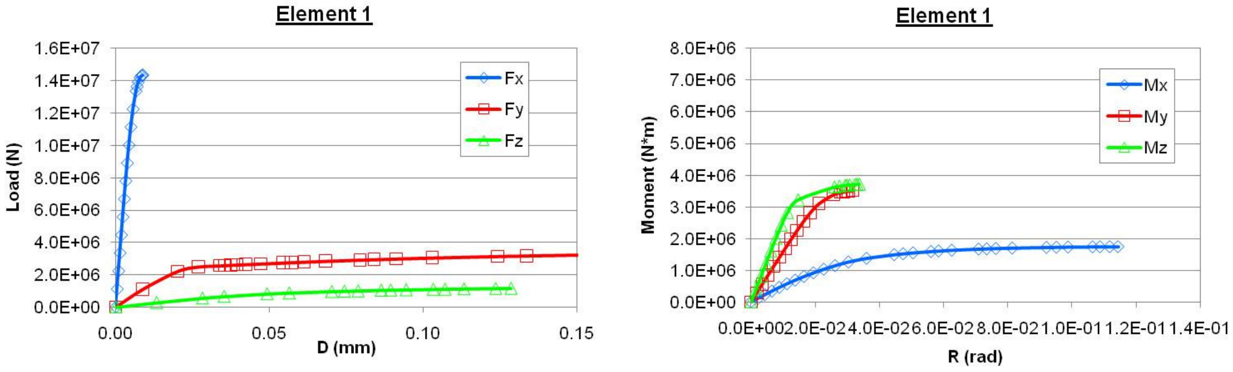

Figure 9.14. Member 1.

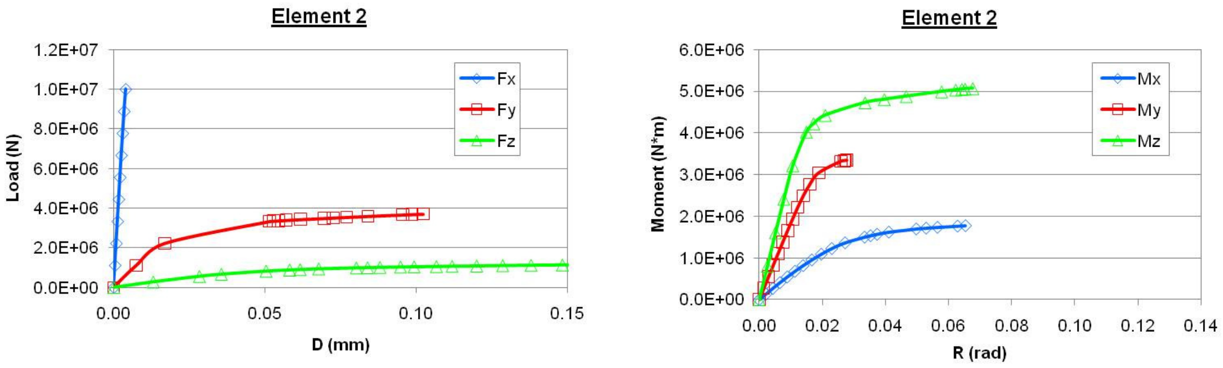

Figure 9.15. Member 2, (the F_x should have been plotted with negative values to be coherent with the XYZ coordinates system, but for simplicity in the graph has been plotted with positive values).

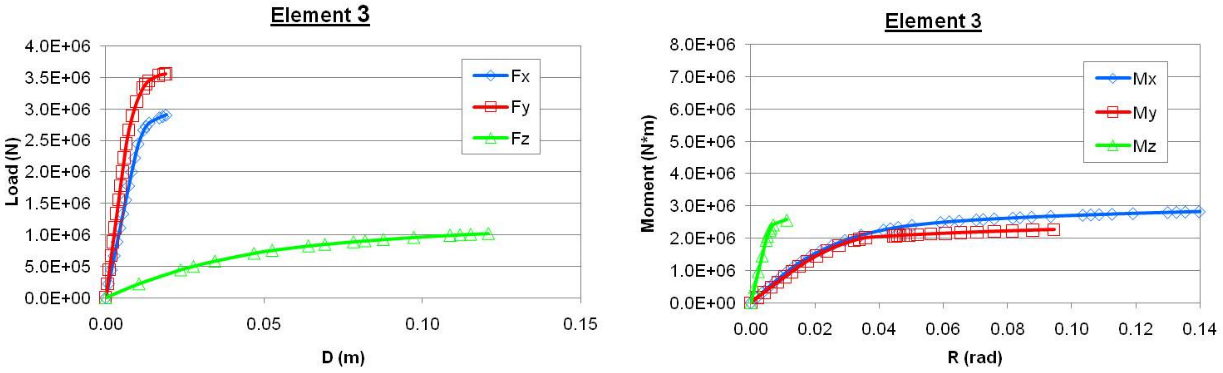

Figure 9.16. Member 3.

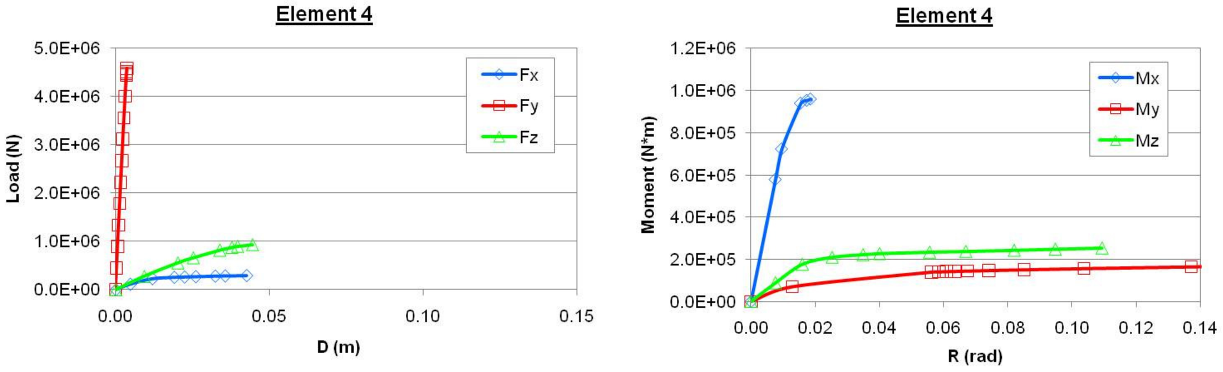

Figure 9.17. Member 4.

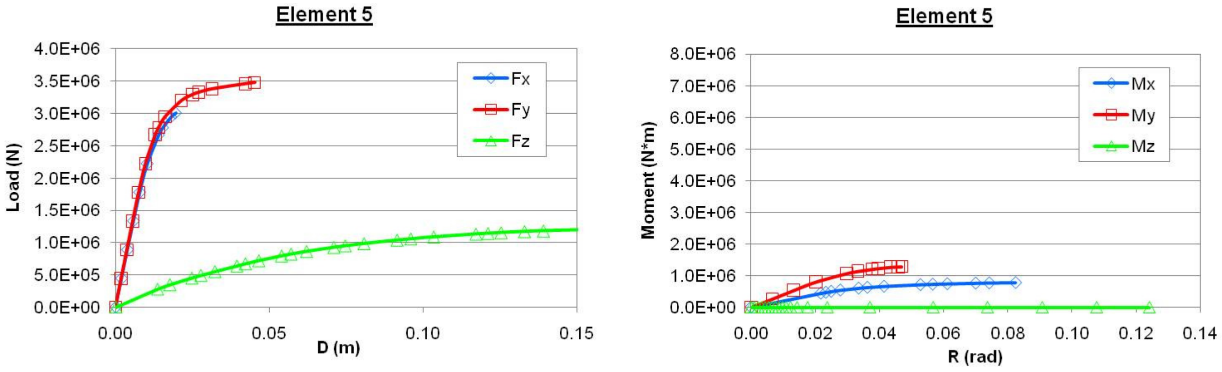

Figure 9.18. Member 5.

9.3.2 NONLINEAR ANALYSES

Analyses with nonlinearity of material and geometry are run. For model 1, with rigid joints, the collapse occurs because of failure in the members by yielding. Figure 9.20 shows where the plastic hinge is localized.

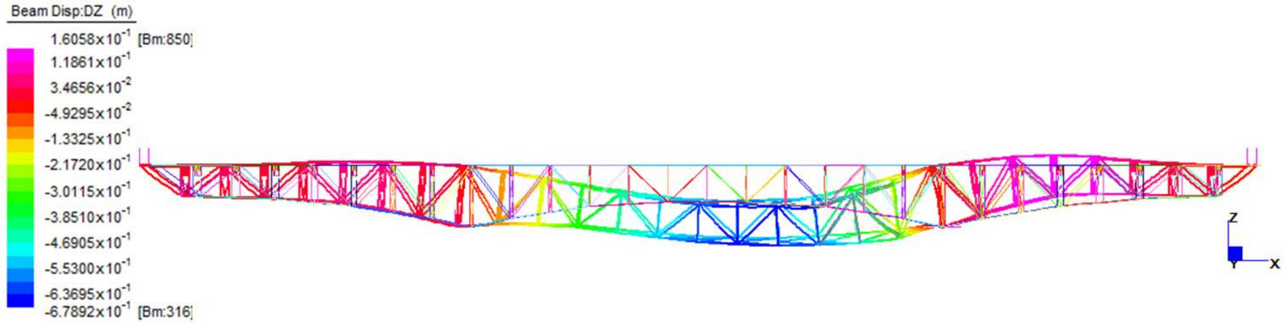
Beam Disp:DZ (m)
1.6058x10^{-1} [Bm:850]
1.1861x10^{-1}
3.4656x10^{-2}
-4.9295x10^{-2}
-1.3325x10^{-1}
-2.1720x10^{-1}
-3.0115x10^{-1}
-3.8510x10^{-1}
-4.6905x10^{-1}
-5.5300x10^{-1}
-6.3695x10^{-1}
-6.7892x10^{-1} [Bm:316]
Z
Y
X

Figure 9.19. Rigid joints model. Deformed shape of 10 scaling at load factor of 6.36.

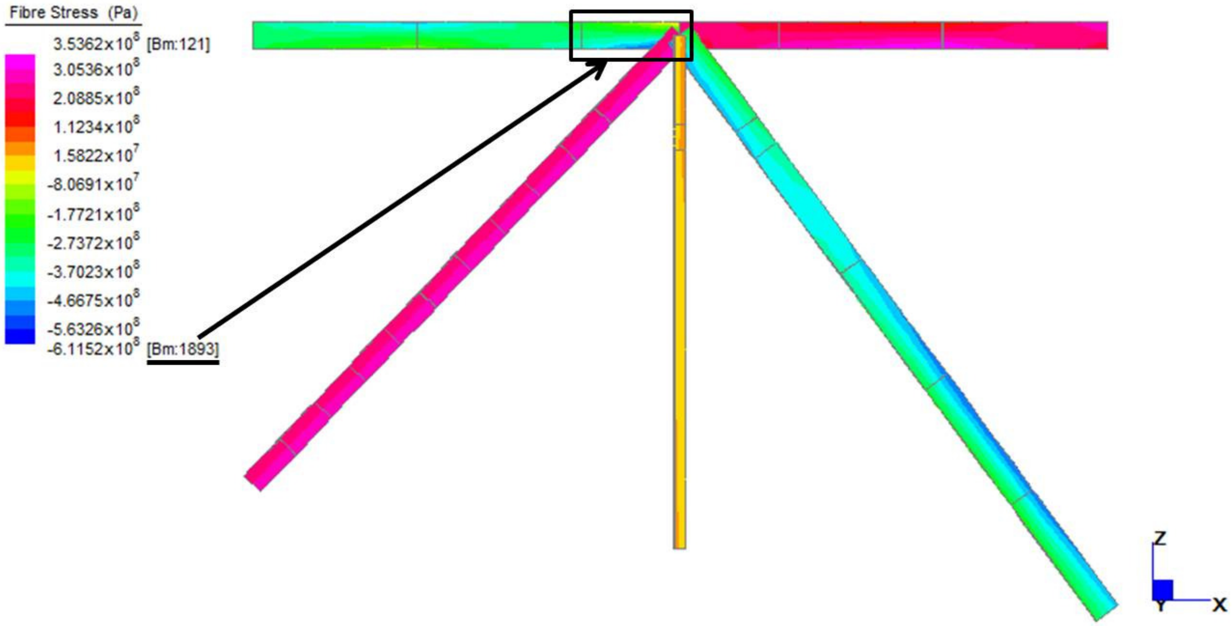
Fibre Stress (Pa)
3.5362x10^8 [Bm:121]
3.0536x10^8
2.0885x10^8
1.1234x10^8
1.5822x10^7
-8.0691x10^7
-1.7721x10^8
-2.7372x10^8
-3.7023x10^8
-4.6675x10^8
-5.6326x10^8
-6.1152x10^8 [Bm:1893]
Z
Y
X

Figure 9.20. Localization of the yield hinge. Trend of stress in the 5 elements around the joint U10-W.

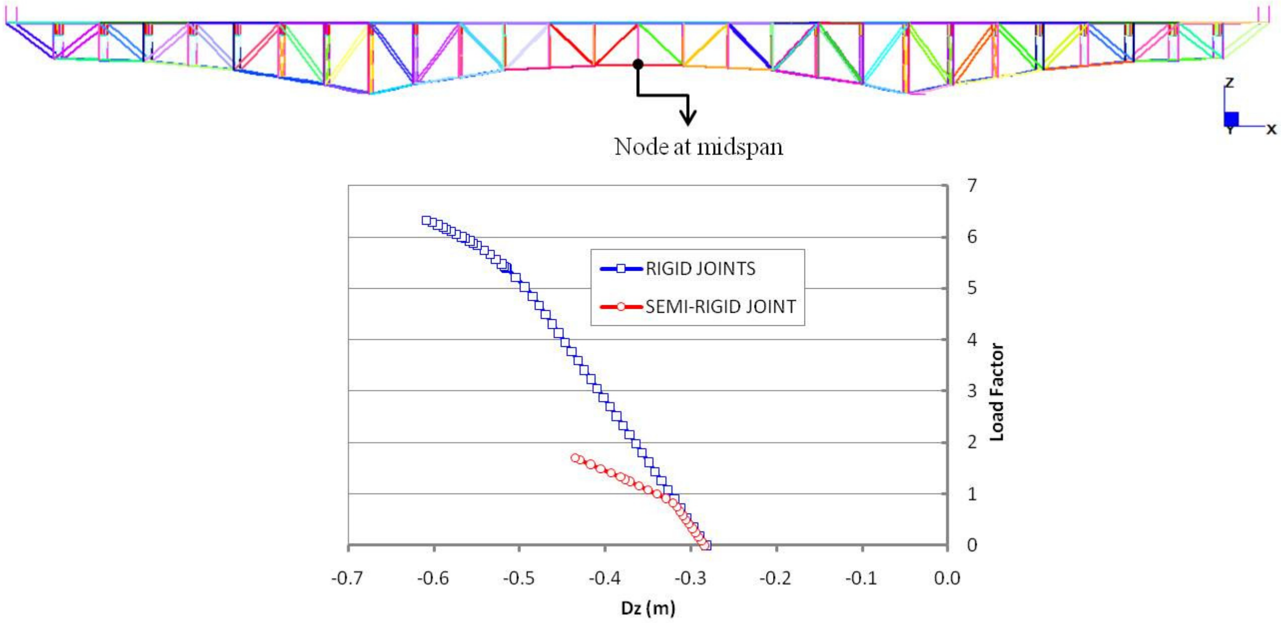

Figure 9.21. Load Factor-Vertical Displacement at the node in the midspan.

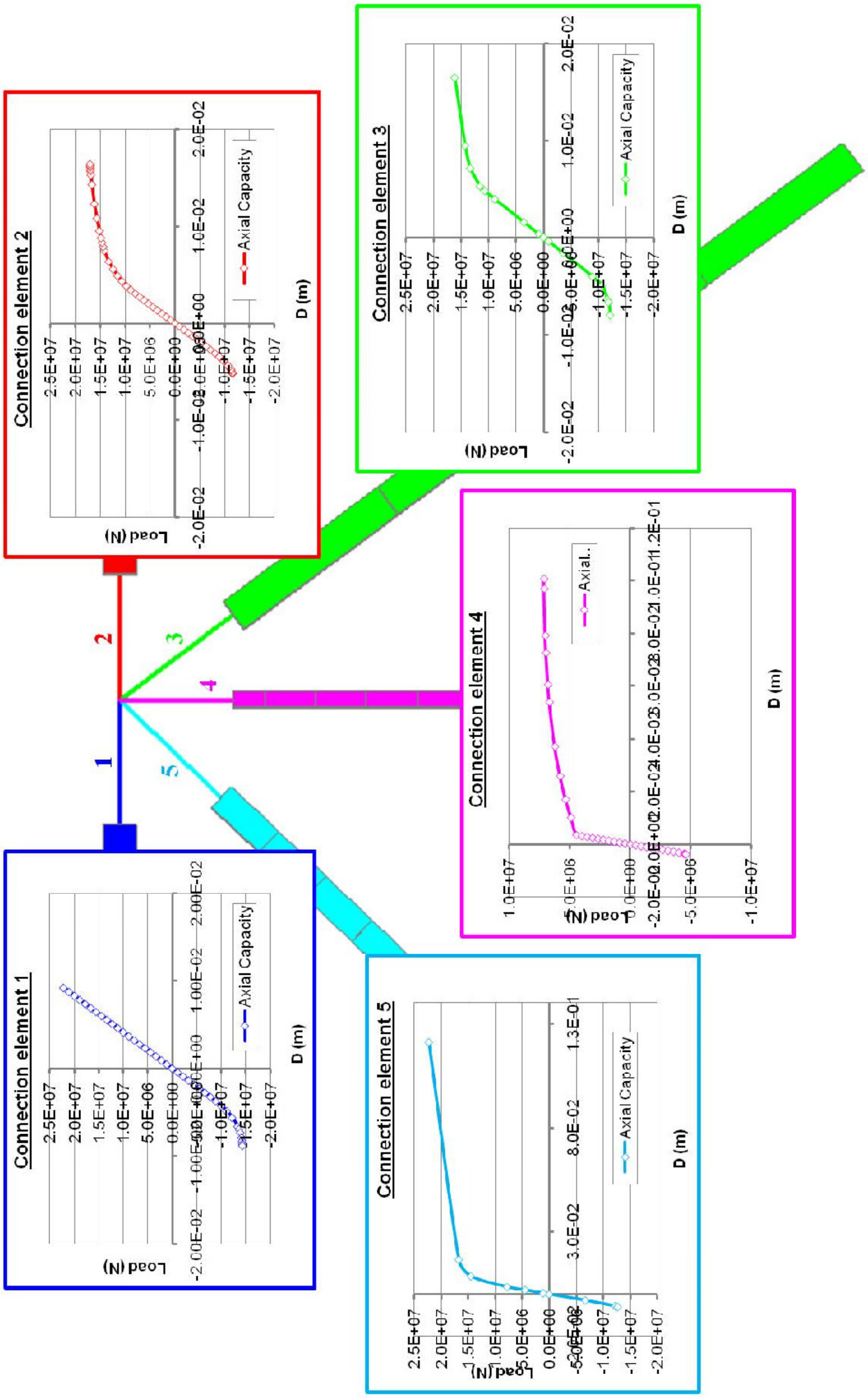

Figure 9.22. Tension and compression axial capacity in the five connection elements, (local coordinates).

The semi-rigid connection provides a much better description of the actual behavior. Whereas the rigid joint model predicts member failure at a load factor of 6.36, the semi rigid joint model predicts that U10 begins to fail at a load factor of 0.92, and completely fails at load factor 1.7, leading to the collapse of the bridge. In Figure 9.22 the trend of the axial forces in the 5 connection elements modeling the joint U10-W is shown. This figure shows that collapse starts because of the achievement of the axial capacity in compression of the connection element 3, which is actually the main reason for the real collapse.

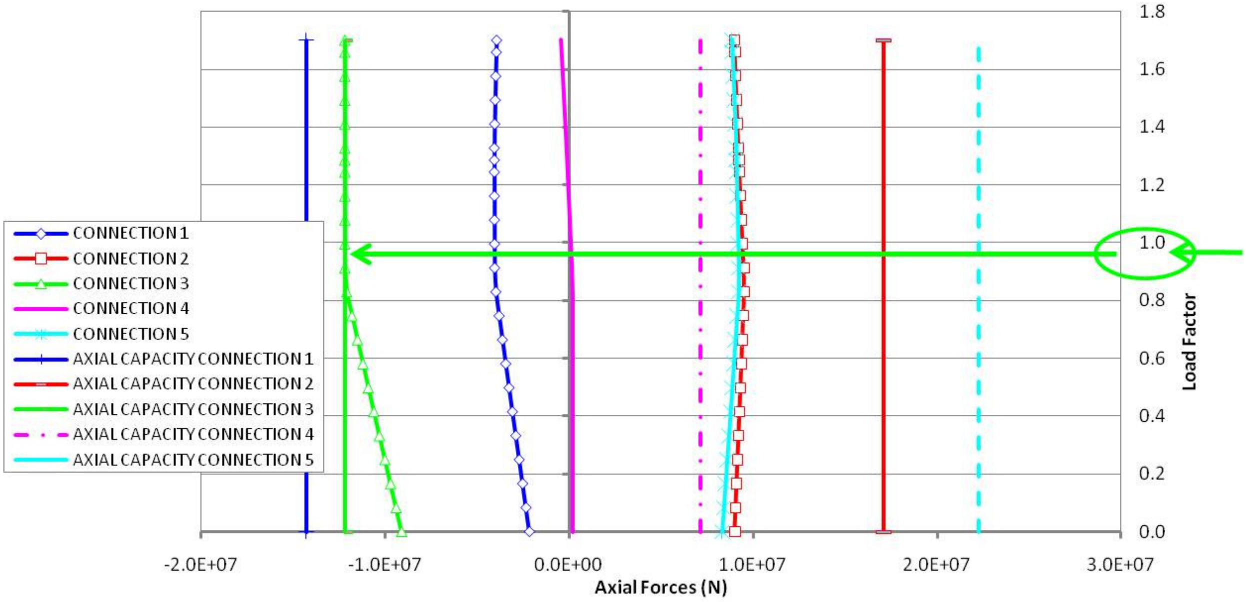

Figure 9.23. Semi-rigid joint. Trend of the axial forces in the 5 connection elements of the chosen joint.

Figure 9.23 shows the deformation in the detailed model in Abaqus with scale factor of 10. This figure refers to the ultimate compression load that the model can carry. It is obvious that failure occurs because of the large displacements on the free edge of the gusset plate.

This particular deformed shape could be made in comparison with the Figure 9.24 where it easy to see the initial deformation that the gusset plate had before the collapse, Figure 9.25.

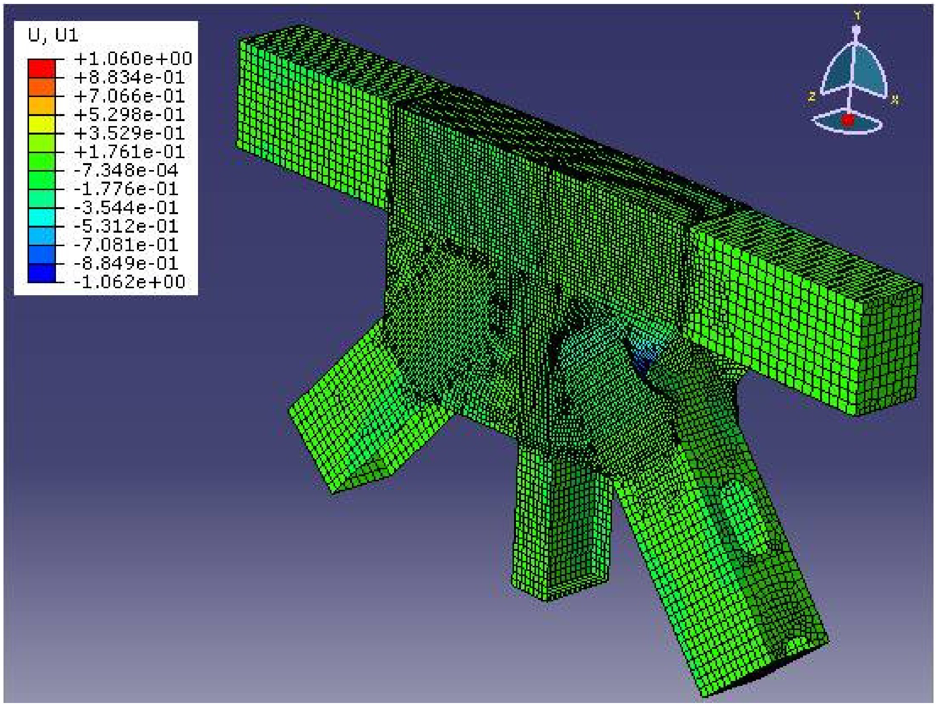
U, U1
+1.060e+00
+8.834e-01
+7.066e-01
+5.298e-01
+3.529e-01
+1.761e-01
-7.348e-04
-1.776e-01
-3.544e-01
-5.312e-01
-7.081e-01
-8.849e-01
-1.062e+00
Y
Z
X

Figure 9.24. Deformation of the detailed model at F (compression) of 1.21E+7.

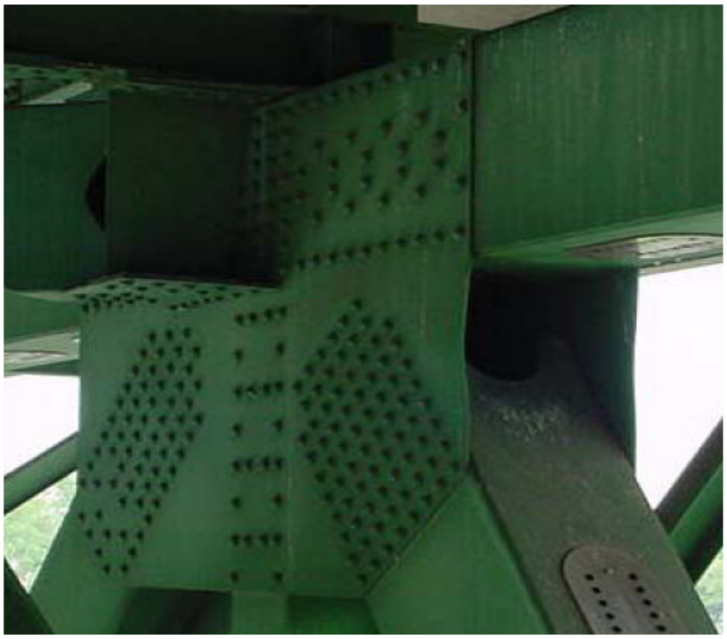

Figure 9.25. Picture of U10 W connection taken on June 2003, [NTSB, 2008].

9.4 CONCLUSION

From the nonlinear analyses on the 3D model of the bridge it has been possible to reproduce the collapse of the bridge.

The correct modeling of the critical joint (U10-W) led the connection element (used to reproduce the gusset plate and the member) to fail (that is just what happened on the real structure). After that, the west truss lost stiffness and resistance and after a while the local failure led the whole structure to fail.

All of that has been possible to achieve because of the correct way of modeling the connection; in fact if this would not have been done, modeling the joint as rigid for example, the ultimate load factor would have been about four times bigger.

Therefore this way to proceed is not only faster and less complicated to deal with but also sufficiently accurate to reproduce the real behavior of the structure under study.

One objection that could be made is anyhow that for this bridge only one connection has been modeled by means of detailed model; therefore it is reasonable to ask what and if the structural response could change in case of modeling all the connections with the five connection elements previously used. The answer to this issue has been given in the appendix.

CONCLUSION

1. CONCLUSION
2. FUTURE WORK

CONCLUSION

1. CONCLUSION

The main goal of this thesis was to develop a method of analysis able to take into account the proper stiffness and strength of the gusset plates in a steel truss bridge.

One of the first questions raised in this thesis was: "how safe is it to model all the connections of steel truss bridges as rigid joints?"

To answer that, the first part of the work focused on reviewing the literature and the recent codes. From that review, it is concluded that there is a gap in knowledge about the way to model the joints in this type of structure. The only rigorous way to do it is by means of finite element analyses that are complex and computationally demanding.

The proposed sub-structuring analysis gives good results both in linear and nonlinear ranges, and is able to capture the actual failure of the gusset plate under study.

Nonlinear analyses run for the specific case of the I35-W, in chapter 9, show that the assumption of rigid joints predicts strength about four times greater than the one with the more correct joint modeling. Moreover, as shown in Figure C.1, it is possible to assess the cause of the collapse that, in this specific case, is the achievement of the axial capacity of the connection element number 3.

This way to proceed gives also good results in terms of computational time saving, as summarized in Figure C.2, which shows the number of elements and the time necessary to run the analyses.

One limitation found in these analyses was that, modeling only one detailed joint, it was impossible to apply the same connection elements to the others joint;, nevertheless a simple application of the method to a simpler steel truss bridge confirms the thesis that if the critical element is known it is enough to model in a detailed way just that one.

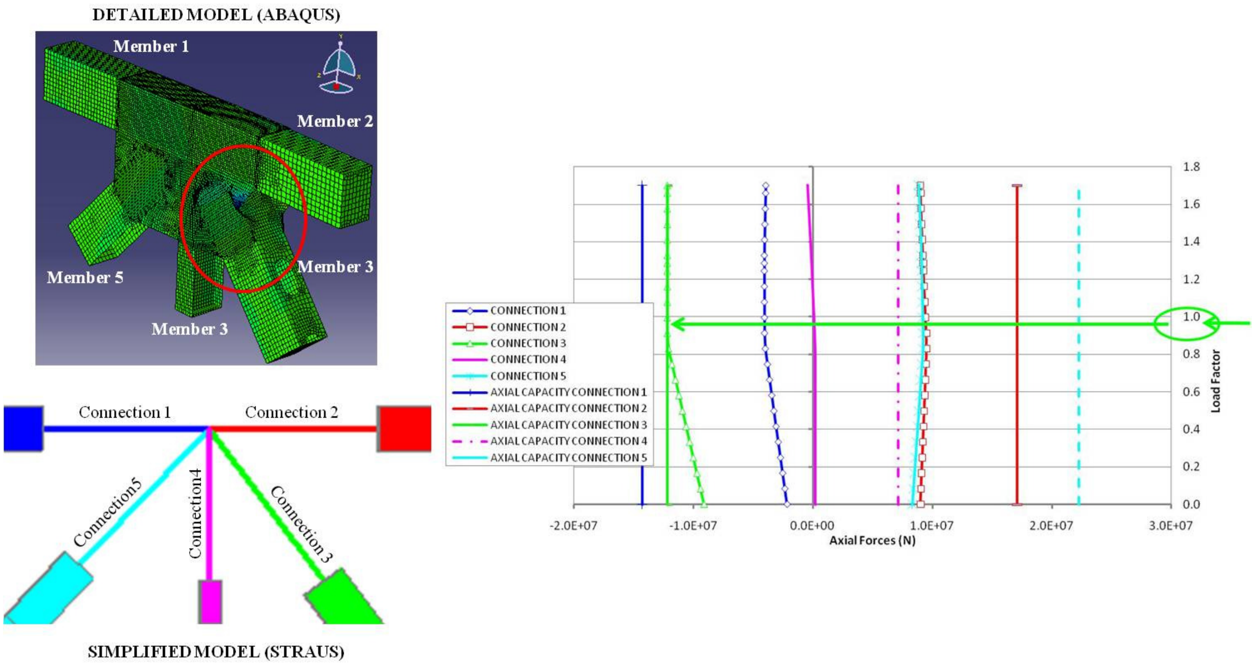

Figure C.1. On the left the detailed and simplified model used to model the joint, on the right the trend of the axial force of each connection elements modeling the join under study.

ABAQUS	STRAUS
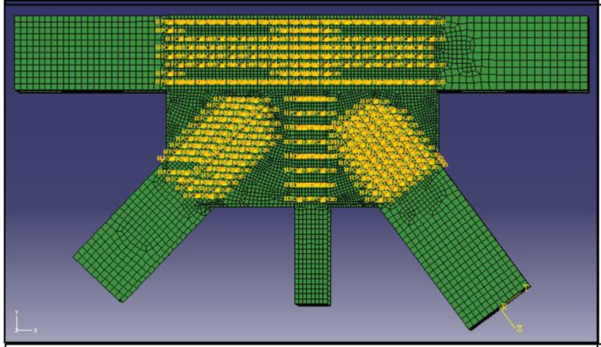	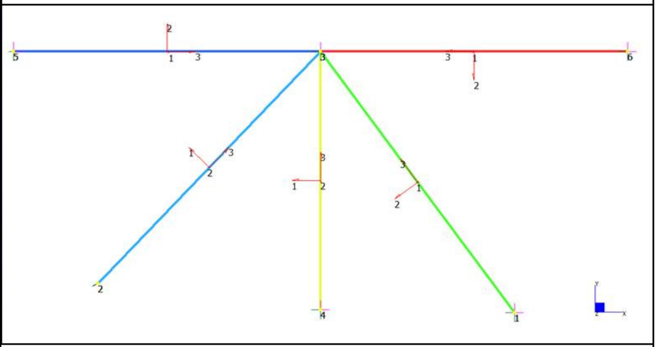
Each gusset plate is composed of 289,000 elements	5 connection elements
Running time of nonlinear analyses: 1h 30 min	Running time of nonlinear analyses: 10 min

Figure C.2. Comparison between the two models used.

2. FUTURE WORK

- FHWA is performing full scale physical tests of gusset plates. It would be interesting to extract spring characteristics directly from these tests, Figure C.3 and C.4. Nevertheless, it is not possible to test all possible bridge configurations; so FEA needs to be relied upon. Parametric studies could be performed, and the spring characteristics related to the physical properties of the gusset plate, thus obviating the need for future designers to perform their own detailed connection study.

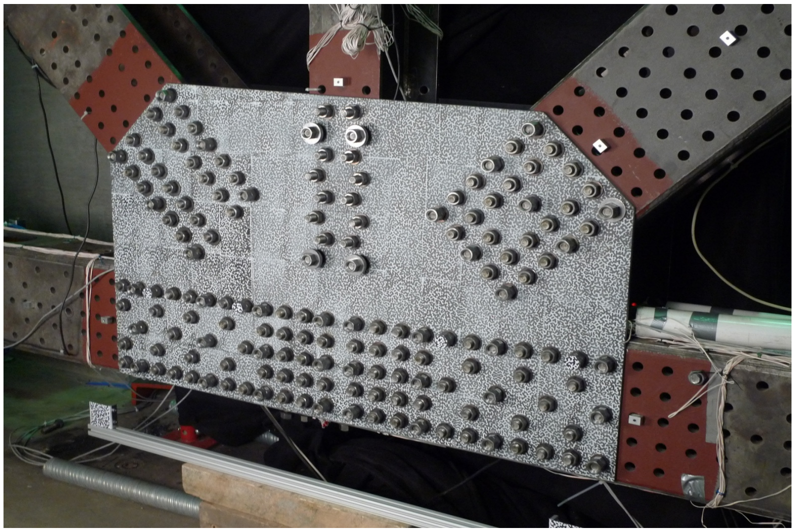

Figure C.3. Test performed at FHWA in Virginia, USA.

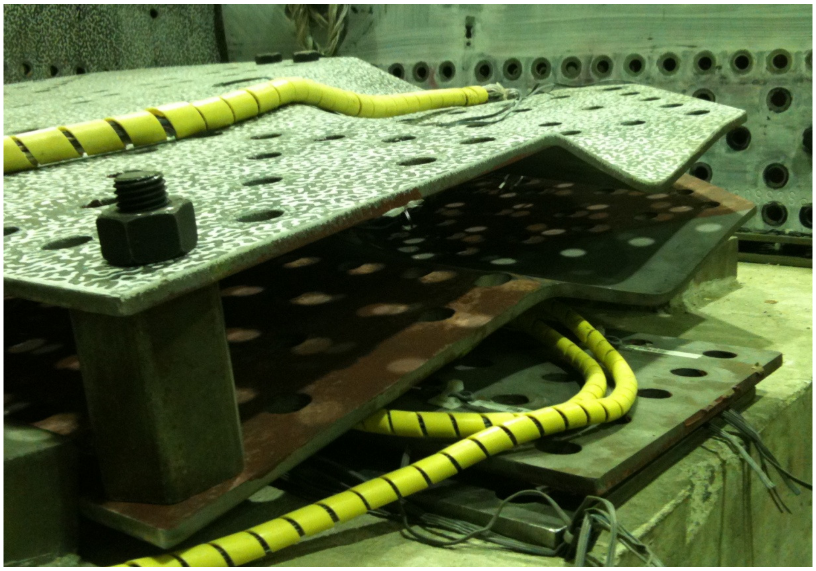

Figure C.4. Results of these tests, buckling of the gusset plates.

- As already said, I-35W Bridge was subjected constantly to inspection to assess its safety but even with that people in charge did not notice that the bridge was about to fail. A future work, linked on what done in this thesis, could be to develop parametric study on some particular shapes of gusset plates in order to identify some "critical" points where, for example, the monitoring of the out-plane displacements, could give to the owners of the bridges a warning of what it is happening in the connection. The main goal would be therefore to improve prediction of actual performance of steel bridges through a better understanding of the behavior of connection. An idea of monitoring could have been done with a technique of monitoring developed by Mark Iadicola (NIST) who focuses his research on two areas of structural health monitoring:

- development of non-destructive techniques; and
- analysis for determining the degraded condition of infrastructural components and their subcomponents.

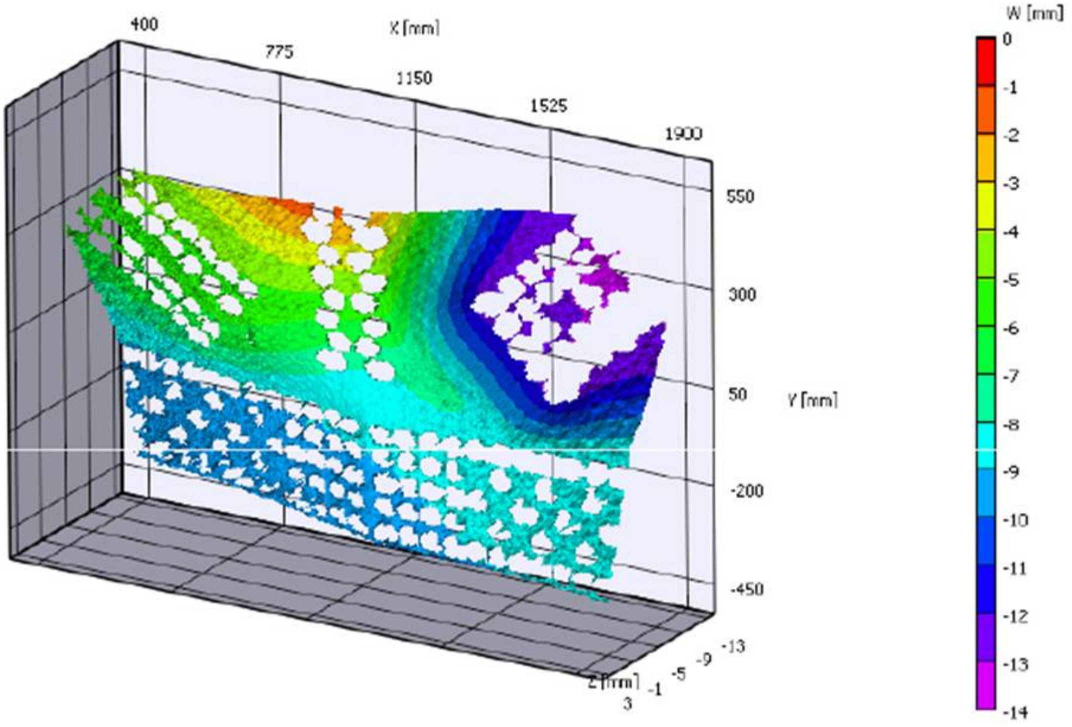

Figure C.5. Displacement monitoring for a gusset plate of the FHWA tests.

Figure C.5 refers to a measure of out of plane displacements of a gusset plate during one of the tests FHWA is running, see Figures C.3 and C.4.

APPENDIX

APPENDIX

The general procedure is applied to a simple steel truss bridge in order to assess the importance of modeling the joints by means of the five- element connection described in Chapter 8. The goal is to show that it is possible to accurately predict the ultimate strength of a truss bridge, accounting for connection behavior, without recourse to vast computer resources. In this example, a model with the same section members as in the joint analyzed in the I-35W Bridge was built. The bridge under study has the geometry shown in Figures A.1 and A.2. For simplicity, the structure considered is planar and almost all its joints are the 5-member connection previously studied. Figure A.3 shows an actual example of this type of bridge, which is based on the Howe truss patented in 1840. The bridge is subject to distributed loads on the top chord which model the traffic, and the dead load and to 3 point loads with different intensity which model the construction loads applied on 3 nodes of the upper chord.

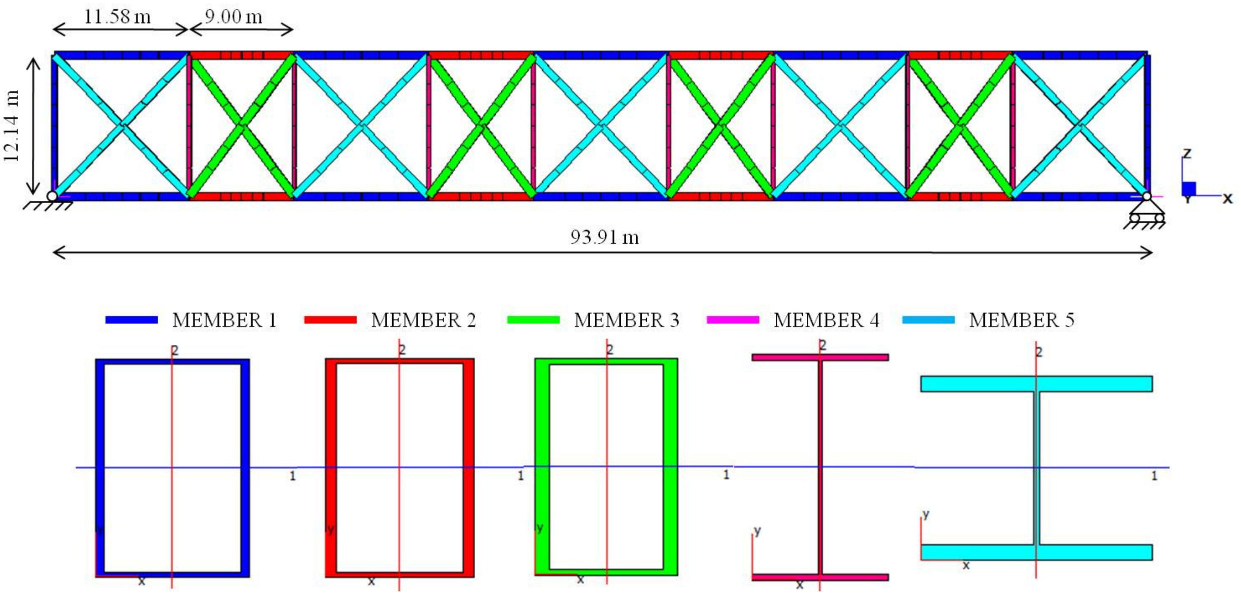

Figure A.1. Geometry of the truss bridge.

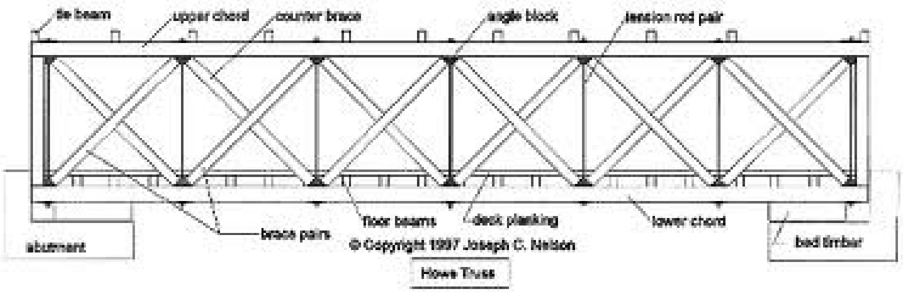
tie beam
upper chord
counter brace
angle block
tension rod pair
abutment
brace pairs
floor beams
deck planking
lower chord
bed timber
© Copyright 1997 Joseph C. Nelson
Howe Truss

Figure A.2. Typical example in literature of bridges with the same geometry.

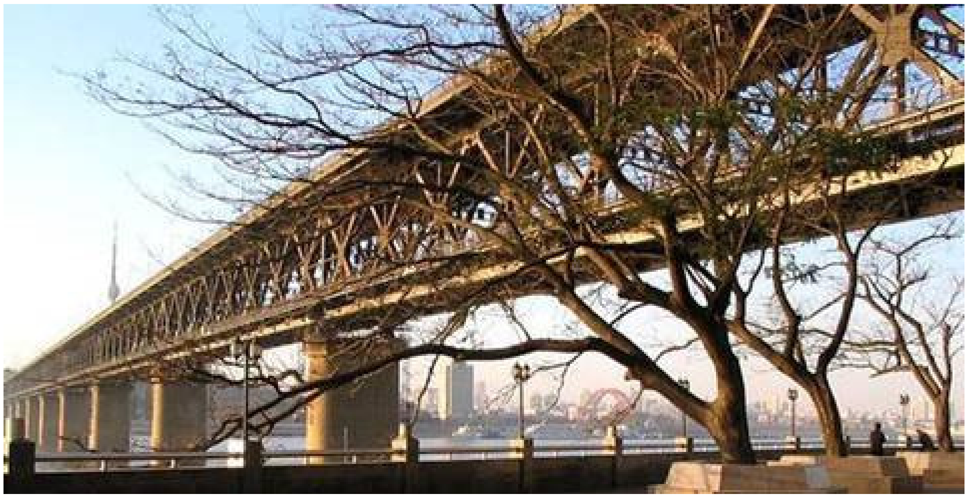

Figure A.3. Bridge with X diagonal, First Whhan Bridge in China. (Wikipedia).

Distributed Load (30 kN/m + 10 kN/m + 8 kN/m)

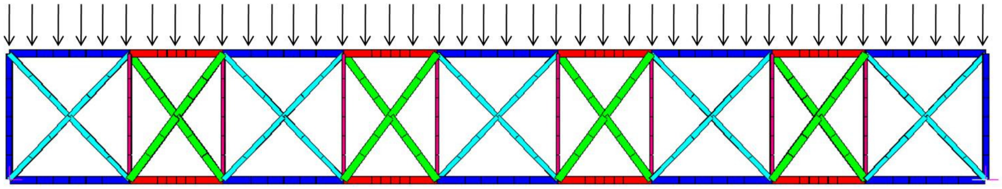

Concentrated Load (80 kN ; 140 kN; 80 kN)

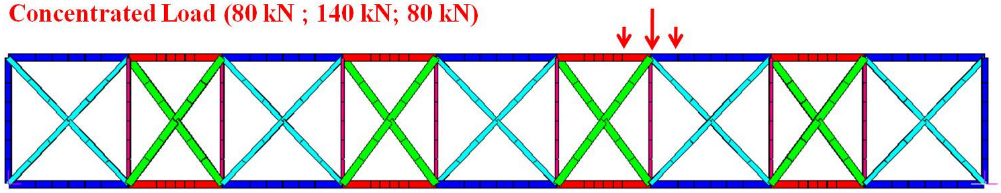

Figure A.4. Two load cases considered.

Four models are considered, which involve different approaches on the modeling of the joints:

1. Rigid joints;
2. Semi-rigid joints with just one joint modeled by the 5-connection elements previously described;
3. Semi-rigid joints, with all the 5-member joints modeled by 5 connection elements previously described;
4. Pinned joints, with all the 5-member joints modeled by hinged joints.

Nonlinear analyses (nonlinearity of material and geometry) are run by applying an increasing load factor to the concentrated loads only, with the uniform load constant.

Figure A.6 shows the load factor-vertical displacement for the four different models considered. This Figure shows the 4 ultimate load factors the structure can carry, which are obviously functions of the different ways to model the joints. As expected model 4 pinned joints, is the one with the lowest value, about 1.4, and the greatest one is the one from model 1 rigid joints, while the models with semi-rigid joints fall in between.

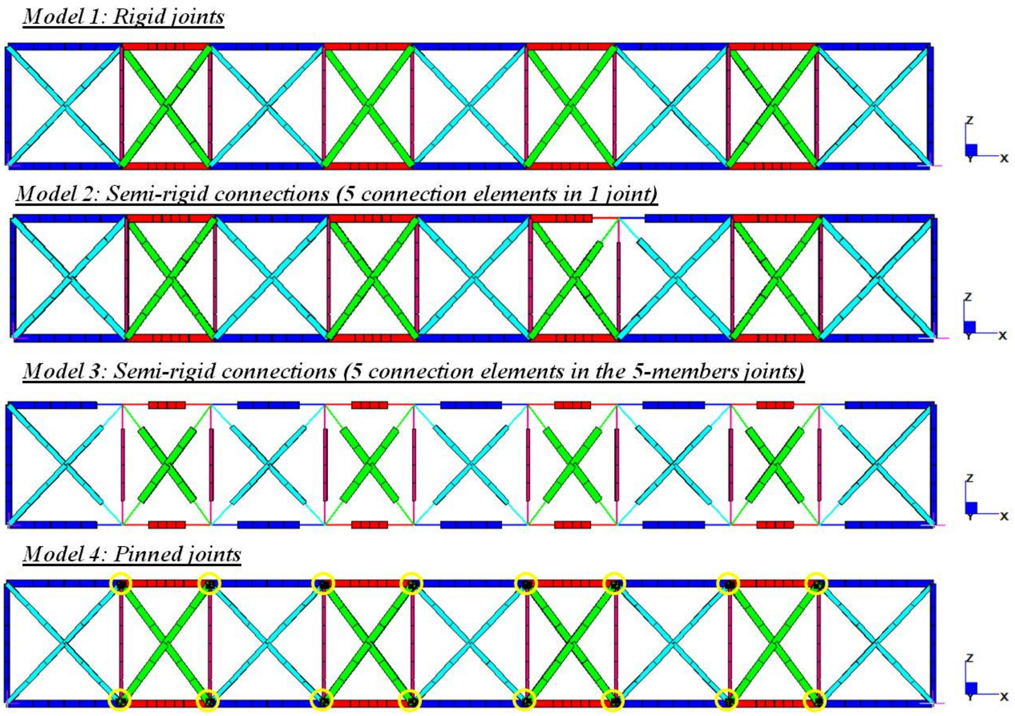

Model 1: Rigid joints

Model 2: Semi-rigid connections (5 connection elements in 1 joint)

Model 3: Semi-rigid connections (5 connection elements in the 5-members joints)

Model 4: Pinned joints

Figure A.5. The four different models considered.

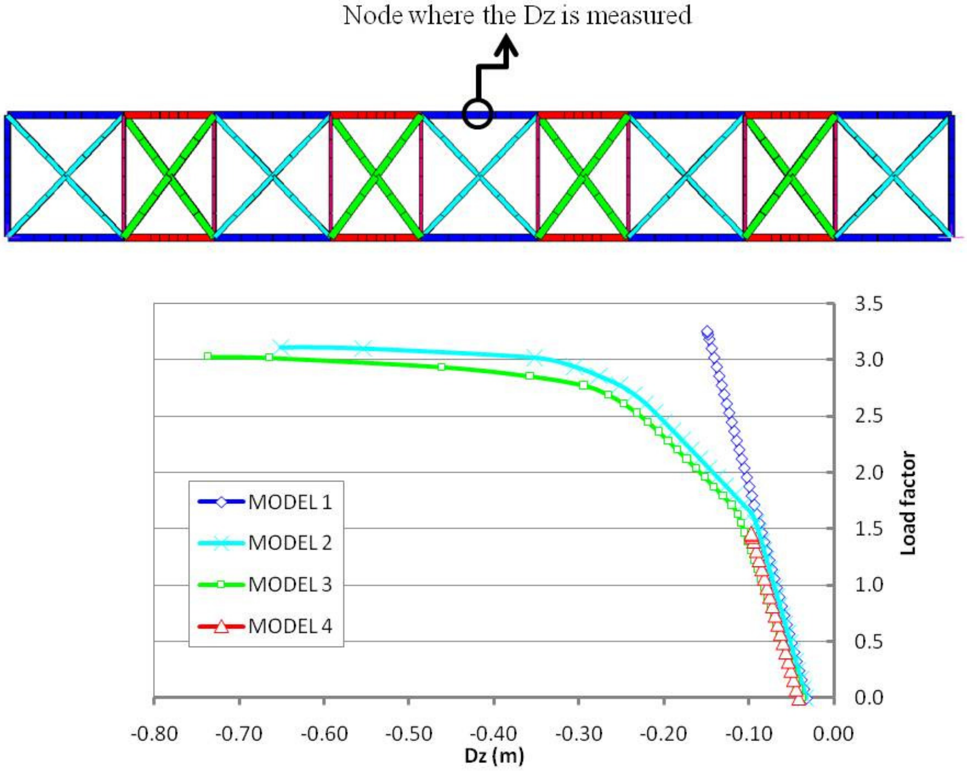

Figure A.6. Load factor-vertical displacement.

Model 1: Rigid joints

Model 1 reaches the ultimate load factor of 3.26. Figure A.7 shows the total stress in the members at the ultimate load factor. That shows as the collapse is reached because of the failure of the members.

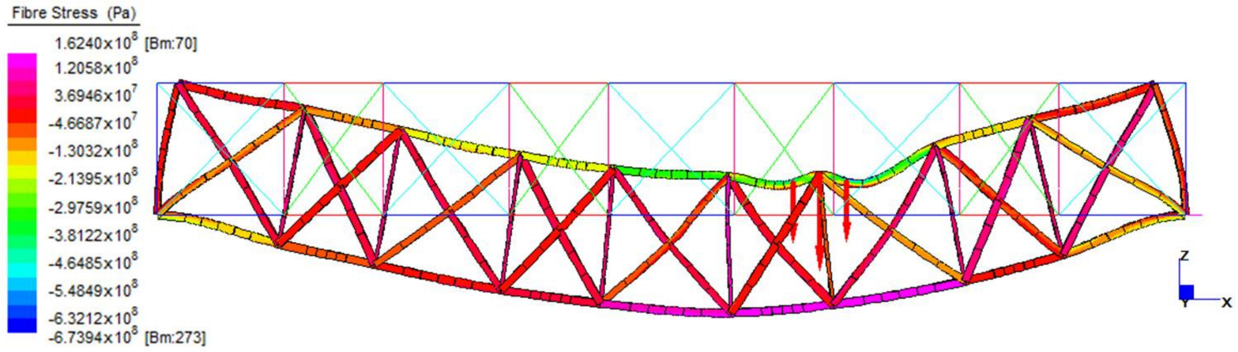
Fibre Stress (Pa)
1.6240x10⁸ [Bm:70]
1.2058x10⁸
3.6946x10⁷
-4.6687x10⁷
-1.3032x10⁸
-2.1395x10⁸
-2.9759x10⁸
-3.8122x10⁸
-4.6485x10⁸
-5.4849x10⁸
-6.3212x10⁸
-6.7394x10⁸ [Bm:273]
Z
Y
X

Figure A.7. Rigid joints, (Deformed scale of 10).

Model 2: Semi-rigid connections (5 connection elements in one joint)

The particular of the joint under study is showed in Figure A.8, the axial capacity of each connection element is plotted in Figure A.9. From this figure the failure of the truss bridge can be easily evaluated and attributed to the achievement of axial capacity of the connections. At around a load factor of 1.98 the connection 2 reaches the axial capacity; then it happened to connection 1 and in the end to connection 3 and 4 which lead to the failure of the bridge.

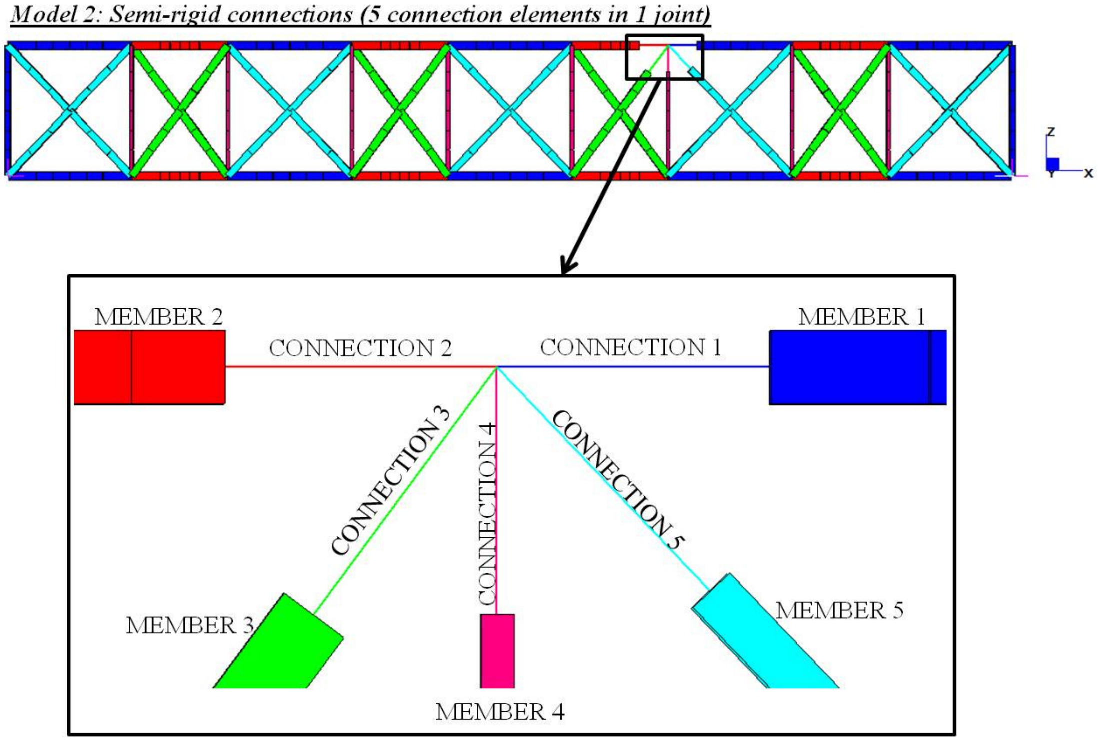
Model 2: Semi-rigid connections (5 connection elements in 1 joint)
Z
X
MEMBER 2
CONNECTION 2
CONNECTION 1
MEMBER 1
CONNECTION 3
CONNECTION 4
CONNECTION 5
MEMBER 3
MEMBER 5
MEMBER 4

Figure A.8. Model 2, Semi-rigid joints, 5 connection elements in one joint.

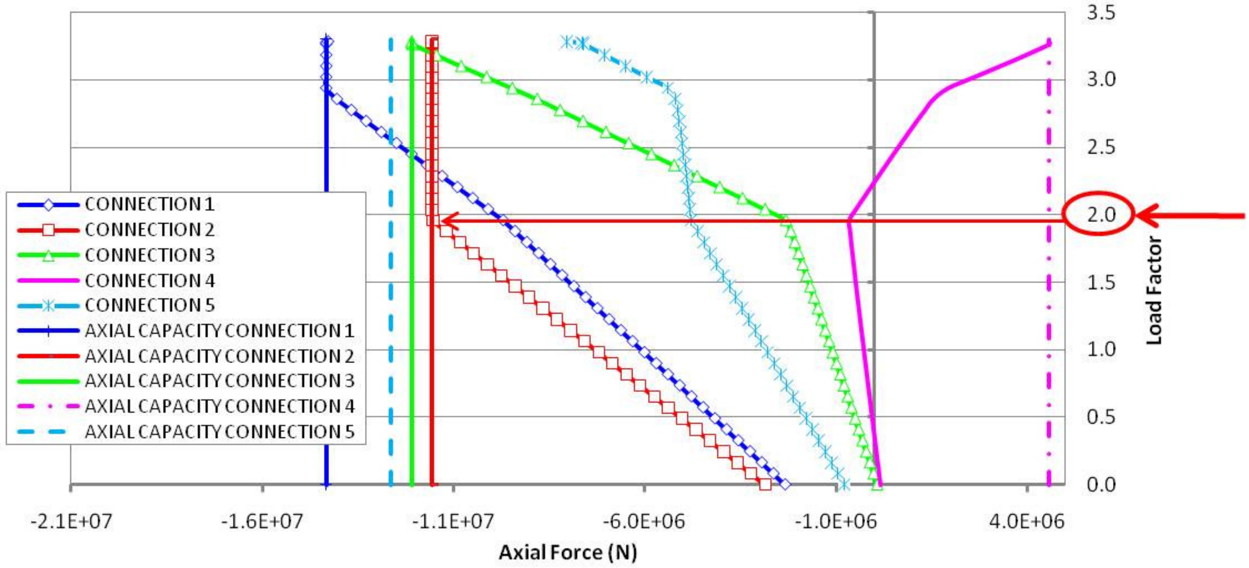

Figure A.9. Model 2, Semi-rigid joints, 5 connection elements in one joint. Trend of the axial forces in the 5 connection elements of the joint chosen.

Model 3: Semi-rigid connections (5 connection elements in the 5-members joints)

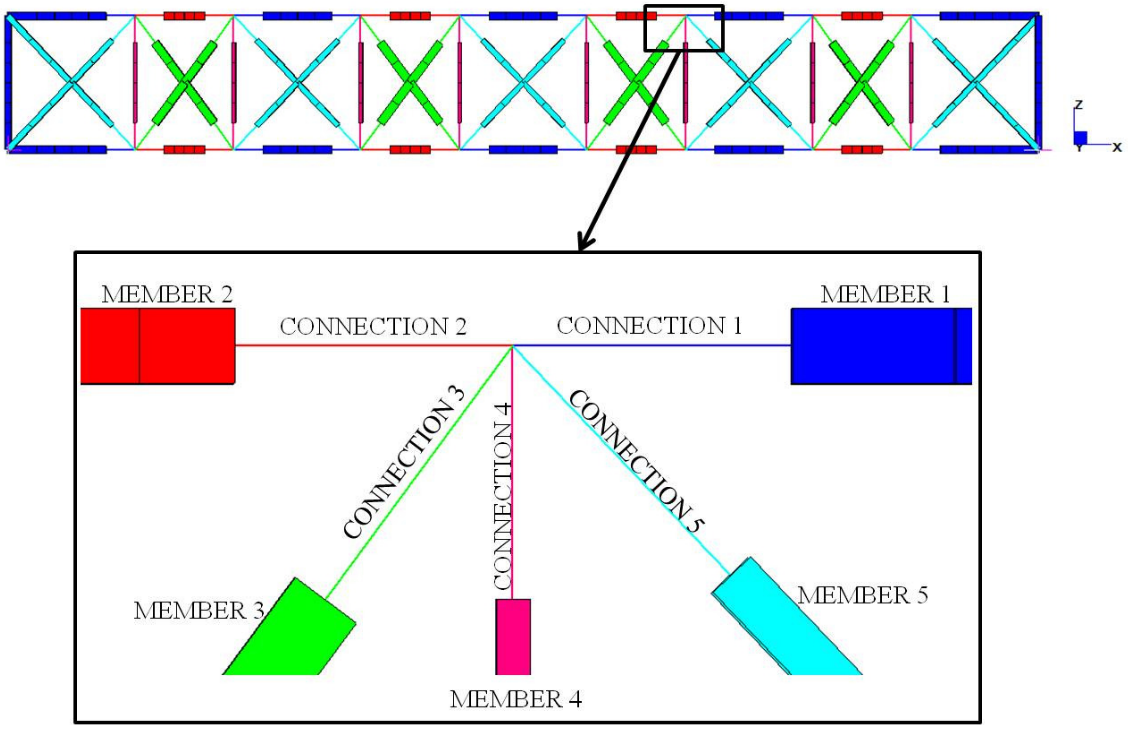
z
x
MEMBER 2
MEMBER 1
CONNECTION 2
CONNECTION 1
CONNECTION 3
CONNECTION 4
CONNECTION 5
MEMBER 3
MEMBER 5
MEMBER 4

Figure A.10. Semi-rigid connections (5 connection elements in the 5-members joints).

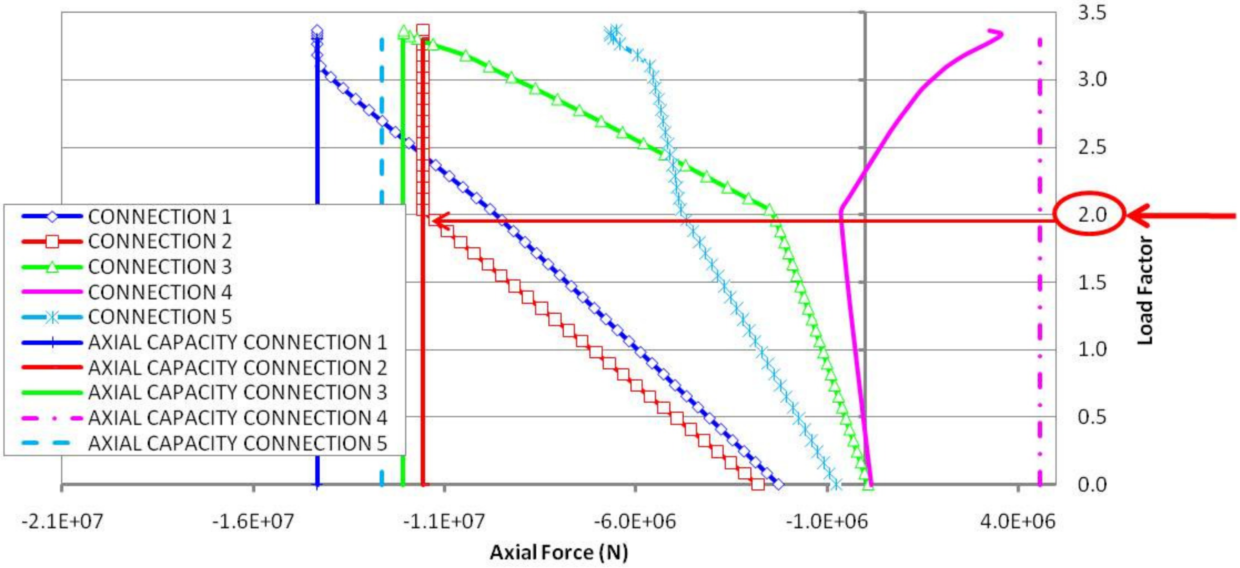

Figure A.11. Model 3, Semi-rigid joints, 5 connection elements in all the 5-member joints. Trend of the axial forces in the 5 connection elements of the joint chosen.

Model 4: Pinned joints

As the last case, the model with pinned joints is analyzed. Model 4 reaches the ultimate load factor of 1.46. Figure A.12 shows the total stress in the members at the ultimate load factor. For this model the failure is reached as soon as a plastic hinge is developed in member 1 of the joint.

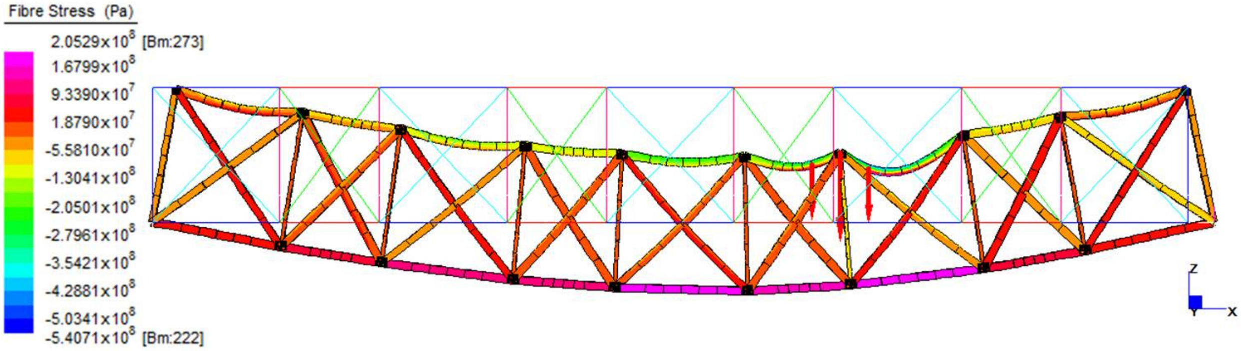
Fibre Stress (Pa)
2.0529x10^8 [Bm:273]
1.6799x10^8
9.3390x10^7
1.8790x10^7
-5.5810x10^7
-1.3041x10^8
-2.0501x10^8
-2.7961x10^8
-3.5421x10^8
-4.2881x10^8
-5.0341x10^8
-5.4071x10^8 [Bm:222]
z
x

Figure A.12. Model 4, Pinned joints, (Deformed scale of 10).

CONCLUSION

Accurate prediction of bridge failure should include proper modeling of connections (in some cases, as above, a hinged model is a close lower bound; in other cases, the rigid joint model may be a close upper bound). This can be done economically and accurately if the same joint model can be used repeatedly at multiple locations, or if multiple load cases must be run. The nonlinear spring model provides a simplified way to model connections and achieve that goal.

REFERENCES

[AASHTO, 1994], American Association of State Highway and Transportation Officials (1994) “*AASHTO LRFD Bridge Design Specifications*,” Washington, D.C. 20001.

[ABAQUS], ABAQUS, http://www.simulia.com/

[Arangio et al., 2010], Arangio S., Bontempi F. and Ciampoli M., (2010). “*Structural integrity monitoring for dependability*”, Journal of Structure and Infrastructure Engineering. In press.

[AISC, 2005], American Institute of Steel Construction, (2005), “*Code of Standard Practice for Structural Steel Buildings and Bridges”* (AISC 303-10).

[AISC, 2010], American Institute of Steel Construction, (2010), “*Specification for structural steel buildings”,* June 2, 2010.

[ASCE 7-10, 2010], ASCE/SEI 7-10, (2010), “*Minimum Design Loads of Buildings and Other Structures*”.

[Astaneh, 1989], Astaneh, A., (1989) “*Simple methods for design of steel gusset plates*,” Proc. ASCE Structures Congress ’89, San Francisco, CA pp 345-354.

[Astaneh, 2010], Astaneh-Asl A., (2010),“*Gusset Plates in Steel Bridges-Design and Evaluation*”, Steel TIPS Report, Structural Steel Educational Council, Moraga, CA, April 2010, 156 pp.

[AASHTO, 1994], AASHTO-LRFD Specifications (1994), by American Association of State Highway and Transportation Officials in Washington, D.C .

[Baldassino, 2010], N. Baldassino, A. Bignardi, R. Zandonini, "Response of end-plate joints under combined forces" in Proceedings of the International Colloquium SDSS'RIO 2010 Stability and Ductility of Steel Structures, Rio de Janeiro: Federal University of Rio de Janeiro and State University of Rio de Janeiro , 2010, p. 183-190.

[Baldassino and Zadonini, 2008], Baldassino N., Zandonini R., "*Il requisito di robustezza strutturale nella progettazione*", Costruzioni Metalliche, v. anno LX , n. Luglio Agosto (2008), p. 49-55.

[Ballio and Mazzolani, 2005] Ballio G., Mazzolani F.M., (2005), “*Strutture in acciaio: sistemi strutturali – sicurezza e carchi – materiale – unioni e collegamenti - resistenza e stabilità”*. Hoepli.

[Beaufait, 1970],	Beaufait F.W., Romain W.H.JR and Hoadley P.G., Hackett R.M., (1970), "*Computer methods of structural analysis*". Prentice-Hall.
[Biondini et al., 2008],	Biondini F., Frangopol D.M. and Restelli S., (2008), "*On Structural Robustness, Redundancy and Static Indeterminacy*", ASCE-SEI Structures Congress 2008, Vancouver, Canada, April 24-26.
[Bontempi, 2006]	Bontempi F., (2006), "*Basis of design and expected performances for the Messina Strait Bridge*", International Conference of Bridge Engineering, Hong Kong, November 1-3, 2006.
[Bontempi et al., 2008],	Bontempi F., Arangio S. and Sgambi L., (2008), "*Tecnica delle Costruzioni: Basi della progettazione Elementi intelaiati in acciaio*", Carocci. 2008.
[Bontempi and Arangio, 2010],	Bontempi F., Arangio S., (2010), "*Dependability of Complex Bridge Structural Systems*". 5th Int. Conf. On Bridge Maintenance, Safety and Management (IABMAS 2010), Philadelphia, Pa. July 11-15 2010.
[Bontempi et al., 2010],	Bontempi F., Ciampoli M. and Arangio S., (20100, "*Dependability of offshore wind turbines*". 12th International Conference on Engineering, Science, Construction and Operation in Challenging Environments, Earth and Space 2010. March 14-17 2010. Honolulu, Haway.
[Brown, 1988],	Brown V.L. (1988), "*Stability of Gusseted Connections in Steel Structures*," Ph.D. thesis, University of Delaware, Newark, DE.
[Brown, 1990],	Brown V.L. (1990), "*Stability Design Criteria for Gusseted Connections in Steel-Framed Structures*," Proc. Annual Tech. Sess. On Stability of Bridges, Structural Stability Research Council, St. Louis, MO, 357-364.
[Chambers and Ernst 2005],	Chambers J.J., Ernst C.J. (2005), "*Brace frame gusset plate research – Phase 1 literature review, volumes 1 and 2*," Dept. of Civil Engg. University of Utah, Salt Lake City, UT 84112-0561.
[Cheng et al., 2000],	Cheng, R.J.J., Grondin, G.Y., and Yam, M.C.H., (2000) "*Design and Behaviour of Gusset Plate Connections*", Fourth International Workshop on Connections in Steel Structures, Oct. 22-25, Roanoke, VA. AISC, Chicago, IL 60601-1802.
[Crosti and Bontempi, 2008]	Crosti C., Bontempi F., (2008), "Performance assessment of steel structure subject to fire action", CST2008 & ECT2008 Conferences, Athens, 2008.
[Ciampoli, 2005],	Ciampoli M., (2005), "*Reliability assessment of complex structural systems*", Proceedings of AIMETA 2005, 11-15 September 2005 Florence. Firenze University Press.

[Crosti and Duthinh, 2009a] Crosti, C., Duthinh, D., (2009), "*Buckling of Steel Gusset Plates"*, 5th Int. Conf. on Bridge Maintenance, Safety and Management (IABMAS 2010), Philadelphia, Pa. July 11-15.

[Crosti and Duthinh, 2009b] Crosti, C., Duthinh, D., (2009), "*Block shear failure of steel gusset plates*", 5th Int. Conf. on Bridge Maintenance, Safety and Management (IABMAS 2010), Philadelphia, Pa. July 11-15.

[Crosti and Duthinh, 2010] Crosti C., Duthinh D., (2011), *"A linear model for gusset plate connections",* SEWC, Como, April 4-6, 2011.

[Crosti, 2010] Crosti C., (2011), "*Toward safer steel bridges through more accurate and affordable modeling of connections*", EUROSTEEL 2011, August 31- September 2, 2011, Budapest, Hungary.

[Dowswell and Barber, 2004], Dowswell B., Barber S., (2004), "*Buckling of gusset plates: a comparison of design equations to test data,*" Proc. Annual Stability Conf. Structural Stability Research Council, Rolla, MO.2004.

[EN 1990], EN 1990: Basis of structural design

[FHWA, 2009], Federal Highway Administration, "*Load rating guidance and examples for bolted and riveted gusset plates in truss bridges*" FHWA-IF-09-014, Washington, DC 20590. 2009.

[FEMA 277, 1996] Report of FEMA Mitigation Directorate and ASCE, (1996), "*The Oklahoma City Bombing: Improving Building performance Through Multi-Hazard Mitigation*", FEMA 277, Reston, Virginia, 30 August 1996.

[FEMA, 1997], FEMA, (1997), "*Seismic Performance of Bolted and Riveted Connections*" Background Reports; Metallurgy, Fracture Mechanics, Welding, Moment Connections and Frame Systems Behaviour, Bulletin No. 288, Federal Emergency Management Agency, Washington, DC.

[Galambos and Surovek, 1998], Galambos T.V., Surovek A.E., (2008), "*Structural stability of steel: Concept and Applications for Structural Engineers*", John Wiley & Sons, inc. 2008.

[Galambos, 2008], Galambos T.V., (1998), "*Guide to stability design criteria for metal structures*", Fifth Edition, John Wiley & Sons, inc. 1998.

[Gioncu and Mazzolani, 2002], Gioncu V., Mazzolani M., (2002), "*Ductility of seismic resistant steel structures*", Spon Press. New York. 2002.

[Giuliani, 2008], Giuliani L., (2008), "*Structural integrity: robustness assessment and progressive collapse susceptibility*", PhD thesis at University of

	Rome "Sapienza", advisor Prof. F. Bontempi, Co-advisor Prof. U. Starrosek, Roma 2008.
[Griffiths et al., 1968],	Griffiths, H., Pugsley, A., and Saunders, O., "*Report of Inquiry into the Collapse of Flats at Ronan Point, Canning Town. London: Ministry of Housing and Local Government*", Her Majesty's Stationary Office, 1968.
[Hsieh and Deierlein, 1991],	Hsieh S.H., Deierlein G.G., (1991), "*Nonlinear Analysis of Three-Dimensional Steel Frames with Semi-Rigid Connections*," Computers and Structures, Vol. 41, No. 5, pp.995–1,009.
[Kachanov, 1974],	Kachanov L.M., (1974), "*Fundamentals of the theory of plasticity*," Mir Pub. Moscow, USSR.
[Hrennikoff, 1934],	Hrennikoff, A., (1934), "*Work of Rivets in Riveted Joints*," Trans. ASCE, vol. 99.
[Huang et al., 2010],	Huang Y.H., Wang R.H, Zou, J.H., and Gan Q., (2010), "*Finite Element Analysis and Experimental Study on High Strength Bolted Friction Grip Connections in Steel Bridges,"* J. Constructional Steel Research, Elsevier, 66, pp. 803-815.
[Huns et al., 2002],	Huns B.B.S., Grondin G.J. and Driver R.G., (2002), "*Block shear failure of bolted gusset plates*", 4th Structural Specialty Conference of the Canadian Society for Civil Engineering, Montreal, Canada, June 5-8, 2002.
[ISO 2394, 1998],	International Standard ISO/FDIS 2394: "*General principles on reliability for structures*", 1998.
[Landolfo,],	Landolfo R., (2008). "*Acciao & Ricerca*". Costruzioni metalliche n.1, 2008, pag. 57-73.
[Leon, 1994],	Leon R.T., (1994), "*Composite Semi-Rigid Construction",* Engineering Journal, AISC, Vol.31. No. 2, 2nd Quarter, pp. 57–67.
[Leon et al., 1996],	Leon R.T., Hoffman J. and Staeger T., (1996), "*Design of Partially-Restrained Composite Connections"*, Design Guide 8, AISC, Chicago, IL.
[Liao et al., 2010],	Liao M., Okazaki T., Ballarini R., M., Schultz A.E. and Galabos T.V., (2010), "*Nonlinear Finite Element Analysis of Critical Gusset Plates in the I-35W Bridge in Minnesota*", Journal of Structural Engineering. Submitted January 13, 2010; accepted July 13, 2010.
[Martin, 1966],	Martin H. C., (1966), "*Introduction to matrix methods of structural analysis*", Mc Graw-Hill.

[Mc Guire, 1968], Mc Guire W., (1968), “*Steel Structures*,” Prentice-Hall.

[Miur, 2008], Miur L.S., (2008) “*Designing Compact Gussets with the uniform Force Method*”. Engineering Journal / First Quarter / 2008 / 13.

[Nast et al., 1999], Nast T.E., Grondin G.Y. and Cheng R.J.J., (1999), “*Cyclic behaviour of stiffened gusset plate-brace member assemblies*”. University of Alberta Structural Engineering Report No. 229, Edmonton, Alberta, Canada.

[NCHRP, 2005], National Cooperative Highway Research, (2005), “*A Synthesis of Highway Practice*”, Transportation Researcher Board, Washington D.C., 2005.

[NTSB, 2008a] National Transportation Safety Board, (2008a), “*Safety Recommendation H-08-1*,” Jan. 15, Washington D.C. 20594.

[NTSB, 2008b] National Transportation Safety Board, (2008b), “*Modeling Group Chairman Final Report 08-119*”, Nov. 12, HWY07MH024, Washington D.C. 20594.

[NTSB, 2008], National Transportation Safety Board, (2008), “*Collapse of I-35 W Highway Bridge, Minneapolis, Minnesota, August 1, 2007*” Accident Report, NTSB/HAR 08/03 PB 2008-916213, Washington D.C. 20594.

[NTSB, 2008], National Transportation Safety Board, (2008), “*Structural and local failure study of gusset plate in Minneapolis bridge collapse*,” Modeling group chairman final report 08-119, NTSBC070010, Nov., Washington D.C. 20594.

[O’Connell et al., 2001], O’Connell H.M., Dexter R.J. and Bergson P.M., (2001), “*Fatigue evaluation of the deck truss of bridge 9340*”, Minnesota DoT Final Report, March 2001.

[Ocel and Wright, 2008], Ocel J.M., Wright W., (2008), “*Finite Element Modeling of I-35 W Bridge Collapse Final Report*”, Federal Highway Administration, Turner-Faibank Highway Research Center Report, October, 2008.

[PrEN 1993-1-8, 2003], PrEN 1993-1-8, (2003), “*Eurocode 3: Design of steel structures, Part 1.8: Design of joints*”, European Standard, CEN, Brussels..

[Ramberg and Osgood, 1942], Ramberg, W. & Osgood, W.R. (1943) “*Description of Stress-Strain Curves by Three Parameters*”, TechNote 902, National Advisory Committee for Aeronautics, Washington, DC.

[Royal Commission, 1971], Royal Commission, (1971), “*Report of Royal Commission into the failure of West Gate Bridge*”. Melbourne: C. H. Rixon, Governament

Printer.

[Schmidt et al., 2008], Schmidt, H., Fastabend, M., Swadlo, P. and Lommen, H.G., (2008) "*Ein ungewöhniches Stabilitätsproblem verursacht Schadensfall*" Stahlbau **77**, 12.

[SIA260], SIA 260 Building Code, Swiss Society of Engineers and Architects, (1982), "*Sicherheit und Gebrauchstauglichkeit von Tragwerken – Weisung des SIA an seine Kommissionen für die Koordination des Normenwerks*", 5. Fassung 1980 und 11. Fassung, September 1982.

[Simon, 1998], Sinon H.A, (1998), "*The Sciences of the Artificial*", The MIT Press, Cambridge.

[Starrosek, 2007], Starrosek U., (2007), "*Typology of progressive collapse".* Engineering Structures Vol. 29 Pages 2302–2307.

[STRAND7 / STRAUS7], STRAUS, http://www.hsh.info/

[Thornton, 1984], Thornton, W.A., (1984), "*Bracing Connections for Heavy Construction*" Engineering Journal AISC, 21, 3, pp. 139-148.

[Thornton, 1991], Thornton W.A., (1991), "*On the analysis and design of bracing connections*," Proc. National Steel Construction Conf., American Institute of Steel Construction, Washington D.C., June, pp. 26-33.

[Topkaya, 2004], Topkaya C., 2004. "*A finite element parametric study on block shear failure of steel tension members*". Journal of Constructional Steel Research, Elsevier, vol. 60, pp. 1614-1635.

[Ziemian, 2010], Ziemian R.D. (2010), "*Guide to Stability Design Criteria for Metal Structures*", 6th Ed.,John Wiley & Sons, Inc., Hoboken, NJ.

[Zoetemijer, 1983], Zoetemijer B., (1983), "*Proposal for Standardization of Extended End Plate Connection based*". (period 1978 - 1983), Rep. No. 6-85-M, Steven Laboratory, Delft, 1983.

[Yam and Cheng, 1993], Yam, C.H.M., Cheng, J.J.R., (1993), "*Experimental investigation of the compressive behavior of gusset plate connections*," Structural Engg. Rep. no. 194, U. of Alberta, Edmonton, Alberta, Canada.

[Yamamoto et al., 1988], Yamamoto K., Akiyama N. and Okumura T., (1988), "*Buckling strength of gusseted truss joints*," ASCE JSE vol. 114, no. 3, Mar. pp. 575-590.

[Walbridge, 1998], Walbridge, S., Grondin, G.Y. & Cheng, R.J.J., (1998), "*An Analysis of the Cyclic Behaviour of Steel Gusset Plate Connections*," Structural Engg. Report No. 225, U. of Alberta, Edmonton, Alberta,

	Canada.
[Whitmore, 1952],	Whitmore R.E., (1952), “*Experimental investigation of stresses in gusset plates*,” University of Tennessee Engineering Experiment Station Bulletin no. 16, May.